TEKTONISCHE ENTWÄSSERUNG AN KONVERGENTEN PLATTENRÄNDERN

DEWATERING AT CONVERGENT CONTINENTAL MARGINS

Abschlußbericht des Vorhabens 03R607 6

**Projektträger Material- und Rohstofforschung
des Bundesministeriums für Forschung und Technologie
am Forschungszentrum Jülich GmbH**

**Herausgegeben von
Erwin Suess
mit zusätzlichen Beiträgen von
Peter Hempel, Peter Linke, Marta Torres,
Wolfgang Kloebe, Stephan Lammers, Christiane Wagner**

GEOMAR
Forschungszentrum
für marine Geowissenschaften
der Christian-Albrechts-Universität
zu Kiel

Kiel 1993

GEOMAR REPORT 18

GEOMAR
Research Center
for Marine Geosciences
Christian Albrechts University
in Kiel

Herausgeber: Jörn Thiede
Redaktion der Serie: Gerhard Haass
Umschlag: Harald Gross, GEOMAR Technologie GmbH

Editor: Jörn Thiede
Managing Editor: Gerhard Haass
Cover: Harald Gross, GEOMAR Technologie GmbH

GEOMAR REPORT
ISSN 0936 - 5788

GEOMAR REPORT
ISSN 0936 - 5788

GEOMAR
Forschungszentrum
für marine Geowissenschaften
D-2300 Kiel
Wischhofstr. 1-3
Telefon (0431) 7202-0
Telefax (0431) 72 53 91, 7 20 22 93, 72 56 50

GEOMAR
Research Center
for Marine Geosciences
D-2300 Kiel / Germany
Wischhofstr. 1-3
Telephone (49) 431 / 7202-0
Telefax (49) 431 / 72 53 91, 7 20 22 93, 72 56 50

INHALT

6.1 Anhang

6.2 Manuskripte

1. „In situ measurements of fluid flow from cold seeps at active continental margins“
2. „Dewatering of sediments along the Cascadian Margin: Evidence from geotechnical properties“
3. „Tectonic history of a non-accreting active margin during the past 400 ka. Results of a submersible survey of the Peru Trench at 5-6°S Part I.“
4. „Continent-derived fluids from the convergent margin off Peru. Deep sea dives of the Nautiperc cruise, Part II.“
5. „Expulsion of shallow gas in the Skagerrak - evidence from sub-bottom profiling, seismic, haydroacoustical and geochemical data“
6. „Barite deposits from the Peru subduction zone“

1. EINFÜHRUNG

1.1 Aufgabenstellung

Die Bilanzierung von Fluiden und Gasen sowie deren Zirkulation im Bereich aktiver Plattenränder sind wichtige Aspekte moderner geowissenschaftlicher Grundlagenforschung. Im Rahmen des BMFT-Projektes „Tektonische Entwässerung an konvergenten Plattenrändern" wurden zwei prominente aktive Ränder im zirkum-pazifischen Plattengefüge untersucht: Die Cascadia-Subduktionszone und der Peru-Kontinentalrand (Abb. 1.1.1). Beides sind „akkredierende" Ränder, aber mit unterschiedlich mächtig ausgebildeten Akkretionskeilen. Die Fluidzirkulation spielt hier eine bedeutende Rolle, wobei die sedimentphysikalischen, geothermischen und geochemischen Eigenschaften durch tektonischen Streß der Plattenkonvergenz beeinflußt werden. Das Ziel des Vorhabens erstreckte sich auf die Quantifizierung der Stoffflüsse aus Subduktionszonen. Die wissenschaftlichen Bemühungen in diesem Vorhaben waren darauf ausgerichtet, folgende übergeordnete Fragen zu beantworten:

Wie groß sind die Transportraten von Fluiden im globalen Plattengefüge ?
Wie groß ist der Eintrag von gelöstem CH_4 und ΣCO_2 in den Ozean ?
Wie groß ist der Gesamteintrag von gelösten Stoffen ?
Welche davon sind juvenilen Ursprungs und welche sind "recycled"; d.h. befinden sich schon innerhalb des marinen Stoffkreislaufes ?
Wie nachhaltig wird die marine Umwelt von diesen Stofftransportvorgängen beeinflußt ?
Welche chemische Evolution machen die Fluide an unterschiedlichen Plattengrenzen durch?
Welche physikalischen Sedimentparameter steuern den Wasserfluß am nachhaltigsten ?
Welchen Tiefen entstammen die Fluide in den verschiedenen Krustenteilen ?

Speziell sollten die advektiven Flüsse abgeschätzt werden, die als tektonisch-gesteuerter Anteil dem marinen Stoffkreislauf zugeführt werden. Weiterhin sollten Anhaltspunkte dafür gewonnen werden, ob die tektonisch-gesteuerten Stoffflüsse großräumig über die Subduktionszonen verteilt oder lokal an tektonisch und stratigraphisch vorgezeichneten "vents" entweichen. Die Ziele des Vorhabens sollten in Teilprojekten zuerst am Beispiel der Cascadia-Subduktionszone und des Peru-Fore-Arc erarbeitet werden.

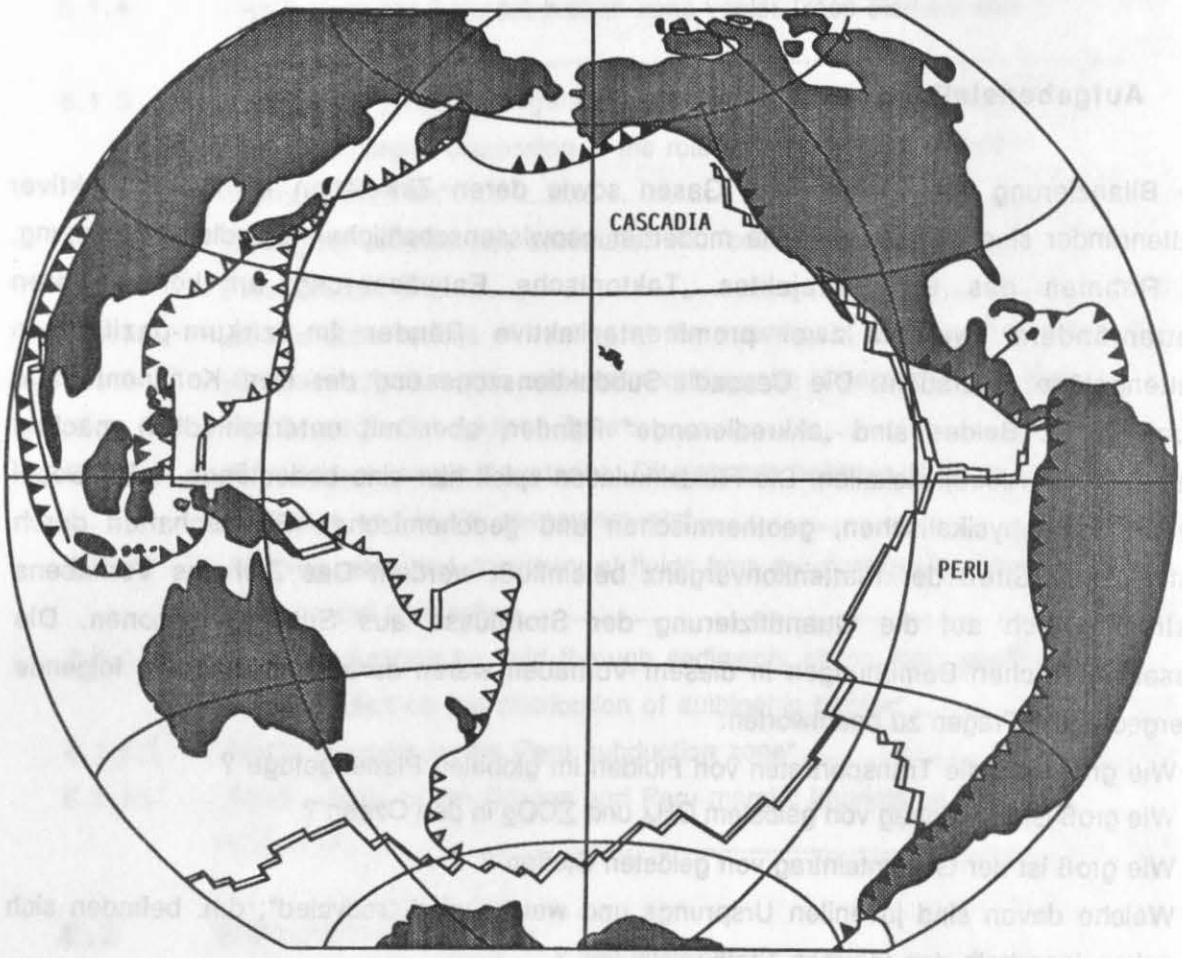

Abb. 1.1.1 Zirkum-pazifische Konvergenzzonen mit akkredierenden und erodierenden Segmenten durch den Subduktionsvorgang; die Untersuchungsgebiete Cascadia und Peru sind besonders markiert.

Der hydrochemische Gesamtstoffffluß aus der Cascadia-Subduktionszone, der in einem früheren Vorhaben gemessen wurde, sollte in eine "regenerierte" benthische Komponente von der Sedimentoberfläche und eine "advektive" Komponente aus den Tiefen des Akkretionskeiles aufgeteilt werden. Regenerationsfluß sollte mit Hilfe der direkten Micro-Kalorimetrie bestimmt werden. Er entstammt erhöhtem biologischem Stoffumsatz um die "vent"-Felder und wird durch den nährstoff- und energiereichen Entwässerungsstrom angeregt und aufrecht erhalten.

Subduktions-"vents" sollten in ausgewählten tektonischen Einheiten der Peru-Subduktionszone mit dem französischen Tieftauchboot NAUTILE und während der SONNE-Reise 78 erkundet, und erste *in situ* Messungen der Ausstromraten durchgeführt werden. Im Peru-Fore-Arc gibt es unterschiedliche tektonischen Stockwerke, aus denen Entwässerungsströme austreten können: dem Akkretionskeil, den Beckenfüllungen des "fore-arcs" und dem Bereich der abtauchenden ozeanischen Kruste. Entsprechend sollten chemische und isotopische "tracer" für die unterschiedliche Herkunft der Flüsse erarbeitet, die Entwässerungsbahnen modelliert und die Größenordnungen der Transportraten abgeschätzt werden.

1.2 Voraussetzungen, unter denen das Vorhaben durchgeführt wurde

Wesentliche Voraussetzung für die erfolgreiche Durchführung des Vorhabens war die Kooperation mit den geologisch und geochemischen Arbeitsgruppen der Oregon State University, U.S.A., und der Université Pierre et Marie Curie, Paris, die es ermöglichte, an den Expeditionen mit den Tieftauchbooten ALVIN und NAUTILE teilzunehmen. Diese Tauchfahrten, zusammen mit der SONNE-Reise 78, erbrachten das notwendige Probenmaterial als wesentlichen Bestandteil des Vorhabens. Die analytischen Möglichkeiten in den Labors von GEOMAR waren in ausreichendem Maße vorhanden, um die gestellten Aufgaben zu erfüllen. Spezialuntersuchungen, für die das notwendige Instrumentarium fehlt, konnten durch die enge Zusammenarbeit mit dem SFB 313, dem Geologisch-Paläontologischen Institut in Kiel und dem Institut für Biogeochemie und Meereschemie, Hamburg, durchgeführt werden.

1.3 Planung und Ablauf des Vorhabens

Zentrale Bestandteile bei der Planung und dem Ablauf des Vorhabens waren Expeditionen zur Cascadia-Subduktionszone und dem Perugraben. Das gewonnene Probenmaterial wurde zum Teil unmittelbar an Bord der Forschungsschiffe analysiert, weitere Proben wurden für die späteren Untersuchungen an Land fachgerecht konserviert.

Im Vorgriff auf das Vorhaben erfolgte eine Expeditionen im September 1989 zur Felderprobung des Mikrokalorimeters und der Porenwasseranalysen im Umfeld von Subduktions-"vents". Im ersten Antragsjahr (1990) erfolgten drei Ausfahrten zur Cascadia-Subduktionszone mit R.V. NEW HORIZON, R.V. WECOMA und R.V. ATLANTIS-II mit mehreren Tauchgängen von D.S.R.V. ALVIN. Im Verlauf der WECOMA-Ausfahrt stand die Extraktion von Porenwässern aus Sedimentkernen und die Gewinnung von Bodenwasserproben und deren Analyse im Hinblick auf die gelösten Nährstoffe und Gase im Vordergrund. Ein Großteil der Parameter konnte bereits an Bord analysiert werden, die übrigen Proben wurden im Anschluß an die Ausfahrt im speziell für diese Untersuchungen eingerichteten Laborcontainer des GEOMAR an Land bearbeitet. Die Tauchgänge mit ALVIN dienten der Bestimmung der Flußraten und chemischen Bestandteile von Fluiden, die an "vent"-Feldern austreten. Hierzu wurde die mit einer Strömungssonde ausgerüstete Gas-Wasser-Probenkammer (benthic barrel) eingesetzt (LINKE et al. in press; Anhang). Die geplanten kalorimetrischen Messungen wurden an Bord der ATLANTIS-II und WECOMA während und vor dem Tieftaucheinatz vorgenommen. Während der WECOMA-Ausfahrt 1989 konnten an insgesamt 4 Stationen Tiefenprofile der Wärmeproduktion im Sediment erfaßt werden. Von ALVIN aus wurden 1990 "vents" direkt beprobt und an Sedimentkernen aus dem Umfeld die Wärmeproduktion bestimmt.

Die geplante Beprobung und sedimentphysikalische Analyse von Kernen, die in den Jahren 1983, 1984 und 1987 von der Cascadia-Subduktionszone gewonnen wurde, konnte ebenso erfolgreich durchgeführt werden, wie die Sichtung und Interpretation der flachseismischen Aufzeichnungen. Die Ergebnisse sind in einem Manuskript zur Veröffentlichung eingereicht (s. HEMPEL and SUESS 1993; Anhang). Versuche zur Isotopenfraktionierung beim Einbau bzw. der Abgabe von Zwischenschichtwasser erfolgten an reinem Smektit. Für die Spurenmetall- und stabile Isotopenzusammensetzung der Karbonatkonkretionen und Organismen wurden *Calyptogena*- und *Solemya*-Muscheln, sowie Bartenwürmer (*L. barhami*) von verschiedenen ALVIN-Tauchgängen geochemisch untersucht.

Im Frühjahr 1991 erfolgte die geplante Teilnahme an der NAUTIPERC-Expedition mit Tauchgängen des D.S.R.V. NAUTILE im Gebiet des Peru-Fore-Arc und die Vorbereitung der SONNE-Reise 78. Die an Bord der R.V. NADIR (Mutterschiff der NAUTILE) erfolgten Analysen von gelösten Nährstoffen und Gasen, wurden durch umfangreiche Messungen an Land ergänzt. Die wichtigsten tektonischen und geochemischen Ergebnisse wurden in zwei Übersichtsarbeiten veröffentlicht (BOURGOIS et al. 1993; DIA et al., 1993). Schwerpunkt der Vorbereitung zur SONNE-Ausfahrt war der Bau der Probenkammer (benthic barrel), die erstmalig von Bord eines Forschungsschiffes eingesetzt werden sollte. Das seismische Prozessing von PARASOUND-Registrierungen konnte zu routinemäßigen Verfahren entwickelt werden.

Die SONNE-Ausfahrt im Frühjahr 1992 galt der bathymetrischen Vermessung ausgewählter Abschnitte des peruanischen Kontinentalhanges und der OFOS-gesteuerten Beprobung von "vent"-Feldern. Aus technischen Gründen wurde von dem Einsatz der *in situ* Porendruckbestimmung mit PUPPI abgesehen und dafür eine einfachere Temperatur- und Drucksonde erworben und eingesetzt. Die Probenkammer konnte mehrfach erfolgreich eingesetzt werden und lieferte, zusammen mit der installierten Strömungssonde, wesentliche Ergebnisse zur Quantifizierung der Fluid- und Gasausstromraten. Die Arbeiten an den Spurenmetallzusammensetzungen und Chloridanomalien konnten anhand des gewonnenen Probenmaterials in geplanter Weise fortgeführt werden.

1.4 Wissenschaftlicher und technischer Stand

Die Quantifizierung der Ausstromraten von Fluiden und Gasen, die durch tektonisch gesteuerte Prozesse am Meeresboden austreten, konnte durch dieses Vorhaben auf eine verläßliche Basis gestellt werden. Hierzu dienten Strömungssonde und Gasanalysen in der Probenkammer, die sowohl von Tieftauchbooten als auch von Bord des konventionellen Forschungsschiffes R.V. SONNE ausgebracht wurde. Die erforderlichen technischen Entwicklungen und gesammelten Erfahrungen sind wegweisend für zukünftige Unternehmen mit ähnlicher Fragestellung. Die wichtigste zusammenfassende Arbeit dazu ist von LINKE et al., 1993 (Anhang): "*In situ* measurement of fluid flow from cold seeps at active continental margins". Von den 15 derzeit existierenden Abschätzungen von Ausstromgeschwindigkeiten resultieren 10 aus dem Einsatz der *in situ* Probenkammer, 3 aus der Analyse von Porositätsänderungen (sedimentphysikalische Geschwindigkeiten) und 2 Wärmestromanomalien.

Bei den geochemischen Untersuchungen der biologischen "vent"-Vergesellschaftungen und autigenen Mineralbildungen zeichnet sich ab, daß die von "vent"-Organismen eingebauten Spurenmetallkonzentrationen entscheidende Hinweise auf die Genese, Modulationen der Fließraten und Herkunftstiefen der Fluide liefern. Die Untersuchungen hierzu sind noch nicht abgeschlossen. Die physikalischen Eigenschaften oberflächennaher Sedimente erwiesen sich als aussagekräftige Parameter bei der Beurteilung tektonisch-bedingter Sedimentdeformationen an aktiven Kontinentalrändern. Es ließen sich aus den Ergebnissen unabhängige Entwässerungsraten bestimmen, die mit den direkt gemessenen Ausstromraten verglichen werden können. Das Prozessing der digitalen sedimentechographischen Aufzeichnungen mit PARASOUND konnte erstmalig mit kommerzieller prospektions-

seismischer Software durchgeführt werden und lieferte entscheidende Detailinformationen zur Beurteilung des akustischen Verhaltens und der Verbreitung oberflächennaher gashaltiger Sedimente.

1.5 Zusammenarbeit mit anderen Stellen

Dieses Vorhaben hätte durch die intensive Zusammenarbeit mit folgenden Forschungsinstitutionen im In- und Ausland nicht in dem Maße erfolgreich durchgeführt werden können:

College of Oceanography, Oregon State University, Corvallis, Oregon (U.S.A.)
Laboratoire Tectonique et Environement de Geologie, Université Pierre et Marie Curie, Paris (France)
Universida Nacional Lima (Peru)
Institut für Umweltphysik, Universität Heidelberg
Fachbereich Geowissenschaften, Universität Bremen
Institut für Biogeochemie und Meereschemie, Universität Hamburg
Geologisch-Paläontologisches Institut, Universität Kiel
Sonderforschungsbereich 313, Universität Kiel
Institut für Meereskunde, Kiel
Reedereigemeinschaft Forschungsschiffahrt, Bremen
Firma Hydrobios, Kiel
Ingenieur-Büro Scholz, Fockbek

2. WISSENSCHAFTLICHE ERGEBNISSE

2.1. Geochemische und isotopengeochemische Untersuchungen an "vent"-Material

Christiane C. Wagner

Spurenelement- und Isotopenuntersuchungen an biogenem Material aus den "vent"-Gebieten vor Peru und Oregon waren eine zentrale Fragestellung des Forschungsprojektes. Die neueren Ergebnisse tragen dazu bei, den Mechanismus, der dem Zustandekommen und der Aufrechterhaltung von "vents" zugrunde liegt, besser zu verstehen. Während der Forschungsfahrt SONNE 78, im Frühjahr 1992, konnte einiges neues Material für diese Untersuchungen geborgen werden, das insbesondere in Verbindung mit direkten Beobachtungen (OFOS) wertvoll ist.

Neue methodische Ansätze

Abweichend von den vorangegangenen Untersuchungen, ist bei den letzten Messungen die Atom Absorptions Spektrometrie als Analysemethode verstärkt zum Einsatz gekommen. Für die zu untersuchenden Materialien wurden spezielle Meßprogramme erarbeitet und auf ihre Eignung überprüft. Haupt- und Nebenelemente wurden mittels ICP-AES (Induced Coupled Plasma-Atom Emissions Spektroskopie) gemessen. Zusätzlich zur analysetechnischen Methodik wurden Interpretationsansätze entwickelt, (1) um eine umfassende Interpretation unterschiedlicher Materialien aus "vent"-Gebieten zu ermöglichen und (2), um die Aussage von Isotopendaten zu untersuchen.

Vergleichbarkeit von geochemischen Daten aus "vent"-Material

Aus den "vent"-Gebieten vor Peru und Oregon sind verschiedene Organismen mit Hart- und Weichteilen untersucht worden. Die untersuchten Materialien lassen sich in zwei Gruppen einteilen:

(1) Carbonate ($CaCO_3$) in calcitischer (Serpulidenröhren, Konkretionen) und aragonitischer Struktur (Schalen der Mollusca)

(2) Organisches Material; Periostracum und Weichteile der Mollusca: Röhren und Weichteile der Vestimentifera, Weichteile der Serpuliden

Die Schalen der Molluscen sind zwar biogen gebildet, weisen jedoch eher anorganische als organische Züge auf. Das hängt damit zusammen, daß die Bildung der Schale nicht unmittelbar aus entsprechenden Epithelzellen erfolgt, sondern aus einer Flüssigkeit (Extrapallialflüssigkeit) abgesondert wird, wobei sich organische Bestandteile eher passiv verhalten (TAYLOR et al. 1969). Die Extrapallialflüssigkeit befindet sich im Raum zwischen Mantel und Schale. Es wird angenommen, daß einzelne Epithelkammern in Kontakt mit dem Seewasser stehen (TAYLOR et al., 1969) und damit deren chemisches Inventar wiederspiegeln.

Von dieser Annahme ausgehend, ist es also nicht verwunderlich, daß verschiedene Bereiche der Schale eines Organismus einen unterschiedlichen Chemismus wiederspiegeln und sich insgesamt ein uneinheitliches Bild ergibt. Von daher ist, da die Mechanismen der Schalenbildung nicht bis in alle Einzelheiten bekannt sind, die Vergleichbarkeit verschiedener Schalen einer Art eingeschränkt. Vergleiche zwischen Schalen unterschiedlicher Arten sind entsprechend nur bedingt möglich. Molluscenschalen und Serpulidenröhren, aragonitisch oder calcitisch, sind außerdem von einem Proteingerüst durchzogen. Dieses kann bei der Reinigung der Proben nicht vollständig entfernt werden und hat damit ebenfalls Einfluß auf Elementkonzentrationen in einer Schale. Auch hier gilt deshalb eine eingeschränkte Vergleichbarkeit.

Zusammenfassend ist eine abnehmende Vergleichbarkeit in folgender Reihe festzustellen:

- innerhalb der Schale/Röhre eines Organismus
- zwischen Organismen einer Art
- zwischen Organismen unterschiedlicher Arten (*Calyptogena/Solemya*)
- zwischen Organismen unterschiedlicher Stämme (Serpuliden/Molluscen)

Die organischen Weich- und Hartteile (Periostracum, Röhren) repräsentieren eine Varietät komplexer organischer Strukturen, die nicht detailliert bekannt sind. Ein direkter Vergleich ist daher kritisch zu betrachten, aber gleichzeitig auch die einzig praktikable Möglichkeit, eine Charakterisierung unterschiedlicher Stoffgruppen nach einem einheitlichen Schema vorzunehmen.

Grundlagen zur Interpretation stabiler-Isotopen-Daten von "vent"-Organismen

Die Interpretation von Daten stabiler Isotope (O,C) an "vent"-Organismen erfordert andere Ansätze, als die Interpretation in Bezug auf paläoozeanographische Fragestellungen. "Vents" zeichnen sich durch Lebensgemeinschaften aus, die an die jeweiligen speziellen Nahrungsquellen ihres Lebensraumes angepaßt sind. Damit sind die Organismen von den großräumigen Umweltbedingungen relativ unabhängig und reflektieren diese als Mischsignal der Isotopien ihrer Hartteile. Durch die Aufzeichnung des "vent"-Milieus sind einzigartige Möglichkeiten der Interpretation gegeben.

Als Ausgangspunkt für die Interpretation der Signale müssen folgende Randbedingungen bekannt sein:

1. Quellen für C und O gelöstes CO_2, HCO_3, CO_3, Stoffwechselprodukte von Organismen und Symbionten (aus biogenem CH_4)
2. Isotopenverhältnisse der Quellen Meerwasser, "vent"-Fluide (extrapoliert aus Probenkammer-messungen)
3. Art der Symbionten Abschätzung von deren Wirkungsgrad in Bezug auf das Isotopensignal

4. Generelle Trends im Isotopensignal über den gesamten Reifeprozeß des Organismus Vergleich mit Organismen aus anderen Lebensräumen
5. Abschätzungen über das Alter der zu untersuchenden Organismen

Mollusca: Calyptogena

In Bivalviern in marinem Flachwassermilieu (*Tridacna, Arca, Pinna, Pecten*) beobachtete saisonale Schwankungen der Isotopenwerte (WEFER 1985, WEFER & BERGER 1991, ROMANEK & GROSSMANN 1989), sind bei *Calyptogena* nicht zu erwarten. Zyklische Schwankungen im Schalenprofil von *Calyptogena* können daher ein unterschiedliches Nahrungsangebot reflektieren, das jedoch nicht saisonal bedingt ist, sondern von den Ausstromraten der "vents" abhängt. Nach Kenntnis der Isotopenverhältnisse im C-Pool der "vents" und des Umgebungswassers sind in der Schale Mischwerte zu erwarten. $\partial^{18}O$ -Werte müßten nach dem bisherigen Kenntnisstand relativ konstant bleiben, da die sedimentären "vents" keine erhöhte Temperatur gegenüber dem Bodenwasser haben. Symbiontische Bakterien können bei *Calyptogena* Isotopenverhältnisse beeinflussen. *Calyptogena* beherbergt chemoautotrophe Bakterien. Diese sind nach Untersuchungen von RUBY et al. (1987) stark ^{12}C-selektiv, sogar in höherem Maße als photoautotrophe Einzeller.

Vestimentifera: *Lamellibrachia*

Für die Hartteile von Bartenwürmern, wie *L. barhami*, liegen bislang keine systematischen Untersuchungen stabiler Isotope vor. Vereinzelte Messungen an der Röhre von SAINO & OTHA (1989), sowie KULM et al. (1986) deuten darauf hin, daß sich auch hier die chemoautotrophe Ernährungsweise der Organismen durch Symbionten in den Hartteilen niederschlägt. Die bisherigen Messungen sind jedoch nur Einzelwerte und lassen daher keine Rückschlüsse auf die Bandbreite möglicher Schwankungen zu. Die Interpretation von Daten stabiler Isotope von *L. barhami* erfordert statistisch signifikante Messreihen, die Aussagen über generelle Tendenzen der Isotopenanreicherung über den Zeitraum der Ontogenie eines Individuums zulassen.

Ergebnisse und Diskussion

Die Ergebnisse der Spurenelement- und Isotopenuntersuchungen werden im Folgenden, nach Gebieten gegliedert, diskutiert. Spurenelementkonzentrationen der Beprobungsgebiete vor Peru sind tabellarisch dargestellt (Tab. 2.1.1). Die erste Zeile gibt jeweils die Maximalwerte, die zweite das "Rauschen", also den Bereich in dem die Hintergrundwerte schwanken, an.

PERU				
	Ba	**Zn**	**Sr**	**Cu**
Chiclayo				
33 Calyptogena (I)	57	12	1	5,5
	10,0-30	1,0-4	?	2,0-3
33 Calyptogena (A)	60	30	1	11
	10 - 15	0-5	0,7-0,9	0-3
33 Serpulide 1	20	45	3,4	
	0-5	15-25	2,9	
Serpulide 2	130	250	3,3	
	5 - 10	40-60	2,9	
Paita				
SP 30/1 Serpulide	25	150	3,3	
	0-20	100	3	
177 Solemya	30	29 (124)	9	
	0-5	1,0-5	5,5-6,5	
177 Calyptogena 1	45		3,3	
	0-5		0-1	
177 Calyptogena 2	45	194	6	8
	1,0-10	1,0-8	?	0-2
30 Calyptogena	16	48	1,25	
	0-5	2,0-10	0,9-1,0	
Chimbote				
8506-1 Calyptogena (A)	4	200		
	0-0,5	10 - 30		
8506-2 Calyptogena (A)		1,3		
		0-0,5		
8506-2 Calyptogena (I)	6,3		0,5	
	1,5-2,5		0-0,1	
163 Solemya	25		7	
	0-1		5 - 6	
163 Serpulide	80	45	3,3	
	30-35	25-30	3	

Tab. 2.1.1 Konzentrationsbereiche der Spurenelemente von karbonatischen "vent"-Biota vor Peru normiert auf Ca, d.h. µmol Ba, Zn, Cu/mol Ca bzw. mmol Sr/mol Ca

Barium, Zink und Kupfer

Die Verteilung von Ba und Zn in den Schalen verschiedener Organismengruppen (*Calyptogena, Solemya, Serpulidae*) ist gekennzeichnet durch starke Variabilitäten. In allen Schalen-/Röhrenprofilen lassen sich Maxima von einer Grundvariabilität unterscheiden. Die höchsten Konzentrationen von Ca^{2+} isomorph ersetzenden Elementen wurden in Serpuliden gemessen (Tab. 2.1.1). Diese besiedeln, wie OFOS-Aufnahmen während SO 78 gezeigt haben, direkt die Austrittsstellen von "vent"-Fluiden. Sie können sich an jede Geländeform anpassen und haben deshalb bei steiler Morphologie (Chiclayo, Paita) den besten Zugang zur Nahrungsquelle. Eine Abnahme der Elementkonzentrationen ist in der Reihenfolge *Serpulidae -> Calyptogena -> Solemya* zu beobachten. Dieses Resultat ist damit zu erklären, daß *Solemya* solitär in der weiteren Umgebung der "vent"-Kolonien lebt. Eine Abstufung zwischen den einzelnen Gebieten

kann auf Grundlage der vorliegenden Ergebnisse noch nicht durchgeführt werden. Generell muß jedoch im Gebiet Chimbote von anderen Ursachen des "venting" ausgegangen werden als in Paita und Chiclayo (Fahrtbericht SO 78). Vermutlich liegt in Chimbote keine tektonische Steuerung vor. Niedrige Ba-Werte unterstützen diese Annahme.

In Schalenprofilen aus den Gebieten Chimbote und Paita wurden in rezenten Schalenabschnitten z.T. sehr geringe Konzentrationen der Spurenelemente beobachtet. Sie zeichnen offenbar entweder eine Ruhepause der "vent"-Aktivität, oder eine Abwanderung des entsprechenden Organismus aus der "vent"-Kolonie nach.

Strontium

Die Anreicherung von Sr in karbonatischen Hartteilen ist, wie die vorliegenden Untersuchungen zeigen, artabhängig. Sie liegen bei Calyptogena im Bereich von 0,1-1mmol/mol Ca, bei Solemya bei 5-9 mmol/mol und bei den Serpuliden um 3-3,4 mmol/mol Ca (Tab. 2.1.1). In den "vent"-Gebieten vor Peru und Oregon sind keine erhöhten Temperaturen gemessen worden (SO 78), wie dies die Anwendung der Temperaturgleichung für Sr in Aragonitschalen (BECK et al. 1992) erfordern würde. Der Sr-Einbau ist danach unter "vent"- Bedingungen nicht temperaturabhängig, noch mineralogisch gesteuert, so daß nur eine schwankende Zufuhr dafür verantwortlich sein kann.

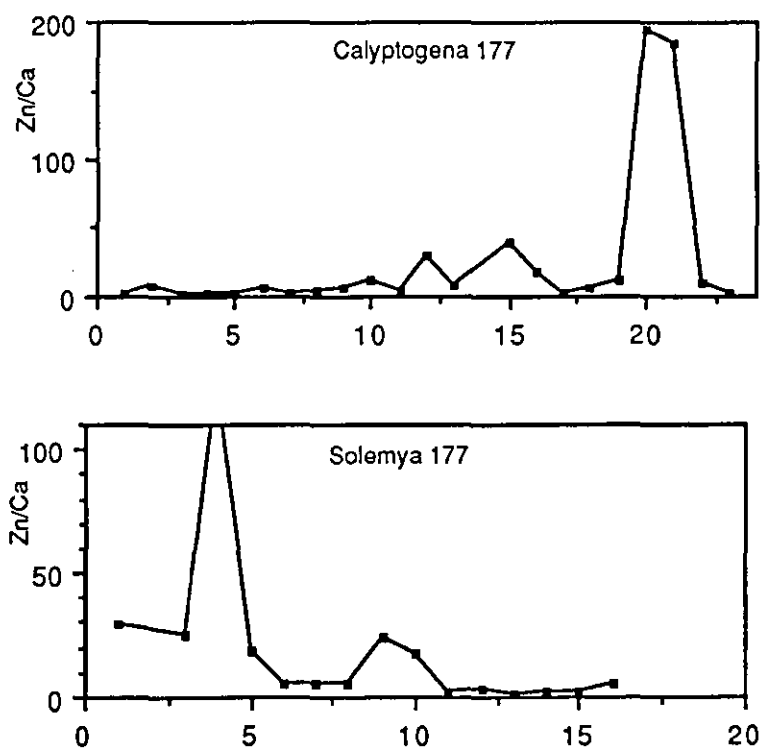

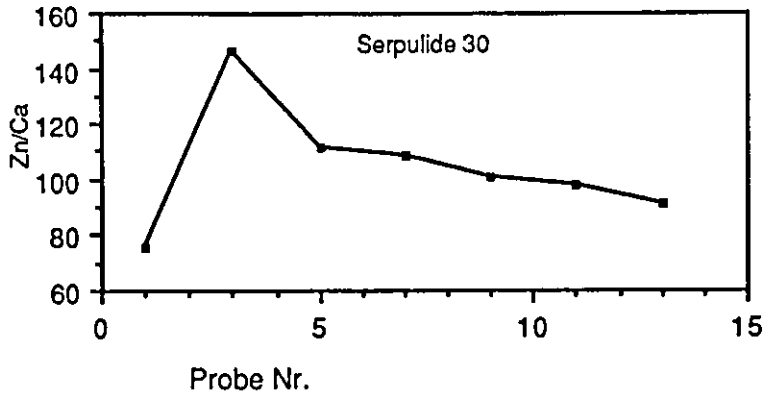

Abb. 2.1.1 Konzentrationsvergleich am Beispiel von Zink; Extremwerte heben sich von einem "Rauschen" ab. Dieses ist am Höchsten bei Serpuliden, am Geringsten bei *Solemya*; die Probennummer bezeichnet sequentielle Abschnitte eine Individuums.

Die Ergebnisse der Spurenelementanalysen im "vent"-Gebiet vor Oregon bestätigen diejenigen vom peruanischen Kontinentalrand. Auch hier variiert der Einbau von Spurenelementen in Hartteile periodisch. Dieses Charakteristikum tritt in karbonatischen Hartteilen, aber auch in organischen Röhren auf (*L. barhami*). Da bei den Röhren ein völlig anderer Mechanismus des Einbaus vorliegt und diese aus komplexen organischen Strukturen aufgebaut sind, ist die Übereinstimmung der Spurenelementmuster zwischen den Organismen bemerkenswert.

An der Lokation 1428 im Untersuchungsgebiet vor Oregon ist eine Schale von *Calyptogena* sogar direkt mit einer Röhre von *L. barhami* vergleichbar (Abb. 2.1.2). Die längste Zeitspanne wird dabei durch die Röhre von *L. barhami* abgedeckt. Diese Organismen sind bereits im Initialstadium der Besiedelung eines "vent" präsent. Die Röhren der beprobten Organismen sind bis zu 1,20 m lang. Da die Verteilungsmuster von Spurenelementen in *L. barhami* und *Calyptogena* gute Übereinstimmungen aufweisen, kann eine relative Wachstumsrate von *L. barhami* im Vergleich zu *Calyptogena* bestimmt werden; diese beträgt 5 : 1 für *L. barhami* zu *Calyptogena*. Da die großen Calyptogenen hier eine Länge von ca. 5 cm haben, ist, bei konstanter Wachstums-geschwindigkeit, das Alter von *L. barhami* 25 mal so hoch, wie das der beprobten Calyptogenen. Die Röhren von *L. barhami* sind daher ebenso wie Sedimentkerne als Speichermedium für geochemische Veränderungen zu betrachten, dessen Datenvorrat mit Hilfe geochemischer Analytik entschlüsselt werden kann.

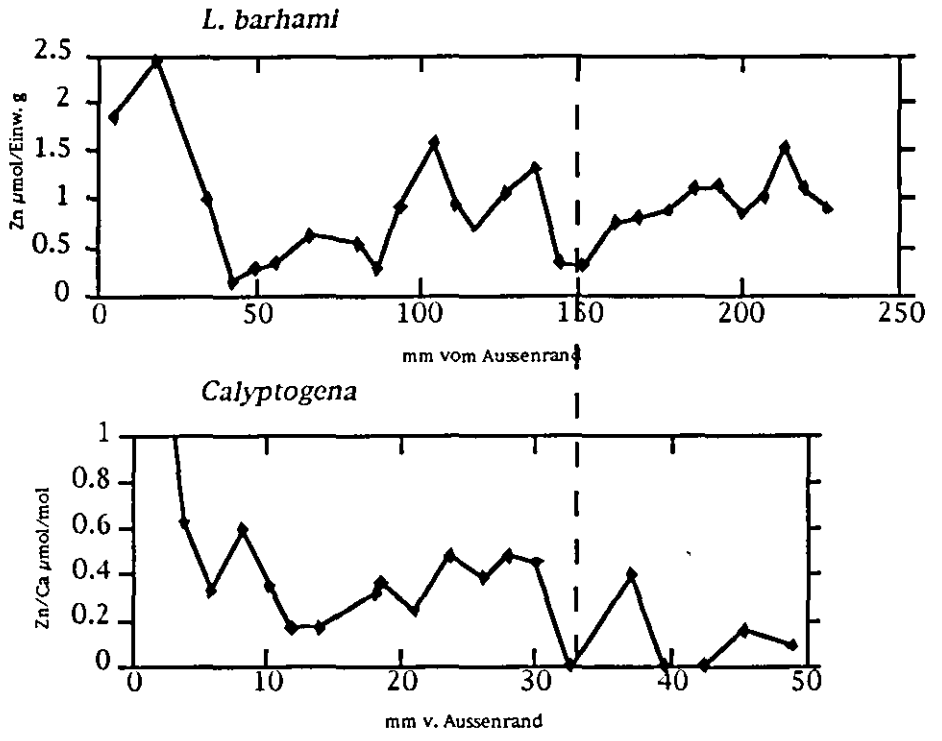

Abb. 2.1.2 Vergleich der Zn-Verteilung in *Calyptogena* (carbonatische Schale) und *L. barhami* (organische Röhre)

Auch in den "vent"-Gebieten vor Oregon zeigt sich, daß jede Lokation ein charakteristisches Konzentrationsniveau unterschiedlicher Spurenelemente aufweist (Tab. 2.1.2). Elemente wie Zn und Cu sind, ebenso wie Ba, z.T stark angereichert. Cadmium erreicht, nach bisherigen Untersuchungen, nur in organischem Material nachweisbare Konzentrationen. In den Röhren von *L. barhami* läuft das Verteilungsmuster von Cd mit dem anderer Spurenelemente konform. Die Messungen einzelner Elemente an unterschiedlichen Organismen fügen sich so Stück für Stück zusammen und sollen zu einer generellen Charakterisierung von "vents" auf geochemischer Grundlage führen.

OREGON				
	Ba	Zn	Sr	Cd
Gebiet 1				
1428 Calyptogena	312	1,6	0,1	55,9
	0,2-0,6	0,5-1	0,07-0,08	0-10
1428 L. barhami				70 (169)
				4,0-12
Gebiet 2				
2046 Calyptogena	6,67	3		
	1,5-1,9	0,1-1		

Tab. 2.1.2 Konzentrationsbereiche der gemessenen Spurenelemente von karbonatischen "vent"-Biota vor Oregon normiert auf Ca, d.h. µmol Ba, Zn, Cu/mol Ca bzw. mmol Sr/mol Ca

C- und O-Isotope

Aus dem Gebiet vor Oregon liegen einige Schalenprofile stabiler Isotope (C+O) von *Calyptogena* und *Solemya*, vor. Auch hier scheint sich, ebenso wie bei den Spurenelementen (insbesondere Sr), eine Entkopplung von den üblichen, klimatisch bedingten Prozessen, anzudeuten. $\partial^{18}O$ und $\partial^{13}C$ zeigen Schwankungen an, die sich teilweise mit den Schwankungen der Spurenelemente parallelisieren lassen (Abb. 2.1.3). Sie zu erklären, ist auf dem gegenwärtigen Kenntnisstand noch sehr schwierig. Falls ein direkter Zusammenhang besteht, müssen komplexe Reaktionen der "vent"-Fluide über Stoffwechselprozesse der Organismen angenommen werden.

Sowohl bei Calyptogena, als auch bei Solemya sind "vent"-induzierte Schwankungen der Isotopenverhältnisse von ontogenetischen überprägt. Es ist jeweils ein Anstieg von $\partial^{13}C$ und $\partial^{18}O$ im ersten Lebensabschnitt zu beobachten. Dieser setzt irgendwann aus. Danach lassen sich Schwankungen innerhalb einer gewissen Bandbreite beobachten (Abb. 2.1.4). Da dieser Effekt ganz durchgängig auftritt, ist er offensichtlich ontogenetisch bedingt und signalisiert eine allmähliche Umstellung des Stoffwechselsystems. Eventuelle "vent"-Effekte können daher nur im akuten Stadium, nach Einpendelung des Systems, beobachtet werden.

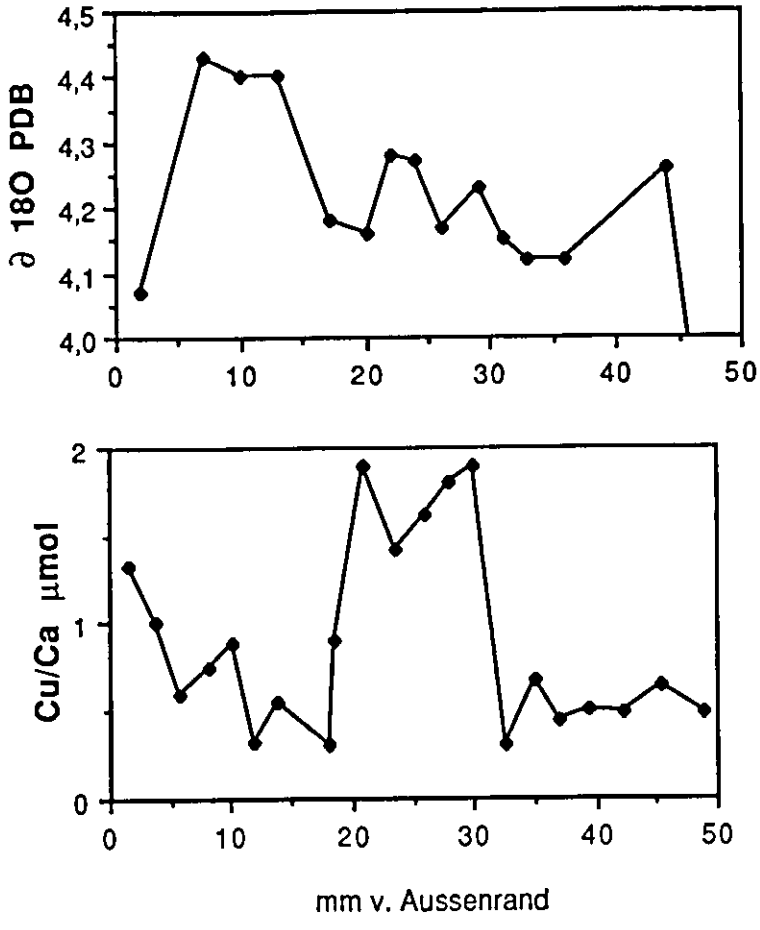

Abb. 2.1.3 Korrelation von $\partial^{18}O$- und Cu-Verteilung entlang eines Schalenprofils von *Calyptogena* (Lokation 1428 vor Oregon).

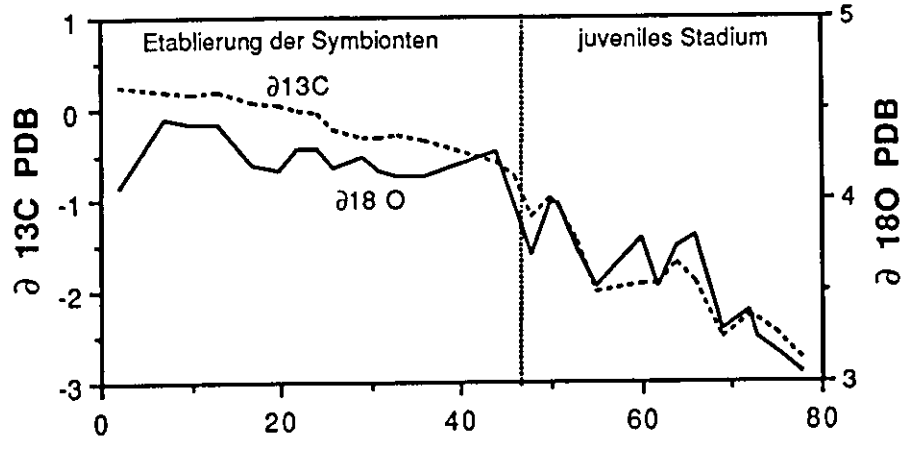

Abb. 2.1.4 Ontogenetische Entwicklung der $\partial^{13}C$ und $\partial^{18}O$-Werte bei *Calyptogena* 1428

Strontium

Sr-Isotope wurden in "vent"-Wässern der Stationen 2046 und 2283 gemessen. Sie deuten auf kontinentale Einflüsse im "vent"-System hin, da sich die Werte deutlich von denen des Meerwassers unterscheiden. Diese Tatsache steht in guter Übereinstimmung mit $\partial^{87}Sr$-Befunden aus Baryten (TORRES et al. 1992).

Ausblick

Wie die oben dargestellten Ergebnisse zeigen, liegt in der Untersuchung von Spurenelementen und stabilen Isotopen im "vent"-Material ein großes Potential, um dem Funktionieren von "vents" in Akkretionskeilen näherzukommen. Schalen-/Röhrenprofile von Organismen können einen zeitlichen Verlauf des Geschehens dokumentieren. Dabei ist *L. barhami* durch seine Langlebigkeit wertvoll. Charakteristische Merkmale der Verteilungsmuster sind nur an einzelnen Beispielen dargestellt. Tatsächlich dokumentieren sie sich in ganzen Gruppen von Spurenelementen, die nach Vervollständigung der Datensätze ausgegrenzt werden sollen. Da die Spurenelemente, die sich in Organismen einlagern, den austretenden Fluiden entstammen, ist so eine Aussage über die Herkunft der Fluide möglich. Leider sind Spurenelementmessungen an den Fluiden nur bedingt möglich, da aufgrund der Beprobungstechnik von einer Kontamination der Proben mit den meisten Spurenmetallen ausgegangen werden kann.

Der Fortgang der Arbeit wird bestimmt durch die Vervollständigung der Datensätze für Spurenelemente aus Organismen aller 6 Beprobungsgebiete. Nach den Hartteilen werden die Weichteile der Organismen analysiert, um organische und anorganische Materialien vollständiger vergleichen zu können. Weitere Isotopenuntersuchungen sollen Hinweise darauf geben, ob und in wieweit Variationen durch das "vent"-Geschehen beeinflußt werden. Falls hier ein Zusammenhang nachgewiesen werden kann, müssen die Mechanismen näher untersucht werden.

Zusammenfassung

- Die Verteilung von Spurenelementen in biogenen Hartteilen zeichnet die Verdünnung austretender Fluide mit dem Umgebungswasser nach. Direkt am Austritt lebende Organismen weisen höhere Gehalte auf, als peripher siedelnde.

- Der Einbau bestimmter C- und O-Isotope, sowie Sr in aragonitische Schalen von *Calyptogena* und *Solemya* erfolgt unabhängig von der Temperatur. Die Variabilität wird über Stoffwechselprozesse bzw. die Zufuhr gesteuert.

- Trotz unterschiedlicher Materialien lassen sich aragonitische Schalen von Molluscen und organische Röhren von Vestimentiferen aus einem Gebiet direkt vergleichen.

- Die Herkunft der "vent"-Fluide der Kontinentalränder vor Oregon und Peru steht in Zusammenhang mit kontinentalen Ablagerungen, wie $\partial^{87}Sr$-Untersuchungen an "vent"-Wässern zeigen.

2.2 Methan- und Sauerstoffverteilungen im Wasserkörper über "vents"

Stephan Lammers

Zielsetzungen

Schwerpunkt der Untersuchungen zum Einfluß subduktionsgesteuerter "vents" auf die Methanverteilungen in der Wassersäule war die Forschungsfahrt SONNE 78 vor der Küste von Peru. Aus zahlreichen Beobachtungen ist bekannt, daß die im Bereich aktiver Kontinentalränder aus akkretierten Sedimenten austretenden Fluide besonders hohe Konzentrationen an gelöstem Methan aufweisen. Neben der Bedeutung, die dieser energiereiche Zufluß für das biochemische Milieu in der unmittelbaren Umgebung der "vents" hat, können Freisetzungen von Methan auch großräumige Anomalien innerhalb der Wassersäule zur Folge haben und so als Indikatoren für aktive Entwässerungsvorgänge herangezogen werden. Außerdem ist in den betreffenden Gebieten ein verstärkter Eintrag von Methan in die Atmosphäre denkbar.

Die Hauptaufgabe der hydrochemischen Arbeit war die Darstellung der Methan- und Sauerstoffverteilungen innerhalb der Wassersäule sowie die Probenahme für Bestimmungen des Heliums samt seiner Isotope und anderer gelöster Edelgase. Darüber hinaus sollte versucht werden, Methanwolken in der Wassersäule quantitativ zu erfassen und ihre Quellgebiete aufzuspüren. Anhaltspunkt für den Erfolg dieser Bemühungen waren aktive Fluidaustritte, die in der Vorbereitung der SONNE 78 Expedition mit Hilfe des Tieftauchbootes NAUTILE lokalisiert werden konnten.

Durchführung

Für die Methanbestimmungen wurden Wasserproben aus der bordeigenen CTD-Rosette in spezielle ventilbestückte und vakuumdichte Glasflaschen blasenfrei abgefüllt. Die Extraktion der gelösten Gase erfolgte durch ein kombiniertes Vakuum/Ultraschall-Verfahren (SCHMIDT et al., 1991). Die Analyse der extrahierten und volumetrisch bestimmten Gasphase wurde unmittelbar danach mit einem Shimadzu GC 14A FID Gas-Chromatographen und einer gepackten 5 Å Molsieb-Säule durchgeführt. Der Fehler des gesamten Aufbereitungs- und Analyseverfahrens war kleiner als 5%. Parallel dazu wurde in allen Tiefen der Gehalt an gelöstem Sauerstoff mit Hilfe einer automatischen Winkler-Titration bestimmt.

Im Verlauf der SONNE 78 Expedition wurden auf 11 Stationen ca. 200 Wasserproben von insgesamt 21 CTD-Profilen auf ihren Gehalt an gelöstem Methan und gelöstem Sauerstoff analysiert sowie Proben für die spätere Messung von Helium, Tritium und gelösten Edelgasen entnommen.

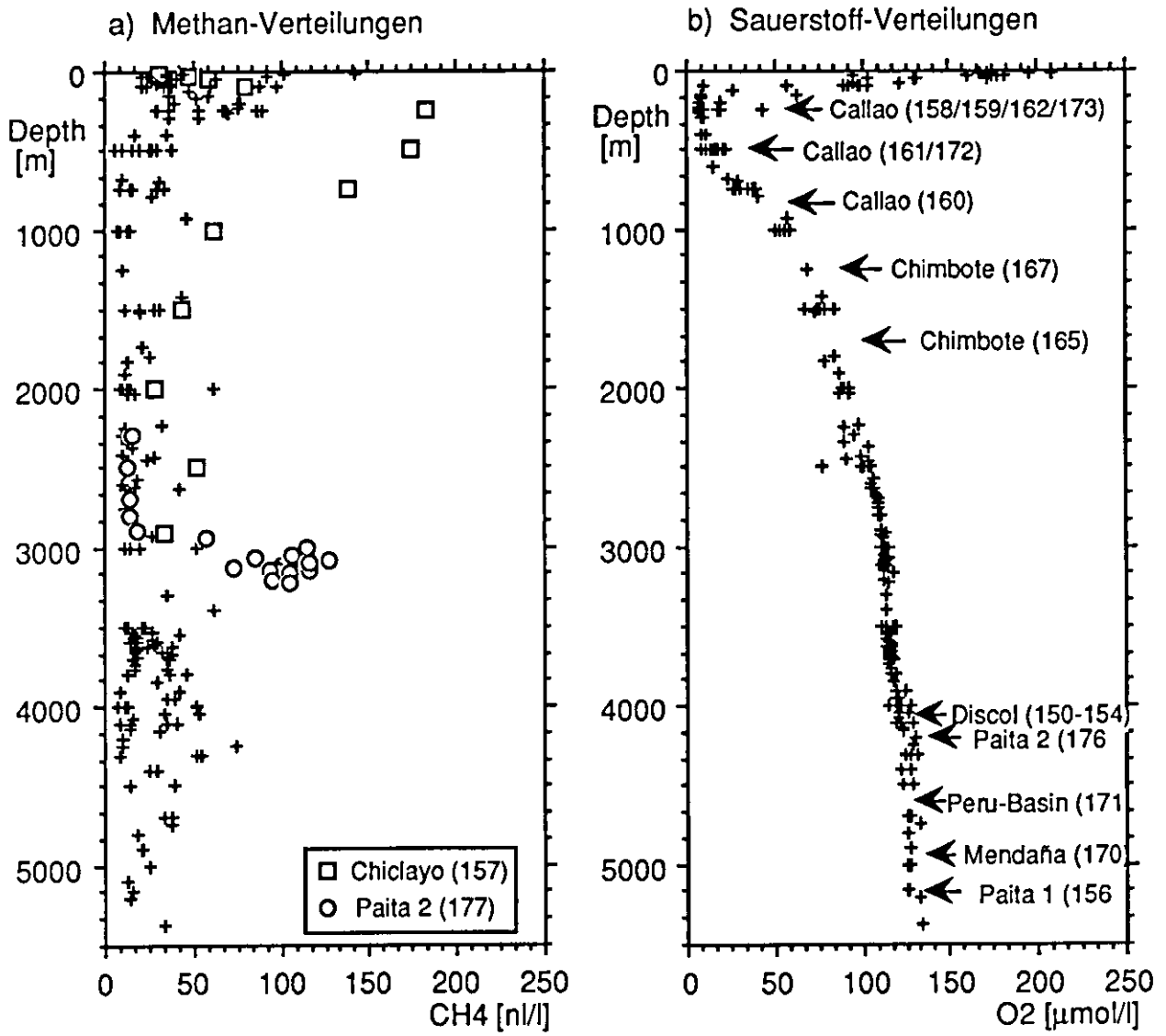

Abb.2.2.1: Übersicht über die Methan- und Sauerstoffverteilungen von SONNE 78. Bei den Methanprofilen (a) sind die Stationen mit den größten Anomalien hervorgehoben. Bei den Sauerstoffmessungen (b) sind außerdem die Tefen-Niveaus der Stationen gekennzeichnet, an denen Sedimentkerne entnommen wurden.

Ergebnisse

Eine Zusammenfassung der gemessenen Methan- und Sauerstoffverteilungen gibt Abb. 2.2.1. Die Sauerstoffprofile zeigen eine weitgehend einheitliche Verteilung in der Wassersäule und eine typische Ausprägung der Minimumzone im Tiefenbereich zwischen 300 und 600 m mit teilweise unter 10 µmol/l. Die Konzentrationen steigen auf durchschnittlich 120 µmol/l in Tiefen über 2000 m und auf bis zu 200 µmol/l in der Nähe der Oberfläche an. Aus den Methanmessungen ergaben sich - abhängig vom Einflußbereich des jeweiligen Arbeitsgebietes - erwartungsgemäß stark unterschiedliche Verteilungsmuster. Als typisches ozeanisches Hintergrundsignal sind die Profile der küstenfernen Stationen im Dicol-Gebiet (152), am Sarmiento Ridge (156) und über der Mendaña-Bruch-Zone (170) anzusehen, mit durchschnittlichen Konzentrationen von 10-15 nl/l in größeren Tiefen und 20-40 nl/l im Bereich der Oberfläche. Die Abweichungen von diesem Hintergrund sind an den küstennahen Stationen besonders in der Zone des Sauerstoffminimums und im bodennahen Bereich ausgeprägt. Die Stationen mit den deutlichsten Anomalien sind in der Abb. 2.2.1a) durch besondere Signaturen hervorgehoben.

Methan- und Sauerstoff in der Deckschicht

Die Abb. 2.2.2 zeigt Ergebnisse der Sauerstoff- und Methanmessungen in den oberen 1000 m. Sie lassen eine Korrelation von Methanmaxima und Sauerstoffminima erkennen. Die Zone des Sauerstoffminimums, deren Zentrum hier am häufigsten in einer Tiefe von ca. 500 m liegt, ist an den küstennahen Stationen ausgeprägt und steigt dort zum Teil bis in Tiefen von 100 m auf (160). Auch Methan zeigt an allen Stationen innerhalb dieser Zone ein deutliches Maximum, dessen Ausprägung mit der Küstennähe und dem Einfluß hoher Produktivität zunimmt (Stationen 156, 160). Der Zusammenhang zwischen Produktionsraten, Sauerstoffmangel und erhöhten Methankonzentrationen ist aus verschiedenen Gebieten, besonders des äquatorialen Ost-Pazifik, bekannt und auf die Zersetzung der Plankton-Biomasse unter suboxischen Bedingungen zurückzuführen. (RASMUSSEN & KHALIL, 1981; CONRAD & SEILER, 1988; CICERONE & OREMLAND, 1988).

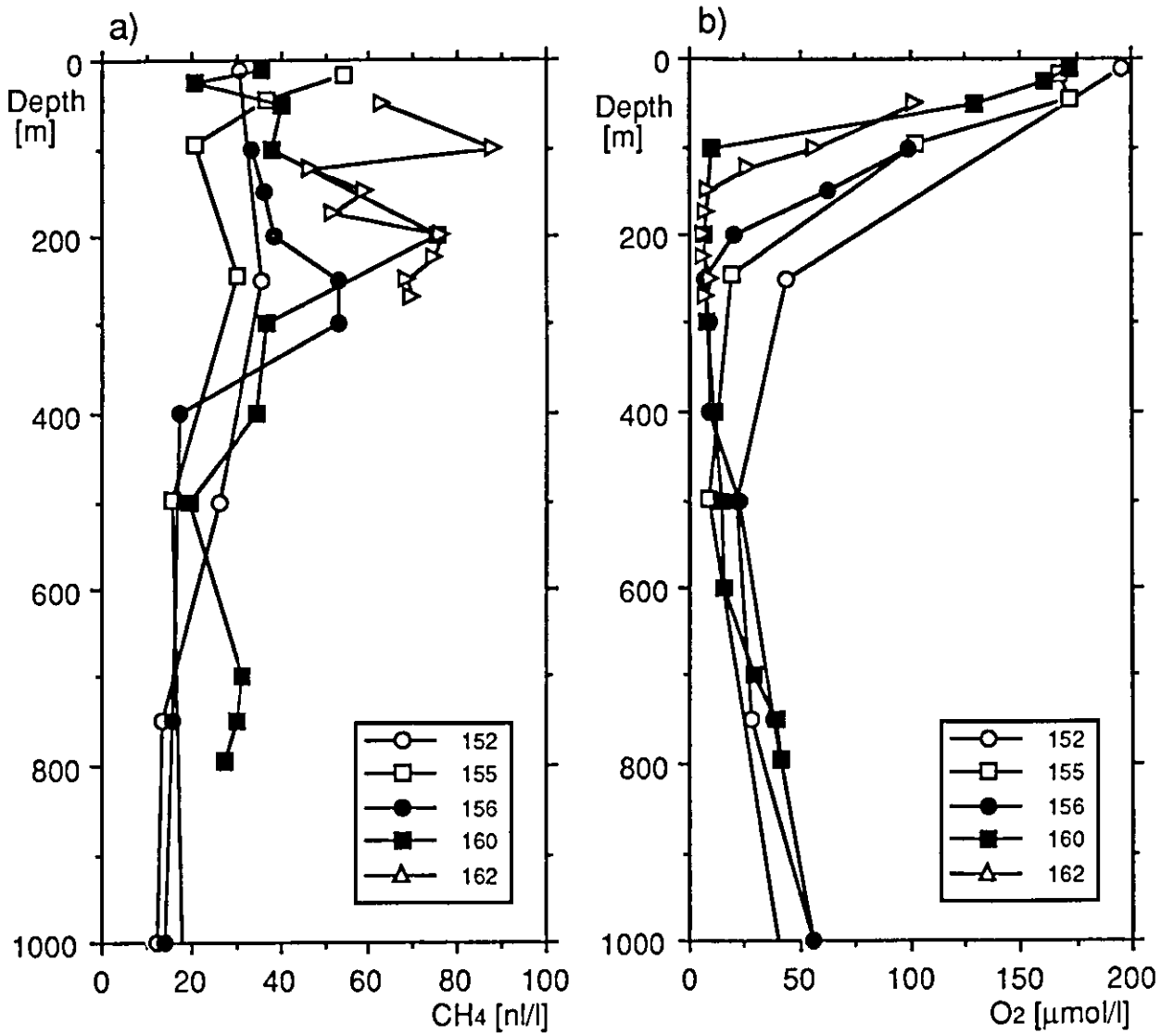

Abb. 2.2.2: Methan- und Sauerstoffprofile der oberen 1000 m.

"Vent"-Einflüsse und Methanverteilung größerer Tiefen.

Die an einigen Stationen beobachteten Methanmaxima in größeren Tiefen korrelieren nicht mit niedrigen Sauerstoffkonzentrationen und beruhen entsprechend nicht auf Methanogenese innerhalb der Wassersäule, sondern sind eine Folge von Injektionen methanreicher Fluide aus den akkretierten Sedimenten des Kontinentalhanges. Im Verlauf der SONNE 78 Ausfahrt waren diese Methan-Anomalien hauptsächlich in der Chiclayo-, Chimbote- und Paita-Region zu beobachten.

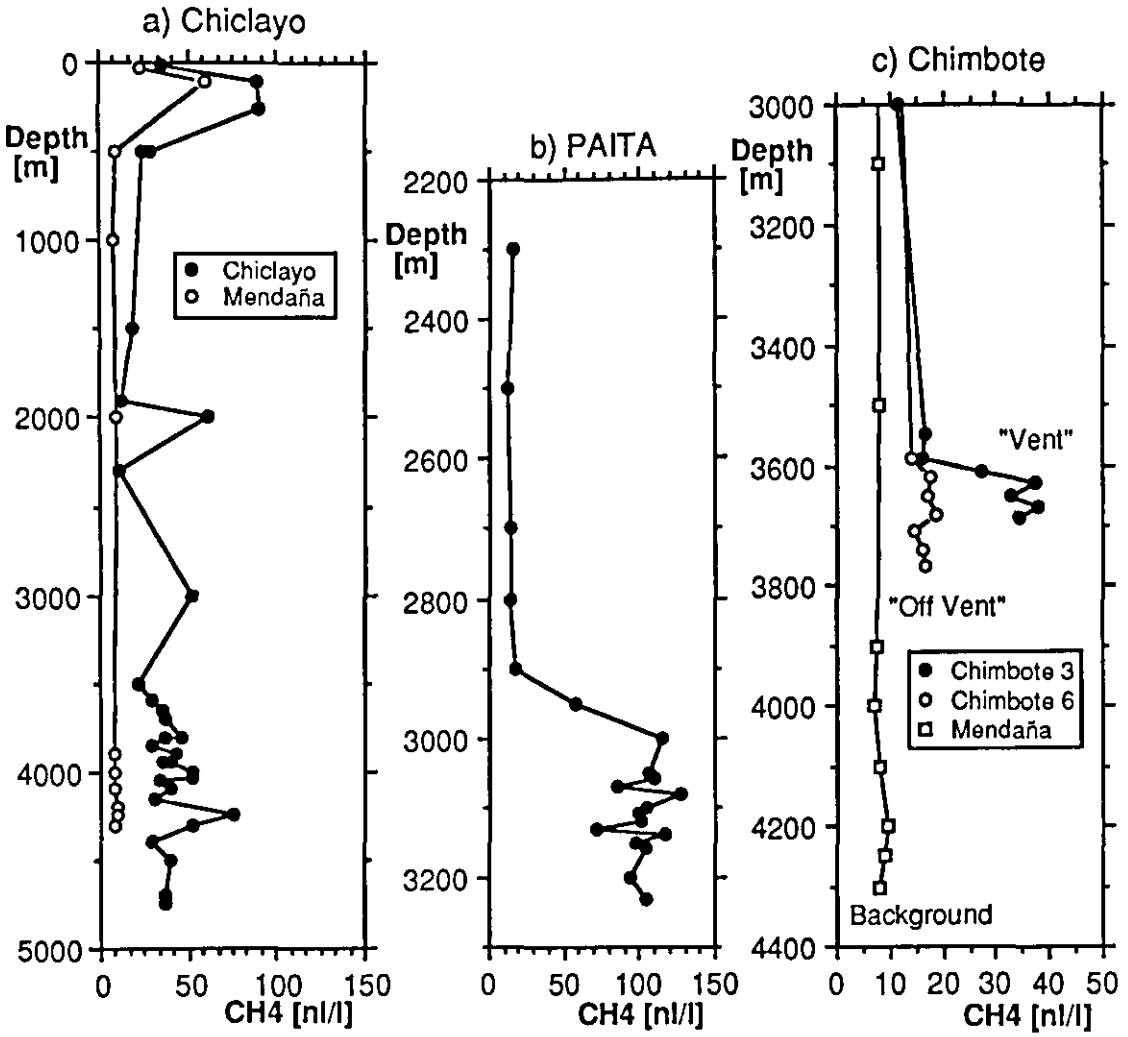

Abb. 2.2.3: Methanprofile der durch "venting" beeinflußten Stationen der SONNE 78 Ausfahrt vor der Küste von Peru. Zum Vergleich ist die Verteilung an Station 170 (Mendaña) als typischer ozeanischer Methanhintergrund wiedergegeben.

Die höchsten Methanmaxima dieser Art in der bodennahen Wassersäule wurden an Station 177 (Paita 2) mit 127 nl/l gemessen und konnten durch Messungen an Wasserproben, die mit der *in situ*-Probenkammer (benthic barrel) gewonnen wurden, eindeutig mit erhöhter "vent"-Aktivität am Boden in Zusammenhang gebracht werden. Die Abb. 2.2.3 gibt eine Zusammenfassung der Profile, die durch aktives "venting" beeinflußt sind. Zum Vergleich ist ein Profil mit normaler ozeanischer Methanverteilung dargestellt, das im Mendaña-Gebiet aufgenommen wurde.

Ein weiteres Ziel war die Verfolgung austretender Methanwolken in der Wassersäule des Chiclayo-Canyon, an dessen Flanken zuvor aktive "vents" beobachtet worden waren. Auf einem ca. 30 Meilen langen Profil, das vom offenen Ozean aus über den Canyon landwärts führte, wurden an insgesamt 6 CTD-Stationen die Sauerstoff- und Methanverteilungen gemessen. Es zeigte sich, daß die eindeutig durch "venting" erzeugten Methan-Anomalien mit den zuvor lokalisierten Austritten korrelierbar und auch über Entfernungen von mehreren Meilen noch nachweisbar waren, obwohl sie mit 30-60 nl/l nur mäßig über dem ozeanischen Hintergrund lagen. Entsprechende Beobachtungen konnten auch bei zwei ca. drei Meilen voneinander entfernten Profilen im südlichen Abschnitt des Chimbote-Gebietes gemacht werden, die einen entfernungsabhängig unterschiedlichen Einfluß derselben Methanwolke zeigen (Abb. 2.2.3c). An der Station 177 (Paita 2) konnte die gefundene Anomalie durch die Aufnahme eines weiteren Profils in zwei Methanwolken (plumes) aufgelöst werden, die von verschiedenen, an einem Steilhang übereinandergeordneten Austritten, freigesetzt wurden (Abb. 2.2.3b).

Insgesamt konnten vor der Peruanischen Küste in der bodennahen Wassersäule deutliche Methan-Anomalien gemessen werden, die horizontal und vertikal über größere Entfernungen zu verfolgen sind und die als Freisetzungen verschiedener Fluidaustritte am Kontinentalhang unterschieden werden können. Die Ergebnisse zeigen, daß das angewandte Verfahren geeignet ist, die Methanverteilungen in der Wassersäule räumlich aufzulösen und, auf der Basis eines geeigneten Meßrasters, zur Quantifizierung der Einflüsse von "venting" beitragen kann.

Sauerstoff im Bodenwasser

Im Verlauf der SO-78 Ausfahrt gezogene Sedimentkerne dienten der Untersuchung der Sedimentationsregimes sowie der diagenetischen Prozesse und Produktivitätsstrukturen. Soweit sie die Verteilung der Organismen und die Konservierung der sedimentierten organischen Substanz betreffen, sind alle diese Prozesse durch die Verteilung gelösten Sauerstoffes in der Wassersäule beeinflußt. Abb. 2.2.1b) zeigt die Stationen, an denen Sedimentkerne gezogen wurden in Relation zur beobachteten Sauerstoff-Verteilung. Diese Stationen umfassen einen weiten Bereich bodennaher Sauerstoff-Konzentrationen von
120 µmol/l an den tieferen Lokationen (DISCOL, Peru-Becken, Mendaña, Paita 1) bis
13 µmol/l an Station 162.

Die Auswirkungen des Sauerstoff-Gehaltes im Bodenwasser auf die Erhaltung organischer Substanz wird gegenwärtig kontrovers diskutiert. Dennoch ist anzunehmen, daß die mit minimalen Sauerstoff-Konzentrationen gekoppelte geringe benthische Aktivität im Callao-Gebiet zu den extrem hohen organischen Gehalten dieser Sedimente beiträgt. Der Gehalt an organischer Substanz in diesen Sedimenten und seine möglichen Beziehungen zum bodennahen

Sauerstoff am Kontinentalhang vor Peru wird ausführlich von REIMERS & SUESS (1981) erörtert.

Methan an der Ozean/Atmosphäre-Grenzschicht

In Ergänzung zu den oberflächennahen Aufnahmen in der Wassersäule wurden an 7 Stationen auch Bestimmungen von Methan in der Luft durchgeführt. Die Luftproben wurden von einem Schlauchboot aus jeweils ca. 1/2 Meile in Luv der Schiffsposition in etwa 10 cm Höhe über der Wasseroberfläche genommen und unmittelbar danach gas-chromatographisch analysiert. Die Probenahme erfolgte in 1 Liter Glasflaschen, die mit jeweils zwei dichtschließenden L&H-Ventilen versehen waren und die durch Absaugen ihres Luftinhaltes mit der Probeluft gefüllt wurden.

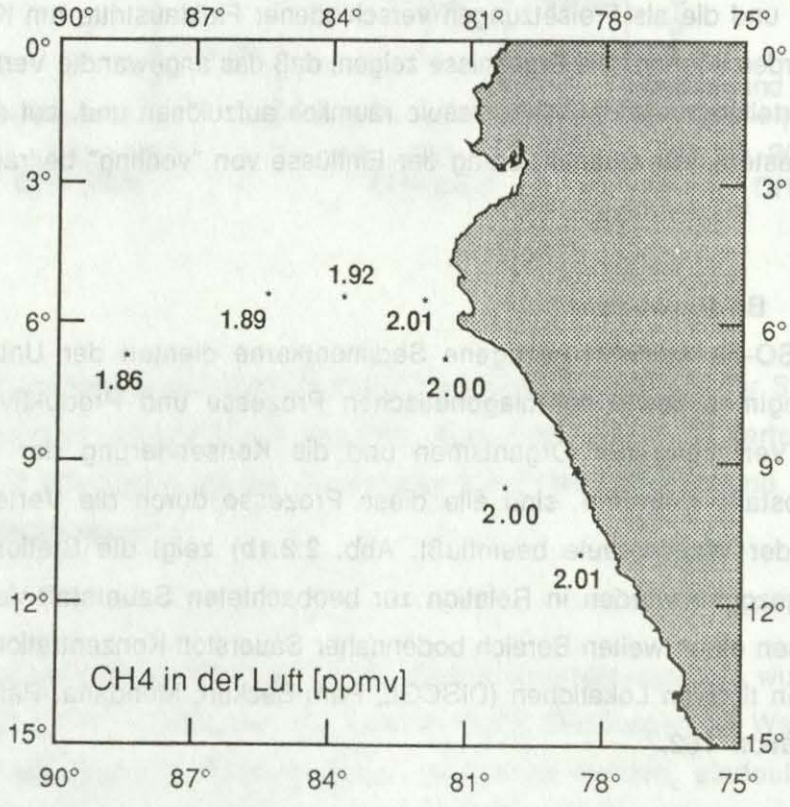

Abb. 2.2.4: Methankonzentrationen in der Luft, gemessen während der SONNE 78 Ausfahrt in ca. 10 cm Höhe über der Wasseroberfläche.

Die Ergebnisse der Messungen, die deutlich über dem heutigen globalen Mittelwert von 1.725 ppmv Methan in der Atmosphäre liegen, sind in Abb. 2.2.4 dargestellt. Die höchsten Werte von bis zu 2.01 ppmv wurden an den küstennahen Stationen 156 und 160 gemessen, während die Konzentrationen an den übrigen Stationen mit der Entfernung von der Küste bis auf 1.86 ppmv (Station 153) abfallen. Ursache ist die in Küstennähe durch eine enorm hohe Produktivität gesteigerte planktogene Bildung von Methan in der Wasssersäule, wie sie auch besonders in den hohen Methanwerten im Bereich der Sauerstoffminimumzone zum Ausdruck kommt. Die besonders über dieser Zone festgestellten erhöhten Konzentrationen in der Luft zeigen, daß hier eine bislang nicht quantifizierte Ausgasung von Methan in die Atmosphäre stattfindet. In den letzten Jahren weltweit intensivierte Messungen haben auch in anderen ozeanischen Bereichen Hinweise auf entsprechende Freisetzungen von Methan in die Atmosphäre geliefert (e.g. OWENS et al., 1991).

Die Tatsache, daß zur Fahrtzeit ein mäßiger ENSO-Event zu verzeichnen war, läßt überdies die Vermutung zu, daß die gemessenen Effekte in diesen Auftriebsgebieten zu anderen Zeiten noch deutlicher in Erscheinung treten. Die Untersuchungen zur Methanverteilung in den Auftriebsgebieten entlang der peruanischen Küste haben zu folgenden weiterführenden Fragestellungen geführt:

1) Welche Prozesse sind innerhalb der Wassersäule für den Verbrauch und die Freisetzung von Methan verantwortlich und haben somit entscheidenden Einfluß auf den atmosphärischen Eintrag ?

2) In welcher Größenordnung beeinflußt das ENSO-Phänomen den atmosphärischen Methaneintrag im Ost-Pazifik ?

3) Wie kann der an aktiven "vents" tektonisch gesteuerte Methaneintrag von dem durch biologische Vorgänge in der Sauerstoffminimumzone produzierte Methanfluß unterschieden werden ?

Die Fortführung der Untersuchungen zum marinen Methanhaushalt sowie zur Rolle des durch "venting" an aktiven Plattenrändern freigesetzten Methans wird u.a. von der Klärung dieser Fragen abhängig sein.

2.3 Einfluß des Ton-Wasser-Systems auf die D/H- und $^{18}O/^{16}O$-Isotopien im Porenwasser und als Ursache der charakteristischen Cl-Anomalien im Porenwasser von Akkretionskeilen.

Wolfgang Kloebe

Chlorid- und Isotopen-Anomalien im Porenwasser sind als weitverbreitete Kriterien von Akkretionskeilen bekannt. Der Einfluß des Ton-Wasser-Systems, vor allem die Rolle des Zwischenschichtwassers, kann für die D/H-, $^{18}O/^{16}O$- und Cl-Anomalien verantwortlich sein. In Verbindung mit anderen geochemischen Signalen soll eine experimentelle Verifizierung die verantwortlichen Prozesse, die in Feldbeobachtungen nachgewiesenen Anomalien, qualitativ und quantitativ klären.

Mögliche Prozesse die zur Verdünnung der Chloridkonzentration des Porenwassers führen sind:

- Zufluß von fossilem oder kontinentalem Süßwasser
- Bildung und Dissoziation von Methanhydraten
- Membranfiltration durch Tone
- Austreibung von Zwischenschichtwasser bei Tonen durch Auflast
- Austreibung von Strukturwasser hydratisierter Minerale bei erhöhterem Druck und Temperatur

Insbesondere bei den Subduktionszonen, in denen keine Methanhydrate vorkommen (Methanhydrate werden als wichtigste Quelle für niedrige Chlorid-Gehalte im Porenwasser angesehen) und dennoch niedrige Chlorid-Gehalte im Porenwasser gemessen wurden, kann die Erniedrigung der Chlorid-Gehalte auf Dehydrierung von Tonen zurückgeführt werden (z.B. Nord Barbados, GIESKES et al, 1990).

Jeder der o.a. Prozesse verursacht eine Änderung der Sauerstoff- und Wasserstoff-Isotopenzusammensetzung im Porenwasser, wobei über den Mechanismus bzw. den Einfluß der Austreibung von Zwischenschichtwasser bei Tonen derzeit diskutiert wird (COLTEN-BRADLEY, 1987; ELDERFIELD et al., 1990; GIESKES et al., 1990; MEHRA & JACKSON, 1960; SUESS & VON HUENE, 1988). Den Einfluß der Wasserstoff- bzw. Sauerstoff-Isotopen-Fraktionierung zu kennen, ermöglicht eine Differenzierung der Prozesse die zu den Chlorid-Anomalien im Porenwasser führen.

Zu dieser Fragestellung wurde ein experimenteller Ansatz zur Isotopenfraktionierung des Zwischenschichtwassers und eine kombinierte Labor- und Feldbeobachtung zum Problem der Cl-Anomalien in Porenwäsern durchgeführt.

Probenmaterial und Aufbereitung zur Charakterisierung des Zwischenschichtwassers

Als Probenmaterial wurde ein Bentonit (Smektit) von der Süd-Chemie AG (Niederbayern) mit folgender Zusammensetzung ausgewählt:

Montmorillonit		94%
Kaolin	ca.	2%
Cristobalit	ca.	1%
Quarz	ca.	2%
Feldspat	ca.	2%

Ein Smektit ist aufgrund seiner spezifischen Eigenschaften, d.h. mit einer relativ hohen Oberflächenladung und einem großen Anteil von Zwischenschichtwasser besonders für die Untersuchung zur Isotopenfraktionierung geeignet. Zudem ist der Smektit in allen Weltmeeren weit verbreitet. Für eine eindeutige Zuordnung der Isotopenfraktionierung zu dem Tonmineral Smektit und um eine möglichst große Isotopenfraktionierung messen zu können, muß der Smektit von Verunreinigungen befreit werden. Aus diesem Grunde wurde der Bentonit chemisch und sedimentologisch aufbereitet.

Aufbereitung

Verunreinigungen des Bentonits durch Eisenoxide sind mit der Dithionit/Citrat-Methode entfernt worden. Dieses Verfahren wurde von MEHRA und JACKSON (1960) entwickelt und von LEMPUT und STUL (1982) verbessert. Die Beseitigung organischer Bestandteile erfolgte in einer Natriumacetat-Lösung unter Zugabe von Wasserstoffperoxid. Diese Verfahren gewährleisten einen geringen Angriff auf die Tonmineralstruktur. Dann wurde der chemisch gereinigte Bentonit in der Atterberg-Anlage in die Korngrößenfraktionen < 2, <1 und <0,5 µm fraktioniert und somit von störenden Begleitmineralien getrennt.

Der gereinigte und fraktionierte Bentonit wurde in einem Dialyseschlauch gegen bidestilliertes Wasser dialysiert, um überschüssige Salze vollständig zu entfernen. Die Korngrößenfraktionen < 2, <1 und <0,5 µm bei sind bei 60^0 C eingedampft worden und wurden anschließend in einer Achat-Kugelmühle homogenisiert.

REM - Aufnahmen und Röntgendiffraktometrie

Zur Überprüfung der Korngrößen der verschiedenen Fraktionen sind REM-Aufnahmen erstellt worden. Zwei Aufbereitungsverfahren wurden angewendet:

1. Auf den Objektträgern mit aufgeklebten Fotopapier wurden die Korngrößensubfraktionen als Pulverpräparat aufgestreut und mit einem Tropfen H_2O zur Bindung benetzt.
2. Auf den Objektträgern mit aufgeklebtem doppelseitigem Klebeband sind die Korngrößensubfraktionen als Pulverpräparat ohne Benetzung aufgestreut worden.

Zur Überprüfung der Reinheit und Quellfähigkeit des Roh-Bentonits und der verschiedenen Korngößenfraktionen des aufbereiteten Bentonits sind von Texturpräperaten (Lufttrocken und mit Etylenglycol gequollen) und Pulverpräperaten Röntgenaufnahmen erstellt worden (Cu-Strahlung, Ni-Filter, 30kV, 40 mA).

Versuchsaufbau zur Isotopenfraktionierung

Der Versuchsaufbau wurde in erster Linie durch zwei Fragestellungen geprägt:
Wie kann man eine Isotopen-Fraktionierung in einem Ton-Wasser-System überhaupt sinnvoll messen (s. 2.3) ? Und wie läßt sich eine Apparatur, die den Anforderungen gerecht wird, mit den vorhandenen Mitteln und Möglichkeiten realisieren?

Um die Aufgaben lösen zu können, ist eine Vakuum-Anlage konstruiert worden. Hierbei waren u.a. folgende Anforderungen zu berücksichtigen:

1. Die Vakuum-Anlage sollte große Probenmengen aufnehmen können, um die apparative Fehlergrenze klein zu halten und den Meßbereich zu optimieren.
2. Der Aufbau der Anlage sollte so variabel gestaltet werden (in einzelne Baueinheiten zerlegbar), daß eine Änderung der Versuchsbedingungen jederzeit möglich ist.
3. Es sollte ein Vakuum unter 10^{-2} mbar erreicht und gehalten werden können.
4. Der Probenbehälter sollte erhitzt als auch gekühlt werden können.

Die Vakuum-Anlage ist in Abb. 2.3.1 dargestellt. Sie setzt sich zusammen aus einer Vakuumpumpe, Druckfühler, Thermostat, Kühlfallen mit Dewar-Gefäßen, Austauschbehälter und einem Probenbehälter, der von einem temperierbaren Mantel umgeben ist.

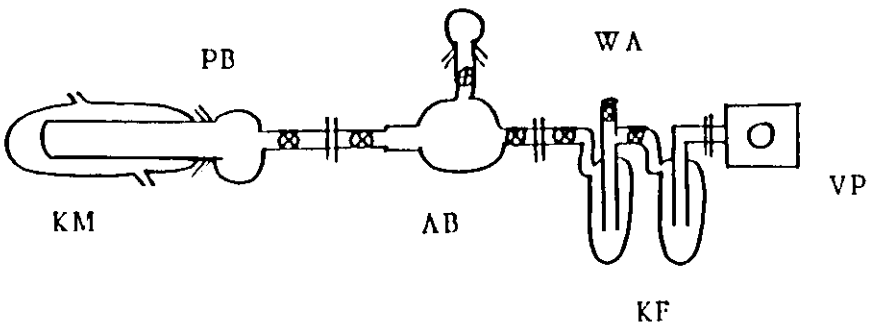

PB	Probenbehälter		Young-Hahn
KM	Kühlmantel		Quetschverbindung
AB	Austauschbehälter		Schliffverbindung
WA	Wasserentnahme zur Analyse		
KF	Kühlfallen		
VP	Vakuum Pumpe		

Abb.2.3.1 Schematisierter Versuchsaufbau

Versuchsdurchführung

Aufgrund der Ergebnisse von SAVIN (1967) ist es notwendig, zur Messung der Isotopenfraktionierung ein geschlossenes System zu verwenden. Er stellte in seinen Versuchsreihen einen Isotopen-Austausch zwischen Porenwasser bzw. der Atmosphäre und Zwischenschichtwasser innerhalb von Stunden bis Tagen fest. Es existiert kein "sauberes" Trennungsverfahren von Porenwasser und Zwischenschichtwasser, da sich erstens die Bindungskräfte überschneiden und zweitens jeder Trennungsversuch (mittels Druck, Temperatur etc.) mit einer Isotopenfraktionierung verbunden ist. Daher ist ein indirektes Verfahren zur Messung der Isotopenfraktionierung erforderlich.

Aus den Untersuchungen von SAVIN (1967) und STEWART (1972) ist eine fast zu vernachlässigende Isotopenfraktionierung zwischen Porenwasser und Zwischenschichtwasser zu entnehmen. Auf der Grundlage dieser Ergebnisse bzw. der angewandten Methoden und der

Kenntnis der physiko-chemischen Eigenschaften von Tonmineralen, ist ein neues Verfahren entwickelt worden. Dieses Verfahren ermöglicht, aufgrund der Adsorbtionskräfte von Smektiten, eine Isotopenfraktionierung bei Smektiten zu messen.

Folgendes Verfahren wurde entwickelt (s. Abb. 2.3.2):
Das Tonmaterial wird in einer Vakuum-Anlage schonend dehydriert, um das Material nicht zu hohen Temperaturen aussetzen zu müssen, die das Adsorptionsvermögen des Tones im hohen Maße beeinträchtigen würden. Nach der Evakuierung wird in die Anlage eine bestimmte Menge Wasser oder Wasserdampf mit einer bekannten Isotopenzusammensetzung zugeführt, so daß der Ton durch Adsorptionskräfte ein Teil des zugeführten Wassers aufnehmen kann. Nach einer genügend langen Austauschphase wird das Restwasser auf die Isotopen-Zusammensetzung analysiert und folglich kann eine Fraktionierung indirekt bestimmt werden.

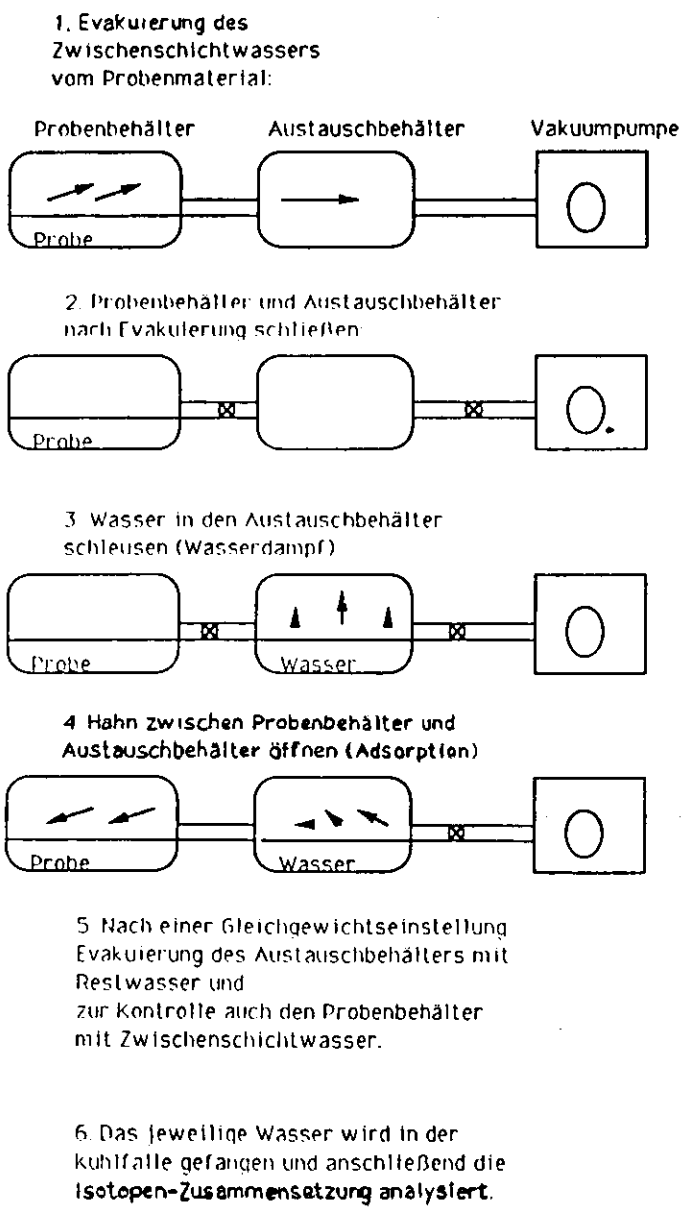

Abb. 2.3.2 Schematischer Versuchsablauf

Experimenteller Teil

Die angewandte REM-Aufbereitungsmethode brachte keine sinnvollen Ergebnisse zur Differenzierung der verschiedenen Korngrößenfraktionen. Deshalb ist die zweite Methode angewendet worden, wo aber auch keine Unterschiede der verschiedenen Korngrößenfraktionen in den REM-Aufnahmen zu erkennen sind. Dennoch ist bemerkenswert:

- daß in allen Korngrößenfraktionen im aufbereiteten Bentonit und im Roh-Bentonit Aggregate von über 100 µm Größe vorhanden sind,
- daß unabhängig von der REM-Aufbereitungsmethode der Roh-Bentonit körniger wirkt, bzw. bei dem aufbereiteten Bentonit die einzelnen Tonmineraloberflächen wie zusammengeschweißt aussehen.

Es erscheint daher fraglich ob eine Differenzierung in Korngrößenfraktionen, nach der Aufbereitung mit einer Eindampfung und anschließendem Mahlen, einen Unterschied im Adsorptionsverhalten, sowie in der Isotopenfraktionierung zeigt.

Die Ergebnisse aus den Röntgenaufnahmen des Roh-Bentonits zeigen einen Quarzgehalt von 1,6%, akzessorische Bestandteile < 1% (Chlorit, Feldspat). Ferner wurden Hinweise auf nicht quellfähige Dreischichttonminerale (Illit), aber in ganz geringen Mengen, beobachtet. Die Charakteristika der Texturpräperate sind wie folgt:

- lufttrocken: Montmorillonit-Hauptreflex: 15,10 Å
- mit Etylenglycol gequollen: Montmorillonit-Hauptreflex: 17,04 Å

Der Roh-Bentonit ist quellfähig und es sind keine Wechsellagerungen vorhanden. Die Röntgenaufnahmen der verschiedenen Korngrößenfraktionen des aufbereiteten Bentonits sind z.Z. in Arbeit.

Vorversuche

Vorversuche zur Bestimmung des Adsorptionsvermögen des Tones sind notwendig, um die einzusetzenden Probenmengen und Wassermengen für eine optimale Messung der Isotopenfraktionierung bemessen zu können. Um für die Versuche vergleichbare Adsorptions-Daten zu erhalten, ist der gleiche Versuchsablauf bei den Vorversuchen angewendet worden:

- den Smektit eine Woche unter Vakuum bei 60° C evakuieren
- den Smektit neun Tage einer Wasserdampf-Phase aussetzen.

In Tabelle 2.3.1 sind die Ergebnisse der Vorversuche zusammengefaßt. Unter diesen Versuchsbedingungen zeigte der Smektit eine Adsorption von 8 Gew.%. Nach COLTEN-BRADLEY (1987) ist eine Dehydrierungs-Temperatur für das Zwischenschichtwasser von Smektit von 195° C unter atmosphärischem Druck notwendig. Der Wassergehalt des Smektits liegt bei 13,4 Gew.% bei einer Trocknung auf 195° C d.h., daß über 2/3 des Gesamtwassergehaltes des Smektits nach der Evakuierung aus der Wasserdampfphase wieder adsorbiert wird.

Tab. 2.3.1 Ergebnisse der Vorversuche zur Isotopenfraktionierung

Versuch Nr. 1 **57 % Restwasser**

D/H Fraktionierungsfaktor:	$^{18}O/^{16}O$ Fraktionierungsfaktor:
a interlayer-free = 0,920	a interlayer-free = 0,984
$\Delta \partial D$ = 45,2 ‰	$\partial\, ^{18}O$ = 9,11 ‰

25 g Smektit + 4,7 ml H_2O-Standard
2,7 ml Restwasser entsprechen 57,45 % RW
2,5 ml H_2O-Standard adsorbiert, d.H. 8 Gew. %

Messung: -1.3 ‰ ∂D
- - $\partial\, ^{18}O$

Versuch Nr. 2 **8,3 % Restwasser**

D/H Fraktionierungsfaktor:

a interlayer free = 0,980
∂D = 51,2 ‰

50 g Smektit + 6,0 ml H_2O-Standard
0,5 ml Restwasser entsprechen 8,33 % RW
5,5 ml H_2O-Standard adsorbiert, d.H. 11 Gew. %.

Messung: -1.3 ‰ ∂D
- - $\partial\, ^{18}O$

Versuch Nr. 3 **66 % Restwasser**

D/H Fraktionierungsfaktor:

a interlayer-free = 0,912

$\Delta \partial D = 36{,}7$ ‰

$^{18}O/^{16}O$ Fraktionierungsfaktor:

a interlayer-free = 0,977

$\partial\, ^{18}O = 9{,}62$ ‰

50 g Smektit + 8,0 ml H_2O-Standard

5,3 ml Restwasser entsprechen 66,25 % RW

2,7 ml H_2O-Standard adsorbiert, d.h. 5,4 Gew. %

Messung: -15,8 ‰ ∂D

+ 1,74 ‰ $\partial\, ^{18}O$

Versuch Nr. 4 **71 % Restwasser (Roh-Betonit)**

D/H Fraktionierungsfaktor:

a interlayer-free = 0,918

$\Delta \partial D = 28{,}4$ ‰

$^{18}O/^{16}O$ Fraktionierungsfaktor:

a interlayer-free = 0,982

$\partial\, ^{18}O = 6{,}1$ ‰

53 g Rohbetonit + 8,0 ml H_2O-Standard

5,7 ml Restwasser entsprechen 71,25 % RW

2.3 ml H_2O-Standard adsorbiert, d.h. 4,34 Gew. %

Messung: -24,1 ‰ ∂D

- 1,78 ‰ $\partial\, ^{18}O$

Standardwasser -52,5 ‰ ∂ D

- 7,88 ‰ $\partial\, ^{18}O$

Versuche

Aus den unveröffentlichten Daten von VROLIJK (1991) ist zu erkennen, daß eine Isotopenfraktionierung meßbar wird, je kleiner das Verhältnis von Wasser/Ton ist. Bei seinen Versuchen erreichte er nie ein Verhältnis < 0,5. Abbildung 3 zeigt eine Rayleigh-Funktion, die durch den Fraktionierungsfaktor a = 0.9993 nach den Daten von VROLIJK erstellt wurde. Aus der Abbildung geht der Zusammenhang von Restwasser, d.h. die nicht adsorbierte Wassermenge in Prozenten, und der Änderung des Isotopenverhältnisses hervor.

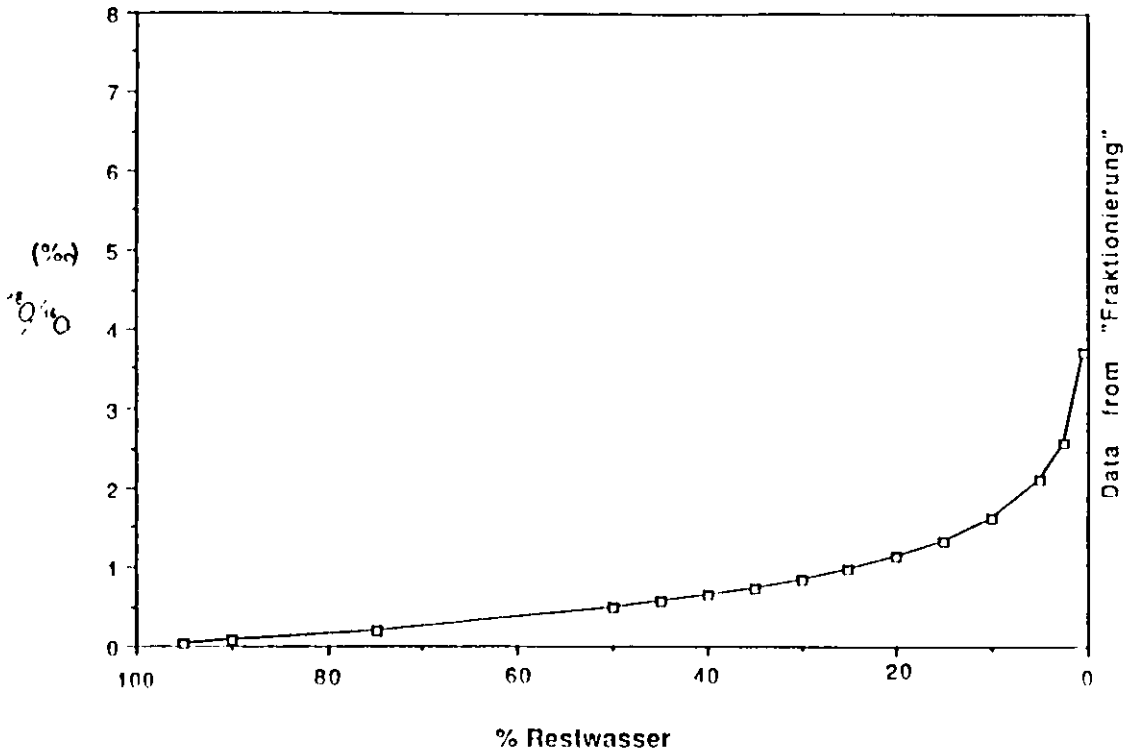

T = 25°C

$\alpha = 0{,}9993$

Abb.2.3.3 Rayleigh-Funktion mit festgesetztem Fraktionierungs-Faktor

In der hier vorgestellten Vakuum-Anlage wird der Meßbereich dadurch optimiert, daß (1) der Ton nur durch Adsorptionskräfte Wasser aufnimmt und ein Wasser / Ton Verhältnis von < 0,15 erreicht wird, (2) das Verhältnis Restwasser / Anfangs-Wassermenge auf unter 50% einzustellen ist.

Die quantitativ eingesetzten Mengen an Tonmaterial und Wasser werden durch folgende Rahmenparameter eingegrenzt:

- das Adsorptionsvermögen des Smektits liegt bei 8 Gew.%
- die Probenmenge an Wasser, die für die Isotopenmessung benötigt wird , d.h. der Restwasser-Anteil muß 1,6 ml betragen
- den gering zu haltenden Restwasser-Anteil im Verhältnis zur Anfangs-Wassermenge um in den interessanten Meßbereich zu gelangen (s. Abb. 2.3.3)

Bis Mitte Juli 1991 wurden drei Versuche durchgeführt. Dabei wurde der zu analysierende Restwasser-Anteil von 58% über 33% bis auf 25% herabgesetzt, was mit einer gleichzeitigen Erhöhung der Probenmenge verbunden ist. Die Isotopenmessungen liegen zur Zeit noch nicht vor.

Feldbeobachtungen und Laborversuche zur Problematik der kompositioneller Anomalien der Porenwässer.

Ziel der Feldbeobachtungen während der Reise SO-78 war es, die Chlorositätsanomalien am Peru-Kontinentalrand zu untersuchen.

Hierzu wurden (1) die geochemischen Parameter Chlorosität, Calcium- und Magnesium des Porenwassers bestimmt; ergänzt wurden diese Beobachtungen durch Laborversuche, um den (2) Einfluß des Ton-Wasser-Systems unter erhöhten Druckbedingungen auf Chlorositätsanomalien zu klären.

Porenwasserproben

Die Porenwasserproben aus den Kastenloten der unten aufgefürten Fahrtgebiete sind auf Chlorositäts- und Calciumgehalte untersucht worden. Allerdings konnte aus dem Callao-Gebiet während der Fahrt nur ein Kastenlot bearbeitet werden. Von dem Kastenlot des Peru Basin ist lediglich der Calcium-Gehalt analysiert worden.

Discol-Gebiet	SO78/151	KAL-3	13 Proben
	SO78/152	KAL-7	27 Proben
Callao-Gebiet	SO78/162	KAL-6	9 Proben
Chimbote-Gebiet	SO78/165	KAL-3	10 Proben
	SO78/167	KAL-2	12 Proben

Mendana-Gebiet	SO78/170	KAL-2	22 Proben
Peru Basin	SO78/171	KAL-2	33 Proben

Das zu untersuchende Porenwasser wurde teilweise mit einer Stickstoff-Presse (3 bar), teilweise mit einer Hydraulik-Presse (50 bar) gewonnen. Die Chlorosität ist titrimetrisch mit Silbernitrat und einer silbersensitiven Elektrode jeweils dreifach bestimmt worden. Die Calciumgehalte sind mittels EGTA (ethylene-bis-(oxyethlenenitrilo)-tetra-acetic acid) komplexometrisch nach der "Super Method" aus Chemical Methods, Aboard Joides Resolution (Technical Note 15), analysiert worden. Diese Methode wurde modifiziert, um eine höhere Auflösung trotz geringerer Probenmenge zu ereichen.

Callao-Gebiet

Die Daten aus dem Kastenlot 162-6 des *Callao-Gebiets* lassen sich gut korrelieren mit denen der Bohrung 680 des ODP Leg 112, da erstens bei zunehmender Sedimenttiefe in beiden Profilen die Chlorosität in den ersten drei Meter zunimmt und zweitens eine Abnahme des Calciumgehaltes mit zunehmender Sedimenttiefe in beiden Fällen zu beobachten ist, wobei eine deutlich stärkere Abnahme des Calciumgehaltes bei den Kastenlotproben zu vermerken ist.

Chimbote-Gebiet

Die gleiche Tendenz der Zu- bzw. Abnahmen der Chlorositäts- bzw. Calciumwerte, wie sie im Callao-Gebiet festgestellt wurden, weisen auch die beiden Profile des *Chimbote-Gebietes* auf. Zu vermerken ist, daß die Porenwasser-Daten des Kastenlots mit der geringeren Wassertiefe (167-KAL-2) deutlich stärkere Gradienten zeigen, als die des Kastenlots (165-KAL-3) aus größerer Tiefe.

Discol-Gebiet, Mendana und Peru Becken

Die drei Beprobungsgebiete liegen zwar räumlich relativ weit auseinander, gehören jedoch alle zu dem Areal jenseits des Peru-Grabens auf der pazifischen Seite. Charakteristisch für diese Gebiete ist, daß sowohl beim Calcium als auch bei der Chlorosität fast keine Gradienten auftreten. Im *Discol-Gebiet* ist auffällig, daß in beiden Profilen einmal bei 250 cm (151-KAL) und einmal bei 280 cm Sedimenttiefe (152-KAL) der Calciumwert von 10 mmol/l jeweils um ca. 0,5 mmol/l zurückgeht, aber tiefer im Profil sofort wieder auf das Ausgangsniveau ansteigt. Das Profil im *Peru Becken* zeigt einen bemerkenswerten Abfall der Calciumwerte (um 50%) in der Sedimenttiefe ab 600 cm, was aber möglicherweise auf den Umstand zurückzuführen ist, daß der tiefere Teil des Profils sich einen Tag an Deck erwärmen konnte, bevor die Probennahme stattfand. Aus den bisherigen Porenwasser-Daten des Callao-Gebietes und des Chimbote-Gebietes, mit ihren zunehmenden Chlorositäts-Werten und den abnehmenden

Calciumgehalten, ist eindeutig der Einfluß der submarinen Salzsole die sich im frühesten Miozän bildete (s. KASTNER et al. 1990) erkennbar. Es ist damit zu rechnen, daß mittels der noch ausstehenden Daten sowie der Literaturauswertung genauere Aussagen über Herkunft und Fließrichtung der Salzsole getroffen werden können.

Druckversuche

Ausgangspunkt der Drucktests war eine Versuchsreihe, in der eine Meerwasser-Smektit-Mischung, die zur Gleichgewichtseinstellung mehrere Monate reagiert hatte, unter maximalem Druck von 5000 psi bei Zimmertemperatur ausgepreßt wurde. Hierbei wurde eine Serie von 24 Porenwasserproben sequentiell gewonnen, deren Zusammensetzung anfangs konstant war und der des Meereswasser entsprach. Gegen Ende des Testes, als ca 89 % des Gesamtwassers ausgepreßt waren, trat eine drastische Änderung der Zusammensetzung ein, dahingehend, daß Cl-, Na- und K-Gehalte abnahmen und Ca- und Mg-Gehalte zunahmen (Abb. 2.3.4a und b). Da eine Ionenbilanz deutlich machte, daß der gesamte gelöste Anteil der ursprünglichen Meerwasser-Ionen reduziert war, wurde eine Verdünnung durch Zwischenschichtwasser als mögliche Erklärung in Erwägung gezogen.

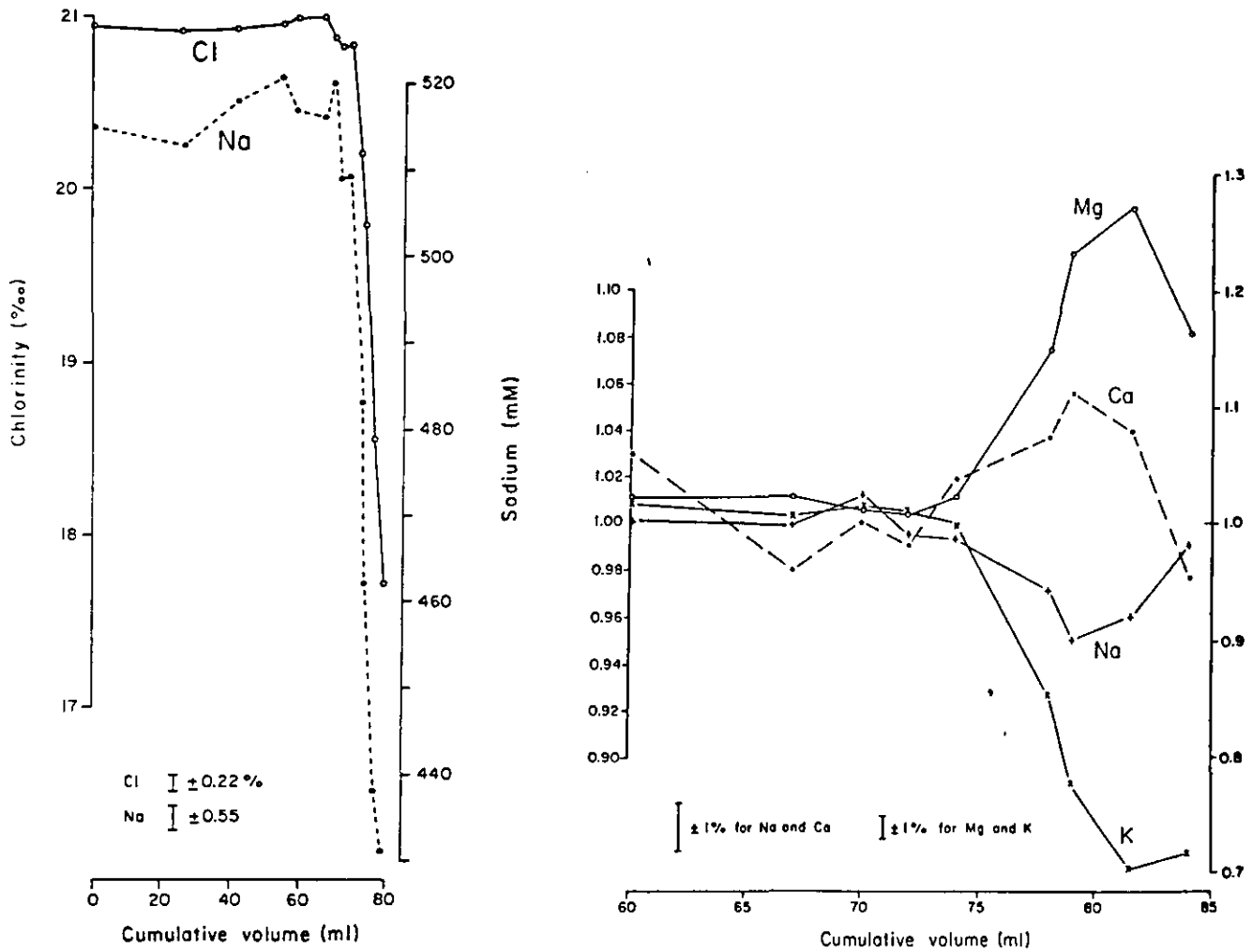

Abb. 2.3.4 Ergebnisse der Druckversuche des künstlichen Ton-Meerwasser-Systems; beachte starke Abnahme der Ionenkonzentration gegen Ende des Versuchs; d.h. bei Abgabe von Zwischenschichtwasser.

Aufbauend auf diesen Ergebnissen wurden natürliche Sedimentproben in ähnlicher Weise behandelt. Dazu wurden ein stark biogen kieseliges Sediment (niedrige Tonanteile M 23410-6) während der Meteor-Reise M-17 und ein stärker toniges Sediment (M 23417-2) und zwei unterschiedlich vorgepreßte Tonproben (mit Drücken von 50 bzw. 90 bar) aus dem Mendana-Gebiet bzw. dem Peru Basin während der SONNE-Reise 78 erneut einem Druck von 150-170 bar ausgesetzt.

Tab. 2.3.2 Chloridabnahmen an ausgepreßten Porenwässern natürlicher Sedimente unterschiedlicher Zusammensetzung

Drucktest kieselig 23410 - 6		Chlorosität mmol/L *
1	20 ml	561
2	50 ml	560
3	10 ml	559,2
Drucktest tonig 23417 - 7		**Chlorosität mmol/L ***
1	40 ml	556,4 ??
2	35 ml	560,8
9	2 ml	552,5

*Standard Meerwasser 560,2 ± 1.1 mmol Cl/L
Mittelwert von 5 Messungen 5,745 ml ±0.012

Erste Analysenergebnisse

Bei der tonhaltigen Sedimentprobe der M-17 Reise wurde, wie bei dem Labortest, eine signifikante Cl-Abnahme gemessen, während die kieselige Probe - wie erwartet - keine Cl-Anomalie im Porenwasser zeigte. Das Ergebnis der beiden Druckversuche mit den Proben der

SONNE-Reise ist, daß trotz verschieden starker Vorpressungen und der unterschiedlichen Herkunft der Proben im Restwasser nahezu identische Abnahmen der Chlorosität gegenüber dem Porenwasser vorhanden sind.

Ausblick

Eine gezielte Differenzierung des Fraktionierungsgrades der Isotopen des Wassers kann erst aufgrund der Ergebnisse der Isotopen-Messungen der o.g. Versuche ermöglicht werden. Die Ergebnisse der Isotopen-Messungen werden zeigen, ob es sinnvoll ist, einen Smektit mit einem höheren Adsorptionvermögen einzusetzen, um noch niedrigere Restwasser-Anteile bzw. einen optimaleren Meßbereich für die Isotopen-Fraktionierung zu erhalten. Um sinnvoll die Versuchszeit zu verkürzen, müßte eine zweite parallel laufende Aparatur erstellt werden. In der Abbildung wird das Arbeitsschema vorgestellt und beinhaltet nachfolgende Schritte:

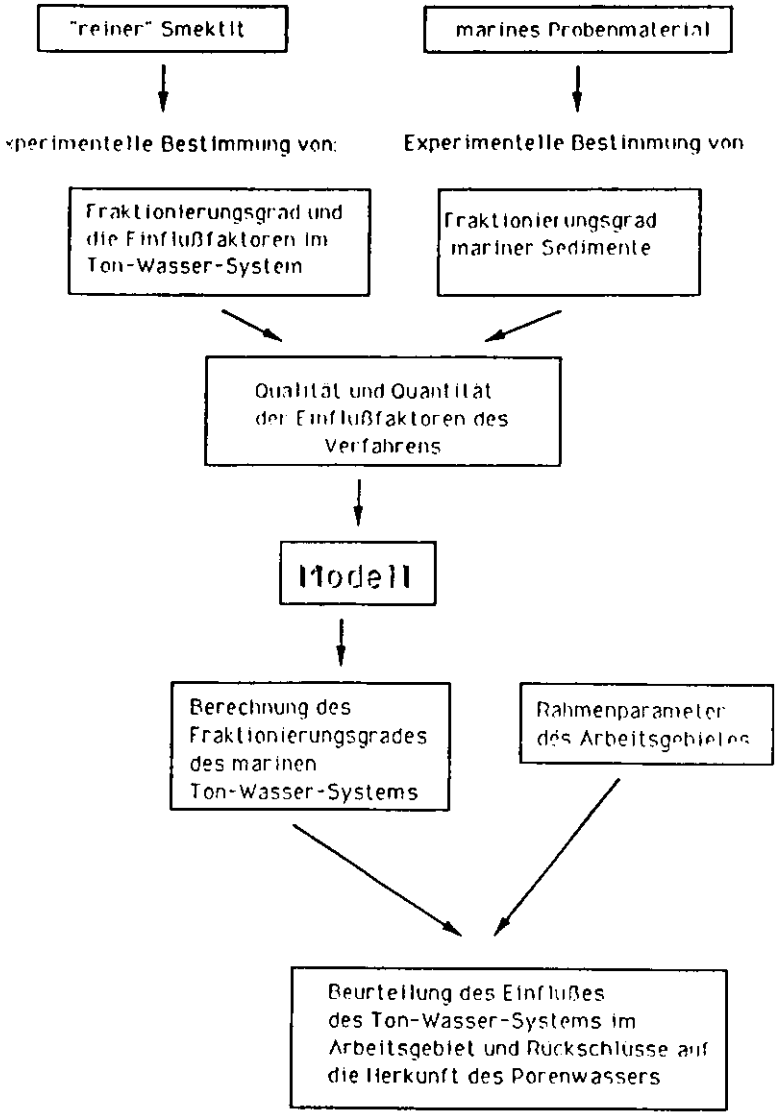

Abb. 2.3.5 Arbeitsschema

Der Einfluß der Kationenbelegung, Korngrößenfraktionen und der Salinität auf eine Isotopenfraktionierung wird untersucht werden, um somit Aussagen über die natürlichen marinen Verhältnisse treffen zu können. Folgen werden Arbeiten zur Charakterisierung des Tones mit seinen spezifischen Eigenschaften wie z.B. Schichtladung, Kationendichte und Zwischenschicht-Kationenaustauschvermögen, mittels der n-Alkylammoniumionen-Methode, um eine Korrelation bzw. bessere Interpretation des Fraktionierungsgrades zu ermöglichen.

Die Feldbeobachtungen und Ergebnisse der Drucktests zeigen - entgegen den bisherigen Befunden anderer Bearbeiter - keine signifikanten Cl-Anomalien, die auf eine Verdünnung durch Zwischenschichtwasser zurückzuführen sind. In Anbetracht der nicht eindeutigen Ergebnisse der Isotopenfraktionierung und der wenig vielversprechenden Feldbeobachtungen und Drucktests wurden diese Arbeiten im Rahmen des Projektes "Plattenrand" mit Ablauf der Finanzierung eingestellt.

2.4 Geotechnische Hinweise der tektonischen Entwässerung

Peter Hempel

Die im Rahmen dieses Vorhabens durchgeführten geotechnischen und diagenetischen Untersuchungen verdeutlichen am Beispiel der Plattenbegrenzungen vor NW-Nordamerika und vor Peru den Zusammenhang zwischen tektonischer Deformation und der damit einhergehenden Entwässerung der Sedimente.

Ergebnisse

An insgesamt 29 Sedimentkernen (Tab. 2.4.1) vom Kontinentalhang vor Oregon und Washington, dem Cascadia Margin, wurde die lithologische Zusammensetzung der Sedimente und deren maßgebliche geotechnische Parameter, wie Dichte, Wassergehalt, Porosität und Scherfestigkeit, bestimmt. Laterale und vertikale Variationen ergeben ein deutliches Abbild der tektonischen Beanspruchung und der Entwässerung der Sedimente in Raum und Zeit. Zeitlich umspannen die untersuchten Sedimente etwa das Holozäns und Spät-Pleistozän. Insbesondere liefern die Scherfestigkeits- und Wassergehaltsprofile deutliche Indizien für den Grad der Kompressionen und daraus resultierenden Kompaktion der Sedimente. Die dem Akkretionskeil vorgelagerten undeformierten Sedimente der Tiefsee-Ebene haben im gesamten Kerntiefenbereich einheitlich hohe Wassergehalte und geringe Scherfestigkeiten. Im Bereich der Deformationsfront erreichen diese Parameter selbst in geringen Teufen extreme Werte (geringe Wassergehalte, hohe Scherfestigkeiten). Die älteren, bereits deformierten Sedimente zeigen einen leichten Rückgang dieser Extremwerte, sind aber dennoch deutlich gegenüber den "Hintergrund-Werten" erhöht (Abb. 2.4.1) (HEMPEL and SUESS, 1993; subm.).

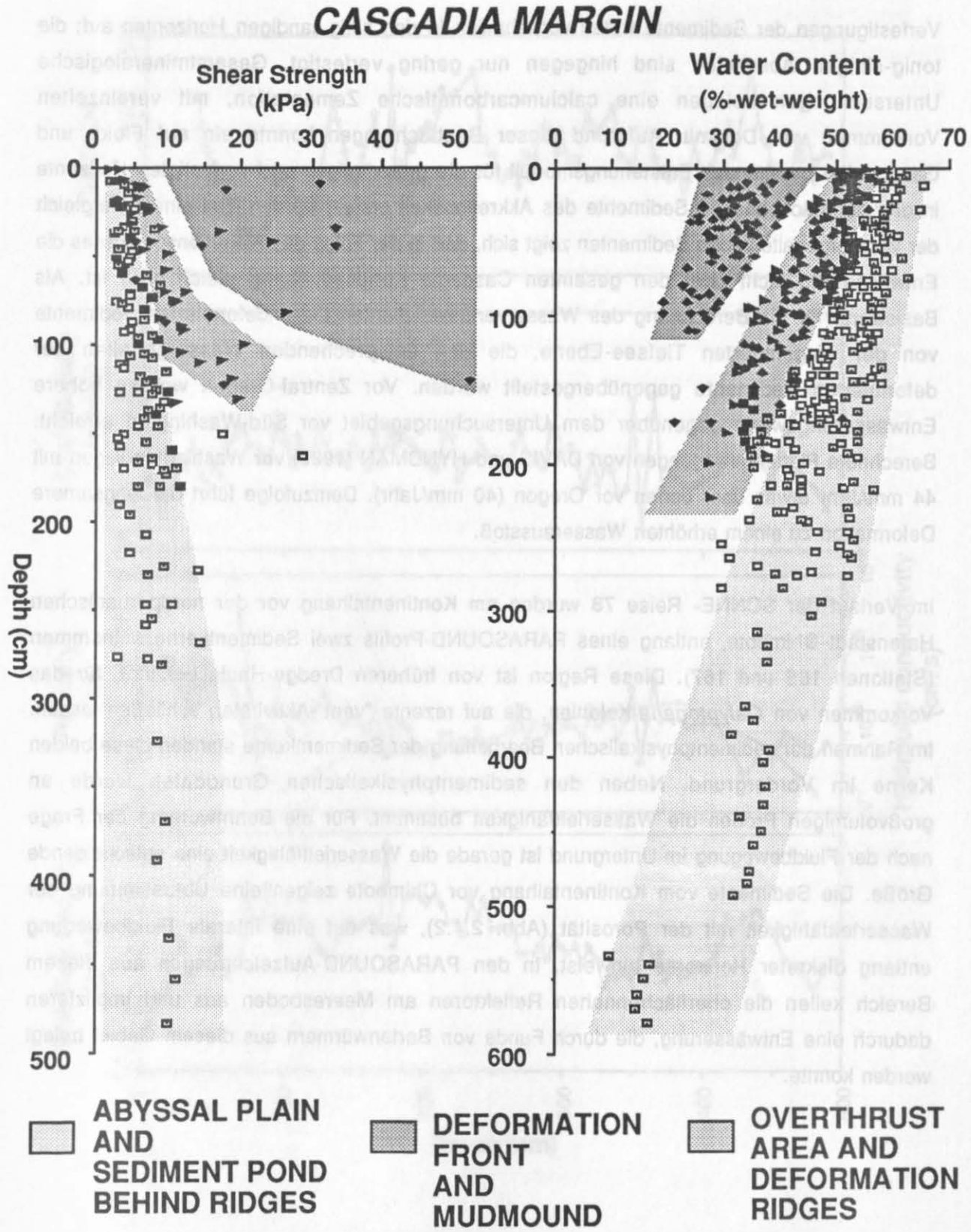

Abb. 2.4.1. Scherfestigkeiten und Wassergehalte der deformierten und undeformierten oberflächennahen Sedimente vom Cascadia Margin. Selbst in geringen Teufen treten im Bereich der heutigen Deformationsfront extreme Scherfestigkeiten und Wassergehalte auf.

Verfestigungen der Sedimente treten vornehmlich in den siltig-sandigen Horizonten auf; die tonig-siltigen Abschnitte sind hingegen nur gering verfestigt. Gesamtmineralogische Untersuchungen belegen eine calciumcarbonatische Zementation, mit vereinzelten Vorkommen von Dolomit. Aufgrund dieser Beobachtungen konnte ein auf Fluid- und Gasaustritte beruhendes Entstehungsmodell für die grobkörnigen und verfestigten Horizonte in den oberflächennahen Sedimente des Akkretionskeil erstellt werden. Bei einem Vergleich der Wassergehalte in den Sedimenten zeigt sich, daß in der Folge des Akkretionsprozesses die Entwässerung nicht über den gesamten Cascadia Kontinentalhang gleich groß ist. Als Basiswerte für die Berechnung des Wasserverlustes dienten die undeformierten Sedimente von der vorgelagerten Tiefsee-Ebene, die den entsprechenden Wassergehalten der deformierten Sedimente gegenübergestellt wurden. Vor Zentral-Oregon werden höhere Entwässerungswerte gegenüber dem Untersuchungsgebiet vor Süd-Washington erreicht. Berechnete Plattenbewegungen von DAVIS und HYNDMAN (1989) vor Washington liegen mit 44 mm/Jahr etwas über denen vor Oregon (40 mm/Jahr). Demzufolge führt die langsamere Deformation zu einem erhöhten Wasserausstoß.

Im Verlauf der SONNE- Reise 78 wurden am Kontinentalhang vor der nordperuanischen Hafenstadt Chimbote, entlang eines PARASOUND-Profils zwei Sedimentkerne entnommen (Stationen 165 und 167). Diese Region ist von früheren Dredge-Hauls bekannt, für das Vorkommen von *Calyptogena*-Kolonien, die auf rezente "vent"-Aktivitäten schließen lassen. Im Rahmen der sedimentphysikalischen Bearbeitung der Sedimentkerne standen diese beiden Kerne im Vordergrund. Neben den sedimentphysikalischen Grunddaten wurde an großvolumigen Proben die Wasserleitfähigkeit bestimmt. Für die Beantwortung der Frage nach der Fluidbewegung im Untergrund ist gerade die Wasserleitfähigkeit eine entscheidende Größe. Die Sedimente vom Kontinentalhang vor Chimbote zeigen eine Überstimmung der Wasserleitfähigkeit mit der Porosität (Abb. 2.4.2), was auf eine laterale Fluidbewegung entlang diskreter Horizonte hinweist. In den PARASOUND-Aufzeichnungen aus diesem Bereich keilen die oberflächennahen Reflektoren am Meeresboden aus und implizieren dadurch eine Entwässerung, die durch Funde von Bartenwürmern aus diesem Gebiet belegt werden konnte.

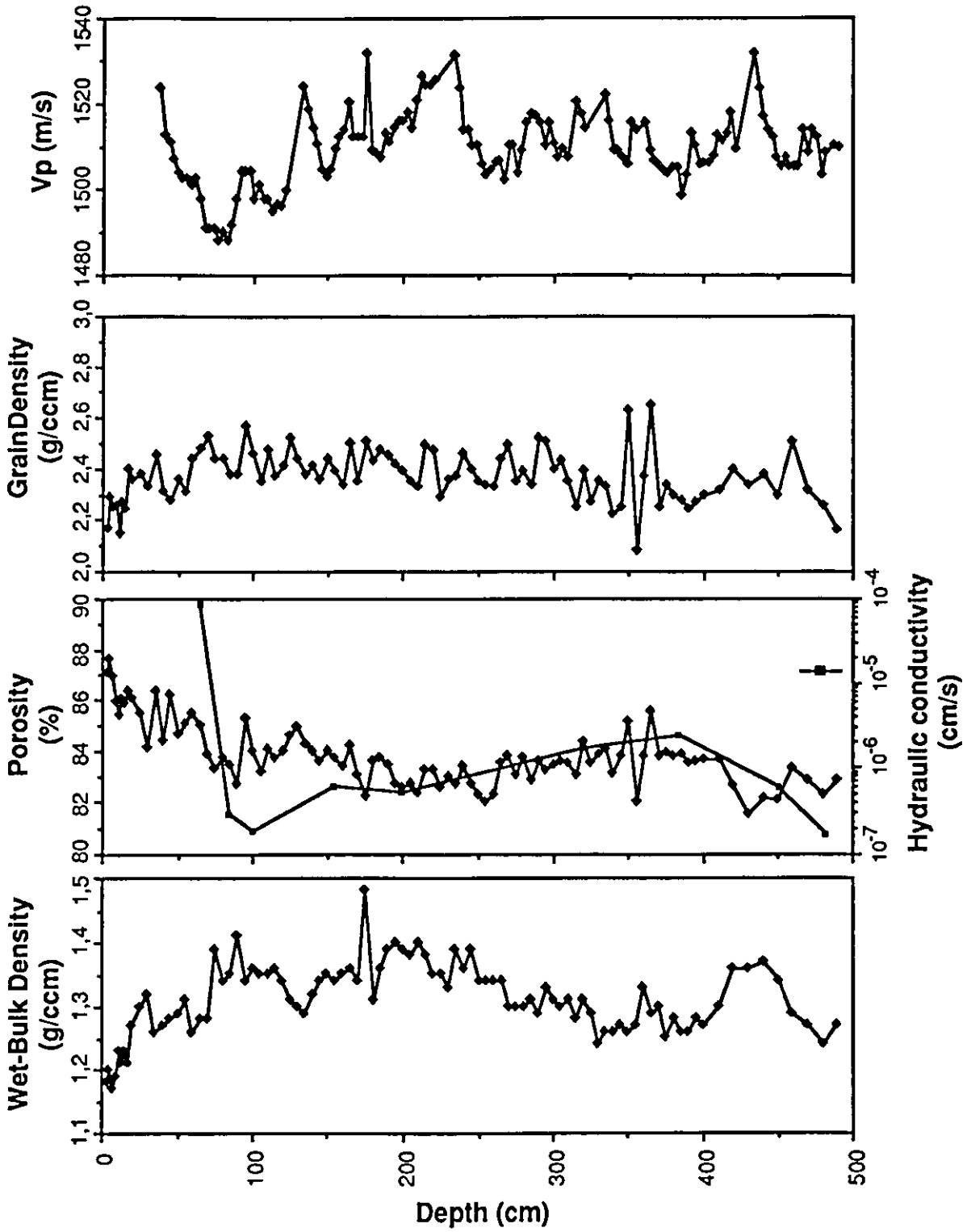

Abb. 2.4.2 Sedimentphysikalische Parameter des Kastenlot-Kernes 165-3. Bemerkenswert ist die Übereinstimmung des Porositäts- mit dem Wasserleitfähigkeits-Profil. Dies deutet auf eine laterale Fluidbewegung in diskreten Horizonten hin.

Zusammenfassung

Folgende herausragende Ergebnisse der geotechnischen Untersuchungen, der gesamtmineralogischen Analysen und der Auswertung der seismischen Aufzeichnungen wurden im Rahmen dieses Vorhabens erzielt:

- Gute Übereinstimmung der geotechnischen Parameter in den tektonischen Einheiten entlang der gesamten Cascadia Plattenbegrenzung.
- Hohe Scherfestigkeiten von > 30 kPa in oberflächennahen Sedimenten im Bereich der Deformationsfront. Erhöhte Werte (5-25 kPa) an den Deformationsrücken.
- Extrem niedrige Wassergehalte (25-45 Gew.-%) im Bereich der Deformationsfront.
- Wassergehaltsunterschiede zwischen den undeformierten Sedimenten der Tiefsee-Ebene und den deformierten Sedimenten im Akkretionskeil betragen bis zu 30%.
- Verfestigte, siltig-tonige Sedimenthorizonte haben die gleiche mineralogische Zusammensetzung, wie die unverfestigten tonigen Abschnitte: als Zementationsmittel dient Calciumcarbonat.
- Karbonatgehalte der undeformierten Sedimente der Tiefsee-Ebene mit Werten bis zu 9 Gew.-% generell höher, als die der deformierten Sedimente (0-3%).
- Dolomit tritt vereinzelt in verfestigten Horizonten auf.
- Verfestigte Horizonte stehen vermutlich in engem Zusammenhang mit der Entwässerung CO_2- und methanhaltiger Fluide.
- Reflexionsseismische und echographische Aufzeichnungen belegen eindrucksvoll die unterschiedlichen Deformationsgrade der tektonischen Einheiten, die durch die geotechnischen Messungen ermittelt wurden.
- Verlauf von Porosität und Wasserleitfähigkeit in den Kernen aus dem "vent"-Gebiet vor Chimbote (Nordperu) sind in bemerkenswerter Übereinstimmung.

Tab. 2.4.1 Position, Wassertiefe und Kerngewinn der untersuchten Sedimentkerne vom Cascadia-Margin.

Core	Latitude	Longitude	Water-depth (m)	Recovery (cm)
Oregon Margin (Overthrust area)				
W8306-1A	44° 56,34'	125° 21,73'	2511	167
W8306-4A	44° 55,91'	125° 18,64'	2008	55
W8306-5A	44° 56,26'	125° 18,45'	1990	103
W8306-6A	44° 55,44'	125° 28,37'	2758	279
Washington Margin (Mound area)				
W8306-2C	47° 13,70'	126° 08,90'	2320	70
W8306-3C	47° 12,50'	126° 19,36'	2445	170
W8306-4C	47° 17,53'	126° 05,67'	1920	135
W8306-5C	47° 17,74'	126° 04,29'	2050	200
Washington Margin (Ridge offset area)				
W8306-9C	47° 27,51'	126° 34,55'	2370	270
W8306-10C	47° 27,42'	126° 23,89'	2320	195
W8306-11C	47° 27,49'	126° 02,15'	1600	195
W8306-12C	47° 27,47'	126° 03,28'	1807	250
W8306-14C	47° 27,50'	126° 04,17'	1810	145
Transit to Oregon Margin (Overthrust area)				
W8306-17C	44° 57,00'	125° 37,92'	2735	195
W8306-18C	44° 57,45'	125° 21,96'	2376	200
W8306-20C	44° 55,98'	125° 14,87'	1260	100
Oregon Margin (Underthrust area)				
W8306-24C	44° 39,78'	125° 19,07'	2420	170
W8306-26C	44° 39,00'	125° 20,50'	2795	165
W8306-27C	44° 39,00'	125° 19,66'	2623	150
W8306-28C	44° 38,99'	125° 17,41'	2014	100
AT8408-4	44° 40,00'	125° 21,60'	2860	230
AT8408-7	44° 39,50'	125° 19,70'	2550	56
AT8408-10	44° 40,00'	125° 17,10'	2180	215
AT8408-11	44° 39,90'	125° 21,50'	2846	120
AT8408-15PC	47° 00,45'	125° 54,78'	2124	588
AT8708-1	44° 40,80'	125° 17,70'	2080	115
AT8708-2	44° 40,80'	125° 17,46'	2091 ?	220
AT8708-3	44° 40,80'	125° 17,46'	2040 ?	122
AT8708-6	45° 11,40'	125° 31,74'	2437	190

W: RV WECOMA AT: RV Atlantis

2.5 Sedimentechographische Charakterisierung gashaltiger Sedimente

Peter Hempel

Gashaltige Sedimente, die in geringer Tiefe unter dem Meeresboden liegen, erscheinen in reflexionsseismischen und sedimentechographischen Aufzeichnungen als transparente Zone. Hervorgerufen wird dieses Phänomen, indem die seismische Energie an freien Gasblasen im Porenraum zu einem großen Anteil gedämpft und stark gestreut wird. Die Dämpfung erzeugt eine abrupte Verringerung der Kompressionswellengeschwindigkeit (Vp), die aus mehrkanaligen reflexionsseismischen Registrierungen berechnet werden kann.

Eine detaillierte Analyse oberflächennaher gashaltiger Sedimente konnte erstmals mit Hilfe der digitalisierten Aufzeichnungen des PARASOUND-Sedimentecholotes durchgeführt werden. Ein ausgewähltes Profil im Skagerrak in der nordöstlichen Nordsee diente als Arbeitsgrundlage. Entlang dieses Profils erfolgten während einer früheren Reise mit F.S. GAUSS mehrkanalige reflexionsseismische Messungen und anschließende Berechnungen von Vp. Es konnte eine oberflächennahe Gaszone festgestellt werden, in der Vp auf 900 bis 1000 m/s zurück geht (Abb. 2.1.5-1). Im Vergleich dazu beträgt Vp im Wasser 1500 m/s und in unverfestigtem Sediment 1500-1700 m/s. Erst die vertikale Auflösung der PARASOUND-Aufzeichnungen ermöglicht die Erkundung der sedimentären Feinstruktur im Bereich der Gaszone.

Im Rahmen dieses Vorhabens wurde die Bearbeitung der digitalen Aufzeichnungen vom Sedimentecholot PARASOUND mittels eines kommerziellen Software-Paketes (GEOSYS, Fa. GECO-Prakla) durchgeführt. Die Digitalisierung der PARASOUND-Signale erfolgt nunmehr routinemäßig an Bord von F.S. METEOR, P.F..S. POLARSTERN und F.S. SONNE. Die Bearbeitung der hochfrequenten Daten in dem für Prospektionsseismik entwickelten GEOSYS war mit Anpassungsschwierigkeiten verbunden. Mit Hilfe einiger Zusatzprogramme kann nun die gesamte im Rechenzentrum des GEOMAR vorhandene Hard- und Software für die Auswertung der PARASOUND-Daten benutzt werden.

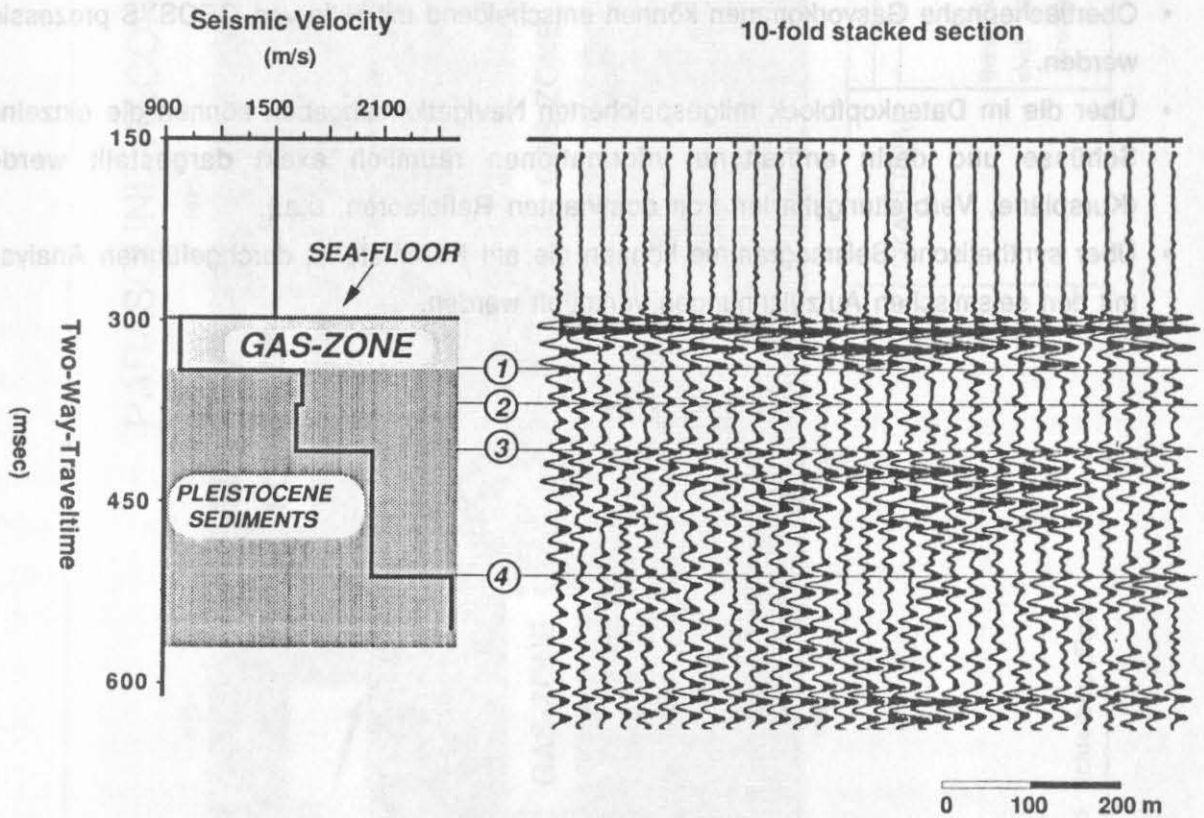

Abb. 2.5.1 Dargestellt ist die berechnete Intervallgeschwindigkeit aus den 10-fach gestapelten reflexionsseismischen Daten.

An ausgewählten Datensätzen aus dem Skagerrak (Abb. 2.1.5-2) und aus dem Europäischen Nordmeer (Vøring Plateau) wurden die digitalisierten Aufzeichnungen unter der Fragestellung der Charakterisierung oberflächennaher Gasvorkommen prozessiert. Das Prozessing erbrachte wichtige Detailinformation über das Amplitudenspektrum, die Signalhauptfrequenz und die engräumige vertikale Abfolge von Reflektoren und erwies sich damit als äußerst hilfreiches Verfahren für eine fundierte seismostratigraphische Interpretation und als großer Informationsgewinn gegenüber den Analogschrieben.

Zusammenfassung

- Digitalisierte PARASOUND-Aufzeichnungen können routinemäßig eingelesen und bearbeitet werden.
- Darstellungen der bearbeiteten Daten kann den Fragestellungen angepaßt werden (Detaildarstellungen, Übersichtsdarstellungen, u.a.).
- Oberflächennahe Gasvorkommen können entscheidend mit Hilfe von GEOSYS prozessiert werden.
- Über die im Datenkopfblock mitgespeicherten Navigationsangaben können die einzelnen Schüsse und darin enthaltene Informationen räumlich exakt dargestellt werden (Kurspläne, Verbreitungskarten von dominanten Reflektoren, u.a.).
- Über synthetische Seismogramme können die am Kernmaterial durchgeführten Analysen mit den seismischen Aufzeichnungen verknüpft werden.

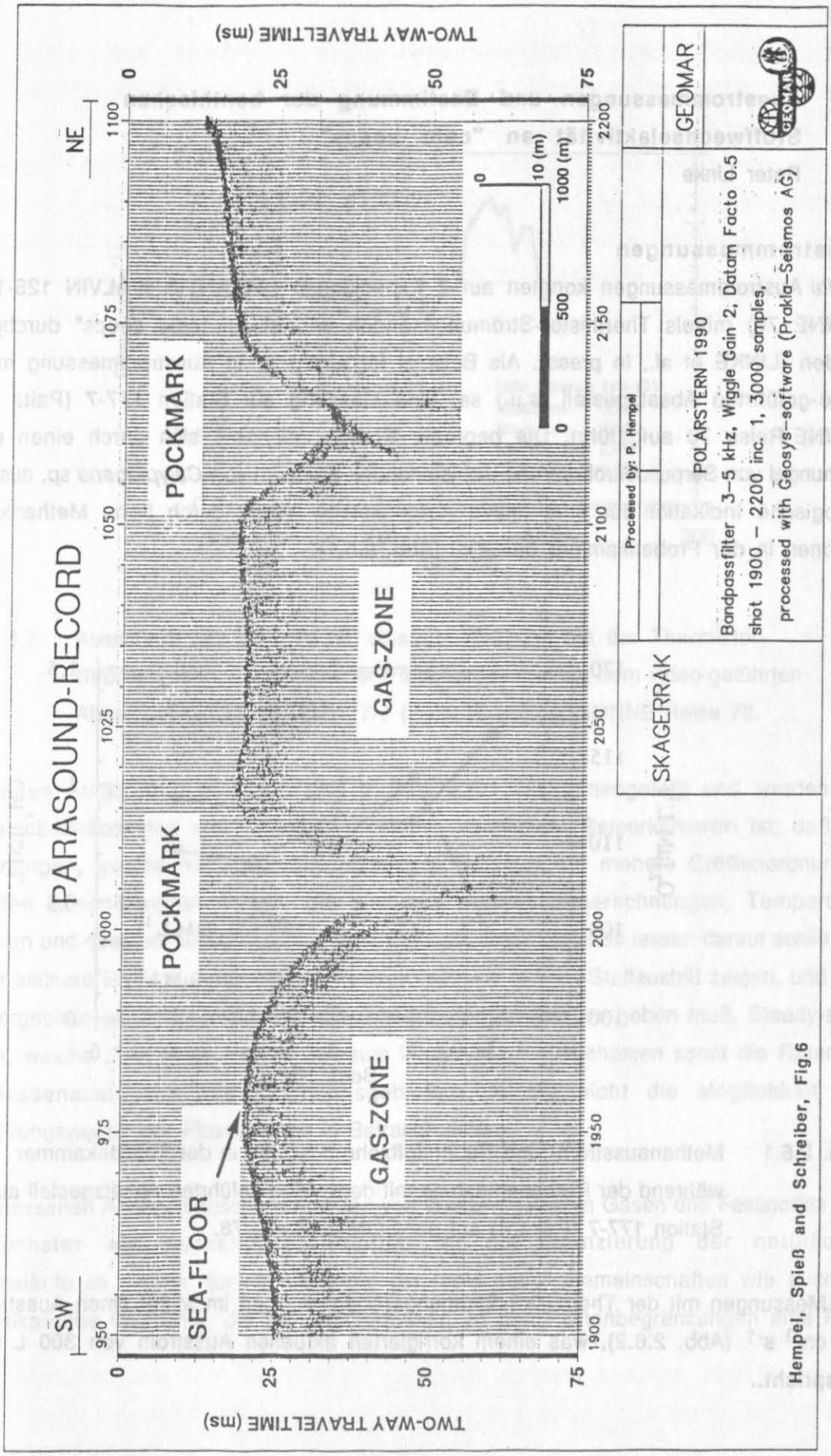

Abb. 2.5.2 Sedimentechographische Aufzeichnung mit PARASOUND. Dieser digitalisierte Abschnitt wurde Bandpass-gefiltert zwischen 3 und 5 kHz. Die geringe Eindringung von etwa 10 m ist auf die hohe Gaskonzentration im Sediment zurückzuführen.

2.6 Ausstrommessungen und Bestimmung der benthischen Stoffwechselaktivität an "cold seeps"

Peter Linke

Ausstrommessungen

In situ Austrommessungen konnten auf 2 Expeditionen (ATLANTIS II/ALVIN 125-12 und SONNE 78) mittels Thermistor-Strömungssonden an aktiven "cold seeps" durchgeführt werden (LINKE et al., in press). Als Beispiel für eine direkte Ausstrommessung mit dem video-geführten Absatzgestell (s.u.) sei eine Messung auf Station 177-7 (Paita II) der SONNE-Reise 78 aufgeführt. Die beprobte Station zeichnete sich durch einen dichten Dschungel von Serpulidenröhren und dichtstehenden Kolonien von *Calyptogena* sp. aus. Diese biologische Indikation für eine aktive Austrittsstelle wurde durch hohe Methankonzentrationen in der Probenkammer bestätigt (Abb. 2.6.1).

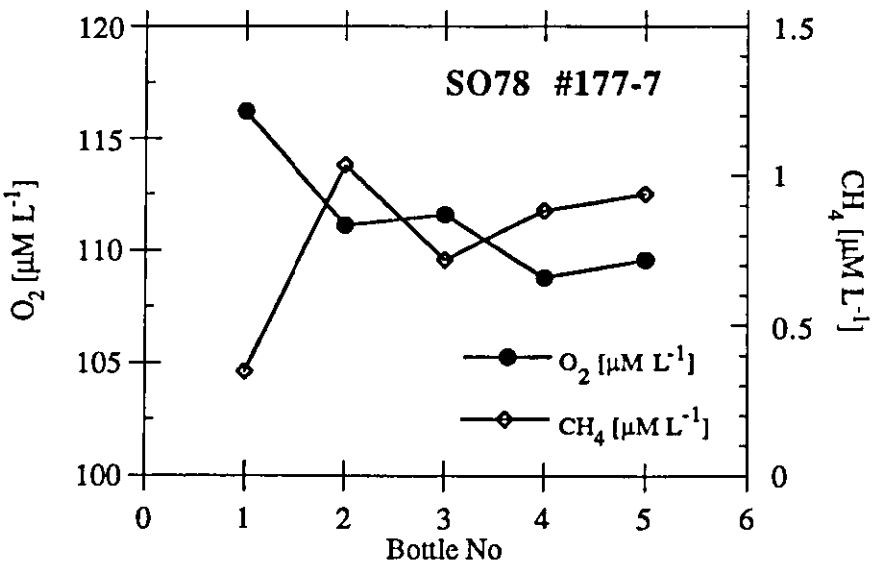

Abb. 2.6.1 Methanausstrom- und Sauerstoffzehrungsraten in der Probenkammer während der Probenentnahme mit dem video-geführten Absatzgestell auf Station 177-7 (Paita II) auf der SONNE Reise 78.

Die Messungen mit der Thermistor-Strömungssonde ergaben im Mittel einen Ausstrom von 2,1 $cm^3\ s^{-1}$ (Abb. 2.6.2), was einem korrigierten aktuellen Ausstrom von 300 L $m^{-2}\ d^{-1}$ entspricht..

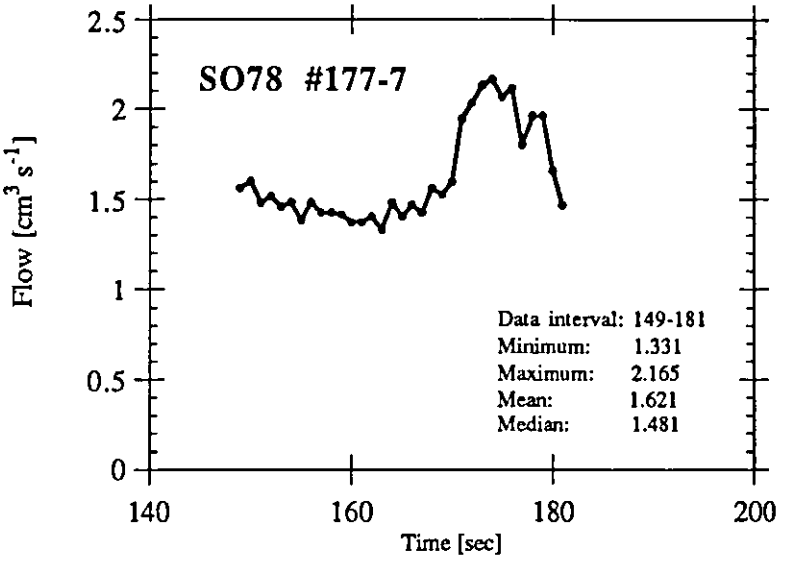

Abb. 2.6.2 Ausschnitt aus einer *in situ* Austrom-Messung mit der Thermistor-Strömungssonde während der Probenentnahme mit dem video-geführten Absatzgestell auf Station 177-7 (Paita II) auf der SONNE Reise 78.

Die übrigen Ausstrom-Messungen sind in Tab. 2.6.1 zusammengefaßt und werden mit Ausstromabschätzungen aus indirekten Ansätzen verglichen. Bemerkenswert ist, daß die Berechnungen, welche auf Porositätsänderungen beruhen, um mehere Größenordnungen unter den Abschätzungen liegen, die sich aus Massenflußberechnungen, Temperaturgradienten und direkten Ausstrommessungen ergeben. Diese Befunde lassen darauf schließen, daß nur kleinere Gebiete der gesamten Konvergenzzone aktiven Stoffaustritt zeigen, und daß es Liefergebiete (recharge zones) für diese aktiven Ausstrittstellen geben muß. Steady-state Modelle, welche über einen langen Zeitraum integrieren, unterschätzen somit die Raten für den Massenaustausch aus Akkretionsgebieten, da sie nicht die Möglichkeit von Rückführungswegen der Flüssigkeiten in Betracht ziehen.

Die gemessenen Ausstromgeschwindigkeiten von Wasser, gelösten Gasen und Feststoffen sind von höchster wissenschaftlicher Priorität für die Bilanzierung der natürlichen Stoffkreisläufe im Ozean, für die Ökologie der "cold seep" Gemeinschaften wie auch für geophysikalische Probleme, die z.B. bei Erdbeben an den Plattenbegrenzungen eine Rolle spielen.

Table 2.6.1.: *List of stations with venting rates obtained from in situ measurements, compared with indirect estimates using fluxes of methane and barium and temperature changes within the sediments.*

LOCATION	LATITUDE LONGITUDE	DEPTH [m]	APPROACH	FLOW RATES [L m^{-2} day^{-1}]	LINEAR FLOW VELOCITY [m $year^{-1}$]	REFERENCES
Cascadia	44° 40.44' N	2046	Mechanical flowmeter	188 ± 20	113	CARSON *et al.*, 1990
Alvin 1907	125° 17.63' W		Methane flux	156 ± 10	95	CARSON *et al.*, 1990
			Porosity reduction	~ 1.8 x 10^{-3}		CARSON *et al.*, 1990
			Porosity reduction	~ 7 x 10^{-4}		HEMPEL and SUESS, 1993
			Heat flow	~ 4 x 10^{-2}		DAVIS *et al.*, 1990
Cascadia	44° 40.42' N	675	Thermistor flowmeter	1765 ± 20	1065	This study
Alvin 2283	125° 07.49' W		Methane flux	1700* ± 50	1023	This study
Cascadia	45° 56.19' N	2424	Thermistor flowmeter	86 ± 20	52	This study
Alvin 2285	125° 20.82' W		Methane flux	50 ± 20	30	This study
Peru margin	9° 35.26' S					
Sonne 168-2	80° 07.70' W	3672	Thermistor flowmeter	441 ± 20	265	This study
Sonne 180-4	5° 36.00' S 81° 38.61' W	3309	Barium flux	970 ± 50	583	TORRES *et al.*, 1992
Peru margin	5° 36.32' S					
Nautile NP2-35	81° 38.63' W	3540	Methane flux	200* ± 50	120	DIA *et al.*, 1992
Nankai Trough			Heat flow		100	HENRY *et al.*, 1992
			Seismic velocity	~ 8 x 10^{-4}	6 x 10^{-4}	BEKINS and DREISS, 1992

Notes: The flow rates indicated by asterics (*) were calculated assuming that the methane concentration in the feed water was the same as that for *Alvin* dive site 1907. The flow rates based on porosity reduction (steady-state dewatering) are averages over the entire prism, and therefore should not be directly compared with the flow rates obtained at an individual venting site. The linear flow velocity was estimated using a constant porosity of 60%.

Bestimmung der benthischen Stoffwechselaktivität (Kalorimetrie)

Die direkte Mikrokalorimetrie ist ein Verfahren zur Bestimmung kleinster Wärmeflüsse. Die gemessene Wärmemenge ist ein Maß für die Stoffwechselaktivität von Sedimentgemeinschaften, aber auch von isolierten Organismen. Die Wärmeproduktion gilt dabei als ein direktes Maß für den Energiefluß, unabhängig vom Typ des Metabolismus. Dies ist in marinen Sedimenten von Bedeutung, da hier verschiedene Metabolismustypen gleichzeitig auftreten. Auf der Reise W8909A der WECOMA konnten 1989 an insgesamt 4 Stationen Tiefenprofile der Wärmeproduktion im Sediment durch Messungen mit dem Mikrokalorimeter erfaßt werden. Im direkten Vergleich dieser Profile wurde die höchste Wärmeproduktion an der vent Station (2 BC, 2070m Wassertiefe, s. Abb. 3) gemessen.

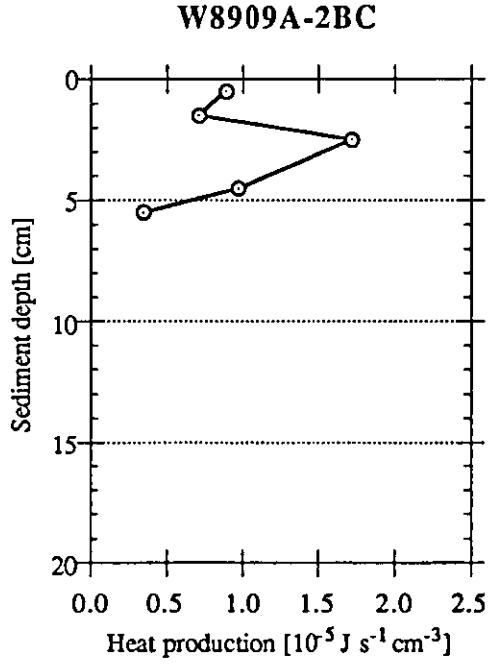

Abb. 2.6.3 Profil der Wärmeproduktion eines Sedimentkernes aus der unmittelbaren Umgebung eines cold seep auf der Reise W8909A der WECOMA.

Generell ist die Wärmeproduktion dieser Sedimente verglichen mit Messungen vom Vøring-Plateau (Norwegische See) als sehr hoch zu bezeichnen. Ähnlich hohe Werte konnten in der Norwegischen See nur nach einem Sedimentationsereignis, einem Nahrungspuls für Tiefsee-Organismen gemessen werden (GRAF, 1989). Wärmeproduktionsmessungen an seep Sedimenten in der Norwegischen See (METEOR-Reise 13/2, Stationen 547 und 576) lagen demgegenüber um fast eine Zehnerpotenz unter diesen Werten. Nachdem diese Ergebnisse aus Proben stammen, die vom Schiff aus genommen wurden, erschloß erst die direkte Beobachtung im Tauchboot die Heterogenität der Sedimente sowie die Größenskalen, in denen "cold seeps" auftreten.

Stoffwechselaktivität

Ein typisches Merkmal der Sedimente von der Cascadia-Subduktionszone ist das Auftreten verfestigter Horizonte, welche vielfach das Eindringen des benutzten Probennahmegerätes (Push corer - PC) verhindern. Dennoch konnten im Jahre 1990 auf der Reise 125/12 der ATLANTIS II "seep"-Sedimente mit dem Tauchboot ALVIN gezielt beprobt werden. Ein Sedimentkern aus der unmittelbaren Umgebung eines "seeps" (#2285PC, 2424m Wassertiefe, s. Abb. 2.6.4a) ergab die höchsten Wärmeproduktionswerte in einer Sedimenttiefe von 14 cm. Dieses Maximum in der benthischen Stoffwechselaktivität findet zudem Übereinstimmung in einem Anstieg der NH_4- und Alkalinitätskonzentrationen im Porenwasser (Abb. 2.6.4b). Demgegenüber zeigen die Wärmeproduktionsprofile aus 2 Sedimentkernen (#2282+2283PC, Abb. 2.6.4C) eines aktiven Gashydratgebietes in 675m Wassertiefe ein oberflächennahes Maximum in der benthischen Stoffwechselaktivität.

Dies läßt vermuten, daß in diesem Gebiet mit den höchsten Ausstromraten (s. Tab. 2.6.1) der maximale Stoffumsatz durch aufsteigende Fluide und geringe Sauerstoffeindringtiefen aufwärts in die Nähe der Sedimentoberfläche verschoben wird. In den Sedimenten von "cold seeps" mit geringeren Ausstromraten und einer dementsprechend größeren Sauerstoffeindringtiefe hingegen sind maximale Stoffwechselaktivitäten in größeren Sedimenttiefen zu erwarten. Diese Phänomene wären dadurch zu erklären, daß die energetische Basis von "cold seep" Gemeinschaften nicht auf der photoautotrophen Primärproduktion der euphotischen Zone, sondern auf der chemoautotrophen Primärproduktion freier und mit verschiedenen Tieren in Symbiose lebendenden Bakterien beruht. Diese gewinnen ihre Energie aus der Oxidation reduzierter Substanzen (z.B. Sulfid, Methan, Ammoniak), die durch zirkulierende Wässer aus der ozeanischen Kruste und dem darauf beruhendem Sediment-Paket herausgelöst werden und durch Konvektion in den Ozean zurückgelangen. Leider war es bisher nur in wenigen Fällen überhaupt möglich, Sedimente von "cold seeps" zu beproben und sie einer eingehenden Untersuchung geochemischer und biologischer Parameter zu unterziehen. Diese Ergebnisse sind jedoch bisher einzigartig und erscheinen, aufgrund der bereits vorliegenden Befunde, als erfolgversprechend und sollten in Zukunft weiterverfolgt werden, um die Frage klären zu helfen, inwieweit Lebensgemeinschaften an "cold seeps" (wie auch an Hydrothermalquellen) im Vergleich zu denen der übrigen Tiefsee als grundsätzlich verschieden herauszustellen sind.

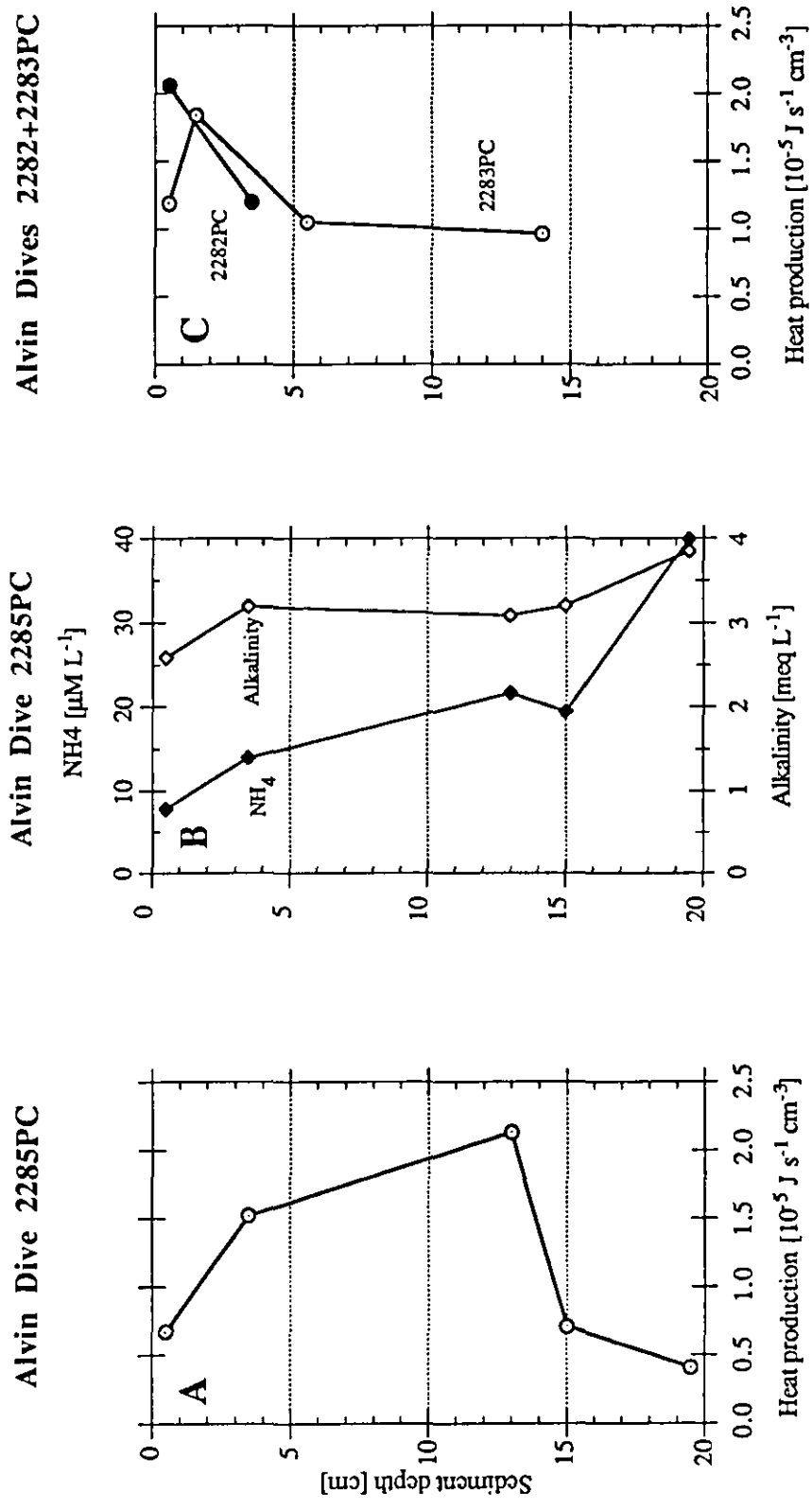

Abb. 2.6.4 Profile der Wärmeproduktion (A) sowie der Alkalinität und des NH_4-Gehaltes (B) eines Sedimentkernes von dem Akkretionsrückens (#2285), einem Gebiet mit geringen Ausstromraten, gegenübergestellt den Wärmeproduktions-profilen von 2 Sedimentkernen aus dem aktiven Gashydratgebiet (#2282+2283).

Zusammenfassung

- ***In situ* Ausstrommessungen** mit der Thermistor-Strömungssonde konnten auf zwei Expeditionen erfolgreich durchgeführt werden;
- die gemessenen Ausstromraten liegen um Größenordnungen über den Abschätzungen, die auf Porositätsänderungen beruhen;
- die Möglichkeit, die Probenkammer sowohl vom U-Boot als auch von konventionellen Forschungsschiffen einzusetzen, eröffnen neue Dimensionen in der Beprobung von aktiven Kontinentalrändern und der Bilanzierung der natürlichen Stoffkreisläufe im Ozean;
- die **Kalorimetrie** ist ein vielversprechendes Verfahren zur Erfassung der Stoffwechselaktivität der cold seep Sedimentgemeinschaften;
- Maxima im benthischen Stoffumsatz lassen sich gut mit Ausstromraten und geochemischen Parametern korrelieren.

2.7 Barite deposits in the Peru subduction zone.

Marta Torres

A program of dives with the deep submersible NAUTILE during the spring of 1990, has provided structural and stratigraphic data on the subducting plate boundary of the Peru margin (BOURGOIS et al., 1992). Communities of clams and serpulae as well as venting fluids were sampled during this project; analysis of these materials have produced important information on the chemistry of fluids and vent organisms in this active margin (DIA et al., 1992; BOULEGUE et al, 1992). Of particular interest was the discovery of large deposits of barite, in the form of crusts, concretions and chimneys which were recovered during the NAUTILE expedition, and subsequently sampled during the R/V SONNE cruise 78.

Results

Barite samples were recovered from the slope of the Peru margin along a failure scarp as well as from the Chiclayo canyon using a submersible during the NAUTIPERC project, and by coring during the SO-78 cruise (Fig. 2.7.1). They occur in the form of light yellow to brown concretions or chimneys, up to 15 cm height, as well as white crusts only a couple of millimiters thick. They are composed of very pure barium sulfate crystals either in dendritic arrangements or in concentric layers. No other phases were identified by XRD in either the chimneys nor in the crusts. Their porous nature results in a low bulk density, ranging from 2.8 to 3.4 g/cc, which compares with a value of 4.5 g/cc for the material density of barium sulfate.

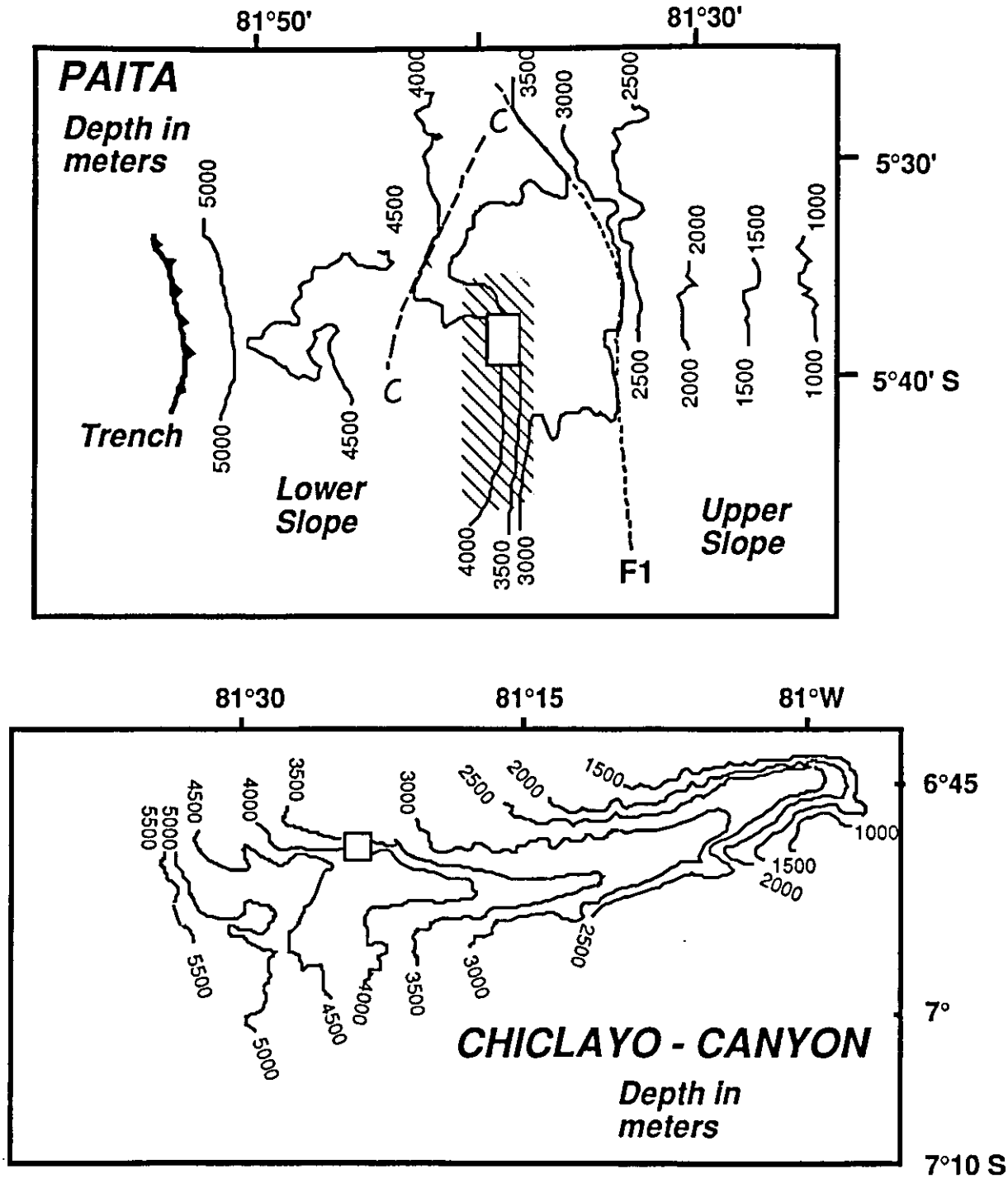

Fig. 2.7.1 Bathymetric contours indicating the areas surveyed by the NAUTILE NAUTIPERC expedition) and the SONNE (cruise SO78). A) Paita area showing the location of the upper and lower venting sites. B) Chiclayo canyon. In both cases the barite deposits are indicated by open squares.

Water samples recovered with the benthic barrel were analyzed for barium by ICP-AES. The sequential water sampling using VESP showed significant changes in the chemical composition of the enclosed bottom water with time; changes in the barium concentration of the fluid are shown in Fig. 2.7.2.

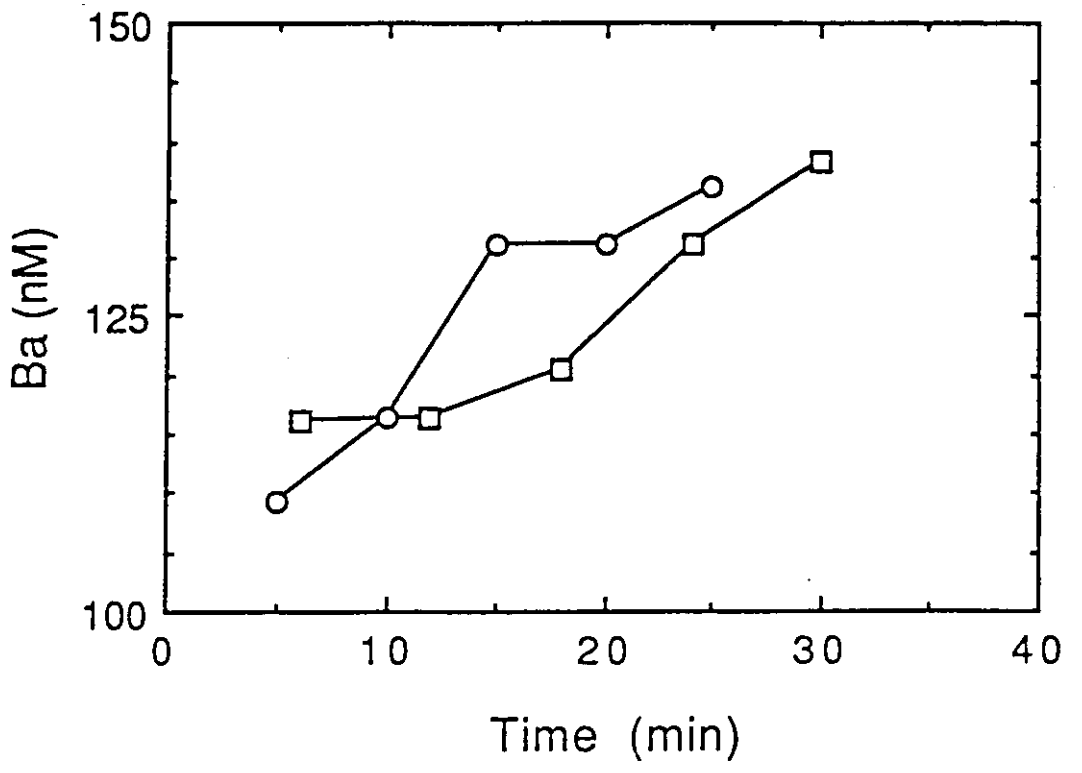

Fig. 2.7.2. Increase in dissolved barium concentration with time for two deployments of the VESP at the Paita venting site. Circles correspond to Station SO78-177-2 and squares represent data from Station SO78-180-4.

During one of the deployments of the VESP at a vent site (Station SO78-180-4), a sediment sample was retrieved and its pore fluid composition determinated. Pore fluids were squeezed immediately after retrieval in a titanium hydraulic press; the dissolved barium content in the pore water was found to be 1.26 µM. The barites were analyzed for their isotopic composition, and the results are discussed in TORRES et al. (1993), s. Anhang.

Source of the barium

It is important to determine the source of the barium in these deposits, as this knowledge might help elucidate the origin of the venting fluids, paths of fluid flow and venting rates. Two scenarios are possible: (1) the barites might have been deposited in association with hot barium-rich fluids which were discharged following the sediment slide by tapping into a hydrothermal reservoir; or (2) the barium associated with biogenic deposition in this high productivity region which is remobilized in the zone of sulfate depletion, is subsequently transported with the fluids to the venting site where it precipitates.

Temperature measurements and geochemistry of the venting fluids (DIA et al., 1992) show no evidence for contemporaneous hydrothermal activity in the Peru slope; on the other hand, recent precipitation is suggested by the fragility of the deposits and by the absence of any significant sediment coating on the chimneys in an environment characterized by extremely high sediment accumulation. These observations lead us to postulate that the barium source is associated with remobilization of biogenic barium, and subsequent transport of the barium-rich reducing fluids to the cold-vent sites. A possible source of barium for the barites recovered at the vent sites, is from the venting fluids in which dissolved barium has accumulated as a result of organic matter diagenesis. Barium concentrations as high as 400 µM have been measured in the pore fluids obtained by deep drilling in the Peru margin.

Isotopic data

Sulfate fractionation during bacterial decomposition of organic matter results in a dissolved sulfate reservoir enriched in the heavy ^{34}S isotope (GOLDHABER and KAPLAN, 1980), so the authigenic barites formed within the sediment column should be isotopically heavy relative to seawater. The values from the barites recovered at the Chiclayo site ($\partial^{34}S$ = 22 $^{o}/_{oo}$) indicate that the Chiclayo deposits formed at the seafloor, from the interaction of barium-rich fluids venting at the margin, with seawater sulfate. The higher isotopic values in the samples from Paita ($\partial^{34}S$ = 25 to 30 $^{o}/_{oo}$) may reflect a component enriched in ^{34}S by bacterial oxidation of organic matter which has been either being generated at the sediment water interface or has been transported to the seafloor from deeper in the sediment section by the venting fluids.

The oxygen isotopes of the sulfate in the Chiclayo canyon barites are consistent with contemporary values for the dissolved seawater sulfate. The Paita samples, however show an enrichment of $S^{18}O_4$ relative to seawater ($\partial^{18}O$ = 16 to 17 $^{o}/_{oo}$). We propose that the enrichment in the heavy oxygen isotope results from bacterial activity near the vents. During sulfate reduction, bacteria preferentially metabolize sulfate containing ^{16}O and ^{32}S (MIZUTANI and RAFTER, 1973; McCREADY and KROUSE, 1980), and thus barite becomes progressively enriched in ^{18}O and ^{34}S. The slight enrichment in ^{34}S and ^{18}O in the Paita deposits may indicate a component of biologically metabolized sulfate. This fractionation, which is only present in Paita and not in Chiclayo, is consistent with the higher sediment cover and the presence of bacterial mats observed in the Paita venting sites. The $^{87}Sr/^{86}Sr$ isotopic ratios of the barites reveal a shift towards radiogenic values. The high values ($^{87}Sr/^{86}Sr$ up to 0.711118) indicate that the fluids responsible for the deposition of the barites may have a continental component. The original fluid must have reacted with a continental crust, since isotopic analysis of bulk sediment samples do not reveal ratios as high as those recorded in the barite deposits.

Venting rates

Concentration increase of barium in the benthic barrel clearly documents a contemporaneous release of Ba to the bottom water from the vent sites (Fig. 2.7.2). This demonstrates that barium can be remobilized from the sediments at low temperatures. We have estimated water flow rates from these vents using the flux rates of dissolved components if the fluids. By assuming that: (1) the barium behaves conservatively during the period of deployment approximately 30 minutes; and (2) that the barium content in the pore fluids feeding the vent is that measured at the sediment surface, an estimate of fluid flow of approximately 970 $L/m^2/day$ was obtained using the barium flux rates from Station 180-4. The good correspondence of venting rates calculated with barium, with those estimated using other dissolved parameters indicates that the barium source is somewhat coupled to the fluids which are enriched in metabolites from decomposition of organic matter.

Source of the fluid

The "instantaneous" flow rates estimated from the dissolved barium, are comparable with rates measured in the Oregon margin. Several studies (Le PICHON et al., 1992; CARSON et al.,1990) have shown that such high values cannot be explained solely by steady-state compactive dewatering processes. This results imply that there must be a recharge zone for the fluids venting at accretionary margins. Accumulation of dissolved barium is driven by remobilization of barite in sulfate depleted sediments; this observation puts un upper limit as to the depth of the penetration of the recharge fluids. Furthermore, the strontium isotopic composition of the barites indicates that the fluid responsible for the transport of biogenic barium to the vent site may have a continental component.

These observations clearly demonstrate that the fluids have either migrated from the continent or have reacted with a continental crust underlying the sediments. In either case, they are not solely due to loss of porosity during compaction of the sediment prism. Furthermore, the evidence suggests that the circulation cell for the fluids venting at this margin is rather large; i.e., the recharge fluids cannot come from a small scale satellite convection around the vent, but rather venting results from a large scale fluid-flow through the sediment section.

Summary

- Large barite deposits were discovered in the Peru margin in association with biological communities indicative of active fluid seepage.

- Sulfur isotopic data suggest that the barites formed at the seafloor, by the interaction of barium-rich fluids and seawater sulfate.
- By comparison with data from drilled sites in this margin, the source of the barium is thought to be the remobilization of biogenic barite from upwelling sediments in the zone of sulfate depletion.
- Strontium isotope data indicate that the fluid responsible for the transport of biogenic barium to the vent site may have a continental component. This in turns supports the idea that venting at this sites results from a large scale fluid-flow through the sediment section.

3. TECHNISCHE ERGEBNISSE

3.1 Probenkammer-Einsatz von ALVIN

Peter Linke

Der Prototyp eines *in situ* Gerätes zum Beproben von "vent"-Fluiden und Registrieren von Ausstrom-Messungen wurde vom Antragsteller noch während der Zugehörigkeit zur Arbeitsgruppe an der Oregon State University entwickelt (Abb.3.1.1). Das Instrument erlaubt ein Volumen von etwa 180 Litern Bodenwasser über einer Austrittsstelle abzuschließen bzw. den Fluß durch eine Verengung so zu führen, daß die Ausstrom-geschwindigkeit gemessen werden kann. Die sechs Wasserprobennehmer im geschlossenen Volumen der Kammer erlauben, über vorgegebene Zeitabschnitte die Zunahme der Gehalte von "cold seep"-Fluiden oder -Gasen zu messen. Auf der Basis dieses Prototypes wurde für eine *in situ* Bilanzierung der Flußraten an den "cold seep" Stationen in Zusammenarbeit mit V. Martens, Institut für Meereskunde Kiel, eine Thermistor-Strömungssonde für den Tiefsee-Einsatz mit dem Tauchboot ALVIN konstruiert (LINKE et al., in press). Die Auslegung dieser Sonde war an Erfahrungen aus Strömungsmessungen im Flachwasser (LaBARBERA & VOGEL, 1976; FORSTER, 1991), im Strömungskanal (ZIEBIS, 1992) sowie an den Vorgaben vorhandener Geräte (Probenkammer, mechanischer Strömungsmesser; CARSON et al., 1990) orientiert.

Auf zwei Stationen (#2283+2285) konnten *in situ* Ausflußraten von "cold seeps" erfolgreich durchgeführt werden. Unmittelbar vor der eigentlichen Messung wurden jeweils die Signale der Strömungssonde bei Nullströmung als Basislinie unter *in situ* Bedingungen (Temperatur, Salinität, Viskosität) aufgezeichnet, um sie dann später vom eigentlichen Meßwert abzuziehen.

Abb. 1: EINSATZ DER PROBENKAMMER VON TAUCHBOOTEN

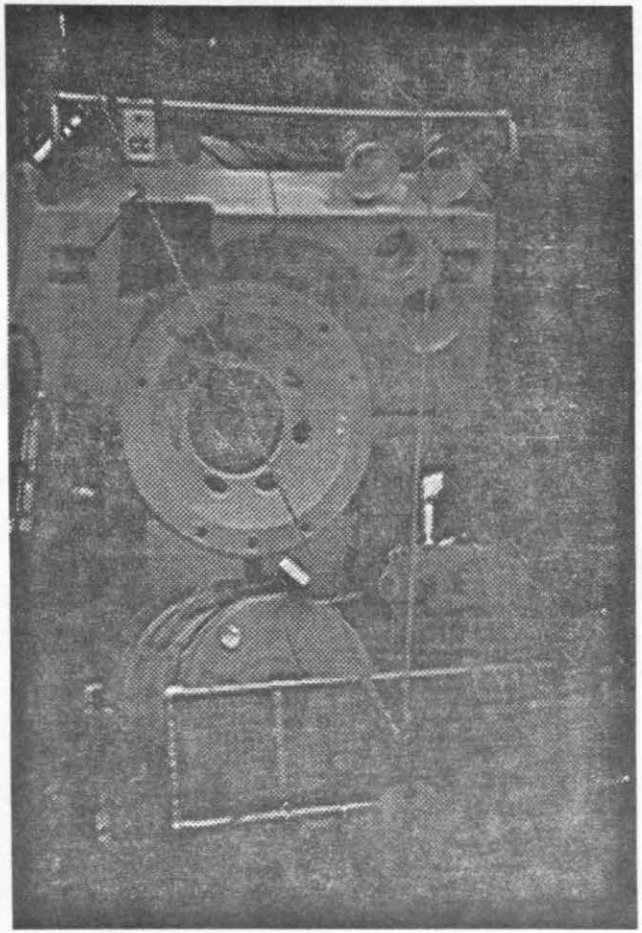

PROBENKAMMERN IM TRANSPORTKORB DES TAUCHBOOTES "ALVIN"

PROBENKAMMER IM EINSATZ

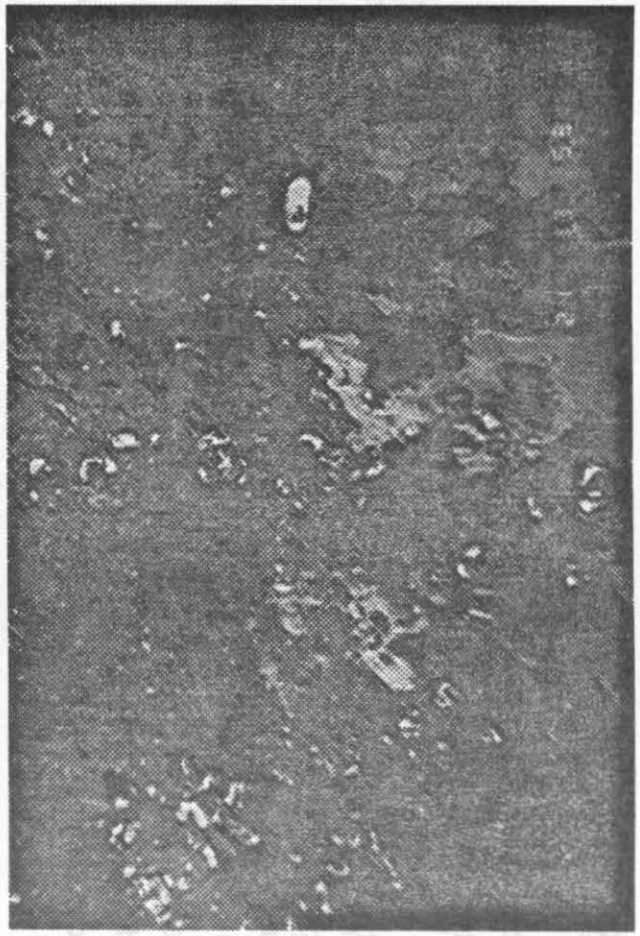

FLÜSSIGKEITSAUSTRITTSSTELLE (VENT) MIT MUSCHELN + BAKTERIENMATTEN

3.2 Probenkammer-Einsatz von NAUTILE

Marta Torres

Auf der Basis des oben beschriebenen Prototypes wurde weiterhin im Rahmen dieses Vorhabens ein verbesserter Nachbau in Zusammenarbeit mit der Fa. Hydro Bios, Kiel, hergestellt. Die neue Probenkammer hat einen Durchmesser von 44 cm und eine Höhe von 70 cm (Abb. 3.2.1). Das PVC-Gehäuse kann etwa 4 cm in den Untergrund eindringen, um damit ein geschlossenes System innerhalb der Probenkammer zu erzeugen. Tieferes Eindringen in das Sediment, das zur Funktionsbeeinträchtigung der Wasserschöpfer führen würde, wird durch Füße verhindert. Innerhalb der Probenkammer befinden sich 5 Wasserschöpfer à 2 Liter, ein Motor mit Auslösemechnismus für die Wasserschöpfer, eine CTD-Sonde und eine Programmiereinheit mit Interspeicher, mit einer Speicherkapazität von 128 kByte. Die Programmiereinheit gewährleistet eine zeit- oder tiefenabhängige Auslösung der Wasserschöpfer und die Registrierung der Daten von der CTD-Sonde. Die Speicherkapazität ist ausreichend für etwa 4 Stunden bei einer Registrierung der CTD-Daten im 1 Sekundenabstand. Die Registrierintervalle sind von 1 Sekunde bis 99 Stunden stufenlos wählbar, womit sich die gesamte Registrierzeit um ein Vielfaches von 4 Stunden erhöhen läßt. Im Anschluß an die Tauchfahrt können die Daten über ein Handterminal abgefragt und auf einen PC, zur späteren Auswertung, transferiert werden (LINKE et al., in press).

Das Auslösen der Wasserschöpfer ist ebenfalls programmierbar, mit Intervallen zwischen einer und 120 Minuten, wobei die Auslöseintervalle zwischen allen 5 Wasserschöpfern konstant sind. Auf Metallteile innerhalb der Probenkammer konnte aus technischen Gründen leider nicht völlig verzichtet werden. Die runde Außenhülle wurde mit Tampen versehen, die das Aussetzen und Einbringen der Probenkammer erleichtern werden. Der Auslösemechanismus für den Schrittmotor und die Registrierung der CTD-Sonde wurden am Deckel angebracht, der durch Ziehen an einem Hebel aktiviert wird. An dem Hebel ist ein Auftriebskörper angebracht, der vom Greifarm des Tauchbootes erfaßt und gezogen werden kann. Die Ausführung dieses Details erfolgte in enger Zusammenarbeit mit Dr. F. Harmegnies (IFREMER, Brest), der über große Erfahrungen mit Einsätzen der NAUTILE verfügt und bei der NAUTIPERC-Tauchkampagne (März-April 1991) selbst teilnahm. Alle in der Probenkammer befindlichen Instrumente, wie Wasserschöpfer, CTD-Sonde und Motor, wurden bis 550 bar entsprechend 5500 m Wassertiefe getestet. Die Integration einer Thermistor-Strömungs-Sonde konnte zunächst aus finanziellen Gründen nicht realisiert werden, stand dann aber für den Einsatz auf der Reise 78 des FS SONNE (s. Kap. 2.2.3.) zur Verfügung. Die Probenkammer wurde termingerecht übergeben.

Abb. 3.2.2-3.2.4 Konstruktionszeichnungen (Fa. Hydro-Bios) der Probenkammer in Vorbereitung auf den Einsatz während der NAUTIPERC-Expedition

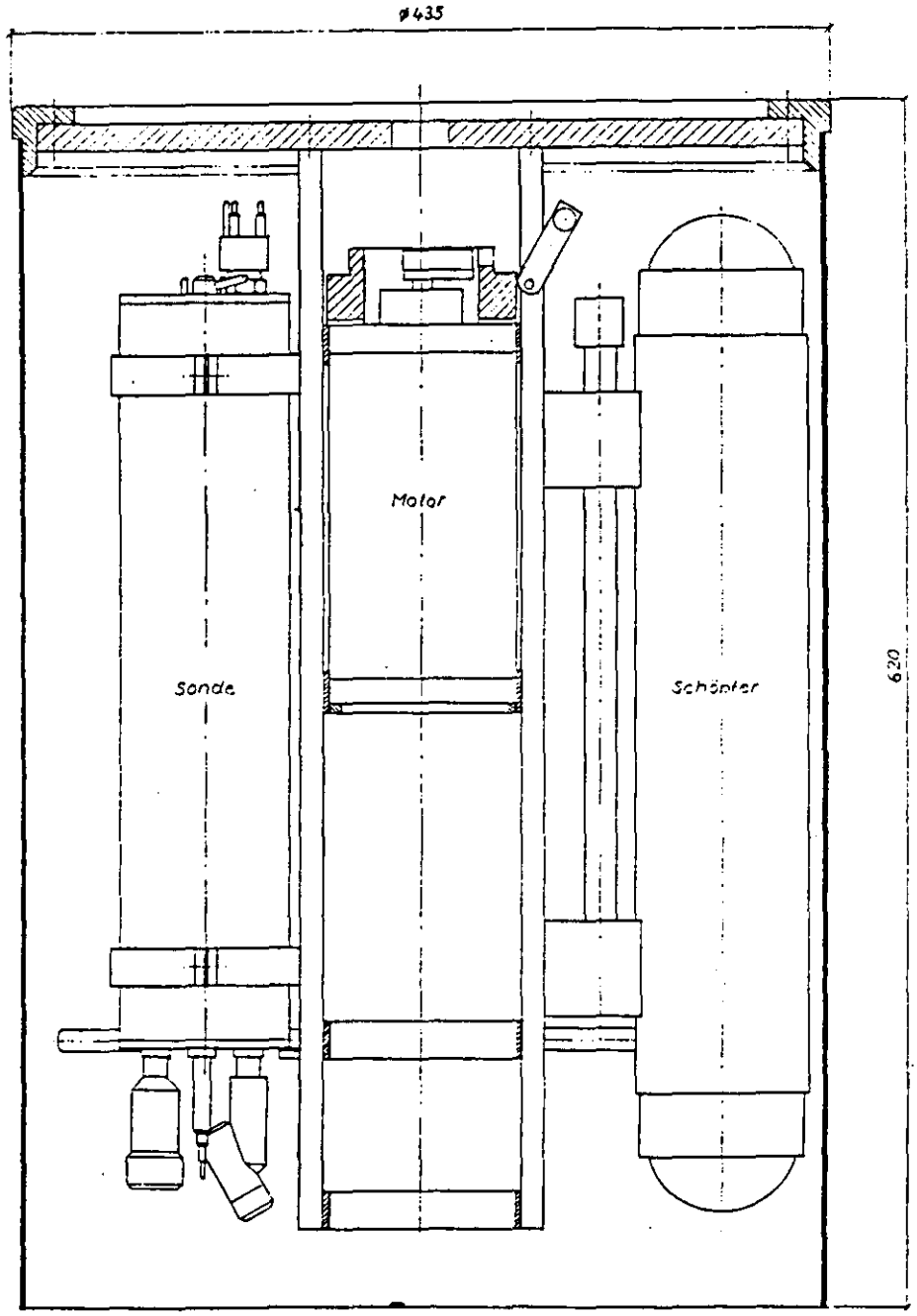

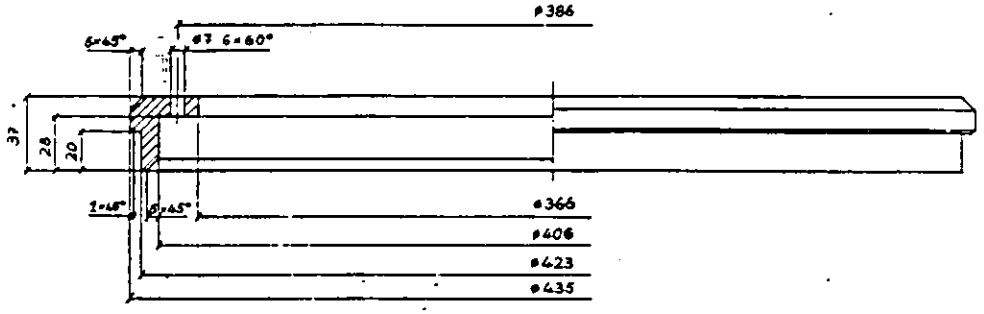

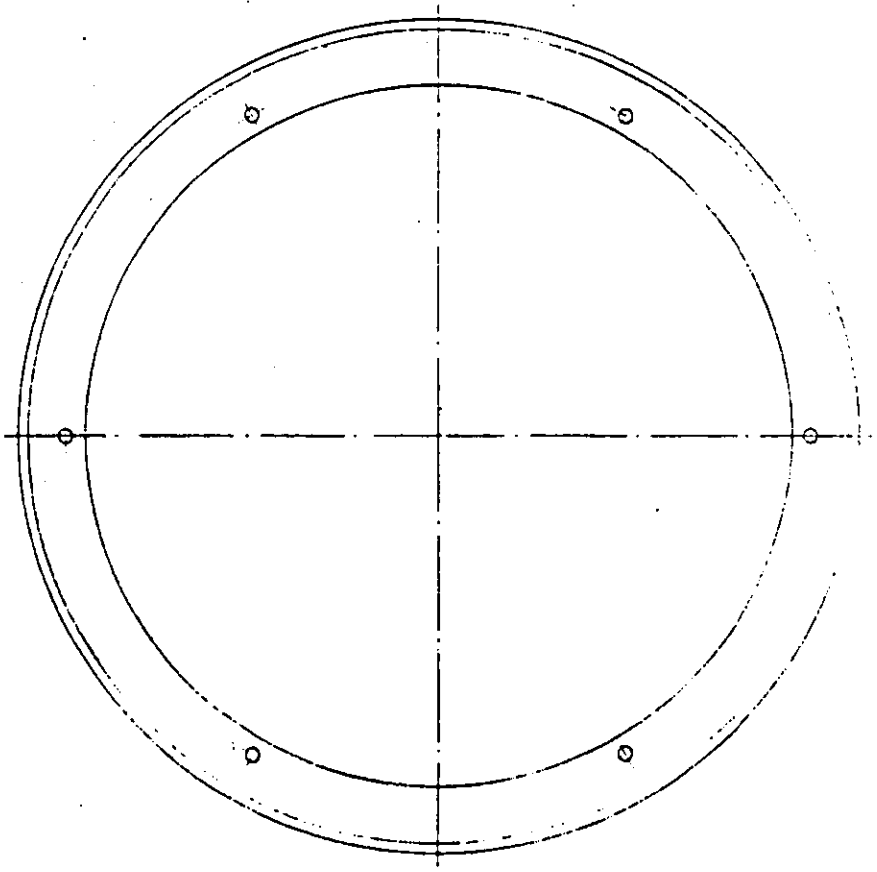

Maßstab 1:2	Gezeichnet	Datum 01.03.91	Name	
uds-Wasser-Schöpfer			Hülltring	
HYDRO-BIOS APPARATEBAU GMBH			Kataog-Nr.	Teil Deck. 1
				Werkstoff PVC

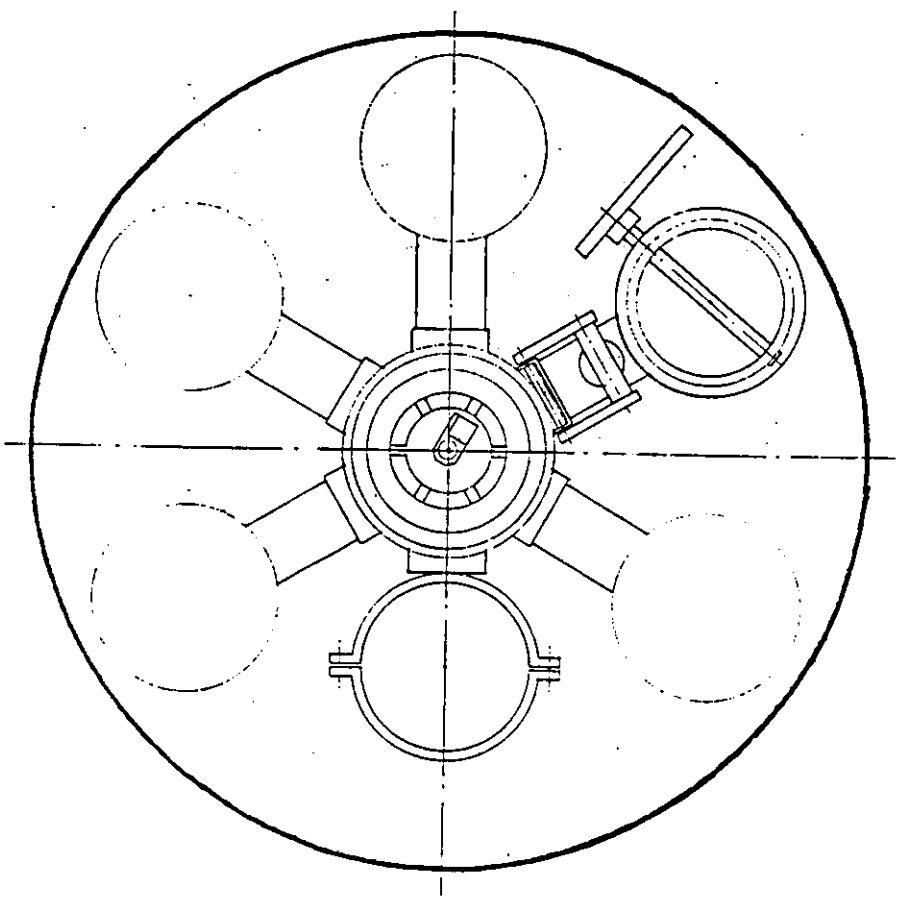

"Vent"-Beobachtungen während der NAUTIPERC-Expedition

Es folgt eine Zusammenfassung der mit dem Tieftauchboot NAUTILE gemachten Beobachtungen. Die Beobachtungen wurden durchgeführt (1) im Bereich zwischen dem Peru-Graben und der Mendaña-Bruchzone bei einer Wassertiefe von 6000m (NP-2-19), (2) am Kontinentalhang vor Chimbote bei 3800m Wassertiefe (NP-2-25) (3) und am Paita-Abhang bei 3600m Wassertiefe (NP-2-28, NP-2-29, NP-2-31, NP-2-35).

NP-2-19

Ziel: Bereich zwischen Peru Trench und Mendaña Bruchzone

Wassertiefe: 6000 m

Eine kontinuierliche N-S-Böschung, mit starker Sedimentbedeckung, bildet den steilen Abhang am Abhang-Graben-Übergang. Kein Hinweis auf Fluid-Austritte, weder durch Subduktion noch durch Wechselwirkung mit der Bruchzone. Die Probenkammer wurde nicht abgesetzt, aber Bodenwasserproben wurden mit Niskin- und Titanflaschen genommen.

NP-2-25

Ziel: Chimbote "vent site"

Wassertiefe: 3800 m

Eine Molluscen-Kolonie wurde exakt lokalisiert. Es ist anzunehmen, daß das "vent" tektonisch kontrolliert wird. Die Probenkammer wurde wegen eines elektronischen Defektes nicht abgesetzt. An einem Bakterien-bedeckten Absatz in 3636 m Wassertiefe wurde der Titan-Wasserschöpfer teilweise gefüllt.

NP-2-28

Ziel: Paita Escarpment

Wassertiefe: 3600 m

Die Absicht dieses Tauchgangs war es, Fluidproben mit der Probenkammer über einem aktiven "vent" in verschiedenen Zeitintervallen zu entnehmen. Die Probenkammer ging, durch einen mechanischen Fehler des Greifarmes, ca. 6m über dem Meeresboden verloren und konnte, aufgrund des steilen Hanges, während dieses Tauchganges nicht wiedergefunden werden.

NP-2-29

Ziel: Paita Escarpment

Wassertiefe: 3600

Während dieses Tauchganges wurde die Probenkammer wiedergefunden und erfolgreich aufgenommen. Die außerordentlich steilen Hänge, sowie die unebene Oberfläche erschweren das Absetzen der Probenkammer im Paita "vent"-Gebiet erheblich. Das Instrument wurde während des Absetzens kontinuierlich vom Greifarm festgehalten, obwohl dies Störungen durch das Tauchboot verursacht. Da der Schließmechanismus an zwei der Niskin-Flaschen versagte, wurde eine Serie von nur drei Proben gewonnen.

NP-2-31

Ziel: Paita Escarpment

Wassertiefe: 3600

Während dieses Tauchganges sollten hauptsächlich Temperatur-Gradienten gemessen werden. Es wurden zwei Versuche gestartet, um mit dem GEOMAR-Strömungsmesser direkte Ausstrommessungen durchzuführen. Der Absatz für 5min über einem Areal von 0,03m^2, wurde an zwei Stellen versucht. Es konnte jedoch kein meßbares Signal (in der Größenordnung von 2nl/min) erkannt werden. Es bleibt fraglich, ob ein zu geringer Fluid-Ausstrom, oder ein experimenteller Fehler, dafür verantwortlich war.

NP-2-35

Ziel: Paita Escarpment

Wassertiefe: 3600

Während dieses Tauchganges wurde ein erfolgreicher Probenkammer-Absatz durchgeführt. Die Topographie an dem ausgewählten Ort ist rauh und steil, so daß der Absatz erschwert wurde und das Gerät 2 Stunden am Ort gehalten werden mußte. Die chemischen und Isotopen-Daten dieses Einsatzes deuten auf eine Ausstromrate von ca. 200$Lm^{-2}day^{-2}$ hin. Die während des Einsatzes aufgezeichneten Temperaturen identifizieren die "vents" des Paita-Abhanges als "cold seeps".

3.3 Probenkammer-Einsatz von konventionellen Forschungsschiffen

Peter Linke

Eine Weiterentwicklung der Probenkammer sollte den Einsatz des oben beschriebenen Instrumentes von konventionellen Forschungschiffen aus ermöglichen und so unabhängig vom Einsatz eines Tieftauchbootes machen. Die Charter von Tieftauchbooten ist nur in Einzelfällen aufzubringen, und die Bundesrepublik Deutschland verfügt derzeit nicht über einen Tiefsee-Roboter (ROV: Remotely Operated Vehicle) mit Einsatztiefen bis 6000 m, über den ein solcher Einsatz möglich wäre. Für den weiteren Verlauf dieses Vorhabens bestand daher dringender Bedarf, die Probenkammer von konventionellen Forschungsschiffen aus einzusetzen.

Basierend auf Erfahrungen mit dem Multicorer sowie einem im Sonderforschungsbereich 313 speziell entwickelten Bodenwasserschöpfer (THOMSEN et al., in press) wurde eine Vorrichtung entwickelt (s. Abb. 3.3.5), mit der die Probenkammer an ein hydraulisch absenkbares Gestell angebracht wurde (VEnt SPider-VESP; LINKE et al., in press). Die Hydraulikvorrichtung bewirkt ein langsames Absenken der Probenkammer auf den Meeresboden. In Kombination mit einer Videokamera zur Bestimmung des Ortes der Probennahme wird sie über das bordeigene Koax-Tiefseekabel abgesenkt und mittels Telemetrieeinheit am Meeresboden abgesetzt und überwacht. Das Gerät ist zusätzlich mit einem Transponder ausgerüstet, damit über das schiffseigene Navigationssystem ständig die aktuelle Schiffs- und Geräteposition im akustischen Transpondernetz überwacht werden kann. Durch die Verbindung des Gerätes zum Forschungsschiff wurden hierdurch auch Einsätze über längere Zeiträume (bis zu 1 Std.) ermöglicht. Bei dieser Entwicklung waren die Erfahrungen aus den Einsätzen mit dem Bodenwasserschöpfer eine entscheidende Hilfe (THOMSEN et al., in press). Um die Verweildauer der Probenkammer am Meeresboden weiter zu erhöhen, wird zur Zeit an der technischen Realisierung einer Loslösung des Gerätes vom Schiff gearbeitet. Weiterhin erlaubt das bestehende Gerät an Stelle der Probenkammer auch einen konventionellen Multicorerkopf zur videounterstützten Entnahme von Sedimentkernen einzusetzen.

Abb. 5: EINSATZ DER PROBENKAMMER VON KONVENTIONELLEN FORSCHUNGSSCHIFFEN

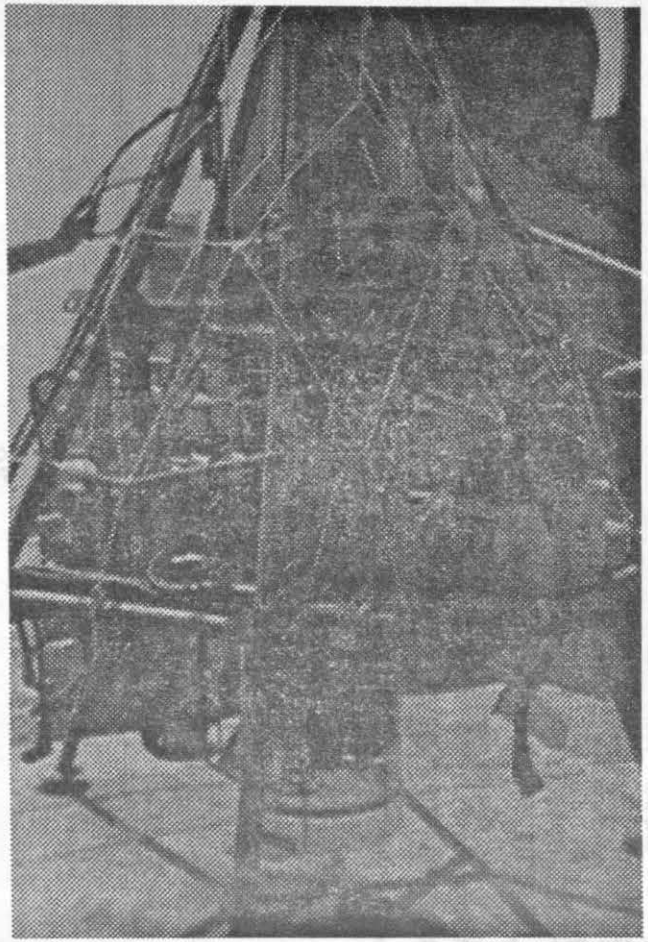

PROBENKAMMER MIT ABSATZGESTELL

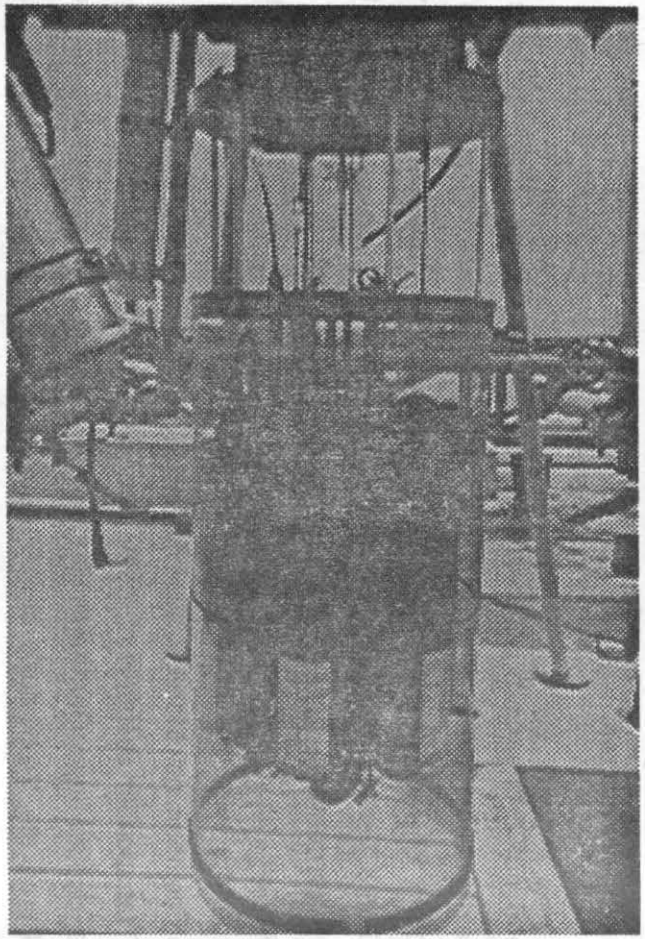

PROBENKAMMER MIT KLARSICHTHÜLLE

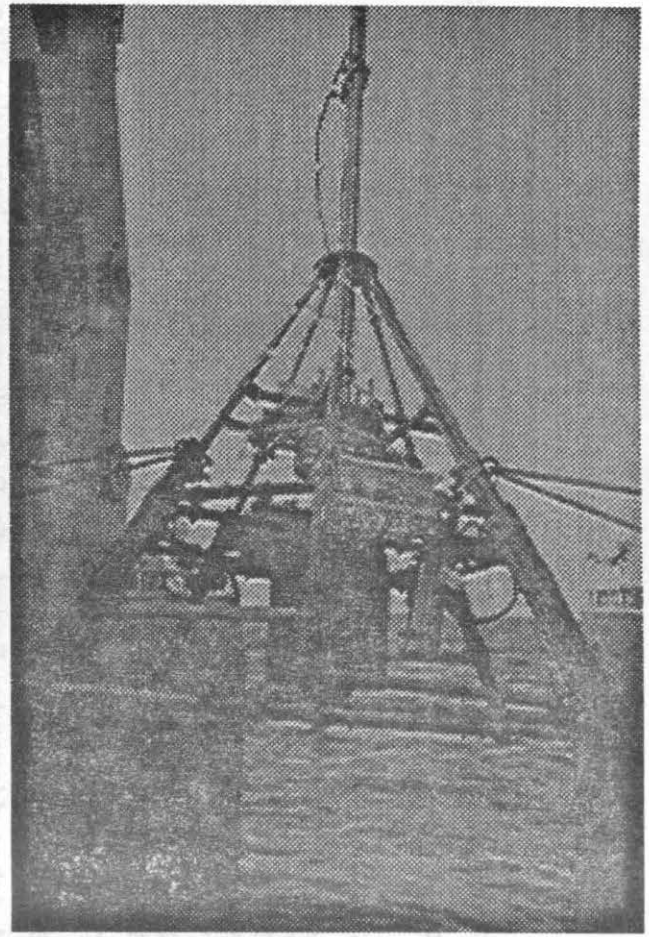

AUSBRINGEN VON VESP - VENTSPIDER

Das Absatzgestell (Fa. Scholz) und die nach dem Einsatz mit dem Tauchboot NAUTILE überarbeitete Probenkammer (Fa. Hydrobios) sowie die nun in die Speichersonde integrierte Thermistor-Strömungssonde (Fa. ADM) wurden erst kurz vor der Verschiffung zum Ersteinsatz auf dem Forschungsschiff SONNE (Reise 78) fertiggestellt. Der Einsatz auf dem Schiff erforderte erhebliche Vorbereitungen bei der Montage des Absatzgestells sowie der Anbringung der Videokamera, Telemetrie-Einheit, Energieversorgung und Transpondernavigation. Die Arbeiten wurden in vorbildlicher Weise durch die Deckschlosserei und die Elektronikwerkstatt der FS SONNE unterstützt.

VESP konnte auf dieser Reise auf insgesamt 14 Stationen eingesetzt werden; auf einem dieser Einsätze (#178-3) wurde das Gerät als Video-Multicorer gefahren (Tab. 3.3.2). Dies erscheint für die Zukunft ein äußerst vielversprechender Weg zu sein, in dem komplizierten Terrain aktiver "cold seeps" geologische und biologische Proben zu gewinnen.

Im Laufe der Expedition wurde mit jedem VESP-Einsatz das Gerät laufend verbessert. So erwies es sich als vorteilhaft, den Probennahmezyklus nicht über einen Magnetschalter, sondern über die Telemetrie-Einheit von Deck aus zu bedienen. Zudem erwies sich die Konstruktion des Absatzgestelles für den Einsatz als zu schwach. Besonders beim Aufnehmen des Gerätes kann durch einen schrägen Zug nach oben das Gerät über den Boden geschleppt werden, wobei die Beine einknicken. Durch zusätzliche Querverstrebungen des Gestells und Versteifungen der Beine konnte das Gerät durch Bordmittel für den Einsatz in dem rauhen Gelände optimiert werden. Weiterhin erwies sich die durchsichtige Plexiglas-Hülle der Probenkammer als zu stoßempfindlich und wurde daher durch eine rigide Polyäthylen-Hülle ersetzt. Das so verbesserte Gerät arbeitete daraufhin einwandfrei, und es konnten mit zunehmender Erfahrung beim Absetzen spezielle Kolonien der "cold seep" Organsimen beprobt werden.

Somit gelang es auf SO78 erstmals, die Weiterentwicklung der Probenkammer mit Hilfe eines video-geführten Absatzgestelles in einem akustischen Transpondernetz am Boden, für jeweils eine knappe Stunde auf den nur wenigen Quadratmetern großen Austrittsstellen abzusetzen, einen Probenahmezyklus zu starten und die Ausstromgeschwindigkeiten der Formationswässer zu registrieren.

Table 1. List of VESP-deployments, fluid sampling, data storage and recovery.

STATION	DEPTH (m)	DESCRIBITION OF DEPLOYMENT SITE	DURATION (MIN.) OF DEPLOYMENT/CYCLUS/STORAGE	WATER SAMPLES (BOTTLES #1-5)	STORED RAM DATA
152-17 (DISCOL)	4162 m	soft and fluffy sediment	31 / 5 / n.d.	contained sediment	all transferred
156-7 (PAITA I)	5171 m	mudstones	31 / 5 / n.d.	look good	n. d., switch failed
156-11 (PAITA I)	5189 m	soft and fluffy sediment	52 / 8 / n.d.	contained sediment	all transferred
163-2 (CHIMBOTE)	I. 3639 m	close to small nest of clams	39 / 15 / 31	#1 + 2 look good	files incomplete
	II. 3715 m	small nest of clams	32 /cyclus interrupted	#3+4, #5 water column	no data
168-2 (CHIMBOTE)	3672 m	bioturbated mudstone	52 / 8 / 54	look good	all transferred
176-4 (PAITA II)		VESP used as BWS, no deployment	- / 5 / 30	look good	all transferred
177-2 (PAITA II)	3352 m	Field of clams and serperlids	29 / 5 / 35	look good	all transferred
177-4 (PAITA II)	3267 m	rocky bottom, dead clams	39 / 5 / 40	#3 did not close	all transferred
177-7 (PAITA II)	3235 m	big field of clams & serperlids	43 / 5 / 40	look good	problems with CTD
178-3 (PAITA II)		VESP used as TV-MUC, very steep	no OSCAR-deployment	no samples	no data
180-1 (PAITA II)	3262 m	soft and fluffy sediment	38 / 5 / 35	no samples	no data, wrong cable
180-3 (PAITA II)	3286 m	big field of clams & serpulids	42 / 6 / 40	no samples	no data, wrong cable
180-4 (PAITA II)	3309 m	big field of clams & serpulids	45 / 6 / 38	very good	all transferred
180-5 (PAITA II)	3243 m	big field of serpulids	52 / 8 / 50	look good	all transferred

3.4 Temperature Probe

Marta Torres

Description of the probe

The SBE SEACAT S/N 989, was customized to contain three thermistors on a sting and a Validyne differential pressure sensor at the tip while deployed on a fixed position. The location of the three temperature sensors from the sting tip are: 50.8 mm, 355.6 mm and 457.2 mm for the bottom, middle and top sensors, respectively. The SEACAT main housing is a cylindrical pressure vessel having an outside diameter of 99 mm and flat end caps. The housing is hard-coat anodized aluminum (7075-T6 alloy), designed for use to depths of 6800 meters. It employs anodes for corrosion protection. SEACAT embodies the sensor elements and Weinbridge oscillator interface (U.S. patent No. 3,675,484). It allows for temperature measurements from -5 to 35 °C with an accuracy of 0.01 and a resolution of 0.001 °C. Powered by internal batteries, the SEACAT probe is capable of recording data for periods of a year or more. Data storage is in low standby-power CMOS static RAM; data may be acquired at intervals equal to any number of integer minutes. Communication with SEACAT is over a 3 wire RS-232 link. The program SCTERM is used to provide status display, data acquisition set-up, data retrieval and diagnostic tests.

Deployment via a multicorer frame

During the SO78 cruise, the heat probe was deployed using the main frame of a multicorer (BARNETT et al., 1984). This allowed for a smooth deployment at the seafloor and for the simultaneous recovery of 5 cores, which permit the determination of thermal conductivity measurements and sediment characterization. The frame is constructed from steel pipes connected by scaffolding clamps (K. SCHOLZ); it has a total height of 3.5 m and a base of 7 m^2. Prior to deployment the probe was checked and programed for taking temperature readings every 15 seconds via a portable computer. The frame was deployed and the probe was left in the sediments for a period of 10 minutes, to allow for temperature equilibration. The data was read immediately upon retrieval; the frequency data was converted to temperature using the calibrations provided by SBE (see appendix: calibrations 989a, 989b and 989c are for the bottom, middle and top sensors respectively). During the SONNE cruise 78, the probe was deployed 8 times in the DISCOL area, as indicated in Table 3.4.1. In all cases temperature data was successfully recorded; examples of the raw data are shown in Fig. 3.4.1 and 3.4.2.

Tab. 3.4.1 Lokalities of deployment of temperature probe

Station	Date	Latitude	Longitude	Depth (m)
150-MUC2	4.3.92	05° 30.08'S	85° 22.37'W	4080
150-MUC3	4.3.92	05° 30.13'S	85° 22.34'W	4080
151-MUC1	4.3.92	06° 34.14'S	86° 11.38'W	4132
152-MUC3	6.3.92	07° 04.42'S	88° 27.63'W	4187
152-MUC8	7.3.92	07° 03.66'S	88° 28.25'W	4170
152-MUC10	7.3.92	07° 04.45'S	88° 26.50'W	4202
152-MUC12	7.3.92	07° 03.32'S	88° 27.04'W	4130
152-MUC3	6.3.92	07° 04.42'S	88° 27.63'W	4187
176-MUC2	7.4.92	05° 37.00'S	81° 42.68'W	4262

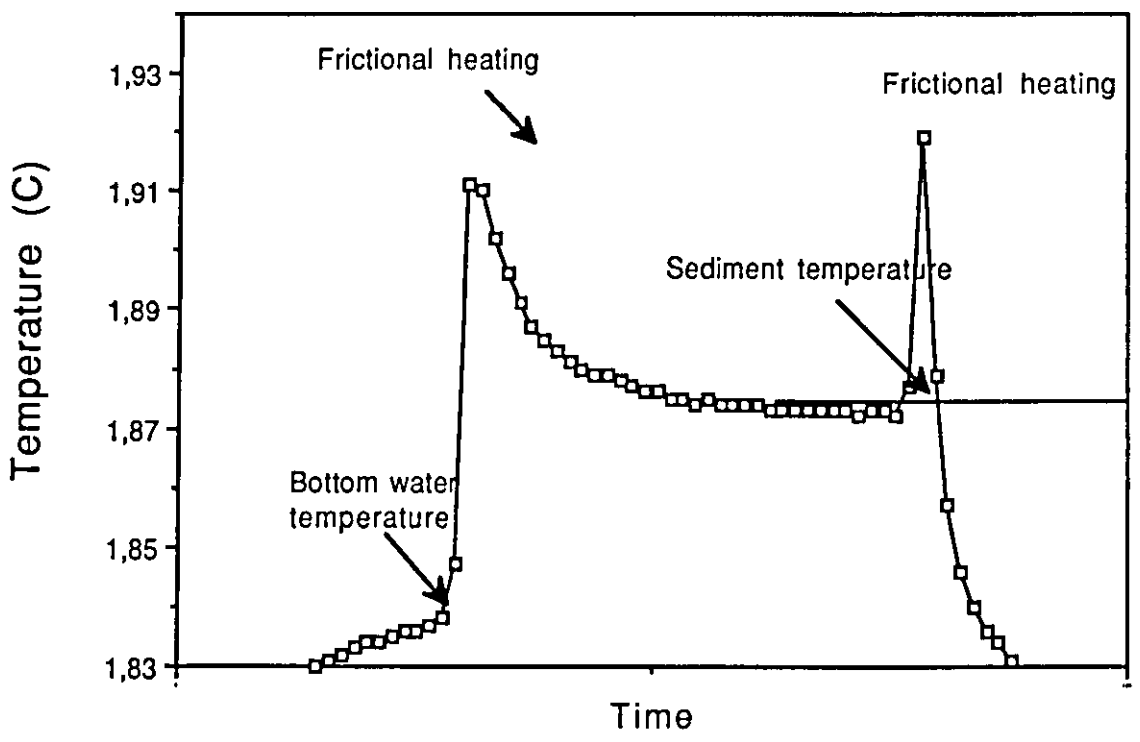

Fig.3.4.1: Raw data obtained by the temperature probe. Upon insertion on the sediments there is frictional heating, followed by a decay to the equilibrium temperature. The sediment temperature is the value extrapolated from the temperature plateau. During removal of the probe there is an additional heating effect.

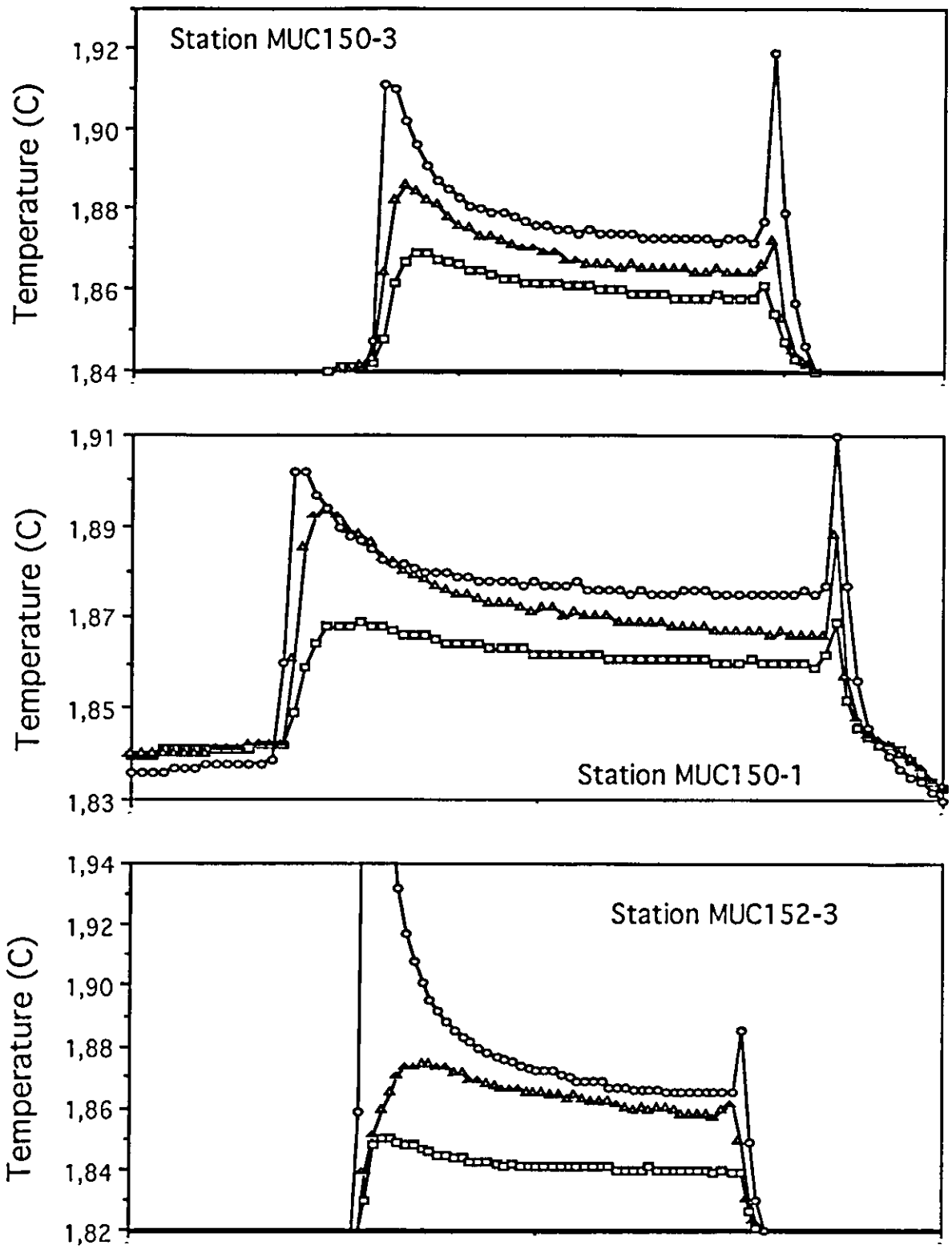

Fig. 3.4.2: Temperature data for the DISCOL deployments of the 3-thermistor sting. In all cases the temperature data for the deepest sensor is displayed by circles, the middle sensor by triangles and the uppermost sensor by squares.

Deployment in the Paita scarp zone was extremely difficult due to the morphology and rough surface at this location. Only one deployment in the lower slope region were soft sediments accumulated was possible; the data for this run (station 176-2) is shown in Fig. 3.4.3. In this situation, all three thermistors recorded the same equilibrium temperature.

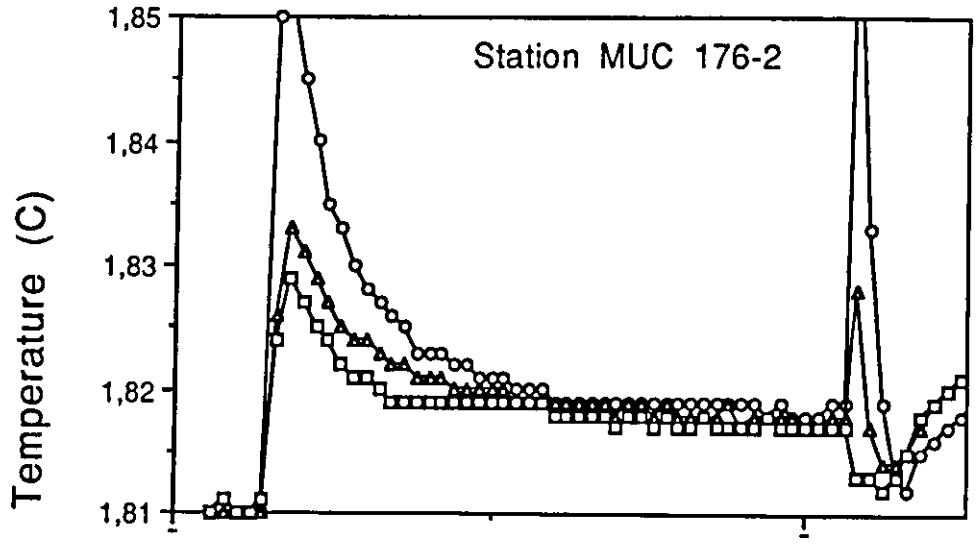

Fig. 3.4.3: Temperature data for the deployments of the probe in the lower slope of the Paita area. Note the equilibrium temperature is virtually the same for all thermistors, the symbols are those described for Fig. 3.4.2.

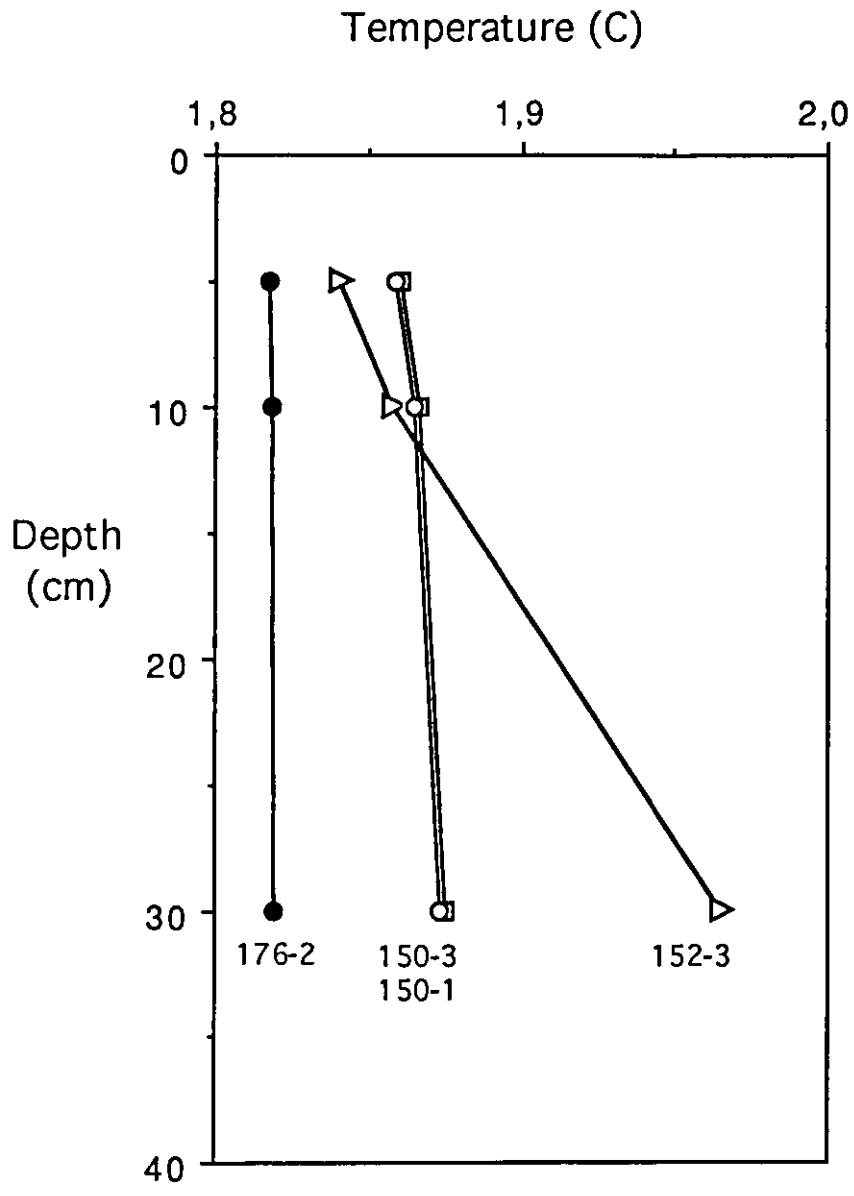

Fig. 3.4.4 Temperature gradients for three stations at the DISCOL area (150, 152 and 176), and the PAITA area (176-2); note excellent reproducibility of the data between subsequent deployments at station 150.

Summary

- The probe was succesfully deployed using the multicorer frame; the temperature data collected is of very high quality.
- No data was obtained in an active seep site, because of the rough nature of the terrain which precluded deployment of the probe.

4. FORTSCHRITTE ANDERER AUF DIESEM FORSCHUNGSGEBIET

Wegweisende Fortschritte auf dem Gebiet der tektonischen Entwässerung von Akkretionskeilen beruhen im Wesentlichen auf Untersuchungen im Rahmen des Ocean Drilling Programs (ODP) und Beobachtungen und Beprobungen von Tieftauchbooten aus. Bei den Fahrtabschnitten 131, 141 und 146 wurden mit Hilfe der JOIDES RESOLUTION an drei pazifischen Akkretionskeilen Bohrungen niedergebracht, um die physikalischen, chemischen und strukturell-tektonischen Bedingungen für den Fluidtransport zu erkunden. Tieftauchexpeditionen mit der ALVIN unter amerikanischer Führung oder der NAUTILE im Rahmen der französisch-japanischen Zusammenarbeit zielten auf eine Quantifizierung der austretenden Fluide und eine systematische Erfassung von "venting" mit topographischen und strukturellen Einheiten am Meeresboden hin.

4.1 Ergebnisse von ODP-Leg 131 im Nankai-Graben

Das Ziel von ODP-Leg 131 am Fuße des Nankai Akkretionskeils vor Japan war es, die Deformationsgeschichte und die assoziierten hydrogeologischen Prozesse zu untersuchen. Es war erstmalig gelungen, die Sedimentabfolgen eines Akkretionskeils bis ins Grundgebirge zu durchbohren. Aus den Porenwasseranalysen lassen sich keine diskreten Entwässerungsbahnen gashaltiger Fluide ablesen, vielmehr wird ein diffuser aufwärtsgerichteter Stoffffluß durch weite Bereiche des Akkretionskeils angenommen. Zwischen dem Meeresboden und 600 m Teufe ist nur wenig Methan vorhanden. Das Kohlenstoff-Isotopensignal deutet auf biologischen Ursprung hin. Längerkettige Kohlenwasserstoffe, wie Ethan und Propan, treten ab 380 m unter dem Meeresboden gemischt mit biogenen Gaskomponenten auf. Unterhalb 1020 m ist nur noch thermogenes Gas vorhanden. Die Gas-Zusammensetzung läßt erkennen, daß die thermogenen Gase in den Tiefenintervallen von 600 bis 800 m und 1060 bis 1280 m *in situ* aus dem organischen Material gebildet werden (TAIRA, HILL, et al., 1991).

4.2 Fluid migration in a thermally and tectonically driven regime at the Chile Triple Junction (ODP Leg 141)

The region of the Chile Trench between about 45° 40' S and 47° S is the site of a collision between the actively-spreading Chile Ridge and the Chile Trench subduction zone. The subduction of an active spreading ridge brings together two of the most active hydrogeological systems: the thermally-driven convective system of the mid-ocean ridge and the predominantly compaction-driven system of an accretionary wedge.

ODP drilling was conducted in five sites in the Chile Triple Junction region during ODP Leg 141. Three sites are located on an east-west transect of the collision zone: one near the base of the trench slope (Site 859), one in the mid-slope region (Site 860), and one on the upper slope of the margin (Site 861). Site 862 is located on the crest of the Taitao ridge, and Site 863 was drilled on the lowermost trench slope, this site is positioned over the rift axis in the subducted rift zone.

Drilling at the Chile Triple Junction produced a vast array of downhole geological, geophysical and geochemical data that document the extremely complex and rapidly changing deformational and hydrothermal processes related to ridge subduction. Research in this area addresses fundamental questions on physical processes and chemical reactions through which fluid flow is responsible for metal deposits, hydrocarbon migration, and tectonic behavior of the rocks via fracturing and cementation. For example, the dissolved chloride distributions reflect a complex fluid regime characterized by fluid migration from deep sources which might have been modified by a variety of yet unquantified processes that include present and past hydrate formation, clay dehydration, and perhaps dissolution of evaporite or hydrothermal deposits.

Site 863 drilled over the subducting ridge constitutes a unique setting for the study of an active fluid-flow field in conjuction with changes in metal and sulfur concentrations within the fluids and their interaction with the parent rock. Pore fluid chemistry at Site 863 indicates that a substantial amount of fluid is migrating upward from deep within the subduction zone to the shallow structural levels. The sulfide-rich sediments recovered in the upper 45 mbsf are indicative of deposition of sulfide-rich fluids of a probable hydrothermal origin. Since the paleomagnetic signal resides in iron oxide and iron sulfide phases, an understanding of the formation of sulfide deposits in this setting is essential to unravel the paleomagnetic signal at this site (LEWIS, BEHRMANN et al., 1992).

4.3 Ergebnisse von ODP-Leg 146 entlang der Cascadia-Subduktionszone

Im Herbst 1992 wurden im Rahmen von Leg 146 der JOIDES RESOLUTION vor der NW-Küste der USA (Cascadia Margin) an drei Lokationen insgesamt 9 Bohrungen abgeteuft (Sites 889-891). Ziel der Bohrungen war es, die Beziehungen zwischen Flüssigkeitsbewegungen und der Tektonik im Akkretionskeil der konvergenten Plattenbegrenzung zu untersuchen.

Die Bohrungen 889A-889D und 890A und 890B vor Vancouver Island hatten zum Ziel, die Veränderungen der Porosität in den deformierten und akkretierten Sedimenten im Zusammenhang mit den Flüssigkeitsbewegungen zu untersuchen und einen in 235 Tiefe gelegenen bottom-simualting-reflector (BSR) vor Vancouver Island zu durchteufen und dessen thermisches, chemisches und hydrogeologisches Umfeld zu erkunden. Chlorid-Anomalien und die Gehalte an Gasen (Methan, Ethan und Propan), sowie Bohrloch-geophysikalische Messungen deuten daraufhin, daß der BSR durchbohrt wurde, obgleich keine Proben des Gashydrats gewonnen werden konnten. Die Bohrungen erbrachten neue Hinweise über den Zusammenhang zwischen dem seismischen Abbild von BSR's und dem Druck- und Temperatur-Stabilitätsfeld von Gashydraten.

Bei den Bohrungen 891A-891C vor Oregon standen Fragen nach den Transportwegen von Flüssigkeiten und darin gelöster Gase im Akkretionskeil im Vordergrund. Hierzu wurden die Bohrungen in unmittelbarer Nähe zur heutigen Deformationsfront abgeteuft und Temperaturbestimmungen, *in situ*-Permeabilitäten der Verwerfungsfläche und die Veränderungen der sedimentphysikalischen Eigenschaften im strukturgeologischen Kontext und der Diagenese untersucht. Mit Hilfe von Porenwasseruntersuchungen lassen sich die erbohrten Sedimente in zwei Zonen unterteilen, die in keinem Stoffaustausch miteinander stehen. In der unteren Zonen, die tiefer als 200 m unterm Meeresboden liegt, deuten erhöhte Methan-Konzentrationen und die Präsenz von langkettigen Kohlenwasserstoffen auf thermogene (hydrothermale) Kohlenwasserstoffbildung und advektiven Transport hin. Die vorhandenen ungesättigten Kohlenwasserstoffe, die über geologische Zeiträume instabil sind, implizieren, daß die Fluide jünger sind als 5.000 Jahre und somit das Zirkulationssystem im Akkretionskeil aktiv ist. Unterschiede der Element-Konzentrationen in verschiedenen Teufen sind ein weiteres Indiz für den advektiven Fluß entlang permeabler Verwerfungs-flächen.

Um die zeitliche Entwicklung des Fluidchemismusses im Akkretionskeil der Cascadia-Subduktionszone zu verfolgen, wurden Bohrlochversiegelungen (Site 889 und 891) angebracht, die im Sommer 1993 geöffnet werden sollen. Im Vordergrund der Untersuchungen steht die erstmals durchgeführte Öffnung und geochemische Beprobung der

Bohrlochversiegelungen CORK durch das Tieftauchboot ALVIN. Die wissenschaftlichen Ziele sind die Quantifizierung des Fluidausstromes, mittels neuentwickelter Strömungsmesser, die Bestimmung des, durch die tektonische Entwässerung bedingten, Stoffflusses von z.B. CH_4 und CO_2 sowie die Bildung und Desintegration fester Methanhydrate. Die zeitliche Entwicklung des Fluid-Chemismusses soll durch Untersuchungen der Spurenelementzonierung in Hartschalen von "vent"-Organismen abgeleitet werden. Entsprechende Vorarbeiten wurden an "vent"-Organismen durchgeführt, die E. Suess 1986, 1987 und 1990 bei ALVIN-Expeditionen vor Oregon beprobte (CARSON, WESTBROOK et al., 1993).

4.4 Die tektonische und thermische Struktur des Kontinentalrandes vor Peru bei 12° S

Im Rahmen eines ODP- und eines PROCOPE-Projektes wird die Subduktionszone vor Peru mit unterschiedlichen modernen geophysikalischen Methoden (Reflexionsseismik, Finite Elemente Prozeßmodellierung, Sandkastenanalogmodellierung) mit den folgenden Zielsetzungen untersucht:

- Ermittlung der tektonischen Struktur anhand von seismischen Profilen
- Berechnung der vertikalen Wärmeflußdichte aus der Tiefe des Bottom Simulating Reflektors (BSR)
- Modellierung des Temperatur- und Fließfeldes
- Rekonstruktion der Entwicklungsgeschichte

Reflexionsseismik

Mit modernen Processing-Verfahren (Pre-Stack Tiefenmigration, Geschwindigkeitsanalyse) werden mehrere Profile, die den Bereich des Peru-Trenchs, des Kontinentalabhanges und des Lima-Beckens umfassen, bearbeitet.

Abbildung 4.4.1 zeigt die Interpretation des seewärtigen Teils eines der bearbeiteten Profile (Shell 1017). Man erkennt, wie auf allen anderen Profilen in diesem Bereich, deutlich einen BSR, der die Basis der Stabilitätszone von Methangashydraten anzeigt. Klar zu identifizieren sind in diesem Profil auch die subduzierte ozeanische Platte, subduzierte Sedimente, das kontinentale Kristallin, ein Bereich mit Abschiebungen (landwärts) und Backthrusting (seewärts) oberhalb des Kristallins sowie die Grenzen des Akkretionskeils.

Die stratigraphische Zuordnung der Sedimentpakete im landwärtigen Teil dieses Profilabschnitts erfolgte anhand von Bohrungen in Höhe des benachbarten Profils 1018 im Rahmen von ODP Leg 112 (SUESS, v. HUENE et al., 1988). Die tektonische Struktur des bearbeiteten Gebietes, die stratigraphisch-petrographische Zuordnung sowie die thermischen oberflächennahen Verhältnisse, die aus der Lage des BSR abgeleitet werden können, gehen in numerische Modellrechnungen zum Fluid- und Wärmetransport ein und sind auch Grundlage für den Aufbau von Sandkastenmodellen.(v. HUENE, and LEE, 1983; KLÄSCHEN, BELYH, et al., 1993).

Sandkastenmodell

Die Rekonstruktion der tektonischen Struktur eines konvergenten Plattenrandes kann mit Hilfe eines Analogmodelles verifiziert werden, das in sich konsistente Ergebnisse liefert. Grundlage des Einsatzes von Sandkastenexperimenten zur experimentellen Untersuchung der Entstehung und des Wachstums eines Akkretionskeils ist die Anwendung der Skalenunabhängigkeit der Coulomb-Theorie.

Im Experiment wird nach dem Aufbau eines Anfangszenarios, in dem die idealisierte Struktur der Subduktionszone vor Beginn der Akkretion wiedergegeben wird, die ozeanische Platte auf den Buttress (= Kontinentaler Kristallinkeil) zubewegt, d. h. unter einem vorgegebenen Winkel subduziert. Dabei lagert sich ein Teil der ankommenden Sedimente vor dem Buttress an und bildet den wachsenden Akkretionskeil, während ein anderer Teil Underplating oder Subduktion erfährt. Der jeweilige Anteil, die Struktur des Akkretionskeils, der sich einstellende Hangwinkel sowie die auftretenden Deformationserscheinungen sind eine Funktion der systemrelevanten mechanischen Parameter, etwa innerer Reibung der beteiligten Materialien, basaler Reibung oder Kohäsion. Die Miteinbeziehung des Porendrucks als weiterer für die Berechnung des kritischen Winkels des Keils relevanter Parameter erfolgt über thermohydroelastische und hydrothermaler FE-Modellrechnungen.

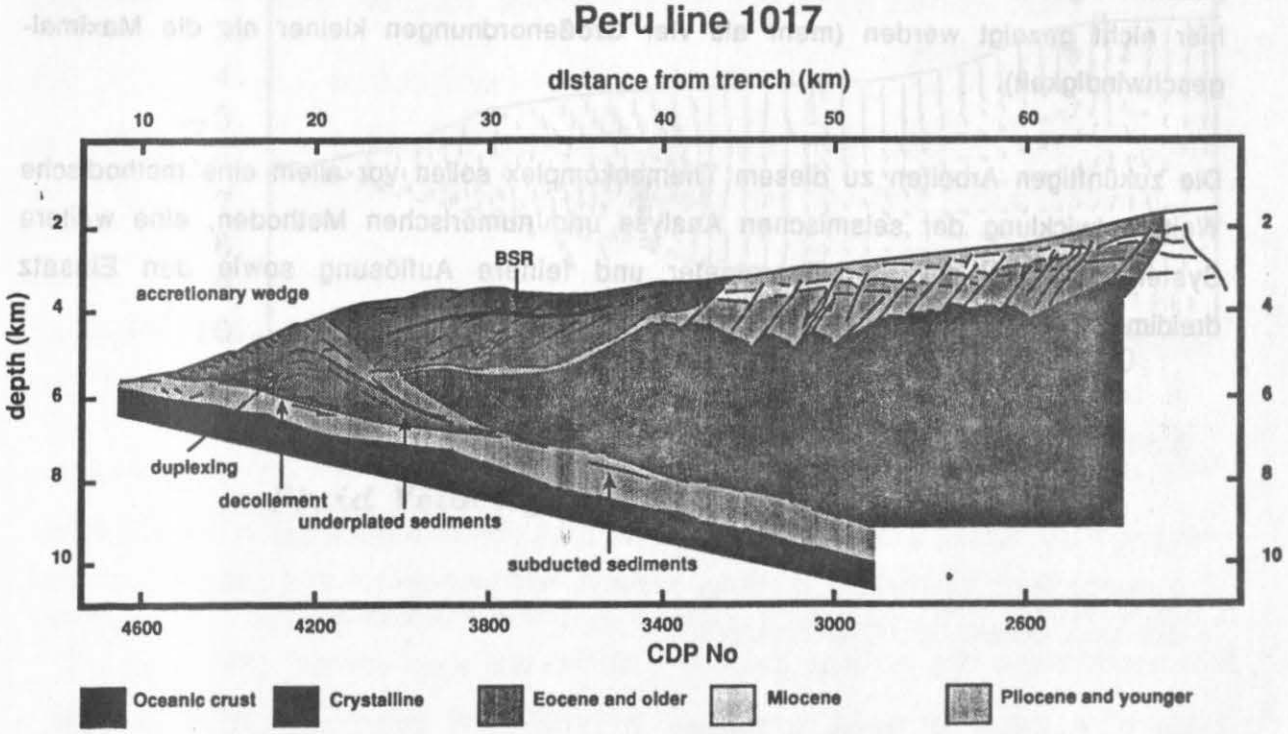

Abb. 4.4.1 Interpretation des seewärtigen Teils des Profils Shell 1018

Numerische Prozeßmodellierung

Die Quantifizierung des Fluid- und Wärmetransportes und die Ermittlung des Temperaturfeldes im tieferen Untergrund erfolgt mit Hilfe von gekoppelten zeitabhängigen finite Elemente Modellrechnungen. Dabei ist eine sehr feine räumliche Diskretisierung der physikalischen Systemparameter (Matrixwärmeleitfähigkeit, Matrixwärmeproduktion, Permeabilität, Porosität, Kompressibilität) möglich.

Die Rechnungen zeigen, daß der Fluidtransport vor allem durch erzwungene Konvektion als Folge tektonischen Antriebs und hervorgerufen durch Permeabilitätsunterschiede erfolgt. Ein regionaler Temperaturanstieg zum Kontinent ist wahrscheinlich auf höhere Wärmeproduktionsraten zurückzuführen, während kleinräumige Variationen im Temperaturfeld aus lokalen Zonen hoher Permeabilität herrühren.

Es bilden sich strukturgesteuerte großräumige Konvektionszellen aus. Dabei kann es, wie im gezeigten Beispiel, zu Umkehrungen der Fließrichtung im Décollement kommen. Fluidgeschwindigkeiten in der schlecht permeablen ozeanischen Kruste sind so gering, daß sie hier nicht gezeigt werden (mehr als vier Größenordnungen kleiner als die Maximalgeschwindigkeit).

Die zukünftigen Arbeiten zu diesem Themenkomplex sollen vor allem eine methodische Weiterentwicklung der seismischen Analyse und numerischen Methoden, eine weitere Systematisierung der Modellparameter und feinere Auflösung sowie den Einsatz dreidimensionaler Modellierungsmethoden beinhalten.

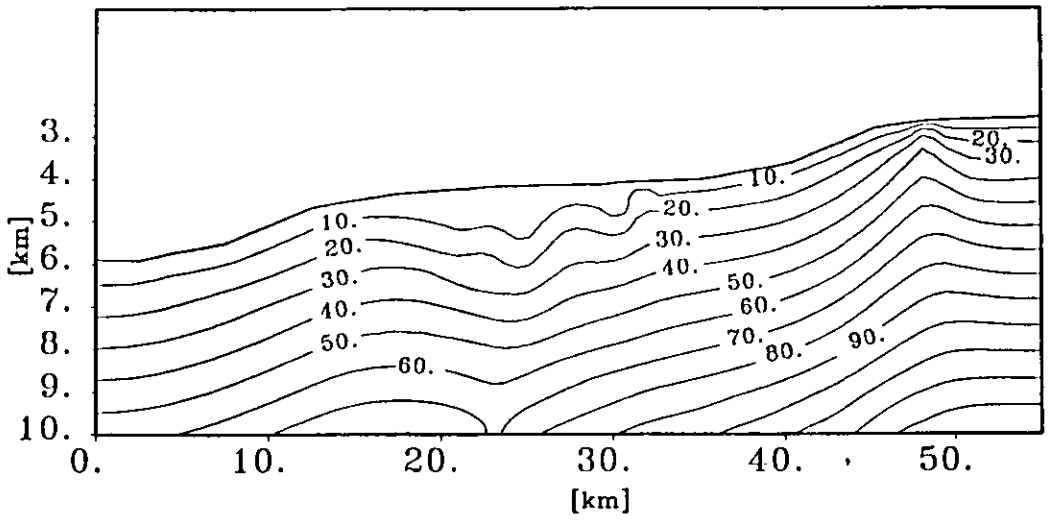

Temperature Field, Peru1152

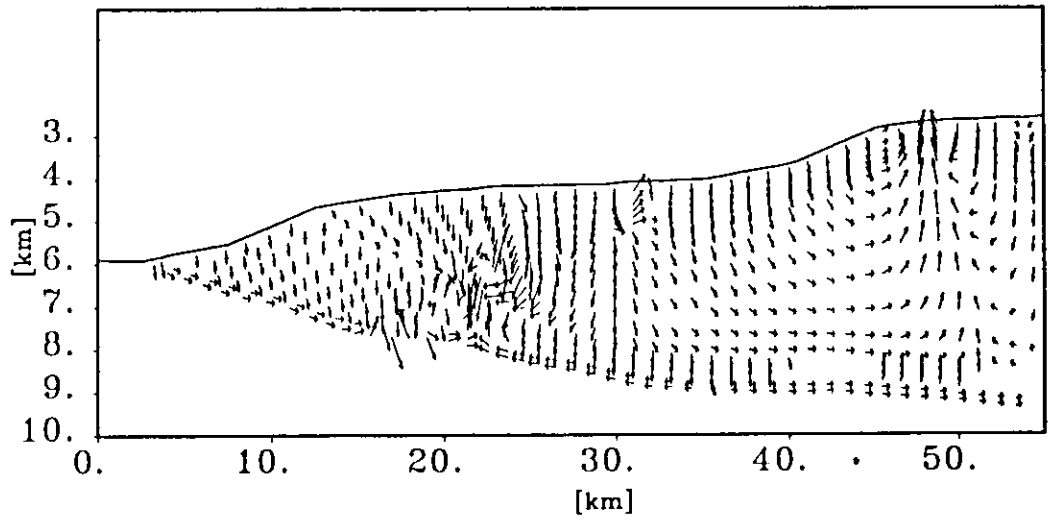

Fluid Velocity, Peru1152

Abb. 4.4.2 Temperaturfeld auf dem Profil Shell 1018 (a), der die im oberen Modellgebietsbereich angetroffenen thermischen Verhältnisse, wie sie aus seismischen Daten abgeleitet wurden sowie das zugehörige Fließfeld (Abstandsgeschwindigkeiten) (b).

5. LITERATUR

Während der Laufzeit dieses Vorhabens wurden auf dem Gebiet der tektonischen Entwässerung wichtige neue Erkenntnisse gesammelt. Eine Reihe von Beiträgen wurde im Rahmen der Konferenz *Fluids in Subduction Zones* vorgestellt und gebündelt in einem Sonderband von *Earth and Plantary Science Letters* ,Vol. 109 von Le Pichon und Kastner herausgegeben. Die *American Geophysical Union* hat bei ihren Herbst- und Frühjahrstreffen jeweils ganze Sessions dem Thema Fluide in Akkretionskeilen gewidmet. Durch die ODP-Legs 131 (Nankai-Graben), 141 (Chile Tripple Junction) und 146 (Cascadia Margin) ist eine Vielzahl von Untersuchungen zum Themenkomplex der tektonischen Entwässerung erschienen oder in Vorbereitung.

5.1 Eigene Veröffentlichungen

Bourgois, J., Y. Lagabrielle, P. De Wever, and E. Suess, 1992. Tectonic history of a non-accreting active margin during the past 400 ka. Results of a submersible survey of the Peru Trench at 5-6° S. Part 1, Geology.

Dia, A. N., L. Aquilina, E. Suess, M. Torres, and J. Boulègue, J. Bourgois, 1992.Continent-derived fluids from the convergent margin off Peru. Deep sea dives of the Nautiperc cruise, Part 2, Geology.

Hempel, P., and E. Suess, 1993 (zum Druck eingereicht). Dewatering of sediments along the Cascadia Margin - Evidence from geotechnical properties. Proc. Init. Res., ODP, 146, Ocean Drilling Program, College Station, TX.

Hempel, P., 1992. Characteristics of gas-charged sediments in the Skagerrak. In: Weydert, M. (Ed.) Proc. European Underwater Acoustics Conference, Luxembourg,14.-18.9.1992, Elsevier, 513-517.

Hempel, P., V. Spieß, and R. Schreiber, 1992. Expulsion of shallow gas in the Skagerrak - evidence from sub-bottom profiling, seismic, hydroacoustical and geochemical data. Estuarine, Coastal, and Shelf Sciences.

Linke, P., E. Suess, M. Torres, V. Martens, W. D. Rugh, W. Ziebis, and L. D. Kulm, 1993.*In situ* measurement of fluid flow from cold seeps at active continental margins. Deep-Sea Res. (in press).

Torres, M., A.N. Dia, Boulegue J., L. Aquilina, and E. Suess, 1992. Barite deposits from the Peru subduction zone.

Kurzfassungen

Aquilina, L., A. Dia, J. Boulègue, A. M. Fouillac, E. Suess, and J. Bourgois, 1992. Geochemistry of Baryte and Carbonate deposits associated with fluid vents in the Peru Convergent Margin off Paita. EOS 73 (14 Suppl.): 153.

Bourgois, J., F. Michaud, M. v Breymann, E. Suess, R. v. Huene, Y. Lagabrielle, T. Juteau, J. P. Foucher, F. Harmegnies, P. Chotin, P. de Wever, E. Fourcade, B. de Lepinay, M. Sosson, L. Aquilina, A. Dia, J. Machare, and F. Monge, 1992. Northern Peru Convergent Margin: Massive slides from the upper plate into the Trench Axis observed from a submersiblel EOS 73 (14. Suppl.): 152.

Dia, A. N., L. Aquilina, J. Boulègue, E. Suess, M. von Breymann, and J. Bourgois, 1992. Fluids from the Peru subduction zone vents: Trace element and isotopic constraints. EOS 73 (14 Suppl.): 153.

Duperret, A., J. Bourgois, Y. Lagabrielle, and E. Suess, 1993. Induced polyphased mega-submarine slides along the northern Peruvian margin. Discussion of the role of tectonic erosion and others processes. Seventh biennial meeting of the European Union of Geosciences Strasbourg, 4.-8. April 1993.

Hempel, P., P. Linke, M. Schumann, E. Suess, and M. Torres, 1993. *In situ* obervations of venting at the convergent margin off Peru. Geol. Vereinigung, Berlin, 25.-27. Feb. 1993. Terra Nostra, 1/93.

Hempel, P., 1992. Sedimentologische und sedimentphysikalische Untersuchungen von der Cascadia-Subduktionszone. ODP-Schwerpunktkolloquium der DFG, Hamburg 3.-5. März 1992.

Lammers, S., 1993. Methane in the water column as an indicator for active vents. Geol. Vereinigung, Berlin, 25.-27. Feb. 1993. Terra Nostra, 1/93.

Suess, E., M. T. von Breymann, P. Linke, R. Bayer, L. Aquilina, A. Dia, J. Boulègue, and J. Bourgois, 1992. Venting rates and chemistry of fluids from the convergent margins off Peru and Oregon. EOS 73 (14 Suppl.): 153.

Suess, E., R. von Huene, M. Torres, and P. Linke, 1993. Convergent margin dewatering: Discrepancy between tectonic estimates and *in situ* measurements. Geol. Vereinigung, Berlin, 25.-27. Feb. 1993. Terra Nostra, 1/93.

Torres, M., and G. Bohrmann, 1993. Barite deposits in the Peru subduction zone. Geol. Vereinigung, Berlin, 25.-27. Feb. 1993. Terra Nostra, 1/93.

von Breymann, M. T., E. Suess, A. Dia, H. Brumsack, and J. Bourgois, 1992. Barium transport by fluids through sediments of the Peru continental margin based on the distribution of authigenic barites. EOS 73 (14 Suppl.): 153.

Wagner, C. C.,1993. Fluid venting at the Oregon and Peru margin: imprints on biogenic material. Geol. Vereinigung, Berlin, 25.-27. Feb. 1993. Terra Nostra, 1/93.

5.2 Verwendete Veröffentlichungen

Beck, J.W., R.L. Edwards, E. Ito, F.W. Taylor, J. Recy, F. Rougerie, P. Joannot and Ch. Renin, 1992. Sea-surface temperature from coral sceletal strontium/calcium ratios. Science 257:644-647.

Boulegue, J., Mariotti, A., Fiala, A. and Bourgois, J., 1992. Geochemistry of clams from subduction zones. EOS 73, 153

Bourgois, J., Lagabrielle, Y., DeWever, P., Suess, E. and the NAUTIPERC Cruise Shipboard Scientists, 1992. Tectonic history of a non-accreting active margin during the past 400 ka, Results of a submersible survey of the Peru trench at 5-6°. Part 1. Geology (in press).

Carson B., E. Suess and J. Strasser, 1990. Fluid flow and mass flux determinations at vent sites on the Cascadia Margin accretionary prism. Journal of Geophysical Research, 95, 8891-8897.

Carson, B., G. K. Westbrook and Scientific Party of ODP Leg 146, 1993. Leg 146 Preliminary Report. Ocean Drilling Program, 46, 100p.

Cicerone, R.J. and Oremland, R., 1988. Biogeochemical aspects of atmospheric methane. Global Biogeochemical Cycles, 2: 299-327.

Colten-Bradley V.A., 1987. Role of pressure in smectite dehydration - effects on geopressure and smectite-to-illite transformation. AAPG Bulletin, 71, 1414-1427.

Conrad, R. and Seiler, W., 1988. Methane and hydrogen in seawater (Atlantic Ocean). Deep-Sea Res., 35(12): 1903-1917.

Davis, E. E., R. D. Hyndman, H. Villinger, 1990. Rates of fluid expulsion across the northern Cascadia accretionary prism: Constraints from new heat flow and multichannel seismic reflection data. Journal of Geophysical Research, 95 A2, B6, 8869-8889.

Dia, A. N., Aquilina, L., Suess, E., Torres, M., Boulegue, J., Bourgois, J. and the NAUTIPERC Shipboard Scientists. 1992. Continent-derived fluids from the convergent margin off Peru. Deep sea dives of the NAUTIPERC cruise, Part 2. Submitted to Geology.

Elderfield, H.; Kastner, M., and Martin, J.B., 1990. Compositions and Sources of fluids in sediments of the Peru subduktion zone. J. Geophys. Res., 95, 8819-8827.

Forster, S., 1991. Die Bedeutung biogener Strukturen für den Sauerstoffffluß ins Sediment. Ber. Inst. f. Meereskunde, Univ. Kiel, Nr. 206, 98pp.

Gieskes, J.M., Blanc, G., Vrolijk, P., Elderfield, H., and Barnes, R., 1990. Interstitial water chemistry-Major constituents, Proceedings of ODP, Final Reports, Part B, vol. 110, Ocean Drilling Program, College Station, TX.

Gieskes, J.M.; Vrolijk, P., and Blanc, G., 1990. Hydrogeochemistry of the Northern Barbados Accretionary Complex Transect: Ocean Drilling Project Leg 110. J. Geophys. Res., 95, 8809-8818.

Goldhaber, M.B. and Kaplan, I.R., 1980. Mechanisms of sulfur incorporation and isotope fractionation during early diagenesis in sediments of the Gulf of California. Mar. Chem., 9:95-143.

Jones, D.S., D.F. Williams, and C.S. Romanek, 1986. Life history of symbiont-bearing giant clams from stable isotopes profiles. Science 231:48-48.

Kastner, M., H. Elderfield, J. B. Martin, E. Suess, K. A. Kvenvolden, and R. E. Garrison, 1990. 25. Diagenesis and interstitial water chemistry at the Peruvian continental margin-major constituents and Strontium isotopes. Proceeding of the Ocean Drilling Program, Scientific Results 112, 413-440.

Kläschen, D., Belyh, I., Gnibidenko, H., von Huene, R., and Patrikeyev, S., 1993. Structure of the Kuril Trench drom seismic reflection records (in prep.).

Kukowski, N., Pecher, I. A., and R. von Huene, 1993. On the characteristics of fluid flow in the Peruvian continental margin at 12°S. Submitted to Geologische Vereinigung.

Kukowski, N., Pecher, I. A., Huene, R. von, Klaeschen, D., and J. Malavieille, 1992. The Peruvian continental margin after subduction of the Nazca Ridge: I. Tectonic evolution and assessment of heat flow from reflection seismic data. II. Mechanical and dynamic-thermal modelling.13. Lateinamerika Kolloquium, Münster.

Kulm, L.D., E. Suess, J.C. Moore, B. Carson, B.T. Lewis, S.D. Ritger, D.C. Kadko, T.M. Thornburg, R.W. Embley, W.D. Rugh, G.J. Massoth, M.G. Langseth, G.R. Cochrane, and R.L. Scamman, 1986. Oregon Subduction Zone: Venting, fauna, and carbonates. Science, 231:561-566.

LaBarbera M., and S. Vogel, 1976. An inexpensive thermistor flowmeter for aquatic biology. Limnology and Oceanography, 21, 750-756.

Lawrence, J.R., and Taviani, M.,1988. Extreme hydrogen, oxygen and carbon isotope anomalies in the pore waters and carbonates of the sediments and basalts from the Norwegian Sea: Methane and hydrogene from the mantle? Geochim. Cosmochim. Acta, 52, 2077-2083.

Le Pichon, X., Kobayashi, K. and the Kaiko-Nankai scientific crew, 1992. Fluid venting activity within the eastern Nankai trough accretionary wedge: A summary of the 1989 Kaiko-Nankai results. Earth and Planet. Sci. Letter, 109: 303-318.

Lewis, S, Behrmann et al., 1992. Regional tectonic setting and drilling objectives for ODP Leg 141, Chile Margin Triple Junction. EOS, 73, (43): 592.

Linke, P., E. Suess, M. Torres, V. Martens, W.D. Rugh, W. Ziebis, and L.D. Kulm, 1993: *In situ* measurement of fluid flow from cold seeps at active continental margins. Deep-Sea Res. (in press).

McCready, R.D.L., and Krouse, H.R., 1980. Sulfur isotope fractionation by *Desulfovibrio vulgaris* during metabolism of $BaSO_4$. Geomicrobiology Jour., 2: 55-61.

Mehra, O.P., and Jackson, M.L., 1960. Iron oxide removal from soils and clays by a dithionite-citrate system buffered with sodium bicarbonate. Clays & Clay Minerals 7, 317-327.

Mitzutani, Y., and Rafter, A., 1973. Isotopic behavior of sulfate oxygen in the bacterial reduction of sulfate. Geochem. Jour., 6:183-191.

Niitsuma N., Y. Matsushima, and D. Hirata, 1989. Abyssal molluscan colony of *Calyptogena* in the Pliocene strata of the Miura Peninsula, central Japan. Palaeogeogr. -climatol. -ecol. 71:193-203.

Owens, N.J.P., Law, C.S., Mantoura, R.F.C., Burkill, P.H. and Llewellyn, C.A., 1991. Methane flux to the atmosphere from the Arabian Sea. Nature, 354: 293-296.

Rasmussen, R.A. and Khalil, M.A.K., 1984. Atmospheric methane in recent and ancient atmospheres: Concentrations, trends, and interhemispheric gradient. J. Geophys. Res., 89: 599-605.

Reimers, C., and Suess, E., 1983. Spatial and temporal patterns of organic matter accumulation on the Peru continental margin. In: Suess, E. and Thiede, J. (Eds), Coastal Upwelling, Its Sediment Record, Part A. NATO Conf. Ser. IV, Mar. Sci., 10A: 311-346.

Romanek, C.S., and E.L. Grossmann, 1989. Stable isotope profiles of *Tridacna maxima* as environmental indicators. Palaios 4:402-413.

Ruby, E.G., H.W. Jannasch, and W.G. Deuser, 1987. Fractination of stable isotopes during chemoautotrophic growth of sulfur-oxidizing bacteria. Applied and Environmental Microbiology, 53:1940-1944.

Saino, T., and S. Otha, 1989. $^{13}C/^{12}C$ and $^{15}N/^{14}N$ ratios of vesicomyid clams and a vestimentiferan tube worm in the subduction zone east of Japan. Palaeogeogr. -climatol. -ecol. 71:169-178.

Savin, S.M., 1967. Oxygen and hydrogen isotope ratios in sedimentary rocks and minerals. Ph.D. Thesis, California Institute of Technology.

Schmitt, M., Faber, E., Botz, R., and Stoffers, P., 1991. Extraction of methane from seawater using ultrasonic vacuum degassing. Anal. Chem., 63 (5): 529-531.

Stewart, G.L. (1972). Clay-water interaction, the behavior of ^{3}H and ^{2}H in adsorbed water, and the isotope effect. Soil Science Society of Am. Proc. 36, 421-426.

Stul, M.S., and Van Leemput, L., 1982. Particle-size distribution, cation exchange capacity and charge density of deferrated montmorillonites. Clay Minerals 17, 209-215.

Suess, E., and von Huene, R., 1988. Ocean Drilling Program Leg 112, Peru continental margin: Part 2, Sedimentary hystory and diagenesis in a coastal upwelling environment. Geology, 16, 939-943.

Taira, A., Hill, J., et al., 1991. Proceedings of the Ocean Drilling Program, Init. Repts.131, College Station (Ocean Drilling Program).

Thomsen, L., Graf, G., Martens, V., and Steen, E., 1993. An instrument for sampling water from the Benthic Boundary Layer. Cont. Shelf Res. (in press).

van der Land, J., and A. Nørrevang, 1977. Structure and relationships of *Lamellibrachia* (Annelida, Vestimentifera). Det Kongelige Danske Videnskabernes Selskab Biologiske Skrifter 21,3 102 pp.

von Huene, R., and Lee, H. J., 1983. The possible significance of pore fluid pressure in subduction zones. Am. Ass. Pet. Geol. Mem., 34, 781-791.

Wefer, G., and W.H. Berger, 1991. Isotope paleontology: growth and composition of extant calcareous spezies. Mar. Geol., 100:207-248.

Wefer, G., 1985. Die Verteilung stabiler Isotope in den Kalkschalen mariner Organismen. Geol. Jahrb., 82(A), 114 pp.

Ziebis, W., 1992. Experimente im Strömungskanal zum Einfluß der Makrofauna auf den bodennahen Partikeltransport. Ber. Sonderforschungsbereich 313, Univ. Kiel, Nr. 37, 83pp.

6.1. Anhang

6.1.1 GEOCHEMISTRY OF BARITE AND CARBONATE DEPOSITS ASSOCIATED WITH FLUID VENTS IN THE PERU CONVERGENT MARGIN

L. Aquilina, A. N. Dia, J. Boulègue, A.-M. Fouillac, E. Suess, M. v. Breymann, J. Bourgois

During the Nautiperc cruise various samples were collected along the continental margin of North Peru at depth ranging from 5400 m to 2500 m, it includes 1) indurated and soft sediments including carbonate cements associated with indurated layers, and 2) barite deposits located in biological colonies.

Thin section observations coupled with microprobe and chemical analyses (major, trace element and carbon, oxygen and strontium isotopic measurements) were performed on these samples.

The sediments related to biological communities can be distinguished from the "local" sediments on the basis of the carbonate, Fe and trace metal contents. This can be related to H_2S and trace metal enrichtments in the sediments recovered in the colonies.

In the indurated layers the dolomitic cement is characterized by positive $\partial^{13}C$ which can be related to diagenesis of organic matter-rich sediments. Calcite deposits due to later fracturation have high Ba content in association with negative $\partial^{13}C$.

In the Paita area and in the Chiclayo canyon, large barite deposits are occurring either at the surface of the sediment or as breccia cement. The high $^{87}Sr/^{86}Sr$ ratios which have been measured in this study on these barites clearly imply that the fluids responsible for these deposits should have mostly leached continental derived minerals and have few strontium from marine origin.

6.1.2 GEOCHEMISTRY OF CLAMS FROM SUBDUCTION ZONES

J. Boulègue, A. Mariotti, A. Fiala, J. Bourgois

Clams were collected at several subducion zones: Japan, Barbados, Peru. The analyses performed on shells and soft tissues are: bulk composition, trace metals, C- and O-isotopes, ^{14}C. Soft tissues were also analyzed for: N-isotopes, methanol dehydrogenase activity, ATP sulfurilase. Ultrastructures of soft tissues were observed by SEM and TEM.

All clams appear to be relying on sulfide based chemoautotrophy through symbiotic bacteria associated with their gills. H_2S is most often provided via decomposition of gas hydrate. Carbon isotopes of soft tissues are all in the range $\partial^{13}C$ = -34 to -39 ‰ (vs PDB). $\partial^{15}N$ depends on nitrogen source: ambient N_2 or N_2 from thermal decomposition of organic matter. Several trace metals are associated to sulfide metabolism: Cd, Zn, Ag, Ba; and to N_2 consumption: Mo, V.

^{14}C of soft tissues indicates that carbon is mostly derived from dissolved CO_2 of bottom water. Input of deep seated carbon via oxidation of methane is limited to less than 10 % of total carbon of soft tissues and shells.

Variations of isotopic compositions of nitrogen of soft tissues at different locations off Japan can be related to plumbing of the vent system in the Nankai subduction area.

6.1.3 NORTHERN PERU CONVERGENT MARGIN: MASSIVE SLIDES FROM THE UPPER PLATE INTO THE TRENCH AXIS OBSERVED FROM A SUBMERSIBLE

J. Bourgois, F. Michaud, M. v. Breymann, E. Suess, R. v. Huene, Y. Lagabrielle, T. Juteau, J. P. Foucher, F. Harmegnies, P. Chotin, P. de Wever, E. Fourcade, B. de Lepinay, M. Sosson, L. Aquilina, A. Dia, F. Monge

Observations from 28 dives with the NAUTILE deep submersible during the Nautiperc Cruise (March-April, 1991) confirm the indications from SeaBEAM bathymetry and seismic records of a massive tsunamogenic slide in the Peru Trench. That slide must have involved at least 315 km^3 of Neogen rock from the mid-slope area which catastrophically slid from 3000 to 5300 m depth.

The middle slope topography is marked by two prominent fault scarps. The upper one is actively slipping and conducts fluids to the seafloor where they now actively vent. The 800 m of slip measured here along a listric normal fault detaches a down-dropped and back-rotated block measuring about 15 by 30 km. The front of the block failed catastrophically during faulting and produced a 30 km wide debris avalanche that flowed 23 km down to the trench axis.

The toe of the slide was observed and sampled during one dive in the trench axis and consists of consolitaded rock from the middle slope area. This slide debris covered the plate boundary and was subsequently thrust faulted during plate movement, after the slide. A reconstruction of movement on that thrust shows that its scarp could be constructed in roughly 10.000 - 12.000 yr.

Five dives across the plate boundary scarp recorded continiuous active slope failure, pervasive fracture, and extensive fluid venting. The estimated 35 cm/yr rate of uplift on the scarp produces

a unique submarine failure morphology not recorded by surface ship instrumentation. Debris aprons from slope failure and pelagic sediment cover the seafloor where the plate boundary should emerge at the surface. Only after rising 200 m from the seafloor at the trench to the top of the slope apron can the fluid channeled along the plate boundary thrust vents to the seafloor. The hydraulic lift must elevate the existing fluid pressure along the plate boundary and may explain the high decoupling which exists between the upper plate and the lower plate in this area.

6.1.4 FLUIDS FROM THE PERU SUBDUCTION ZONE VENTS: TRACE ELEMENT AND ISOTOPIC CONSTRAINTS

A. N. Dia, L. Aquilina, J. Boulègue, E. Suess, M. v. Breymann, J. Bourgois

Extensive geophysical, geochemical, geological and biological studies were conducted from the deep submersible Nautile across the Andean convergent margin off Northern Peru.

19 active fluids emanating from the accretionary wedge have been recovered from depth ranging from 5400 m to 2500 m. Vent sites were discovered closely associated with biological communities and often characterized by presence of large barite deposits.

Mg, Ca, Sr, Ba, Li, K, Rb, Mn, Cu, Mo and Cd contents have been measured in these fluids and showed variations as compared to bottom seawater. The chloride content of the fluids collected in the Paita and Chiclayo areas is higher than the content measured in the reference seawater. The Ba content measured in these same samples exhibits large variations with strong enrichment as compared to seawater. Variations in the Ba concentrations of fluids have to be related to the precipitation of authigenic barites in proximity to the fluid venting.

Furthermore, oxygen, hydrogen and strontium isotopic measurements have been performed on the fluid samples. The Sr isotopic results provide the evidence of radiogenic source (at least for one of the components) for the fluids. Reactions between seawater and continental derived material can be suggested to explain such high $^{87}Sr/^{86}Sr$ rations in the fluids. The fluids responsible for the deposit of the barite has mostly a continental derived component origin.

6.1.5 INDUCED POLYPHASED MEGA-SUBMARINE SLIDES ALONG THE NORTHERN PERUVIAN MARGIN. DISCUSSION OF THE ROLE OF TECTONIC EROSION AND OTHERS PROCESSES

A. Duperret, J. Bourgois, Y. Lagabrielle, E. Suess

Previous seismic (Miller et al., 1986), bathymetric (Bourgois et al., 1986; von Huene et al., 1989) and submersible data acquired along the active margin of northern Peru have been merged

with a hydrosweep survey of the R/V Sonne cruise 78, which extends from 5°15'S to 6°10'S, along the Paita area. The data reveal the occurence of three major curved scarps. They are respectively named from upslope to the trench: upper slope scarp (USS), middle slope scarp (MSS) and lower slope scarp (LSS).

The area located below the USS shows a dome-shaped slope profile combined with a curved directional fabric. This structural pattern could result from a gravitational mass movement, which occurs along the USS.

The MSS extends for 40 km along the middle slope area with an average slope gradient varying from 10° to 30° over a distance of 1 km. The slide covers the entire lower slope and extends widely southward across the trench axis. The main part of rock slide is assumed to have come from the MSS.

The LSS is located 14 km eastward from the trench. It appears as an amphitheatre-shaped scarp of 6 km length along which an entire detached block of about 500 m heigth has slid down.

The overal geometry of the LSS is remarkably similar to that produced experimentally by Malavielle and Calassou (1992). A sand box experiment reproduced the subduction of oceanic horsts and graben under a stable margin subjected to basal erosion. Then, a well define amphitheatre-shaped scar was induce at the edge of the margin subjected to basal erosion. These results suggested that the failures are highly retrogressive, originating on the lower slope and progressevely expanding upslope to the middle slope.

The initial instability is most probably produced by frontal erosion and possibly basal erosion due to the subduction of oceanic horsts and graben. However, the upward progression of such failures may be also controlled by the peculiar structure of the northern Peruvian margin in the Paita area.

6.1.6 BIOLOGICAL COMMUNITIES ASSOCIATED WITH COLD VENTS IN THE PERU TRENCH

A. Fiala-Médioni, M. Sibuet, M. Segonzac, J. Bourgois

Spots of biological activity were observed during the Nautile dives of the Nautiperc Cruise (March-Avril 1991) in the Peru Trench. The more common and densest activities were found in the Paita zone between 3000 and 5200 m. The biological activities are clearly associated with major tectonic features such as main faults and represent indicators of fluid venting.

On the lower slope, many clam colonies with up to 80-100 individuals are half buried in sediments extending along fractures or among eboulis. These large elongated clams (12-16 cm long) belong to one species of *Calyptogena* which is close to *C. phaseoliformis*. Solemyid shells are frequent in this zone.

The main biological activity was found in the middle slope between 3500 m and 3600 m with the largest site extending along a fault covered by eboulis (180 m long and about 25 m large). Colonies (up to 800-1000 individuals per m^2) of clams 4-12 cm (*Calyptogena* n. sp.) and clusters of Serpulids (12-15 cm high) are the main organism. Galatheids, anemones and annelid worms are associated with the clam-serpulid community. Bacterial spots were especially frequent in this zone around small venting holes.

On the middle slope, medium sized *Calyptogena* clams (*C. laubieri*) and small *Vesicomya*, completely buried in the sediment, were collected in cores.

6.1.7 *IN SITU* OBSERVATIONS OF VENTING AT THE CONVERGENT MARGIN OFF PERU

P. Hempel, P. Linke, M. Schumann, E. Suess, M. Torres

In situ observations of vent sites with their specific benthic community and sea floor settings were made by a camera system attached to the deep diving submersible NAUTILE and the remotely operated OFOS (Ocean Floor Observation System) during SONNE cruise 78. Surveys were made at a steep scarp face off Paita, generated by a giant land slide, where gas and water expulsion occurs and at a site in proximity to the subduction zone where lateral compaction processes lead to the expulsion of gas-charged water at the seafloor. Vent sites are dominated by the occurence of great populations of the clam *Calyptogena* and widespread bacterial mats. Active venting can be distinguished from extinct sites by the dominance of dead or alive clams. Single vent sites are a couple of meters across and are separated by distances ranging from a few meters to tens of meters. The great number of vent sites indicates that venting is a widespread phenomenon along the convergent margin off Peru. To quantify the contribution of the escaping gases to the ocean's budget a watersampler combined with a flow meter was positioned by means of OFOS at the vent sites.

6.1.8 SEDIMENTPHYSIKALISCHE UND SEDIMENTOLOGISCHE UNTERSUCHUNGEN VON DER CASCADIA-SUBDUKTIONS-ZONE

P. Hempel

Sedimentphysikalische und sedimentologische Untersuchungen an Sedimentkernen vom Kontinentalhang vor Oregon und Washington (Cascadia Margin) geben Einblick in die Prozesse der tektonischen Entwässerung und der Genese von verfestigten, oberflächennahen Horizonten. Den Schwerpunkt der Untersuchungen bilden die Scherfestigkeits- und Wassergehaltsverteilungen in den Sedimenten, als Abbild der tektonischen Beanspruchung. Diese beiden Sedimentparameter liefern wichtige Hinweise auf die Fluidbewegungen im oberflächennahen Bereich des Akkretionskeils und der Quantifizierung des Fluid- und Gasausstromes am Meeresboden.

In den Scherfestigkeitsprofilen sind die drei tektonischen Einheiten entlang des konvergierenden Kontinentalrandes deutlich erkennbar: (1) Die undeformierte Tiefsee-Ebene mit geringen -, mit zunehmender Teufe leicht ansteigenden Scherfestigkeiten , (2) dem Bereich der Deformationsfront, mit extrem hohen Scherfestigkeiten in geringer Sedimenttiefe und (3) den Deformationsrücken mit erhöhten Werten gegenüber denen von der Tiefsee-Ebene. Ebenso charakteristisch verhalten sich die Wassergehaltsprofile.

In einer Reihe von Sedimentkernen sind erhebliche Wassergehaltsunterschiede zwischen den unverfestigten und verfestigten Sedimentabfolgen erkennbar. Hohe Wassergehalte treten in den unverfestigten siltig-tonigen Abschnitten auf; geringe Wassergehalte in den verfestigten sandig-siltigen Horizonten. Die höheren Wassergehalte deuten auf einen erhöhten Wassertransport in den unverfestigten Schichten hin. Der Hauptentwässerungsstrom innerhalb des Akkretionskeils erfolgt sicherlich entlang der zahlreichen Verwerfungsflächen und nur zu einem geringen Anteil in den feinkörnigen Sedimentpaketen.

Die Entstehung der verfestigten Horizonte ist auf die Entwässerung und Entgasung am Meeresboden direkt zurückzuführen.

6.1.9 CONVERGENT MARGIN DEWATERING: DISCREPANCY BETWEEN TECTONIC ESTIMATES AND *IN SITU* MEASUREMENTS

E. Suess, R. v. Huene, M. Torres, P. Linke

Dewatering mechanisms and rates of accreted sediment are fundamental parameters during plate convergence. Estimates of steady-state dewatering over geologic time scales are in the range of 10^{-3} to 10^{-2} L• m^{-2} • day^{-1}based on actual porosity reduction , derived porosity reduction from seismic velocity models, or from heat transport models.

For the first time, data on actual fluid venting rates at the Cascadia and the Peru margins are now available from in situ deployment of flow meters by deep submersible and remotely by surface ships. A sufficiently large number of point measurements indicate rates of flow of between 10^2 and 10^3 L · m^{-2} · day^{-1}.

This large a discrepancy can be reconciled by invoking focussed dewatering (i.e. along fault- or lithology-controlled vents) and projecting the point measurements to <1% of the area of convergent margins and by requiring recirculation (i.e. recharge zones) in certain convergent tectonic settings.

6.1.10 VENTING RATES AND CHEMISTRY OF FLUIDS FROM THE CONVERGENT MARGINS OFF PERU AND OREGON

E. Suess, M. T. v. Breymann, P. Linke, R. Bayer, L. Aquilina, A. Dia, J. Boulègue, J. Bourgois

Active venting of fluids and gases has been documented and measured with *in situ* benthic chamber from different tectonic settings along two segments of the prominent eastern Pacific convergent margins. Extensive biological, geophysical, and geochemical studies accompanied these measurements made by the deep submersibles ALVIN, off the Cascadia margin and NAUTILE, off the South American continental margin. Off Peru fluids emanate from the accretionary wedge at >5000 m of depth and from a failure slope scarp at 3500 m. Off Oregon a vent site was observed which is fed by a decomposing gas hydrate layer on the landward accretionary ridge in 680 m of water. This discovery adds to the vents already known from the Cascadia margin at the deformation front: (>2500 M) and the seaward accretionary ridge (2046 M).

The fluid and gas chemistries from the *in situ* banthic chamber deployments indicate a large range of methane expulsion from <2 to >2000 g m^{-2} y^{-1}. The hydrate vent off Oregon showed gas phase separation indicating that methane is at saturation as the fluids exit to the seafloor; at all other sites methane is dissolved and transported by the vent water. Fluids from the hydrate vent off Oregon also showed a chloride decrease consistent with its source as gas hydrate water.

Off Peru a slight decrease in dissolved chloride and sulfate indicate that the fluids may originate from the same onoxic interstitial waters that characterize the organic-rich upwelling sediments and which were encountered during ODP drilling. The helium isotopic signatures, with values as light as -13% ∂^3He (off Oregon) and +14% ∂^3He (off Peru), strongly support a fluid source from the sediment for these accretionary sites. The initial deformation front of Oregon, however, shows an oceanic crustal signature of +23% ∂^3He. Barium, strontium, calcium, sulfate, sulfide, ammonium, oxygen and ΣCO_2 concentrations from the benthic chamber deployments illustrate the enormous complexity of biogeochemical turnover reactions at these "cold" seep sites.

6.1.11 BARIUM TRANSPORT BY FLUID THROUGH SEDIMENTS OF THE PERU CONTINENTAL MARGIN BASED ON THE DISTRIBUTION OF AUTHIGENIC BARITES

M. T. v. Breymann, E. Suess, A. N. Dia, L. Aquilina, J. Boulègue, H. Brumsack, J. Bourgois

Venting of fluids on a slope failure scarp in 3500 m of water on the Peru continental margin off Paita has been thoroughly documented by biological, geophysical, and geochemical studies. The interaction of the barium-rich sulfate-depleted vent fluids with seawater results in the precipitation of barite chimneys near the venting sites. Similar deposits have been reported in the Gulf of Mexico and the Sea of Okhotsk, also in association with fluid seeps.

ODP drilling had previously recovered several modes of authigenic barites in the sediments of the Peru margin, an area where intensive high productivity results in a large flux of biogenic barium to the ocean floor. In sediments undergoing strong anoxic diagenesis this labile biogenic-barium concentrations in the pore fluids at Sites 683, 685 and 688. Upward barium diffusion to the sulfate reducing zone leads to the *in situ* formation of crystalline barite in the sediments. This authigenic mineral was recovered at two places in at Site 684 in the upper slope of the Peru margin. In areas of fluid venting, as those of enhanced barium transport off Paita, this same mechanism leads to the formation of authigenic barites at the seafloor.

The preferential utilization of the lighter isotope by bacteria during organic carbon oxidation results in depletion of ^{32}S in the dissolved pore-water sulfate. This is reflected in the heavy $\partial^{34}S$ values of the diagenetic barites ($\partial^{34}S$ up to +83.8 ‰) relative to the chimneys which are formed at the seafloor by the reaction of dissolved barium in the vent fluids with bottom-water sulfate.

Preliminary mass balance calculations highlight the need for a biogenic input as a source for the barium in the barite deposits at the vent sites. Detrital barium associated with clays, even if it were totally remobilized by diagenesis, is not enough to account for the barium needed for the formation of barite observed in the slope scarp deposits off Paita. On the other hand, the origin of the fluid responsible for the transport of biogenic barium to the vent site may have a continental component, as suggested by the Sr isotopes of the barites and low chloride fluids sampled over the vents.

6.1.12 BARITE DEPOSITS IN THE PERU SUBDUCTION ZONE

M. Torres, G. Bohrmann

A program of dives with the deep submersible Nautile during the spring of 1990, has provided structural and stratigraphic data on the subduction plate boundary of the Peru margin. Of particular interest was the discovery of large deposits of barite which were recovered during the Nautile expedition and during R/V Sonne cruise in March/April 1992.

Barite occurs in the form of light yellow to brown concretions or chimneys, up to 15 cm high, as well as white crusts only a couple of millimeters thick. They are composed of very pure barium sulfate crystals either in dendritic arrangements or in concentric layers. Their porous nature results in a low bulk density, ranging from 2.8 to 3.4 g/cc. SEM and thin section observations as well as microbe analysis were performed in these samples. Sulfur isotopic analysis of the barites reveal values consistent with bottom seawater sulfate.

Sequential water sampling over a vent site, using a benthic chamber (VESP) shows significant changes in the chemical composition of the enclosed bottom water with time. The increase in barium concentrations with time clearly documents a contemporaneous release of Ba to the bottom water from the vent sites. During one of the VESP deployments a sediment sample was retrieved for analysis of its pore fluid composition; the dissolved barium content in the pore water was found to be 1.26 µM.

Temperature measurement show no evidence for contemporaneous hydrothermal acitvity in the Peru slope: on the other hand, recent precipitation is suggested by the fragility of the deposits and by the absence of any significant sediment coating on the chimneys, in an environment characterized by extremely large sediment accumulation rates. These observations lead us to postulate that the barium source is associated with remobilization of biogenic barite within the sediment column dur to sulfate depletion, and subsequent transport of the barium-rich, reducing fluids to the cold-vent sites. Barium accumulation in the pore fluids (concentrations as high as 600 µM) has been documented by deep sea drilling in the Peru margin.

6.1.13 FLUID VENTING AT THE OREGON AND PERU MARGIN: IMPRINTS ON BIOGENIC MATERIAL

C. Wagner

Vent organisms from different geological settings in the Oregon and Peru convergent margins were collected by submersible and by box coring and dredges from a research vessel. In all instances, vent communities indicate expulsions of fluid triggered by tectonic forces.

The specific composition of the venting fluids is thougth to produce an imprint on the biogeochemical composition of the organisms depending on the characteristic chemistry of the venting fluids at each site. At a given location, hard parts from different benthic genera show similar patterns of trace element distribution. Trace element profiles taken from sections across entire shells of *Calyptogena* and *Solemya*, as well as from turbe sections of *L. barhima*, have been used to trace back the development and activity of venting fluids. The present-day fluid chemistry was inferred using the section of the shells farthest away from the hinge of organism that were collected alive. Trace element make-up of actual fluids taken from these vents confirm the inferences.

The isotopic composition of shells, tubes and soft parts gives evidence for the fact that venting fluids constitute a food source for these organism. However, it is likely that the carbonate buildup of shell material utilizes both, the venting fluids and the surrounding seawater.

A preliminary biogeochemical inventory, presented here for the first time, provides important insights on trace element fluxes associated with fluid venting on accretionary prisms.

In situ measurement of fluid flow from cold seeps at active continental margins

P. Linke[1], E. Suess[2], M. Torres[2], V. Martens[3], W. D. Rugh[4], W. Ziebis[2], and L. D. Kulm[4]

[1] Sonderforschungsbereich 313, Kiel University, D-2300 Kiel, Germany

[2] GEOMAR Research Center for Marine Geosciences, D-2300 Kiel, Germany

[3] Institut für Meereskunde, D-2300 Kiel, Germany

[4] College of Oceanography, Oregon State University, Corvallis, OR 97331-5503 U.S.A.

Abstract-*In situ* measurement of fluid flow rates from active margins is an important parameter in evaluating dissolved mass fluxes and global geochemical balances as well as tectonic dewatering during developments of accretionary prisms. We have constructed and deployed various devices that allow for the direct measurement of these parameters. An open bottom barrel with an exhaust port at the top and equipped with a mechanical flowmeter was initially used to measure flow rates in the Cascadia accretionary margin during an *Alvin* dive program in 1988. Sequentially activated water bottles inside the barrel sampled the increase of venting methane in the enclosed body of water. Subsequently, a thermistor flowmeter was developed to measure flow velocities from cold seeps. It can be used to measure flow velocities between 0.01 to 50 cm s^{-1}, with a response time of 200 ms. It was deployed again by the submersible *Alvin* in subsequent visits to the Cascadia margin seeps (1990) and in conjunction with sequentially activated water bottles inside the barrel. We report the values for the flow rates based on the thermistor flowmeter and estimated from methane flux calculations. These results are then compared with the first measurement at Cascadia margin employing the mechanical flowmeter. The similiarity between water flow and methane expulsion rates over more than one order of magnitude at these sites suggests that the mass fluxes obtained by our *in situ* devices may be reasonably realistic values for accretionary margins. These values also indicate that there is an enormous variability in the rates of of fluid expulsion within the same accretionary prism.

Finally, during a cruise to the convergent margin off Peru, another version of the same instrument was deployed via a TV-controlled frame within an acoustic transponder net from a surface ship, the RV *Sonne*. The venting rates obtained with the thermistor flowmeter used in this configuration yielded a value of 441 L m^{-2} day^{-1} at an active seep on the Peru slope. The ability for deployment of deep-sea instruments capable of measuring fluid flow rates and dissolved mass fluxes from conventional research vessels will allow easier access to these seep sites and a more wide-spread collection of the data needed to evaluate geochemical processes resulting from venting at cold seeps on a global basis. Comparison of the *in situ* flow rates with rates from steady-state compactive dewatering models differ by more than 4 orders of

magnitude. This implies that only a small area of the margin is venting and that there must be recharge zones associated with venting at convergent margins.

INTRODUCTION

Fluid venting at subduction zones is a current research frontier (SUESS *et al.*, 1985; KULM *et al.*, 1986; MOORE, MASCLE *et al.*, 1987; BOULÈGUE *et al.*, 1987; CARSON *et al.*, 1990, CARSON and HOLMES, 1991; MOORE, 1991; MOORE *et al.*, in press). Rates of water discharge and dissolved material flux rates are parameters of the highest significance to marine scientists but only a few attempts of direct measurements exist (CARSON *et al.*, 1990; SAYLES and DICKINSON, 1991 and references cited therein). Very high temperatures coupled with jet-like discharge velocities of fluids at mid-ocean ridge systems require special corrosion-resistant materials for these vents to become accessible to direct experiments. Fluid venting at plate subduction zones, on the other hand result in small temperature anomalies at the sediment/water interface (cold seeps) and the water is expelled at imperceptibly slow rates.

We have developed a concept for determining water and dissolved material flux rates at subduction zones, and have designed a simple instrument to isolate, collect and measure the flow rates of vent fluids. In designing this equipment we made use in the beginning of existing and proven technologies which could be assembled with off-the-shelf components. This initial instrument, which we termed the "Benthic Barrel", was successfully deployed several times by the DSRV *Alvin* in 1987, 1988 and 1990 at vent sites of the Cascadia subduction zone and some of the initial measurements from these deployments have already been published (CARSON *et al.*, 1990). In this paper we document the initial design of the (*OSU*) Benthic Barrel, which has not been published in all details, subsequent improvements involving a more sophisticated flowmeter, and present additional data sets of methane flux and water flow rates for the Cascadia accretionary margin (675 m and 2424 m water depth, Table 1). These results show the applicability of using short-term experiments from submersibles to obtain such data.

Furthermore, we report the recent development of a TV-controlled device (*VE*nt *SP*ider - *VESP*) for deployment of a new (*GEOMAR*) Benthic Barrel from a conventional surface research vessel, eliminating the need and associated costs of deployment by submersible. This device was sucessfully deployed on a seep site on the Peru margin from board the RV *Sonne*. The results obtained are compared with those from a background station in the abyssal plain of the northern Peru Basin. These direct measurements of fluid flow rates are then discussed in the context of estimates obtained using hydrologic models (BEKINS and DREISS, 1992) and subbottom temperature measurements (LE PICHON *et al.*, 1992; HENRY *et al.*, 1992) from the Nankai accretionary margin.

CONCEPT

The Benthic Barrel is a cylindrical chamber with a large opening at the bottom and a small exhaust port at the top. The chamber is deployed over a suspected vent site with the purpose of channelling the effluent from the sea floor into a semi-enclosed environment. The internal volume of the chamber is initially flooded with ambient seawater and is then slowly replaced by vented fluids. In this way a water mixture develops within the chamber with increasing amounts of vent fluid. Sequentially timed water samples are collected during deployment by bottles mounted inside the chamber. Changes in the concentration of dissolved components among these bottles are then used to calculate their flux rates (CARSON *et al.*, 1990).

The exhaust port at the top of the chamber accepts either a mechanical flowmeter or a hot-bead-thermistor flowmeter, both calibrated for a wide range of flows. The mechanical flowmeter is inserted by the manipulator arm of a submersible into the exhaust port upon completion of the internal water sampling cycle. The thermistor flowmeter can be permanently mounted at the Benthic Barrel, and it directly records the flow rate from the chamber. The reading of the mechanical meter is monitored photographically from the submersible, whereas the signal of the thermistor flowmeter is continuously recorded and stored via cable on board the submersible during the entire sampling period. Temperature changes are also monitored during the deployment period by a temperature sensor mounted inside the chamber.

Since the charter costs of deep-sea submersibles are rather high, we developed a TV-controlled device for deployment of the Benthic Barrel from a conventional surface research vessel. The barrel is attached to the central piston of a modified multicorer frame (BARNETT *et al.*, 1984), which operates on a water hydraulic basis and assures gentle deployment of the barrel once the frame settles on the sea floor. The *GEOMAR Barrel* is equipped with 5 water bottles and a storage CTD probe which is used to activate the water-sampling cycle and to continuously record conductivity, temperature, pressure and flow data.

INSTRUMENTATION

OSU Barrel

A commercially available 55-gallon polyethylene barrel constitutes the shell of the benthic chamber (Fig. 1). It is fitted with a removable lid, an O-ring seal and a bolt-on retaining ring. The internal instrumentation is attached to the lid and can be easily removed from the shell as a unit, giving access to the water bottles and timer for sampling and staging. A 3.3-cm diameter hole -the exhaust port- is centered on two polycarbonate plate rings in the lid. This opening allows fluid to escape and serves as a port for inserting the flowmeter. The barrel is open at the bottom so that it can be pushed into the sediment a short distance thereby forming a seal over the seep site. A flared skirt about 25 cm wide, made of three overlapping sections of silicon rubber, can be fitted around the bottom edge of the barrel to ensure a seal at sites where poor sediment penetration is expected. An anchor chain or other weights may be wrapped around the outside of the barrel (about eight inches above the bottom edge) to facilitate penetration and to add vertical stability (Plate I D). Two stainless steel bands (not shown in Fig. 1 but visible in Plate I D), mounted to the outside of the barrel with polypropylene line, provide a harness for deploying, positioning, and recovering the instrument via submersible. The barrel encloses 0.26 m^2 of the bottom surface area and has an internal displacable volume of 180 L.

Six General Oceanics 2-L *Niskin*™ bottles are mounted vertically around a cylindrical polycarbonate frame. The bottles are tripped sequentially by a motor-driven plate with a wedge mounted off-center (Fig. 1). As the plate turns, the wedge consecutively depresses the tripping

piston of each *Niskin*™ bottle. The motor, controller-electronics and batteries are contained in an aluminum pressure case mounted in the center of the polycarbonate frame. The controller, a model IV "Tattletale" Micro-computer (Onset Computer Corporation) provides motor control and position sensing, analog to digital conversion and internal battery level monitoring. It is powered by a single 9-volt battery. Sample collection times are pre-programmed to the desired day/hour/minute before the dive. The high-torque DC gear motor is powered by 4 standard 9-volt batteries. The motor shaft coupled to a drive shaft penetrates the pressure case through a double O-ring seal. The shaft also drives a concentric cylinder in which 6 narrow slots are cut; these slots pass between an infra-red emitter-detector pair to give positional signals. Temperature readings (to an accuracy of 0.01°C) are taken before each sample is collected and the data are stored in the controller. In contrast to the much smaller device of SAYLES and DICKINSON (1991) the *OSU Barrel* does not contain a stirring device for mixing of the internal volume; this was not deemed necessary due to the stirring effect that results from the closing of the bottles by means of the 2 large plungers on each end.

Flowmeters

The mechanical and thermistor flowmeters are mounted in interchangeable assemblies (Fig. 2), which are inserted into the opening at the top of the barrel (Plate I, D + E). Each assembly consists of a flowmeter mounted inside a PVC pipe (2.6-cm inner diameter) and a stainless steel cage with a T-bar handle for manipulation by the submersible. The end of the PVC-pipe is fitted with a silicon rubber O-ring (Fig. 2) to provide a seal between the flowmeter and the polycarbonate ring in the barrel lid.

The mechanical meters, three *Gilmont*™ precision flowmeters were calibrated for separate but overlapping ranges from 0.01 to 4.0 mL min^{-1}, so that a wide range of fluid flow rates could be measured *in situ*. Calibration of this flowmeter is an elaborate procedure described elsewhere (CARSON *et al.*, 1990); it includes fluid viscosity as a function of temperature, pressure and salinity as well as material compressibilities. The calibration also compensates for the reduction of flow induced by back-pressure when the natural flow of vent water from the

sampling area (0.26 m^2) is channelled through the small orifice of the flowmeter (approx. 3 mm^2). The correction factor for calculating the "true" flow from the "metered" flow is non-linear and depends on the total magnitude of flow.

The thermistor (hot-bead) flowmeter (modified after LABARBERA and VOGEL, 1976) can be used to measure flow velocities from about 0.01 to 50 cm s^{-1} with a response time of about 200 ms and a spatial resolution of about 1 mm. The circuit has low power requirements due to a self-balancing bridge circuit that minimizes the requisite thermistor heating. Data are encoded in terms of frequency and continously recorded on a casette tape recorder. The flowmeter is centered in the pipe mounted on the exhaust port of the barrel and consists of a stainless steel rod with a plastic *Eppendorf*™ pipette tip. The tip is filled with epoxy resin, embedding the two bead thermistors (Fig. 2B). The bead at the top of the tip is used as the sensing thermistor (Fenwal Electronics, GD22J1, 200 Ω/25°C, stub end glas coated, 0.9 mm in diameter), whereas a glass encapsuled bead (Fenwal Electronics, GB 35J1, 5 KΩ/25°C) serves as the temperature compensator.

In this design, the potential difference across the bridge circuit is approximately proportional to the logarithm of the flow velocity. The nonlinear scale can be a disadvantage in some applications, but it does allow high sensitivities to low-speed flows without interruptions due to momentary exposures to higher speeds (such as passing waves). The flowmeter is connected to the submersible by a 9 m long cable, that allows the data to be recorded inside the submersible. The potential across the bridge circuit is amplified and the voltage needed to heat the sensing thermistor in stagnant (zero flow) water is subtracted. The amplifier contains a voltage-to-frequency converter with a (low power) timer (Texas Instruments ICM7555) used as an astable multivibrator. The pulse repetition rate varies from about 300 to 1,500 Hz and is recorded on an inexpensive battery-powered tape recorder. A rechargable power pack (24 - 30 V, current drain 100 - 200 mA) provides the possibility of having a fully portable and power independent board unit. To recover the data from the magnetic tape a frequency-to-voltage converter is used.

Calibration of the thermistor flowmeter unit

The flowmeter was temperature compensated in two water baths with stagnant (zero flow) water (after LABARBERA and VOGEL, 1976) at -1 and +4° C. The calibration was conducted in an arrangement similar to that described by VOGEL (1981), where water emerges from a long pipe (1.2 m length; 0.98 cm radius) at rates which are measured with the aid of an overflow and a graduated cylinder. Both procedures were carried out in a temperature-controlled room at +1°C. The signals of the flowmeter, which is positioned at the end of the pipe, are visible on the 0 - 50 µA meter of the amplifier and are recorded on a strip chart recorder and encoded on tape. Assuming laminar flow, the mean velocity (U) can be calculated by dividing the water flow (F = volume per time) by the area (A) of the pipe:

(1) $U\ [cm\ s^{-1}] = F\ [cm^3\ s^{-1}] / A\ [cm^2]$.

As shown in Fig. 3 A the output of the flowmeter approximates a logarithmic function, indicating a higher sensitivity of the flowmeter for smaller velocities. On a semi-logarithmic plot (Fig. 3 B) the conversion of the flowmeter signal on the strip cart recorder [mm] to velocity corresponds to the regression of the calibration graph which is described by the function:

(2) Flowmeter signal [mm] = a x log U + b

(3) $U\ [cm\ s^{-1}] = 10^{([mm] - b) / a}$

Therefore, by using the regression of the calibration graph (Flowmeter signal [mm] = 74.64 x log U + 62.24; $r^2 = 0.99$; in Fig. 3 B) the flowmeter signal can be converted to velocity:

(4) $U\ [cm\ s^{-1}] = 10^{([mm] - 62.24) / 74.64}$.

The linear correlation (Fig. 3 C) between flowmeter signal [mm] on the strip chart recorder and the observed meter readings [µA] is described by the function:

(5) Flowmeter signal [mm] = 2.38 x [µA] - 2.34; $r^2 = 1$.

The encoded (recorded on tape) flowmeter signals are decoded (played back from tape) on the strip chart recorder and converted to velocity according to the regression shown in Fig. 3 D (decoded signal [mm] = 14.82 x log U + 77.77; $r^2 = 0.93$):

(6) $U\ [cm\ s^{-1}] = 10^{([mm] - 77.77) / 14.82}$.

VESP (VEnt SPider) and GEOMAR Barrel

For TV-guided remote deployment from a conventional surface research vessel the barrel is lowered to the sea floor using the main frame of a modified multicorer (BARNETT *et al.*, 1984, see Plate II A). The frame is constructed from steel pipes connected by scaffolding cramps (K. Scholz); it has a total height of 3.5 m and a base that covers 7 m^2. The addition of further diagonal scaffolding poles provides more stability, and a platform for mounting of accessory equipment. The frame carries an underwater video-telemetry system (Preussag Meerestechnik 1987) consisting of a telemetry unit (Preussag, GC 1-87/U1), a low light TV-camera (Osprey, OEO111-6006), two flood lights (ROS, 24V, 150W halogen) and two batteries (Ocean Power, each 12V, 230 Amph). The underwater telemetry unit (Preussag, GC 1-87/B1) communicates with that aboard ship and controls the various functions such as data and video transfer, power supply and triggers the sampling cycle of the barrel. The cable harness is attached to the frame (Burton underwater plugs). The frame also carries a transponder (EG&G, 723A used as subtransponder, 11 KHz receive-interrogate, 9 KHz reply-transmit) for exact positioning of the instrument within a transponder field; as well as a camera (Benthos, Edgerton standard camera, 372) and flash (Benthos, standard flash, 382) for documentation of the deployment site.

The *GEOMAR Barrel* is attached to the central piston of the above described multicorer frame, which operates on a water hydraulic basis and assures gentle deployment of the barrel on the sediment surface once the frame has reached the sea floor (Plate II B). The depth of penetration depends on the softness of the sediment and can be adjusted by a stopper cramp to the height of the barrel. The outer shell of the barrel is exchangable: during deployment from a submersible as was the case with the DSRV *Nautile* (DIA *et al.*, 1992) a transparent PVC-shell is advantageous, whereas for deployment from a surface vessel a more rigid polyethylene shell is required. For deployment during the RV *Sonne* cruise in 1992 we used a commercially available 55-gallon polyethylene barrel as the shell of the benthic chamber. The bottom of the barrel is cut away as with the *OSU Barrel* so that it can be pushed into the sediment forming a

seal over the vent site. It encloses 0.238 m^2 of the sediment surface and has an internal displacement volume of 284 L. The transparent PVC shell used alternately covers 0.135 m^2 of the sediment surface and has an internal displacement volume of 100 L.

A 6 cm diameter hole -the exhaust port- is centered in the lid to allow fluids to escape and to serve as a port for mounting the thermistor flowmeter. The flowmeter is centrally mounted near the top end of a thick-walled tube, which at its lower internal circumference is funnel-shaped to channel the outflowing fluids from the barrel into the pipe (33.5 mm inner diameter; 8.81 cm^2 orifice). The thermistor flowmeter was calibrated (using the procedure described above) at 1.7 °C, close to the *in situ* temperature at the deployment sites.

The internal instrumentation is attached to a central stand and the shell can be easily removed from it to provide access to the water bottles and the storage CTD probe for sampling, programming and data recovery. Five 2-L water bottles (Hydrobios) are mounted vertically around a cylindrical stainless steel frame; the bottles are tripped sequentially by a motor in the center of this frame just as is the case with the *OSU Barrel*. The sampling cycle is activated either by a reed contact switch, pulled by the mechanical arm from a submersible or by the buoyancy of a small piece of syntactic foam or, in case of deployment from a surface vessel, by the telemetry unit on board ship.

A storage CTD probe (ADM Elektronik GmbH) is also mounted on the frame. Both the motor and the storage CTD probe are contained in a titanium pressure case (Hydrobios, 6000 dBar). The electronic components are mounted on a main logic board and consist of a AC/DC converter, RS 232 transmitter/receiver, microprocessor (32 kB EPROM), storage unit (4 kB and 124 kB RAM), quartz clock and 6 bridge circuits. The storage CTD probe can be connected to a portable hand terminal (ADM, Termi 120), which serves as a control, display and storage unit. With this device the water sample sequence (the trigger interval, which can be set between 1 and 120 minutes), the calibration coefficients, the setting and installation of the sensors (time or pressure dependent), the duration of one measuring cycle (0.5 to 32 cycles s^{-1} or min^{-1}) and the averaging of scanned data are preprogrammed before deployment. Thereby the storage probe can be optimally adjusted for the duration of a deployment.

Deployment procedure

The *VESP* (*VE*nt *SP*ider) is lowered from the surface vessel by the ship's (RV *Sonne*) coaxial cable (18.2 mm diameter, 7100 m length, 50 Ω). Thirty meters above the instrument 2 syntactic foam floats (Euroshore, FM 280, each 27.9 kp buoyancy) are attached to the cable to keep it away from the instrument during deployment. *VESP* is lowered to 2-5 m above the sea floor and a place for deployment is selected by observing the TV-monitor while the ship proceeds at a speed of about 1 kn. The position of *VESP* is tracked within the transponder net for exact positioning or to repeatedly visit an attractive location (e.g. an active vent site as indicated by clusters of living *Calyptogena* clams). If the vent site is considered active, the *VESP* is then lowered immediately (within a few seconds) to the sediment surface and approx. 20 m of slack cable are released. Depending on weather, current velocities, positioning capabilities and navigatory skills of ship and crew, further slack has to be given to avoid disturbance during the sampling procedure. When the frame achieves bottom contact, the central piston with the attached barrel is slowly drawn down by its own weight towards the sediment surface. The penetration and sealing of the barrel is observed on the TV-monitor, as well as any movements of the frame due to insufficient slack of the ship's cable. After waiting for the resuspensed particles to settle or being swept away, the water sampling sequence and the data recording are activated by the trigger from the on-board telemetry unit.

RESULTS

Submersible-guided deployments

During *Alvin* Dive 2283 the *OSU Barrel* was placed for approximately 3 hours over a densely populated colony of *Calyptogena* clams and bacterial mats (Plate 1 A - C), a benthic community known to thrive at active vent sites (SUESS *et al.*, 1985). A zero flow signal of 7 µA was observed and recorded while the thermistor flowmeter remained in a bucket mounted on the transport basket of the DSRV *Alvin*. After inserting the flowmeter into the exhaust port

at the top of the barrel and establishing a stable flow signal of 30 - 35 μA (mean 33 μA) for about 10 minutes, the signal was recorded on tape. By using the linear regression between observed flowmeter signal [μA] and output on the strip chart recorder [in scale units of mm] described in equation (5) the difference between both signals (measurement - zero flow), approximating 62 scale units, amounted to an actual outflow velocity of 0.99 cm s^{-1} based on the equation of the calibration graph (4).

The continuous record of flow data at the seep site (*Alvin* 2285) taken onboard the submersible revealed a signal of 81 scale units (after decoding the flowmeter readings from the tape recorder), whereas a zero flow signal of 75 scale units was recorded. After converting these signals to velocity (1.65 and 0.65 cm s^{-1} respectively, see Fig. 4 A) by using equation (6) the difference between both measurements yields an actual outflow velocity of 1 cm s^{-1}, which is in very good agreement with the velocity obtained from the observed ampere meter readings. Thus the actual fluid flow calculated according to equation (1) amounts to 5.31 cm^3 s^{-1}. This yields a flow of 459 L day^{-1} from the barrel, which has a bottom surface area of 0.26 m^2, and therefore a total fluid flow rate of 1765 L m^{-2} day^{-1} (Table 1).

During this deployment an enormously vigorous methane flux was obtained from the sequential water sampler inside the barrel. Methane was stripped from the samples and measured by gas chromatography using an FID detector (SCHMITT *et al.*, 1991); the sensitivity of the method ranges from 10 to 30 nl CH_4 L^{-1} (better than 0.001 μmol CH_4 L^{-1}). The concentration of methane rose from 13 μmol L^{-1} to 458 μmol L^{-1} over a period of 162 minutes; normally vent waters contain about 1 to 10 μmol CH_4 L^{-1}. The increase in methane content inside the barrel was not linear but increased with increasing time of deployment (Fig. 5 A). This could be due to initially incomplete mixing of the incoming vent water with the enclosed ambient bottom water or could be due to consumption of methane during the deployment. Hence we would underestimate the methane flow. These and other implications in deriving total mass fluxes from concentration measurement with the Benthic Barrel are discussed elsewhere (SUESS *et al.*, in prep.), it suffices here to report that the minimum CH_4-flux measured at *Alvin* dive site 2283 was 118 mmol m^{-2} day^{-1}.

During *Alvin* Dive 2285, the barrel was deployed for 90 minutes over a sparsely populated *Solemya* clam field at 2424 m of depth. The continuous record of flow data over a period of 50 minutes at this site revealed a signal of 82.18 scale units, whereas zero flow amounted to 82 scale units. After converting these signals to velocity (1.98 and 1.93 cm s^{-1} respectively, see Fig. 4 B) by using equation (6) the difference between both measurements yields an actual outflow velocity of only 0.05 cm s^{-1}. This corresponds to an actual fluid flow rate of 86 L m^{-2} day^{-1} (Table 1). The concentration of methane rose from 0.015 µmol L^{-1} to 0.051 µmol L^{-1} during the 90 minutes of the deployment (Fig. 5 B).

TV-guided remote deployments

Several *VESP*-deployments were conducted in April 1992 during the RV *Sonne* cruise 78 to the continental margin off Peru (SUESS, 1992). A previous survey with the French deep-sea submersible *Nautile* revealed active vent fields in two tectonic settings: in the accretionary prism at the base of the continental slope and along a fault-scarp created by a submarine landslide (BOURGOIS *et al.*, 1992). A preliminary deployment of *VESP* in the northern Peru basin (07°04.6´S; 88°27.8`W, 4162 m water depth) was performed to obtain information about the background values for the chemical constituents (e.g. oxygen, methane, helium, trace metals) and the actual fluid flow in an area not influenced by subduction processes and active venting. Figure 6 shows the actual record obtained from the thermistor flowmeter during the background deployment in the northern Peru basin. During the first 2 minutes the flow measurements showed higher flow values, probably due to the generation of internal turbulences immediately after deployment of the barrel on the seafloor. The flow gradually declines to a constant value of 0.25 cm^3 s^{-1} (mean 0.44 cm^3 s^{-1}), which can be regarded as a baseline flow under *in situ* conditions (temperature, pressure, salinity and viscosity), but without active venting. The sediment surface at this station was very soft, and thus a very good seal between the barrel and surface sediments was achieved (Plate II C). Therefore, an outflow due to an insufficient sealing at the sediment surface can be excluded. Figure 6 shows also the results of a successful deployment over an active seep site at the Peru margin (3672 m water

depth, Table 1), where a mean fluid flow rate of 1.99 $cm^3 s^{-1}$ was directly measured. The sediment surface at this site was rough and covered with mudstone ledges and clam shells and only a thin layer of sediment (Plate II D), allowing little penetration of the barrel. The actual fluid flow estimated from these values amounts to 441 L m^{-2} day $^{-1}$ (Table 1). The accompanying methane flux at this site was insignificant, although a regionally elevated CH_4-anomaly pattern was observed (SUESS, 1992 in prep.). This was surprising since at all other vent sites previously investigated, CH_4 always was the most obvious indicator for venting. However, an unusual discovery of liquid higher hydrocarbons, emanating from this seep site, could explain the minor role which methane played here.

DISCUSSION

The flow of fluids, dissolved material and gases from accretionary prisms and the mechanisms of tectonic dewatering in the global plate tectonic framework, are current research themes of the highest priority in marine geosciences. The discovery of active discharge of fluids and gases in subduction zones, collision zones of oceanic and continental plates and from areas which are not obviously effected by plate tectonic forces, has opened up new aspects in existing views of the marine cycle of matter. The magnitude of material transport from these geological settings are still largely unknown and are predominantly unquantified. It is certain, however, that the chemically mobile compounds of carbon, methane and carbon dioxide play a prominent role in the dewatering of collision zones just as they do in oceanic spreading zones. In these environments several attempts have been made to determe water and dissolved material flux rates by the use of submersibles (CARSON *et al.*, 1990; SAYLES and DICKSON, 1991). These attempts consisted essentially of placing a sampling chamber "a benthic barrel" over active vent sites.

In this paper we have presented the results of the direct measurement of fluid flow from a submersible with a thermistor flowmeter from two deployments at the Cascadia subduction zone during *Alvin* dives 2283 and 2285 in 1990. During an earlier deployment in 1988 (Dive 1907), *Alvin* visited an active seep site located at 2046 m of depth atop the back-thrust of the first accretionary ridge; a tectonic setting described by KULM *et al.* (1986) and MOORE *et al.* (in press). At this deployment the *OSU Barrel* was equipped with the mechanical flowmeter and with six *Niskin*™ bottles as reported by CARSON *et al.*, 1990. Water samples were collected sequentially inside the barrel while it was placed over the seep site for 207 minutes. After completion of the sampling cycle, the flowmeter was inserted and a constant reading recorded for at least 15 minutes. The corrected water flow reported by CARSON *et al.* (1990) was 188 L m^{-2} day^{-1}. The flux rate of methane, assuming no consumption during deployment, was 10.3 mmol m^{-2} day^{-1}. Using this flux rate and the methane concentration in the sediment pore fluids which feed the seep, an estimated flow rate of 156 L m^{-2} d^{-1} can be obtained (CARSON *et al.*, 1990). The "true" water flow rate at *Alvin* dive site 1907, therefore, lies between 156 and 188 L m^{-2} day^{-1}. The two estimates are independent of each other, yet were both obtained by a single deployment of the *OSU Barrel.*

We may now compare the results reported by CARSON *et al.* (1990) to the new measurements obtained with the thermistor flowmeter (Table 1). This improvement allows for the continuous recording over extented periods of flow, more accurate and sensitive measurements, and the avoidance of back-pressure effects inherent in the mechanical flowmeter which required correction with a large uncertainty (CARSON *et al.*, 1990). The deployment during *Alvin* dive 2283 was at 675 m of water depth on the second accretionary ridge along a fault off-setting the seafloor. This fault intersects a subsurface gas hydrate layer and thereby gives rise to vigorous venting of methane (CARSON, 1991; CARSON and HOLMES, 1991; MOORE *et al.*, 1991). This site as well as *Alvin* dive site 1907 are presently being drilled by the *JOIDES Resolution* to determine the deeper plumbing system.

Alvin dive site 2285, in contrast, is characterized by low methane fluxes; however, venting at this site was inferred by the presence of numerous individuals of the bivalve *Solemya* sp. This

site was located at the deformation front on the abyssal plain, under 2424 m of water, and is thought to emit deeply sourced fluids from the oceanic basement (MOORE *et al.*, 1991). Site 2285 also yielded a short sediment core from which methane was extracted by the blender method described by FABER and STAHL (1983). The total methane concentration measured in two samples from this core yielded values of 6.25 ± 0.06 µmol kg^{-1} of wet sediment. This methane content includes a large fraction of adsorbed methane (approximately 60%) which is not capable of freely moving with the vent water and has to be subtracted. Therefore, we can estimate the free methane in the feed water to be 8 ± 3 µmol CH_4 L^{-1}, using a value for the wet bulk density of 1.4 g ml^{-1} and assuming a porosity of 80%. Using the methane concentration in the feed water, in conjunction with the methane flux measured in the barrel samples (Fig. 5), we obtained an independent fluid flow rate of 50 ± 20 L m^{-2} day^{-1} at this site (Table 1).

No sediment core, however, could be obtained for the characterization of the feed water at dive site 2283, because little sediment is being deposited at this site. Assuming that the water and the methane fluxes are both accurate at these sites, the feed water at dive site 2283 should contain approximately 66 µmol CH_4 L^{-1}. This is identical to the value previously obtained from the pore water at dive site 1907; an assumption that we consider valid given the proximity of the two sites and the similiarity in subsurface plumbing and fluid source. Hence, we think that the same type of fluid is vented at the first and second ridge at the Cascadia margin off Oregon, albeit at very different rates (Table 1). This is also demonstrated by the very good agreement between the flow rates measured with the thermistor flowmeter and the methane fluxes for all the three sites surveyed (Fig. 5 C).

The consistency between water flow and methane expulsion among the Cascadia dive sites over almost two orders of magnitude may be reasonably realistic for different tectonic settings in accretionary margins and show the applicability of using short-term experiments from submersibles to obtain such data. Furthermore, the mass fluxes of methane reported here for the first time clearly illustrate the enormous variability in the rates of fluid expulsion even within the same accretionary prism.

As described above, the results from the Peru margin, using the TV-controlled frame for deployment of the barrel, provide yet another measurement of fluid flow from cold seeps in convergent margins. Table 1 sumarizes the values obtained by *in situ* measurements of flow in three settings on the Cascadia margin and from one station on the Peru slope. These values are compared with estimates using dissolved flow rates at these sites, as well as other indirect approaches used in the Nankai accretionary margin. These, to the best of our knowledge, are all the data available so far. Calculations using dewatering estimates based on porosity reduction (CARSON *et al.*, 1990; BEKINS and DREISS, 1992) are orders of magnitude lower than expected from mass flux calculations, subbottom temperature and direct flow measurements (LE PICHON *et al.*, 1992; CARSON *et al.*, 1990). This implies that only a small area of the total convergent margin is actually venting and in addition that there must be recharge zones associated with venting at these sites. Furthermore, steady-state compactive dewatering models, integrating over a long period of time, clearly underestimate mass transport rates from accretionary margins by not taking into account recirculation pathways.

The *in situ* flow measurements and indirect estimates from methane fluxes in the Cascadia margin yield surprinsingly similar rates at each site; lending credibility to the approach of an *in situ* instrumentation of the sea floor as developed by us. Vertical subbottom temperature profiles made inside a clam colony on Nankai in 1985 were used to infer an upward Darcy flow of about 100 m $year^{-1}$ (HENRY et al., 1989). Further measurements during the Kaiko-Nankai submersible survey confirmed the estimates of Darcy flow velocities in the range of 70 to 150 m $year^{-1}$. These results correspond approximately to the values obtained at *Alvin* dive site 1907 in the Cascadia margin. For comparison all *in situ* flow measurements are converted to vertical flow velocities either assuming realistic porosities or using actual geotechnical data obtained from sediment cores at *Alvin* dive site 2285 and 1907.

In situ measurements and indirect estimates of fluid flow on the Peru slope give values of 441 and 200 L m^{-2} day^{-1}. All these data show the variability of venting rates among convergent margins, and even within the same tectonic setting, and clearly stress the need for a wider data base in order to extrapolate these results in the global context of material cycling. Direct

measurements and indirect estimates using dissolved mass balances and subbottom temperatures are all valid and independent means to evaluate fluid flow mass transport rates. The ability for deployment of instruments capable of performing these measurements from conventional research vessels using the TV-deployment system described here, will allow easier access to seep sites and a more wide-spread collection of the data needed to evaluate geochemical processes resulting from venting at cold seeps on a global basis.

Acknowledgements-We wish to thank the pilots of the DSRV *Alvin* and crews of the RVs *Atlantis II* and *Sonne* for logistical support, skillful deployment and recovery of the different experimental instruments. We greatly appreciate the technical support of Peter Kalk (Oregon State Univ.), Arnim Flügge (Geology Dept. Univ. Kiel) and Peter Schymatzek (Technical support staff R.V. *Sonne*). Financial support for this project was provided by the Bundesministerium für Forschung und Technologie (Projects 03R607 6 and 03R418 9) and by the National Science Foundation (Project OCE 8609789). This is publication no. 157 of the Sonderforschungsbereich 313, supported by the Deutsche Forschungsgemeinschaft.

REFERENCES

BARNETT P. R. O., J. WATSON and D. CONELLY (1984) A multiple corer for taking virtually undisturbed samples from shelf, bathyal and abyssal sediments. *Oceanologica Acta* **7**: 399-408.

BEKINS B. A. and S. J. DREISS (1992) A simplified analysis of parameters controlling dewatering in accretionary prisms. *Earth and Planetary Science Letters*, **109**, 257-287.

BOURGOIS J., Y. LAGABRIELLE, P. DEWEVER, E. SUESS and THE NAUTIPERC CRUISE SHIPBOARD SCIENTISTS (1992) Tectonic history of a non accreting active margin during the

past 400 ka. Results of a submersible survey of the Peru Trench at 5-6°. Submitted to *Geology*.

BOULÈGUE J., J. T. LIYAMA, J.-L. CHARLOU and J. JEDWAB (1987) Nankai Trough, Japan Trench and Kuril Trench: Geochemistry of fluids sampled by the submersible *Nautile*. *Earth and Planetary Science Letters*, **83**, 363-375.

CARSON B., E. SUESS and J. STRASSER (1990) Fluid flow and mass flux determinations at vent sites on the Cascadia Margin accretionary prism. *Journal of Geophyshsical Research*, **95**, 8891-8897.

CARSON, B. and M. L. HOLMES (1991) Fluid expulsion sites imaged on Cascadia margin. *News from the JOI/U.S. Science Support Program Associated with the Ocean Drilling Programm*, **4**, 5+12.

DIA A. N., L. AQUILINA, E. SUESS, M. TORRES, J. BOULÈGUE and J. BOURGOIS (1992) Continent derived fluids from the convergent margin off Peru. Deep sea dives of the Nautiperc cruise, Part 2. Submitted to *Geology*.

FABER E. and W. STAHL (1983) Analytical procedure and results of an isotope geochemical surface survey in an area of the British North Sea. In: *Petroleum, Geochemistry and Exploration of Europe*, J. BROOKS, editor, Blackwell Science Publisher, London, pp. 51-63.

KULM L.D., E. SUESS, J. C. MOORE, B. CARSON, B. T. LEWIS, S. D. RITGER, D. KADKO, T. M. THORNBURG, R. EMBLEY, W. RUGH, G. MASSOTH, M. LANGSETH and G. COCHRANE (1986) Oregon margin subduction zone: Venting, Fauna and Carbonates. *Science*, **231**, 561-566.

HENRY P., S. J. LALLEMANT, X. LE PICHON and S. E. LALLEMAND (1989) Fluid venting along Japanese trenches, tectonic context and thermal modelling. *Tectonophysics*, **160**, 277-292.

HENRY P., J.-P. FOUCHER, X. LE PICHON, M. SIBUET, K. KOBAYASHI, P. TARITS, N. CHAMOT-ROOKE, T. FURUTA and P. SCHULTHEISS (1992) Interpretation of temperature

measurements from the Kaiko-Nankai cruise: Modelling of fluid flow in clam colonies. *Earth and Planetary Science Letters*, **109**, 355-371.

LABARBERA M. and S. VOGEL (1976) An inexpensive thermistor flowmeter for aquatic biology. *Limnology and Oceanography*, **21**, 750-756.

LE PICHON X., K. KOBAYASHI and KAIKO-NANKAI SCIENTIFIC CREW (1992) Fluid venting activity within the eastern Nankai Trough accretionary wedge: A summary of the 1989 Kaiko-Nankai results. *Earth and Planetary Science Letters*, **109**, 303-318.

MOORE J. C. (1991) Geophysicists meet bioherm: Seepy story surfaces. *News from the JOI/U.S. Science Support Program Associated with the Ocean Drilling Programm*, **4**, 1-3.

MOORE J. C., A. MASCLE and LEG 110 SHIPBOARD SCIENTISTS (1987) Expulsion of fluids from depth along a subduction-zone decollement horizon. *Nature*, **326**, 785-788.

MOORE J. C., K. M. BROWN, F. HORATH, G. COCHRANE, M. MACKAY and G. MOORE (1991) Plumbing accretionary prisms: effects of permeability variations. *Philosophical Transactions of the Royal Society London* A, **335**, 275-288.

SAYLES F. L. and W. D. DICKSON (1991) The seep meter: a benthic chamber for the sampling of low velocity hydrothermal vents. *Deep-Sea Research*, **38**, 129-141.

TORRES M., A. DIA, J. BOULÈGUE, L. AQUILINA and E. SUESS (1992) Barite deposits from the Peru subduction zone. Submitted to *Earth and Planetary Science Letters*.

SCHMITT M., E. FABER, R. BOTZ and P. STOFFERS (1991) Extraction of methane from seawater using ultrasonic vacuum degassing. *Analytical Chemistry*, **63**, 529-532.

SUESS E., B. CARSON, S. D. RITGER, J. C. MOORE, L. D. KULM and G. R. COCHRANE (1985) Biological communities at vent sites along the subduction zone off Oregon. In: *The hydrothermal vents of the Eastern Pacific: an overview*, M. C.JONES, editor, *Bulletin of the Biological Society of Washington*, **6**, 475-484.

SUESS E. (1992) FS Sonne. Fahrtbericht SO 78 Peruvent. Balboa, Panama - Balboa, Panama 28.2.1992 - 16.4.1992. *GEOMAR Report*, **14**, 120 pp.

VOGEL S. (1981) *Life in moving fluids. The physical biology of flow*. Willard Grant Press, Boston, 352 pp.

Table 1: List of stations with venting rates obtained from in situ measurements, compared with indirect estimates using fluxes of methane and barium and temperature changes within the sediments.

LOCATION	LATITUDE LONGITUDE	DEPTH [m]	APPROACH	FLOW RATES [L m^{-2} day^{-1}]	LINEAR FLOW VELOCITY [m $year^{-1}$]	REFERENCES
Cascadia	44° 40.44' N	2046	Mechanical flowmeter	188 ± 20	113	CARSON *et al.*, 1990
Alvin 1907	125° 17.63' W		Methane flux	156 ± 10	95	CARSON *et al.*, 1990
			Porosity reduction	(1.8×10^{-3})		CARSON *et al.*, 1990
Cascadia	44° 40.42' N	675	Thermistor flowmeter	1765 ± 20	1065	This study
Alvin 2283	125° 07.49' W		Methane flux	1700* ± 50	1023	This study
Cascadia	45° 56.19' N	2424	Thermistor flowmeter	86 ± 20	52	This study
Alvin 2285	125° 20.82' W		Methane flux	50 ± 20	30	This study
Peru margin	9° 35.26' S					
Sonne 168-2	80° 07.70' W	3672	Thermistor flowmeter	441 ± 20	265	This study
Sonne 180-4	5° 36.00' S	3309	Barium flux	970 ± 50	583	TORRES *et al.*, 1992
	81° 38.61' W					
Peru margin	5° 36.32' S					
Nautile NP2-35	81° 38.63' W	3540	Methane flux	200* ± 50	120	DIA *et al.*, 1992
Nankai Trough			Temp. measurements		100	HENRY *et al.*, 1992
			Porosity reduction		(6×10^{-4})	BEKINS and DREISS, 1992

Notes: The flow rates indicated by asterics (*) were calculated assuming that the methane concentration in the feed water was the same as that for *Alvin* dive site 1907. The flow rates based on porosity reduction (steady-state dewatering) are averages over the entire prism, and therefore should not be directly compared with the flow rates obtained at an individual venting site. The linear flow velocity was estimated using a constant porosity of 60%.

FIGURE CAPTIONS

Fig. 1 Schematic diagramm of the Benthic Barrel and its components shown deployed on the sediment.

Fig. 2 **A.** Mechanical (Bernoulli-type) and **B.** thermistor flowmeter mounted inside a stainless steel cage with T-bar handle; the opening with the O-ring seal fits the exhaust port of the barrel; radius of the pipe: 1.3 cm.

Fig. 3 **A.** Thermistor flowmeter calibration plot, mean velocity (U) versus flowmeter signal on a strip chart recorder, demonstrating that the output of the flowmeter approximates a logarithmic function.

B. Semilogarithmic thermistor flowmeter calibration plot, log U versus flowmeter signal on a strip chart recorder. The regression of the calibration graph is used for the conversion of the flowmeter signal to velocity.

C. Linear calibration plot with flowmeter signals observed as meter readings versus recorded signals on a strip chart recorder.

D. Semi-logarithmic thermistor flowmeter calibration graph, log U versus flowmeter signal after recovery from the magnetic tape on a strip chart recorder.

Fig. 4: **A.** Fluid flow at *Alvin* dive sites 2283 and 2285 **(B)** measured with the thermistor flowmeter inserted into the exhaust port of the *OSU* Barrel. A zero flow signal (*in situ* baseline) was recorded while the flowmeter remained in a bucket mounted on the transport basket of the submersible *Alvin*. Flow data were calculated according to equation (6) from the strip chart recorder readings after recovery from the magnetic tape.

Fig. 5: **A/B.** Increase in methane concentration with time for deployments at *Alvin* dive sites 2283, 2285 (this study) and 1907 (CARSON *et al.*, 1990); the flow rates measured directly with flowmeters at each site are indicated by the letter "F". Note the different scales.

C. Relationship between mass fluxes of methane and fluid expulsion rates measured with the mechanical flowmeter at site 1907 (CARSON *et al.*, 1990) and with the thermistor flowmeter at sites 2283 and 2285 (this study).

Fig. 6: Fluid flow recordings when *VESP* was deployed from the RV *Sonne* in the northern Peru basin (station 152-17) to obtain a baseline under *in situ* conditions but without active venting, and the recordings at the Peru margin (station 168-2) on an active seep site. The fluid expulsion rate at station 168-2 was calculated using the increase of fluid flow over the background values (Table 1).

Plate I **A.** Active seep site with clam colonies consisting of live and dead *Calyptogena* sp. in clusters around cold seep. Size of clams: 10-15 cm.

B. White streaks on the rock surface (arrow) reveal an active seep surrounded by *Calyptogena* sp. clams and bacterial mats (C).

D. *OSU* Barrel deployed at Cascadia seep site (*Alvin* Dive 2283); the barrel is 92 cm high, the exhaust port atop the barrel is open (without flowmeter inserted) and a heavy chain aids in forming a seal at the sediment surface. During the deployment of the *OSU* Barrel at the active gas hydrate site a vigorous methane flux was measured from the sequential water samples taken within the barrel.

E. *OSU* Barrel with inserted thermistor flowmeter.

Plate II **A.** *VESP* (*VE*nt *SP*ider) on Deck of the RV *Sonne*. The main frame, a modified multicorer carries: **1.** an underwater video-telemetry system, **2.** a low-light TV-camera, **3.** two flood lights, **4.** two batteries, **5.** a transponder used as subtransponder, **6.** a camera and 7. a flash for a TV-controlled deployment, exact positioning and documentation of the deployment site.

B. View on the *GEOMAR Barrel* with the transparant shell (inner diameter 41.4 cm) on Deck of the RV *Sonne*. The internal instrumentation is attached to the central piston of the multicorer; the shell can be easily removed. Five 2-L water bottles and a storage CTD are mounted vertically around a cylindrical stainless stell frame; the bottles are tripped sequentially by a motor in the center of this frame. The central exhaust port (arrow) allows fluids to escape, which are channelled in a pipe to the centrally mounted thermistor flowmeter.

C. TV-guided deployment of the *GEOMAR Barrel* from the RV *Sonne* at station 152-17 in the northern Peru Basin. This deployment is regarded as a background station without active venting to obtain an *in situ* flow baseline (see Fig. 6). Note the good seal between the soft sediment surface and the transparant barrel shell.

D. TV-guided deployment of the *GEOMAR Barrel* from the RV *Sonne* at station 168-2, an active seep site at the Peru margin. The sediment surface at this site was rough and covered with mudstones and clam shells, but with only a thin layer of sediment, allowing only little penetration of the polyethylene barrel shell.

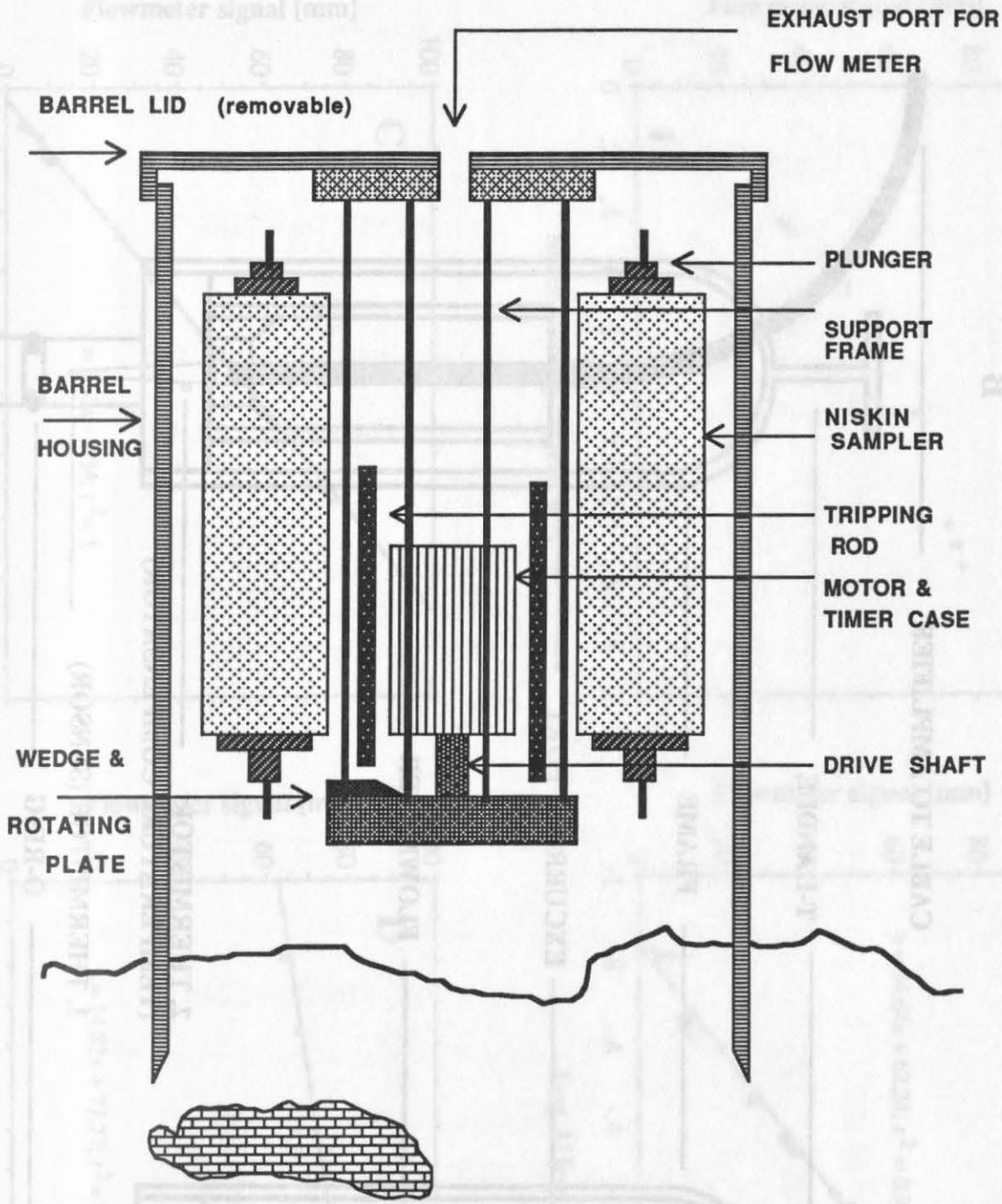
EXHAUST PORT FOR
FLOW METER
BARREL LID (removable)
PLUNGER
SUPPORT
FRAME
BARREL
HOUSING
NISKIN
SAMPLER
TRIPPING
ROD
MOTOR &
TIMER CASE
WEDGE &
ROTATING
PLATE
DRIVE SHAFT

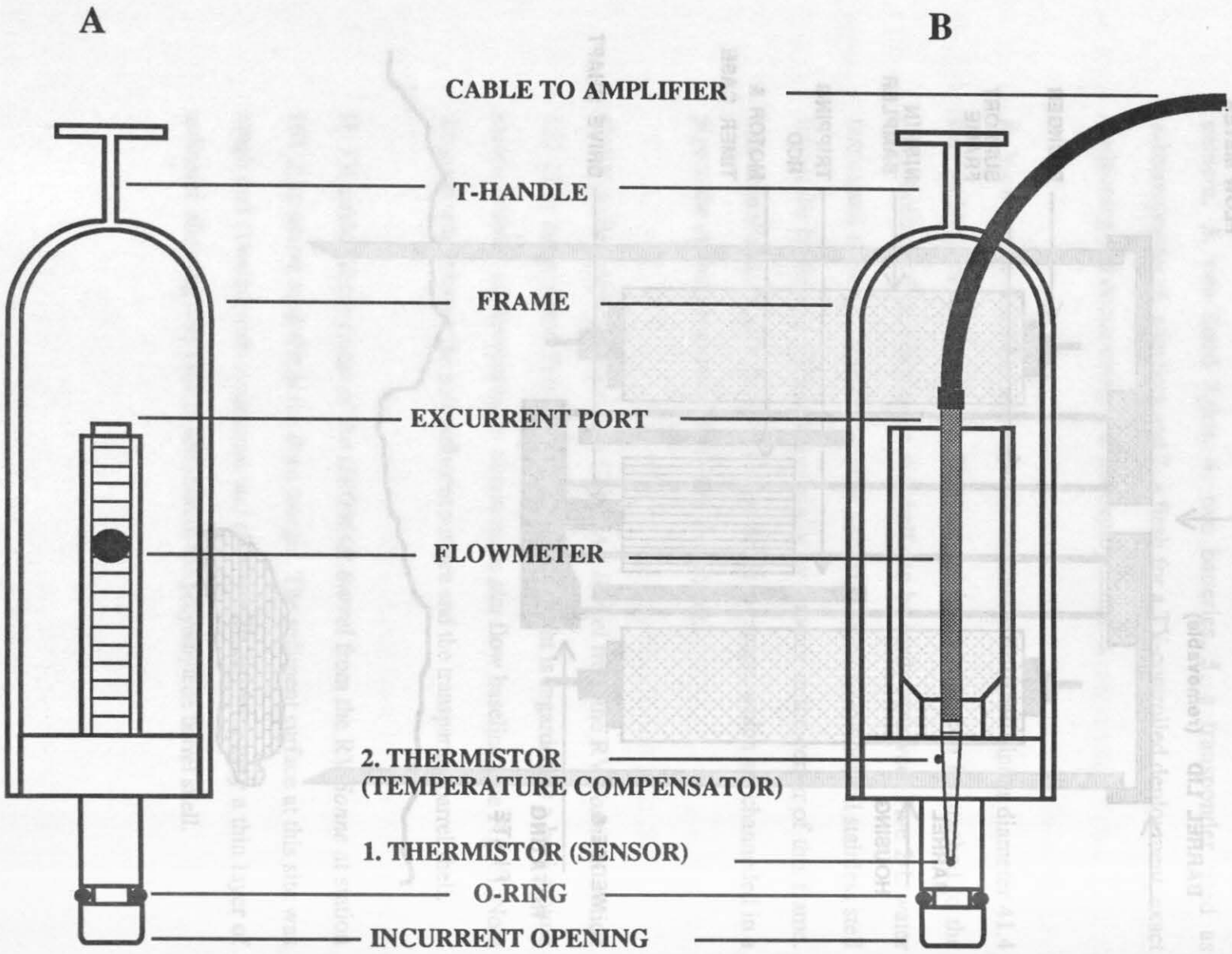
A
B
CABLE TO AMPLIFIER
T-HANDLE
FRAME
EXCURRENT PORT
FLOWMETER
2. THERMISTOR
(TEMPERATURE COMPENSATOR)
1. THERMISTOR (SENSOR)
O-RING
INCURRENT OPENING

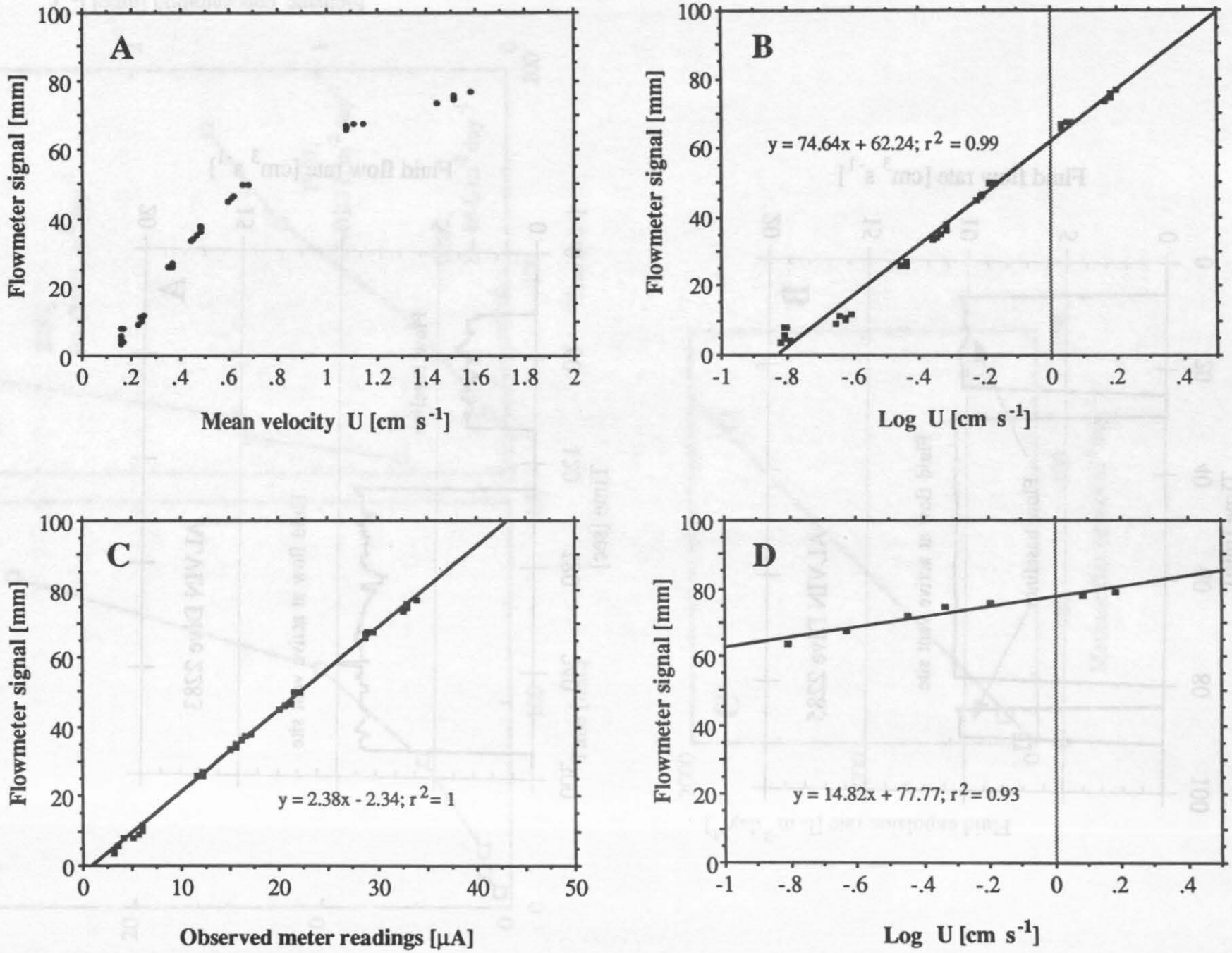
A
Flowmeter signal [mm]
Mean velocity U [cm s-1]
B
y = 74.64x + 62.24; r2 = 0.99
Log U [cm s-1]
C
y = 2.38x - 2.34; r2 = 1
Observed meter readings [µA]
D
y = 14.82x + 77.77; r2 = 0.93
Log U [cm s-1]

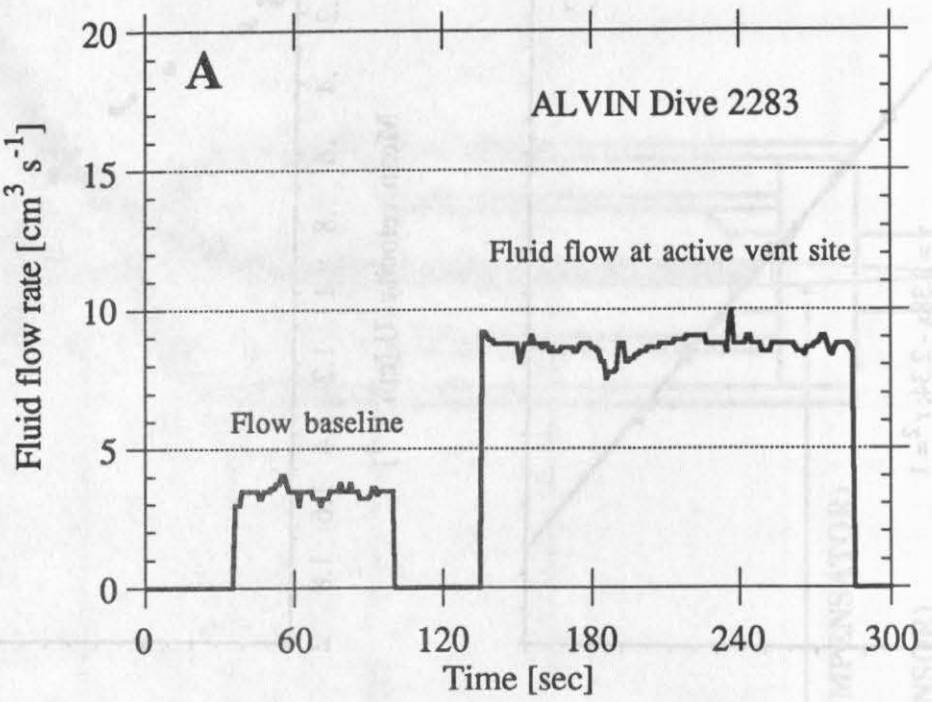
A
ALVIN Dive 2283
Fluid flow at active vent site
Flow baseline
Fluid flow rate [cm^3 s^{-1}]
Time [sec]
0
5
10
15
20
0
60
120
180
240
300

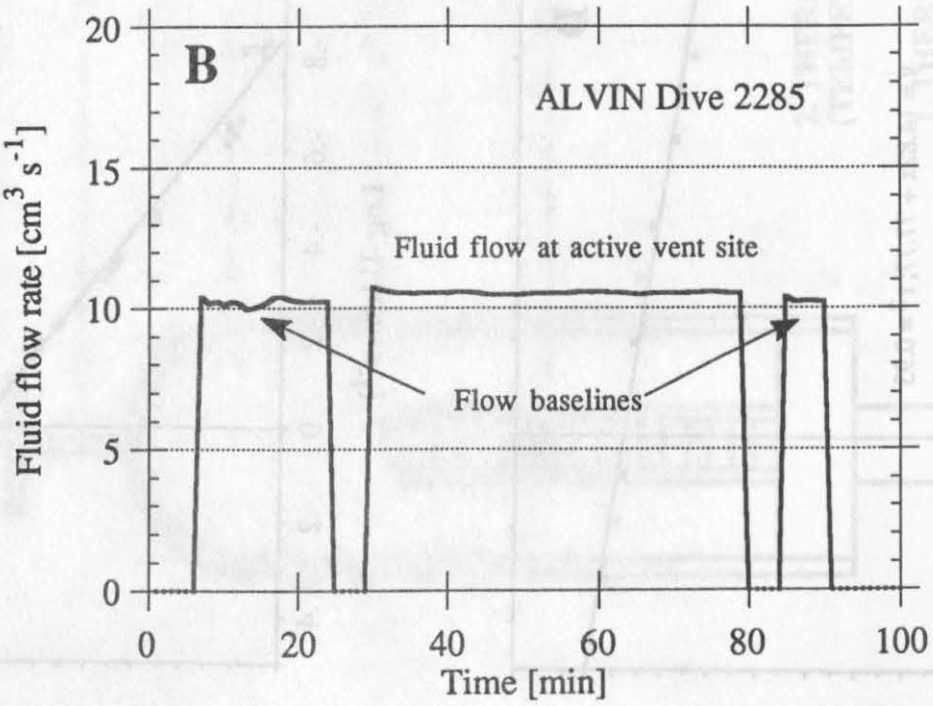
B
ALVIN Dive 2285
Fluid flow at active vent site
Flow baselines
Fluid flow rate [cm^3 s^{-1}]
Time [min]
0
5
10
15
20
0
20
40
60
80
100

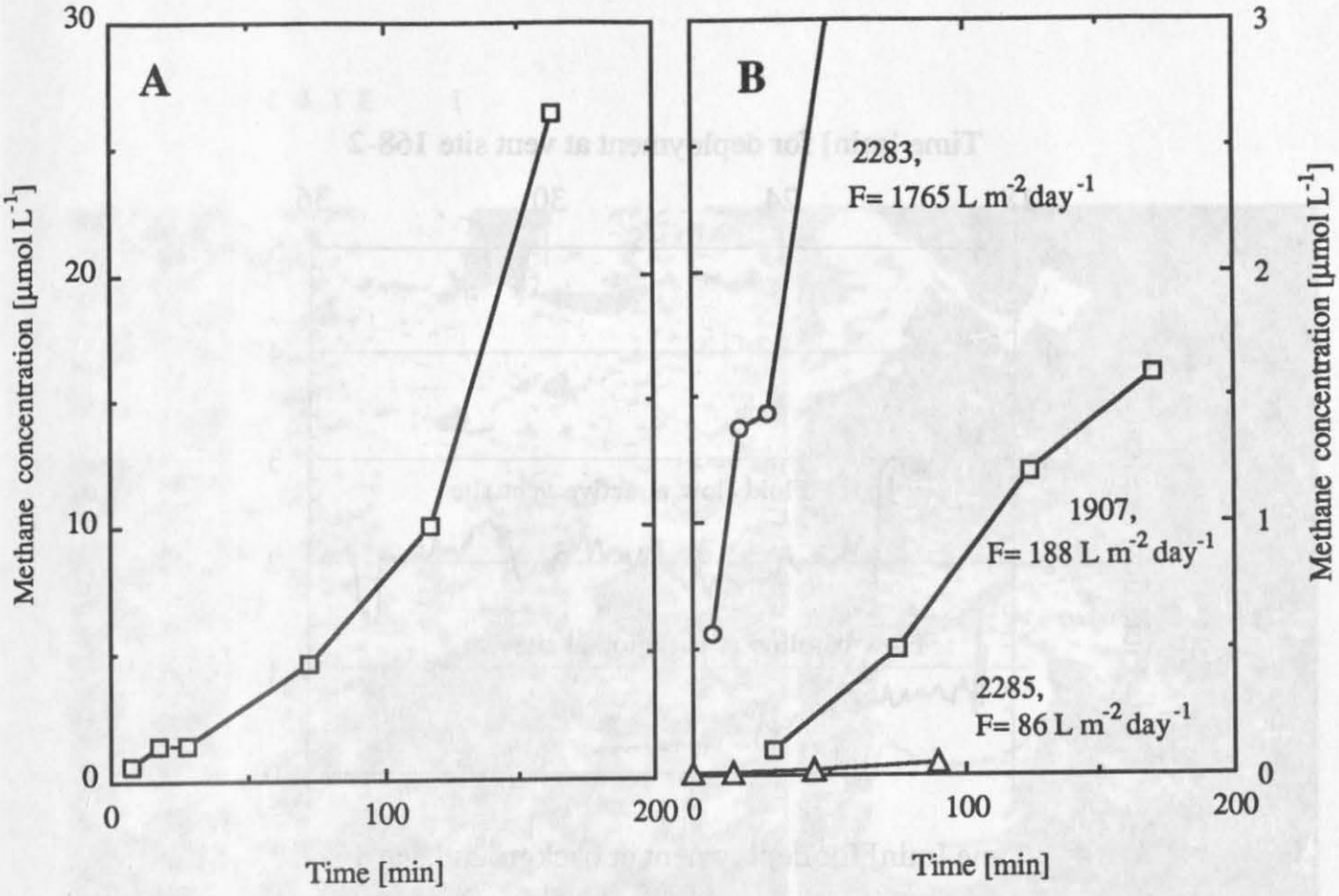
A
B
Methane concentration [µmol L-1]
Time [min]
2283,
F= 1765 L m-2 day-1
1907,
F= 188 L m-2 day-1
2285,
F= 86 L m-2 day-1
0
10
20
30
100
200
1
2
3

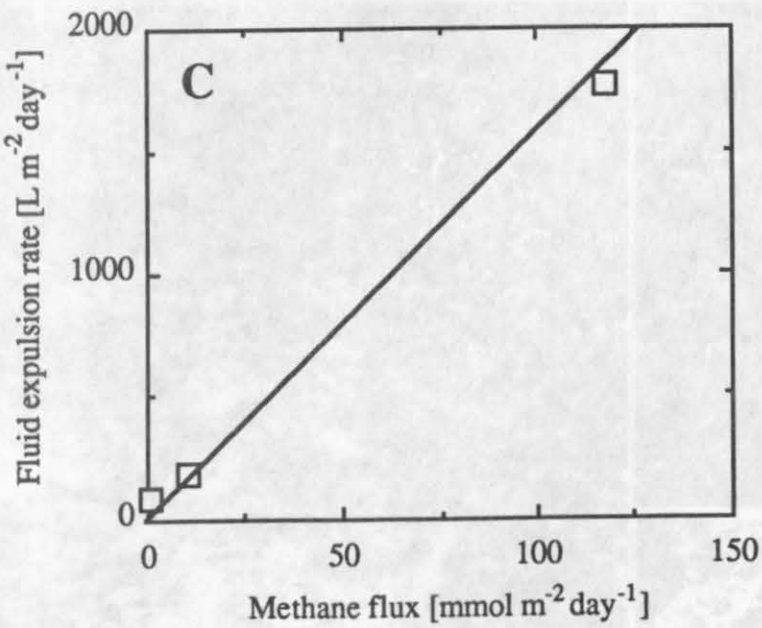
C
Fluid expulsion rate [L m-2 day-1]
Methane flux [mmol m-2 day-1]
0
1000
2000
50
100
150

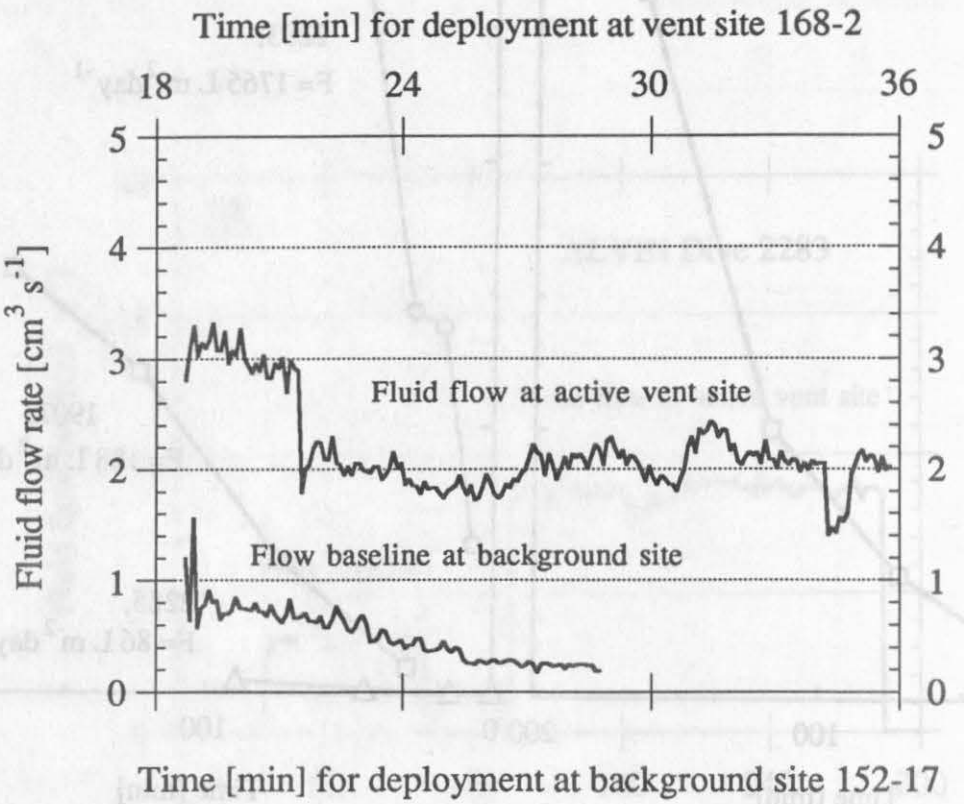
Time [min] for deployment at vent site 168-2
18
24
30
36
5
4
3
2
1
0
Fluid flow rate [cm^3 s^{-1}]
Fluid flow at active vent site
Flow baseline at background site
Time [min] for deployment at background site 152-17

PLATE I

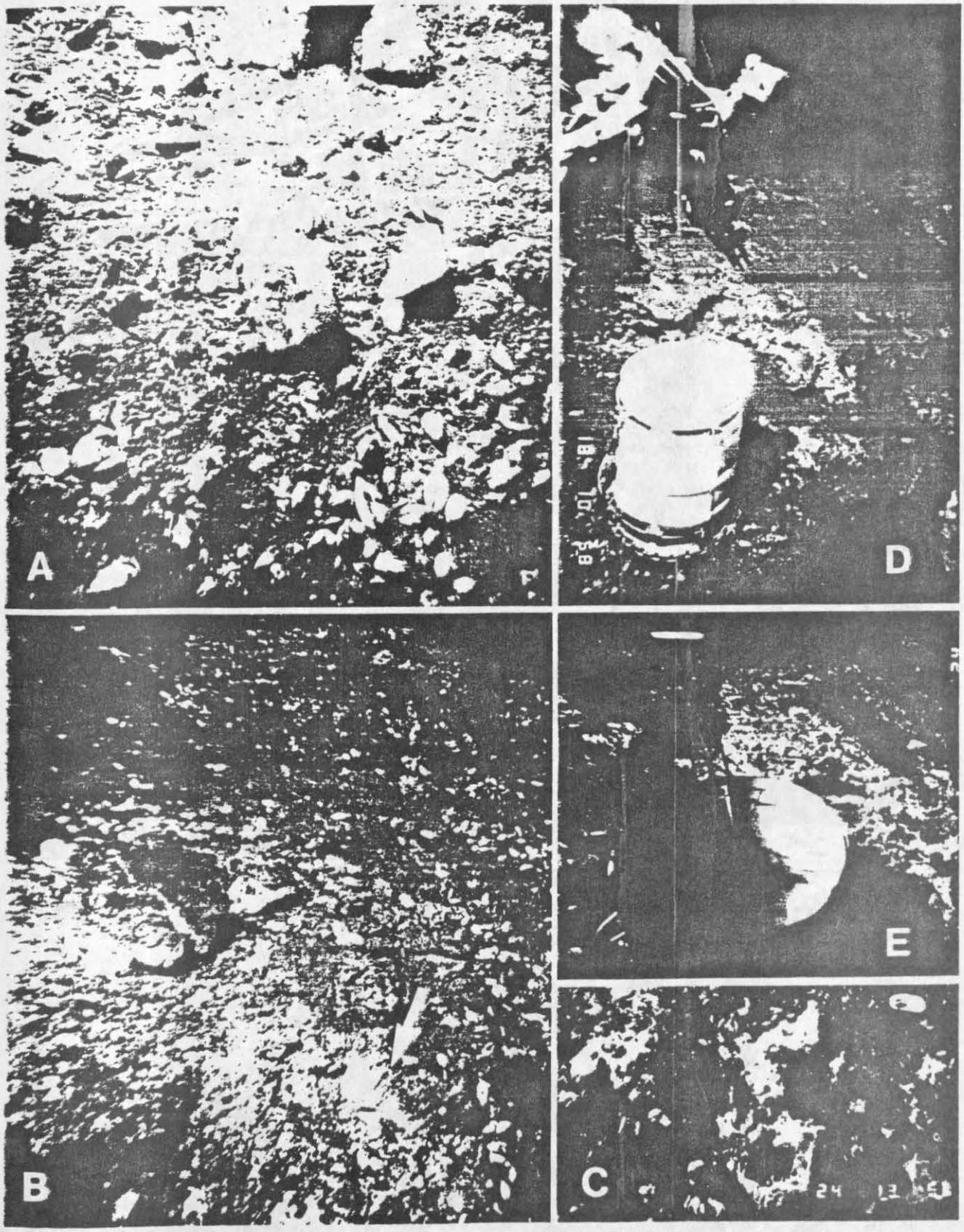

PLATE II

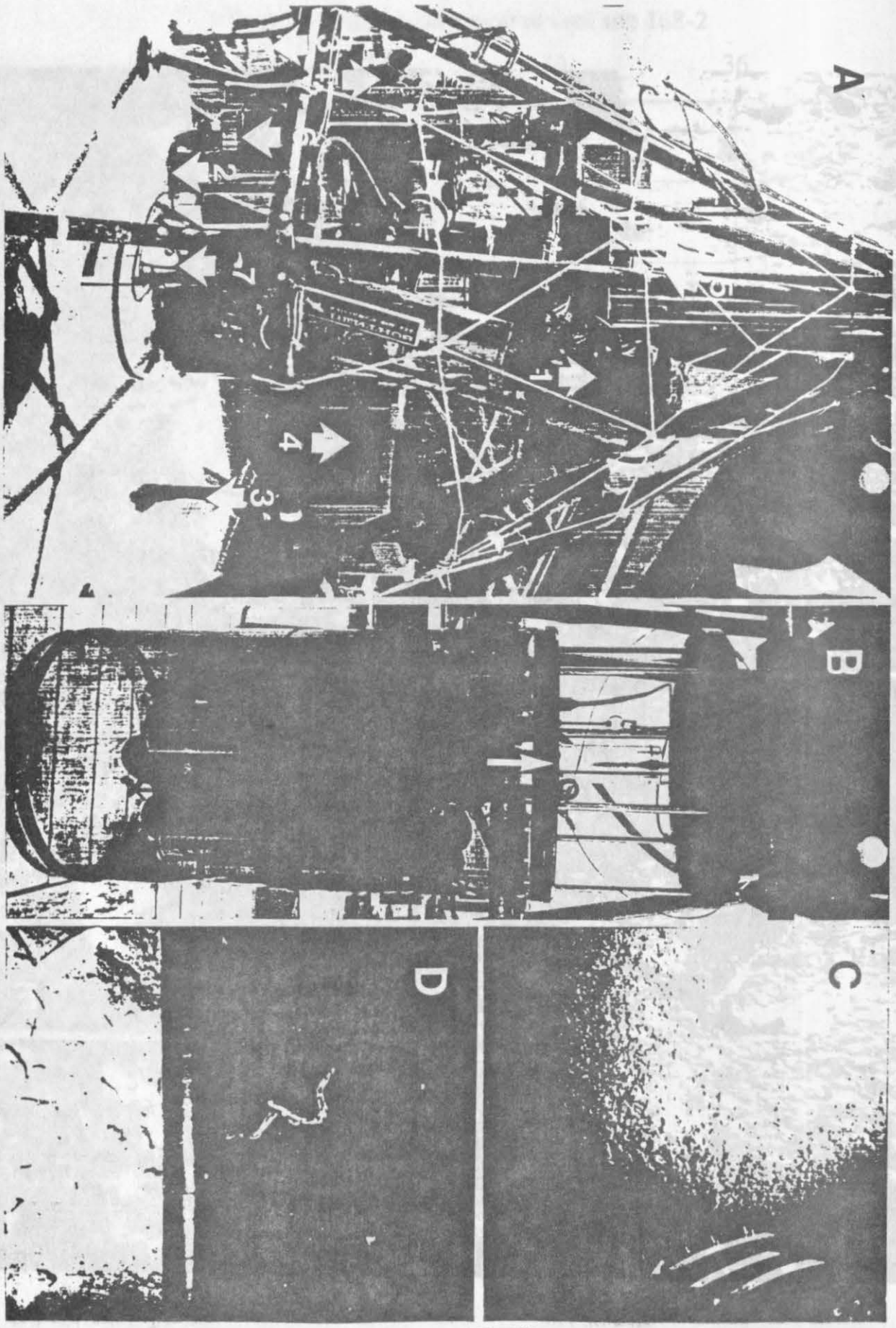

Dewatering of sediments along the Cascadian Margin: Evidence from geotechnical properties

P. Hempel und E. Suess

GEOMAR, Wischhofstraße 1-3, 2300 Kiel 14, Germany

submitted: Proc. Init. Repts., ODP, 146

Abstract

The lithological composition and the physical properties of sediments recovered by kasten coring at 29 sites in the Cascadia Margin give insight into the processes of tectonic dewatering from the Pleistocene to the present. Shear strength and water content, in particular, reveal the degree to which tectonic influence has modified the sediments at this setting. The undeformed sediments at the abyssal plain have low shear strength and high water contents throughout the core depths. Contrastingly, in the vicinity of the deformation front the sediments are characterized by extremely high shear strength and low water contents. Between these two end members the sediments from the deformation ridges show intermediate shear strength and water content values. There is a close relationship between the water content/porosity and the degree of consolidation of the sediments. High water contents are restricted to the unconsolidated silty to clayey intervals, whereas low water contents appear in the cemented sandy to silty layers. From these data we infer patterns of fluid migration within the uppermost section of the accretionary prism and calculate rates of fluid expulsion at the sea floor of $2 \cdot 10^{-4}$ [$L \cdot m^{-2} \cdot d^{-1}$]. The results indicate that fluid expulsion is higher off central Oregon compared to the area off southern Washington.

Based on the bulk mineralogical composition of the sediments examined and some grain size analyses, we conclude that the generation of the consolidated layers at shallow depth beneath the seabed are closely related to the dewatering processes, a widespread phenomenon along the Cascadia margin evidenced in "vent"-fields. Single ^{14}C-datings reveal sedimentation rates of 20 to 27 [$cm \cdot kyr^{-1}$] during the Holocene.

Introduction

The deformation history of accretionary prisms, its effects on the physical properties of the sediments in conjunction with the geochemistry and mechanisms of fluid flow along convergent margins, has received considerable attention over the past years. It is most emphatically expressed by the dedication of five drilling legs of the *JOIDES Resolution* to these objectives [Leg 110, Barbados accretionary prism (Moore, Mascle et al., 1988); Leg 112, Peru margin (Suess, v. Huene et al. 1989); Leg 131, Nankai Trough (Hill, Taira et al. 1991); Leg 141, Chile Tripple Junction (Behrmann, Lewis et al. in press), and finally Leg 146, Cascadia margin (this volume)]. The results of these drilling campaigns gave insight into the tectonic and derived processes which are active within the accretionary prisms. In addition a number of dives by deep diving submersibles have allowed direct observations of the expulsion of fluids and gases at the sea floor (Ritger et al. 1987; Carson et al. 1990), as well as the sampling of rocks and cements formed by the interaction of venting fluids with bottom seawater (Suess and Whiticar 1989; Kulm and Suess 1990).

Studies along the Cascadia margin off Oregon and Washington have resulted in one of the most comprehensive data sets of any convergent margin. It includes observations from submersibles and remotely operated camera systems (Kulm et al. 1986; Suess et al.1985), *in situ* measurements (Davis et al., 1990), surficial samples recovered by coring and dredging, and reflection seismic lines (Davis and Hyndman, 1989). During cruises of RV *Wecoma* in 1983 and RV *Atlantis* in 1984 and 1987 a series of sediment cores were recovered along transects perpendicular to the continental margin off Oregon and southern Washington. Pore water analyses of the sediments from the cores and surficial samples demonstrated the presence of fluids migrated from

greater depths to the surface and the generation of precipitation products (Han, 1988; Han and Suess, 1989; Suess and Whiticar, 1989). In this paper we present the results of physical property measurements and diagenetic investigations of these sediments with the emphasis on their relation to the tectonic history. The objective is to close the gap between the sea floor observations and the drilling results of Leg 146 by: (1) delineating the paths of upward directed fluid flow within the accretionary prism and (2) demonstrating the effects of tectonic deformation and venting on the bulk mineralogy and physical properties of sediments from the youngest geological past.

Geological setting

The Juan de Fuca oceanic plate converges with the North American plate off Oregon and Washington (Fig. 1) at a present rate of 40-44 mm per year (Davis and Hyndman 1989). At the convergent margin a portion of the sediments loaded on the Juan de Fuca plate is off-scraped during subduction and added onto the North American plate; this process forms the Cascadia accretionary complex along the lower continental slope (Silver 1972; Carson et al. 1974; Kulm and Fowler 1974). The accretionary complex consists of a series of folded and thrusted ridges trending perpendicular to the direction of convergence (Han and Suess 1989). The ridges become progressively older from the west to the east across the complex; the youngest ridges at the deformation front are less than 0.3 M.y. old (Carson et al. 1974; Kulm et al. 1986). Sediment cores were recovered from areas along four transects spanning the tectonic elements of the abyssal plain across the landward and seaward vergent deformation ridge (Fig. 3). The two northern transects (Figs.2a, 2b, 3a) are located in the central Washington overthrust area. The central transect is in the Oregon overthrust area (Figs. 2a, 2b, 3b). The

southern transect is located in the Oregon underthrust area (Figs. 2a, 2b). The locations of the sampling stations and their surrounding tectonic environment are described in detail by Han and Suess (1989) and are summarized in Table 1.

Material and methods

A total of 29 sediment cores were sampled at the core repository of the College of Oceanography at Corvallis (Oregon/USA). These cores were recovered from the continental margin off southern Washington and Oregon during two cruises of RV *Wecoma* (W8306A and W8306C) in June 1983 and of RV *Atlantis* AT8408 and AT8708 in August of 1984 and 1987, respectively. All cores were stored undisturbed for a time span of up to 7 years at 4°C and were in good condition. Previous studies on these cores were restricted to porewater chemistry (Han, 1988), analyses which were performed on whole round samples taken directly on board. The core location is shown in Figure 2.

The sediments are characterized by fairly homogeneous soft hemipelagic muds and oozes with consolidated layers ranging in grain size from silty clay to very fine sand. These consolidated layers prevented, in most places, the penetration of the kasten corer deeper than 3 m. Biogenic components are only present to a minor amount and restricted to siliceous particles. In total 459 samples were taken, 114 shear strength measurements performed and 402 samples analyzed for water content and density. These analyses supplement the sparse physical property measurements made on board and result in a 10-cm sample spacing for all cores. Duplicate samples from the same intervals than those sampled on board revealed a difference of less than 10% in water content. Of the 18 samples taken for ^{14}C-dating, only 3 samples with sufficiently high organic carbon contents were suitable

for this purpose. In addition to the measurement of physical properties and dating of the sediments, the samples were also analyzed for carbonate and organic carbon and a subset of 39 samples for mineralogy by XRD. Grain size analyses on selected samples were restricted to the <63 µm fraction.

The samples were kept cool until they were processed at the laboratory of GEOMAR at Kiel. The following measurements were determined on $10cm^3$ samples, using gravimetric and volumetric determinations: wet-bulk density, dry-bulk density, grain density, porosity, and water content. Measurements of wet and dry weights and volumes allowed us to calculate various related index properties. The wet volume was precisely obtained by cutting the sample with a stainless steel cylinder with a defined volume of 10 cm^3. Wet and dry weights were determined using a Sartorius analytical balance to an accuracy of ± 0.01 g. Water content was determined by weight loss of freeze-dried samples. Wet-bulk density was calculated from the ratio of the weight of the wet sediment to the wet sediment volume, dry-bulk density is given by the ratio of the weight of dry sediment to the volume of wet sediment. Grain density was determined independently by weighing the dry sample and measuring the dry volume with a Penta Pycnometer®. The results were used to calculate the porosity on the basis of the equations given by Boyce (1976); other calculations follow the conventions of the Ocean Drilling Program.

Shear strength measurements were performed on undisturbed sections of the sediment cores with a motorized shear vane device perpendicular to bedding. A vane (10 mm x 8 mm) was inserted 1 cm into the sections and a torsional stress of 4 rpm applied to the sample. The shear strength was calculated using the stress at failure and a geometric-size constant for the vane. The values presented are in most

cases the mean of two to three measurements performed at one interval.

The carbonate and organic carbon contents were determined on the same samples used for the physical property determinations. The measurements were performed on samples treated with 2 n HCL using a LECO CS 244 Carbon Sulphur Analyzer. Measurements with the LECO device yielded the total carbon and organic carbon content of the samples, from which the carbonate content was calculated, by difference. On a set of surface samples recovered by dredging, stable carbon and oxygen isotopes were determined at the mass spectrometer facility of Scipps Institution of Oceanography. The results are listed in Table 3.

Sampling for bulk mineralogical studies focussed on cemented horizons apparent in numerous cores. All samples were mechanically ground and mixed with an internal standard of corundum (α-Al_2O_3) at a ratio of 2:1, further grinding in an agate vial with acetone enhanced homogenization. Samples were then prepared as randomly oriented, press-powder slides and XRD measurements carried out using a Philips PW 1729 generator and $Co_{K\alpha}$ radiation. The goniometer velocity was set at 0.02° 2Θ/s and scans were run between 2°-40° 2Θ. The data was processed using APD-1700 software (Philips) on a Micro PDP 11 computer system.

For the quantification of quartz, the ratio of d(101) of the quartz peak height (at 3.343 Å) to the d(012) corundum peak height (at 3.479 Å) was used. The absoulte amount of quartz was then estimated from a standard curve of 11 mixtures of different amounts of quartz with a monomineralic matrix of smectite. Sediment dating was performed with conventional ^{14}C-metho-dology of the organic carbon (C_{org}) on 3 samples of core AT8408-11. Since the organic carbon content of the

samples is about 1 % of the wet-weight, 250 g of sediment were required, covering an interval of 6-8 cm. The measurements were carried out at the ^{14}C-Laboratory of Kiel University.

Results

The tectonic and depostional history of this margin is most evident from sea floor topography and the reflection patterns of high resolution seismic data. Along the transects across the continental margin sediment cores were recovered at sites selected on the basis of reflection seismic registrations. Although a direct link between seismic reflectors and physical properties of the sediment cores can not been drawn, there is an obvious influence of the large scale deformational processes on the near-surface sediments. The physical properties of the sediments originating from the same tectonic setting are quite similar. They are parallel to the continental margin in north-south direction, since the locations are characterized by the same subduction-induced processes of the Washington/Oregon margin. Considerable differences, however, occur along the transects perpendicular to the margin, from the undeformed abyssal plain over the deformation front and the older deformation ridges to the sediment basins. In general the physical properties of the sediments indicate a stronger deformation of the sediments within the overthrust area off Washington relative to the underthrust area off Oregon.

Continental margin off southern Washington

The seismic profile across the deformation zone off southern Washington (Fig. 2b) reveals the tectonic elements of the youngest deformation. The presentation of the data will be carried out from west to east. The depositional sequence to the west of core W8306-10C is

undisturbed, as evidenced by the numerous reflectors running parallel to the sea floor (Fig. 3a) and by the continuous profiles of the physical parameters, like water content, wet-bulk density, and shear strength, against depth in core W8306C-09 (Fig. 4). Single point excursions from this trend originate in distinct turbiditic horizons, which are higher consolidated and contain higher amounts of the >63µm-fraction. Core W8306-02C (Fig. 5) sampled a collapsed mud mound at the base of the continental margin, in the vicinity of the deformation front, where the reflection pattern is chaotic (Fig. 3a). Collapsing of the mud mound led to a complete detoriation of the sedimentary structure, resulting in porosities and shear strength of 50% and 33 kPa, respectively at a depth of about 40 cm. These values are normaly encountered at burial depths of several hundred meters even at convergent margins (Bray and Karig 1988).

At the crest of the first deformation ridge there are single, bent reflectors visible in the seismic records (Fig. 3a). These reflectors indicate a less pronounced deformation and hence suggest that consolidation of the near-surface sediments in core W8306-04C (Fig. 6) is smaller than in core W8306-02C from the mud mound. Nevertheless, the higher shear strength values of about 20 kPa at a depth of 1 m, parallel a steady decrease of porosity down to 55%. This is also apparent in the physical properties of samples from cores W8306A-04 and W8306A-05 from the flank of the second deformation ridge (Figs. 3b and 7).

Landward of the first and youngest deformation ridge a sediment basin is located. The basin fill is characterized by undisturbed deposits evidenced by smooth and parallel running reflectors (Fig. 3a), dispite the deformed sequences in the vicinity of the diapirs. Physical property measurements of sediment samples from core W8306-11C (Fig. 7)

supports the seismic image by showing a continuous increase of wet-bulk density [1.32 $g \cdot cm^{-3}$ to 1.82 $g \cdot cm^{-3}$] and shear strength to about 10kPa and a simultaneous decrease of porosity (80-55%) with depth.

Continental slope off Oregon

Northern profile (overthrust area)

From the reflection seismic profile recorded perpendicular to the slope (Figs. 2b, and 3b), the different tectonic units can clearly to be distinguished in the reflection characteristics and associated physical properties of the sediments, they are similar to those described above for the Washington deformation zone. The coring localities were selected to sample all zones of the tectonic environments. Undeformed sediments reveal only minor physical property variations with depth, as shown in core W8306C-09 (Fig. 4). Two sediment cores (W8306-02A and W8306-18C) recovered from the vicinity of the first defomation ridge exhibit extreme physical properties even at shallow depth, which correspond to those observed in core W8306C-02 (Fig. 4) in a similar setting off southern Washington. They originate from the most recent shear and compaction movements associated with sediment accretion. Physical property profiles of near surface sediments from the second deformation ridge also reveal strong tectonic influence. At a depth of 80 cm the wet-bulk density of core W8306-05A increases from 1.5 $g \cdot cm^{-3}$ to 1.9 $g \cdot cm^{-3}$ (Fig. 8). These values are associated with shear strength of about 26 kPa and a decrease in porosity to about 38%. In core W8306-04A these values are present as shallow as 40 cm below sea floor (Fig. 8).

Southern profiles (Underthrust area)

Two profiles were sampled across the deformation front and the seaward deformation ridge off central Oregon along 44°40'N and 44°39'N latitudes (Fig. 2b). As it was the case in the other profiles described above, the physical properties of the near surface sediments reflect the different tectonic regimes. The strongest tectonic influence is visible in a core (W8306-26C) from the deformation front region where the shear strength reach maximum values of 51 kPa at a depth of about 120 cm (see Appendix). The profiles of the physical properties vs. depth in all cores recovered from the different tectonic settings (W8306C-24, -26, -27, -28, AT8408-04, -07, -10, -11, AT8708-02, -03) are in the same range as those reported from the northern transects above (see Appendix). The response of the shear strength and water contents to the different deformational regimes, including all data from the southern Washington and Oregon cores, are summerized in Figures 9 and 10.

Bulk mineralogy and carbonate content

The aim of the diagenetic investigations was to resolve the composition and genesis of the consolidated horizons present in numerous cores at various depths. A surprising result is the homogeneity of the bulk mineralogy of the sediments recovered from the various tectonic environments and water depths; a finding that implies that differences in burial depth and degree of consolidation have no influence upon the mineralogical composition, nor that the provenance varied greatly. XRD-de reveal quartz to be by far the most dominant lithogenic component, with maximum intensities of the 101-peak (d = 3.433Å). Additionally, in all samples, felspar and clay minerals, were identified. Clay is dominated in the form of muscovite

and chlorite. Despite the generally homogeneous bulk mineralogical composition, dolomite was documented by a 104-peak (d = 2.882 Å) in samples from cores AT8408-04 and AT8408-11 and in core W8306A-05. The first two cores are located in the deformation front area, whereas the other is from an active vent site (Suess and Whiticar, 1989). Dolomite presumably forms by precipitation from methane and CO_2-containing pore fluids. The dolomite is restricted to compacted, coarse grained (silty sand to fine sand) layers, which are suggestive of high permeability closely related to venting processes (Ritger et al. 1987).

Carbonate contents are consistently below 10 wt.-%, nevertheless, there is a difference between the deformed and undeformed sediments. The carbonate content in the undeformed sediments from the abyssal plain and sediment basins separating the ridges, range from 6 to 9%, in the deformed sediments the maximum values are 3%. Based on single carbonate measurements Han (1988) concluded that the deformed sediments are characterized by higher carbonate contents than the undeformed sediments; an observation that could not been verified by the more numerous carbonate analyses made in this study.

Sedimentation rates at the continental slope off Oregon

The determination of sedimentation rates at the continental margin off northwestern America is hampered by the difficulty of dating the sediments biostratigraphically and by oxygen isotopes. The occurrences of foraminifers are too sparse to establish a reliable oxygen isotope record by conventional mass spectrometry. The need of about 250 g of sediment (due to a content of about only 1% of organic carbon) to obtain a single date with standard ^{14}C-methodology, restricted the vertical and therefore time resolution, considerably. The

samples for ^{14}C-dating span an interval of about 8 cm in the cores to obtain a sufficient amount of organic carbon. Samples of core AT8408-11 from the abyssal plain, just in front of the deformation zone, were used for ^{14}C-dating and the subsequent calculation of sedimentation rates. The position of the core gives a crude idea of the sedimentation rate along the continental margin until more dates are available. The age depth-profile extends to a depth of 106 cm, corresponding to about 7200 years before present, resulting in a mean sedimentation rate of 27.5 $cm \cdot kyr^{-1}$ for the uppermost 31 cm (4,000±100 years) and 27.5 cm in the interval from 31 to 71 cm (5,500±110 years) and about 20 cm/kyr in the depth interval from 71 cm to 106 cm (7,200±130 years). The sedimentation rate of 27.5 $cm \cdot kyr^{-1}$ for the last 4000 years reflects the assumption of a ^{14}C-age of 2900 years of the surface sediments. The results are shown graphically in Fig. 11 and listed in Table 2.

Dewatering along the Cascadia Margin

The water content of all samples of the 37 sediment cores from the Cascadia Margin were determined. Although the cores are spread over a distance of 350 km along the continental margin, they are effected by the same tectonic influence of the subduction of the Juan de Fuca plate beneath the North American Plate. In most cores there exists a substancial difference in the water content between the unconsolidated and consolidated sections. High water content characterize the unconsolidated silty and clayey sediments, whereas lower water contents occur in the cemented silty to sandy horizons. This general picture allows the assumption that the present migration of fluids from depth to the sea floor occurs within the unconsolidated sediment intervals and is hampered by the coarse grained layers. This hypothesis can be confirmed by permeability tests, which unfortunately, were not

possible to carry out at the available samples. Certainly, the main transport of fluids and gases within the accretionary prism occurs along the numerous fault planes (Wang et al. 1990) and to a reduced degree within the sediment strata. Figure 12 illustrates the loss of water through tectonic dewatering as a consequence of deformational processes, which is calculated from the difference in water content between the undeformed and deformed sediments. The water contents from sites of the abyssal plain were used as background from which the water contents of the sites at identical depths have been subtracted yielding the water loss. This simple calculation gives the amount of water expelled through the sea floor by lateral compaction during the last 8,400 years of deformation. Accordingly expulsion rates of $2 \cdot 10^{-4}$ [$L \cdot m^{-2} \cdot d^{-1}$] were obtained by using the maximal difference in water content of 30% between the undeformed and deformed sediments down to a depth of 2 m, for which ^{14}C-dates exist encompassing a time span of 8,400 years. This expulsion rate agrees within an order of magnitude with those based on porosity reduction of $2 \cdot 10^{-4}$ [$L \cdot m^{-2} \cdot d^{-1}$] and published by Carson et al. (1990). The expulsion rates calculated from porosity reduction are four to five orders of magnitude smaller than those obtained by direct flow measurements in venting areas (Linke et al., in press). This difference presumably is related to the unknown area of venting at the deformation front; e.g. whether 0.1%, 1.0% or 10% of the total area from which the sediment cores were taken, are actively venting. On the other hand, the direct fluid flow measurements made by submersible were always taken at the highly focussed vent sites and thus are biased towards active venting areas. A further uncertainty with the calculation of expulsion rates is related to possible recirculation within the uppermost sediment column.

Discussion

Pelagic carbonate deposition and authigenic carbonate precipitation

Our carbonate analyses and those of Scamman (1981) from surface samples of the same area combined with carbon isotopic analyses give insight into the origin of carbonates in this hemipelagic environment controlled by tectonic activity. The carbon isotopie values can be separated into 6 groups (Fig. 13). There is a clear frequency maximum in Group II (0 to -3‰ PDB) representing samples containing modern benthic foraminifers with an isotopic composition of +0.5 to -1‰ PDB typical for this region (Zahn, pers. comm.) Group VI with $\partial^{13}C$-values of -40 to -70‰ PDB represent carbonates derived from oxidation of a mixture of thermogenic and biogenic methane (Suess and Whiticar 1989). Groups III and IV with $\partial^{13}C$ values of -6 to -20 ‰PDB are present in minor amounts, and samples with carbon isotopic signatures of -20 to -40 ‰PDB are absent. The division of $\partial^{13}C$-groups can be directly related to differences in the amounts of carbonate present in the samples. The most frequent carbonate values correspond to Group III and not Group II as did the $\partial^{13}C$-isotopic values. In all other groups there is agreement between the frequency distribution of carbonate content and the isotopic signatures (Fig. 13). Figure 14 shows the carbonate contents and $\partial^{13}C$-isotopic ratios of samples from two adjacent dredge hauls (Fig. 15). Dredge 19 is typical for Group II with carbonate contents of up to 6% and $\partial^{13}C$-values of 0 to -3‰ PDB. Samples of Dredge 16 show that high carbonate contents of up to 60% correspond with light $\partial^{13}C$ values of -50‰ PDB, characteristic for Group VI.

This indication of $\partial^{13}C$-values corresponding with carbonate contents of the surface samples is taken to infer the isotopic ratios from the carbonate contents measured in the sediment cores, since isotopic analyses have so far not been performed on samples from the

sediment cores. The frequency distribution of carbonate contents obtained from the cores show a maximum in Group I and II (0-5 wt.-% carbonate). The corresponding carbon isotopic ratios should hence be between +1 and -3‰ PDB, which indicates that the carbonate is almost exclusively biogenically produced. Carbonate contents between 5 and 10 % (Group III), reflecting carbon iosotopic values of -3 to -5‰ PDB, are only present in single samples and carbonate contents of > 10% are completely missing. This implies that there is no methane-derived carbonate present in disseminated form in the cores. This result, however, does not exclude possible authigenic carbonate production, since higher carbonate contents could be dissolved by interaction with the pore waters.

Origin of cemented layers

A typical phenomenon in a great number of cores from the Cascadia Subduction Zone is the appearance of cemented horizons at various depths. They prevented on several occasions the deeper penetration of the coring device. The cemented horizons can be recognized in the visual core description as well-defined horizontal layers of up to 20 - 30 cm in thickness. They are composed of a higher amount of the coarse fraction than the surrounding soft silty to clayey sediments. Grain size analyses support the macroscopic observations of an upward gradation from coarser to finer deposition within the cemented layers. The X-ray diffraction analyses performed on samples from the uncemented and cemented sediments exhibit a great similarity in bulk mineralogy. Bulk mineralogy seems to be unaffected by the degree of consolidation, as there are only very minor differences in the overall composition and the refraction intensities of single minerals. The carbonate content tend to be slightly higher in the cemented horizons compared to the surrounding sediments.

A possible mechanism to generate the cemented layers may be seen in their close genetic relationship to venting processes. In Figure 16a to 16d the generation of a cemented layer in the context of venting is schematically illustrated. A typical sea floor setting in a venting area (Fig. 16a), which summarizes the observations from submersible dives; i.e. the presence of colonies of tubeworms associated with clam fields and carbonate chimneys (Suess et al., 1985; Ritger et al., 1987). Within the seabed there are randomly distributed cemented lenses of coarse grain sediments at different depths and various lateral extention. Already slight motions along numerous and locally restricted faults allows the upward migration of fluids and dissolved gases in the accretionary complex and subsequently their expulsion at the sea floor. With the presumably sudden onset of venting the fine sediment particles are blown away (Fig. 16b), and the coarser components remain at the site. Vent organisms are attracted and settle at the new site of nutrient supply. The flow rates remain constant over an as yet unknown time span before the onset of a slow decline (Fig. 16c). This leads to an upward mixing of coarse remnant particles and pelagic sedimentation with a result of gradational bedding at the vent site and its close vicinity. In Fig. 16d the coarse grained layer is illustrated as part of the sediment column.

In this scenario the cementation of the sediments within the presumably lense-shaped graded layer is a syn- and post sedimentary process, caused by authigenic carbonate precipitation of ΣCO_2- and CH_4- containing fluids. This is expressed by the occurrence of dolomite in some of the cemented layers (Fig. 17). Long-term expulsion of these fluids results in the generation of carbonate chimneys and concretions of various shapes and sizes at the sea floor as observed by submersible dives (Ritger et al. 1987) and dredged by fishermen.

The coarse grained layers do not originate from turbidite deposition, which is certainly present in this steep continental margin, but instead, they are generated by venting processes. This is evident from the simultaneous higher degree of consolidation of the layers and the restricted occurrence of dolomite to these horizons. Furthermore, cores (AT 8408-04, AT 8408-11) separated by only about 200 m, reveal cemented horizons at different subbottom depths (Fig. 18). Over this distance the turbiditic events should be preserved in both cores at the same depths. *In situ* observations from submersibles show that in an area of venting activity single vent sites are only few meters across and separated by tens of meters. The two cores have presumably sampled individual vent sites, which have been active at different time intervals.

Conclusion

Physical properties of sediments recovered by gravity cores from the Cascadia Margin exhibit the deformational processes along this convergent margin. Strongest lateral stress occurs at the present deformation front expressed by abnormally high shear strength values and low porosity values, even at shallow burial depth. Older deformation ridges exhibit values differing significantly from those obtained from the undeformed sediments present at the abyssal plain and the basins between the deformation ridges.

Physical property measurements combined with grain size, carbonate and bulk mineralogy analyses provided a comprehensive data set to verify the composition of the cemented layers encountered at different depths in numerous cores. There appears to be a coincidence of coarser (silty to sandy) sediments with high shear strength and lower water content compared to the otherwise homogeneous clayey to silty unconsolidated intervals. Despite few occurrences of dolomite in

some of the cemented layers, there is no difference in the bulk mineralogy between the uncemented and cemented sediments. Quartz, felspar and clay minerals (illite and chlorite) are the dominant lithogenic components. Carbonate contents between 1 and 3% are most frequent with single samples reaching values of up to 10%. Apart from the very homogeneous mineralogical composition, dolomite was detected in some of the cemented horizons, which is presumably a precipitation product of the CO_2-containing fluids being expelled.

Based on the observations of the numerous cores a model for the generation of the cemented, coarse grained and graded horizons is developed. Since these horizons appeared at two adjacent cores in different depths intervals we conclude that they are derived from venting processes and are not deposited by turbiditic events.

By comparing the water contents of the cores from the undeformed abyssal plain and the deformed part of the continental margin, it was possible to calculate the water being expelled during the deformation process, as being 2×10^{-4} $L \cdot m^{-2} \cdot yr^{-1}$ It could be shown that dewatering is enhanced off central Oregon compared to the margin off southern Washington. In order to obtain an idea about the rates of sedimentation along the Cascadia Margin for the uppermost sediments we dated an undisturbed core recovered from the abyssal plain close to the deformation front. ^{14}C-dates yield sedimentation rates of 20.6 $cm \cdot kyr^{-1}$ to 27.5 $cm \cdot kyr^{-1}$ for the last 7,200 years BP.

Acknowledgements

We would like to acknowledge the most helpful assistence of A. Ungerer during sampling at the core repository at OSU, Corvallis. The sediment cores were collected between 1983 and 1987 with financial support through the NSF Grant OCE-86-09789 to L.D. Kulm (OSU) and E.

Suess. Financial support to the core repository at OSU is provided by NSF grant No. OCE88-00458. Physical property measurements were conducted with the help of S. Utschakowski and U. Peters at Geomar, Kiel. We would like to express our sincere appreciation to P. Holler and F. Kögler (U. Kiel) who made available the shear strength device. Many thanks are due to G. Bohrmann and the technical staff of the Alfred-Wegener-Institute for Polar and Marine Research (Bremerhaven) for performing the XRD-measurements. We thank H. Willkomm and the staff of Radiocarbon Laboratory (U of Kiel) for the ^{14}C-dating, as well as J. Killingley (formerly Scripps Institution of Oceanography) for stable isotope measurements. We most gratefully acknowledge the critical and helpful comments of M. Torres (Geomar) which improved the manuscript considerably. Financial support for this investigation was provided by BMFT-grant 03R6076.

References

Behrmann, et al., *Proc. Init. Res., ODP*, 141, College Station, TX: Ocean Drilling Program, in press

Boyce, R.E. 1976. Definitions and laboratory techniques of compressial sound velocity parameters and wet-water content, wet-bulk density, and porosity parameters by gravimetric and gamma ray attenuation techniques. *Init Repts., DSDP*, 33, (U.S. Govt. Printing Office), Washington,: 931-958.

Carson, B. 1977. Tectonically induced deformation of deep-sea sediments off Washington and Northern Oregon: Mechanical consolidation. *Marine Geology*, 24: 289-307.

Carson, B., E. Suess, and J.C. Strasser. 1990. Fluid flow and mass flux determinations at vent sites on the Cascadia Margin accretionary prism. *Journ. Geophys. Res*, 95: 8891-8897.

Davis, E.E., and Hyndman, R.D. 1989. Accretion and recent deformation of sediments along the northern Cascadia subduction zone. *Geol. Soc. Am. Bull.*, 101: 1465-1480.

Davis, E.E., Chapman, D.S., Forster, C.B., and Villinger, H. 1989. Heat-flow variations correlated with buried basement topography on the Juan de Fuca ridge flank. *Nature*, 342: 533-537.

Davis, E.E., G.C. Horel, R.D. MacDonald, H. Villinger, R.H. Bennett, and H. Li. 1991. Pore pressures and permeabilities measured in marine sediments with a tethered probe. *Journ. Geophys. Res.*, B4: 5975-5984. .

Han, M.W. and E. Suess. 1989. Subduction-induced pore fluid venting and the formation of authigenic carbonates along the Cascadia continental margin. Implications for the global Ca-cycle. *Paleogeogr. Paleoclimatol. Paleoecol.*, 71: 97-118.

Hill, I., A. Taira, et al. 1991. *Proc., Init. Repts., ODP*,131, College Station, TX: Ocean Drilling Program.

Kulm, L.D., and Fowler, G.A., 1974. Oregon continental margin structure and stratigraphy: A test of the imbricate thrust model. In *The Geology of continental margins.*, ed. C.A. Burk and Drake, C.L., Springer Verlag,New York: 261-283. .

Kulm, L.D., Suess,E., Carson,B., Lewis,B.T., Ritger,S.D., Kadko, C., Thornburg, T.M., Embley, R.W., and Rugh, W.D. 1986. Oregon subduction zone: venting, fauna, and carbonates. *Science*, 231: 561-566.

Kulm, L. and E. Suess. 1990. Relationship between carbonate deposits and fluid venting: Oregon accretionary prism. *Journ. Geophys. Res.*, 95: 8899-8915.

Linke, P., E. Suess, M. Torres, V. Martens, W. D. Rugh, W. Ziebis, D. Kulm. 1993. *In situ* measurements of fluid flow from cold seeps at active continental margins. *Deep-Sea Research,* in press.

Moore, J.C., A. Mascle, et al. 1988. *Proc. Init. Repts., ODP*, 110: Ocean Drilling Program. College Station, TX

Ritger, S., Carson, B., and Suess, E. 1987. Methane-derived authigenic carbonates formed by subduction-induced pore-water expulsion along the Oregon/Washington margin. *Geol. Soc. Amer. Bull.*, 98: 147-156.

Shi, Y., C Wang -Y., W.-T. Hwang, and v. Huene R. 1989. Hydrogeological modeling of porous flow in the Oregon accetionary prism. *Geology*, 17: 321-323.

Silver, E.A. 1972. Pleistocene tectonic accretion of the continental slope off Washington. *Marine Geology*, 13: 239-249.

Suess, E., Carson, B., Ritger, S.D., Moore, J.C., Jones, M.L., and L.D. Kulm and Cochrane, G.R. 1985. Biological communities at vent sites along the subduction zone off Oregon. *Biol. Soc. Wash. Bull.*, 6: 475-484.

Suess, E., R. Von Huene, et al. *Proc. Init. Res., ODP*, 112, College Station, TX: Ocean Drilling Program, 1987.

Suess, E. and M.J. Whiticar. 1989. Methane-derived CO_2 in pore fluids expelled from the Oregon Subduction Zone. *Paleogeogr. Paleoclimatol. Paleoecol.*, 71: 119-136.

Wang, C.-Y., Shi, Y., Hwang, W.-T., and Chen, H. 1990. Hydrogeologic processes in the Oregon-Washington accretionary complex. Journ. Geophys. Res., 95: 9009-9023.

FIGURE CAPTIONS

Figure 1. Overview of the study areas off Washington and Oregon with the main structural features.

Figure 2. Study areas along the Cascadia Margin as shown by the hatched areas in fig. 1. A) Bathymetry and study areas off Washington and Oregon. Contour intervals are 500 m water depth. B) Detailed view of coring localities off Washington (I) and central Oregon (II, and III) (after Han, 1988).

Figure 3. Seismic sections with location of sampling sites across the lower continental slope (a) off Washington and (b) off central Oregon. RK-C and RK-A denotes cores taken during *Wecoma*-cruise W8306-A and W8306-C. For reference see Fig. 2 and Table 1.

Figure 4. Physical properties of core W8306C-09 from the abyssal plain with typical values reflecting the pelagic depositional environment. Dissolved calcium values in the pore water are those reported by Han (1988).

Figure 5. Physical properties of sediment core W8306C-02 from a mud mound at the deformation front. Note the high shear strength values at shallow depth and the low porosity and water content values.

Figure 6. Core W8306C-04 originates from the top the seaward ridge with intermediate shear strength values, porosity and water content values.

Figure 7. The physical properties of core W8306C-11 reflect the unconsolidated nature of the sediments within a sediment pond situated between two deformational ridges.

Figure 8. The cores W8306A-04/-05 were recovered from the western slope of the second deformation ridge The physical properties show only minor tectonic influence on the recovered sediments.

Figure 9. Shear strength versus depth in relation to the tectonic environment.

Figure 10. Water content versus depth in relation to the tectonic environment.

Figure 11. Age depth profile derived from ^{14}C-dating on samples from core AT8408-04 and the calculated sedimentation rates.

Figure 12. Dewatering of the sediments as a consequence of deformation along the Cascadia subduction zone. The difference in water content in percent of the wet-weight between the undeformed sediments of the abyssal plain and the deformed sediments of the deformation area indicates considerably higher amount of dewatering off central Oregon compared to the sites off southern Washington

Figure 13. Relation and classification of $CaCO_3$-content and $\partial^{13}C$-values in samples of all anticipated tectonic environments along the Cascadia-margin. Part of the carbonate contents are taken from Scamman (1981).

Figure 14. Comparison of carbonate contents and $\partial^{13}C$-values of samples from Dredge hauls 16 and 19. For location see Fig. 15.

Figure 15. Location and $\partial^{13}C$-values of surface samples from the Cascadia Margin.

Figure 16a - 16d. A diagramatic illustration of the origin of cemented coarse grained layers in venting areas.

Figure 17. X-ray diffractogram of sample AT8408-11, 114-116 cm representing the mineralogic composition of a cemented horizon with the high quartz intensity (occuring in all samples) of the 101-peak at 3.443 Å (2Θ). In addition this sample is characterized by a pronounced dolomite occurrence with the 104-peak at 2.8859 Å (2Θ).

Figure 18. Lithology and water contents of cores AT8408-04 and AT8408-11. Both sites are separated by only a couple of meters, and thus the difference in depth of the cemented, coarse grained layers is striking. This observation supports the idea that the layers are not originated from turbiditic events but instead are produced by venting, which is widespread along the margin but with a limited spatial extent of a single vent site of only a couple of square meters. The water content profiles reflect the lower values in the cemented horizons relative to the unconsolidated sections. Therefore, fluid flow takes place predominantely in the unconsolidated hemipelagic oozes and muds.

TABLE CAPTIONS

Table 1. Coring sites, their positions, water depth, and recovery of each core.

Table 2. Sedimentation rates of core AT8408-04, calculated from conventional ^{14}C-datings on the total carbon content.

Table 3. Oxygen and carbon isotopic values from surficial and coring samples. Carbonate contents are taken from Scamman (1981).

Appendix:

Physical properties of all samples analyzed onboard and at the shore-based laboratory up to seven years later. Shipboard data lack porosity and grain density values.

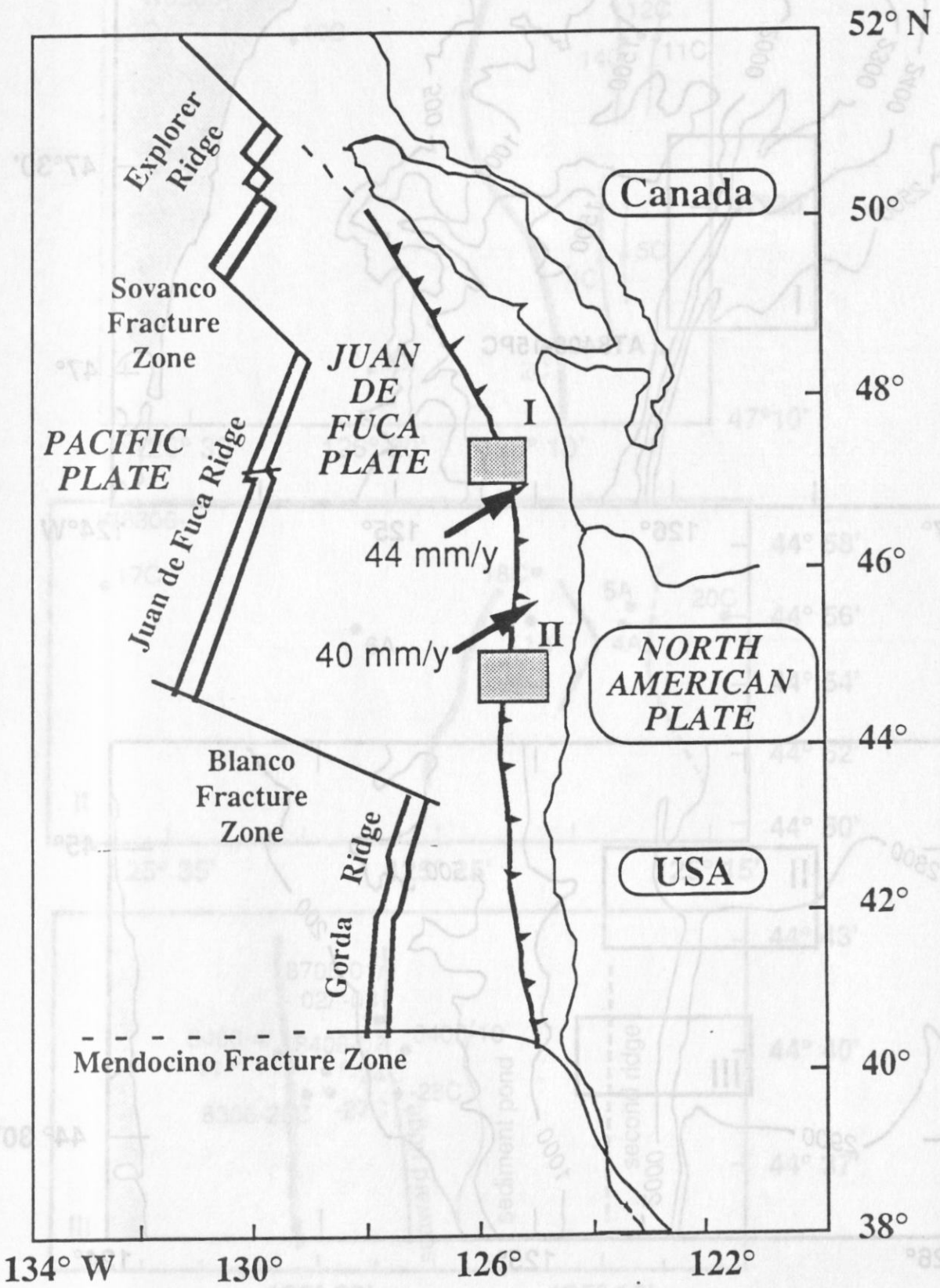
52° N
50°
48°
46°
44°
42°
40°
38°
134° W
130°
126°
122°
Explorer Ridge
Sovanco Fracture Zone
PACIFIC PLATE
Juan de Fuca Ridge
JUAN DE FUCA PLATE
Canada
I
44 mm/y
40 mm/y
II
NORTH AMERICAN PLATE
USA
Blanco Fracture Zone
Gorda Ridge
Mendocino Fracture Zone

Fig. 1

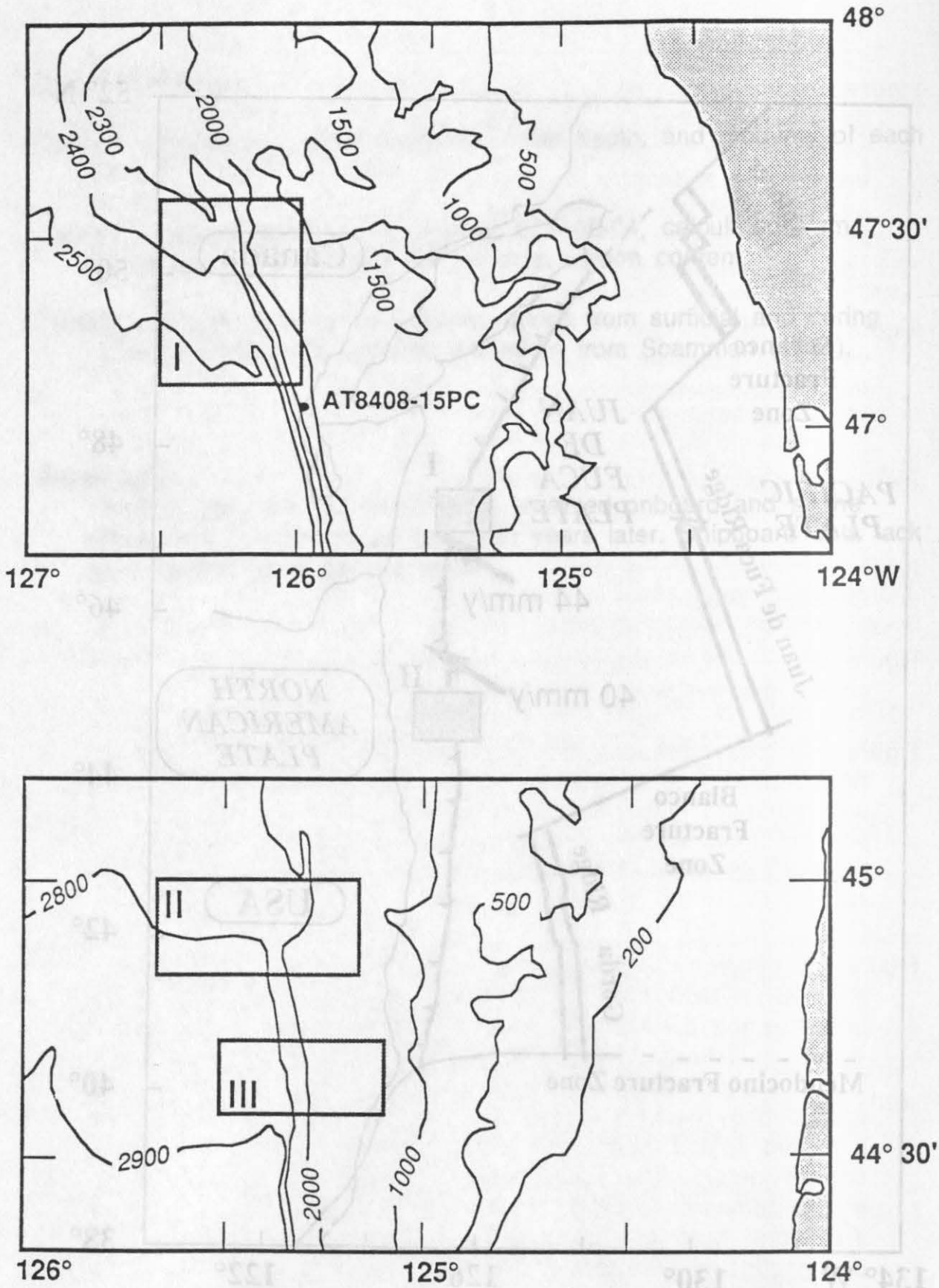
48°
47°30'
47°
2000
1500
500
2300
2400
1000
2500
1500
I
AT8408-15PC
127°
126°
125°
124°W
45°
2800
500
200
II
III
2900
2000
1000
44° 30'
126°
125°
124°

Fig. 2a

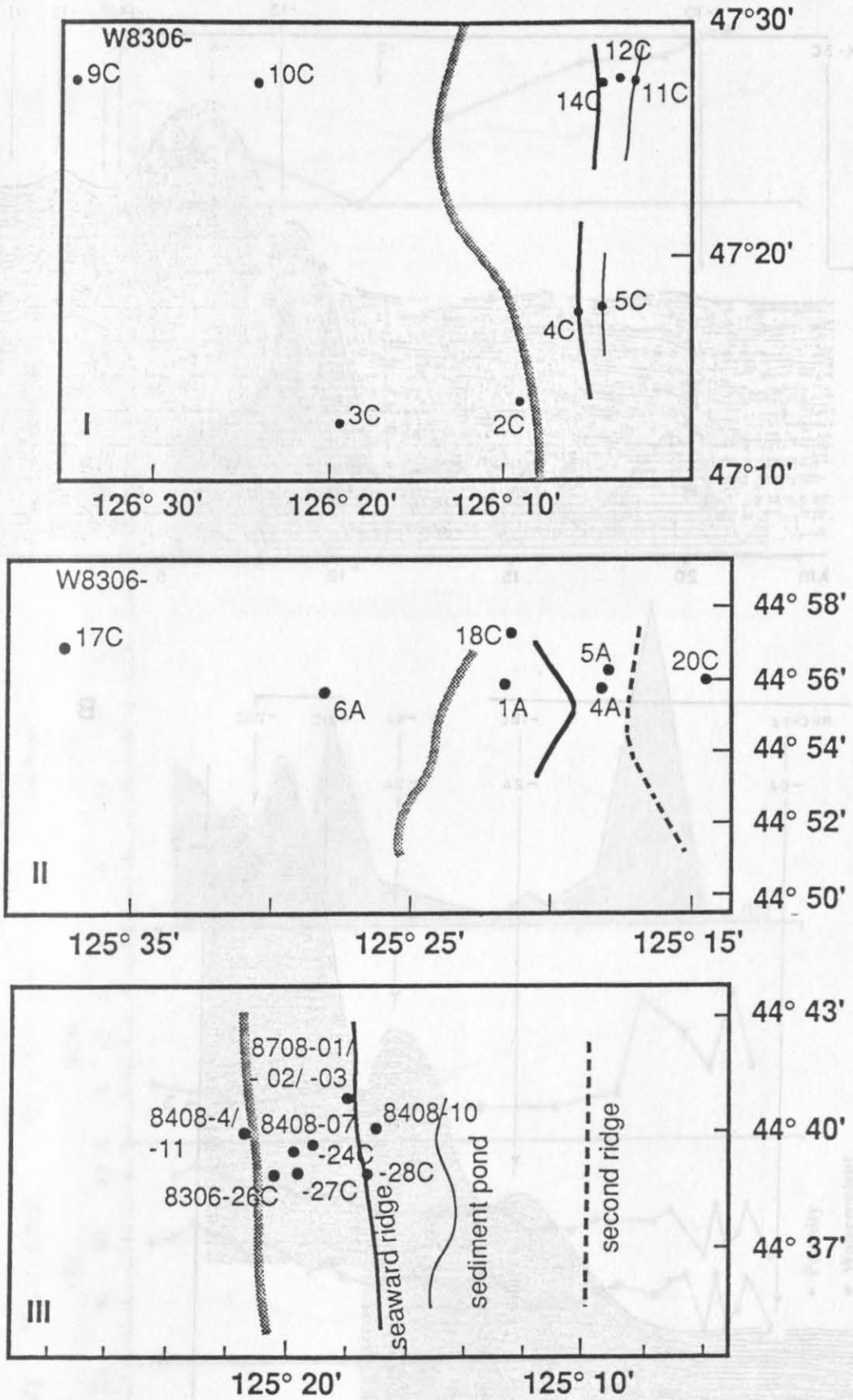
W8306-
9C
10C
12C
14C
11C
47°30'
47°20'
4C
5C
I
3C
2C
47°10'
126° 30'
126° 20'
126° 10'
W8306-
17C
18C
5A
20C
6A
1A
4A
44° 58'
44° 56'
44° 54'
44° 52'
44° 50'
II
125° 35'
125° 25'
125° 15'
44° 43'
8708-01/
- 02/ -03
8408-4/
-11
8408-07
8408-10
-24C
-28C
8306-26C
-27C
seaward ridge
sediment pond
second ridge
44° 40'
44° 37'
III
125° 20'
125° 10'

Fig. 2b

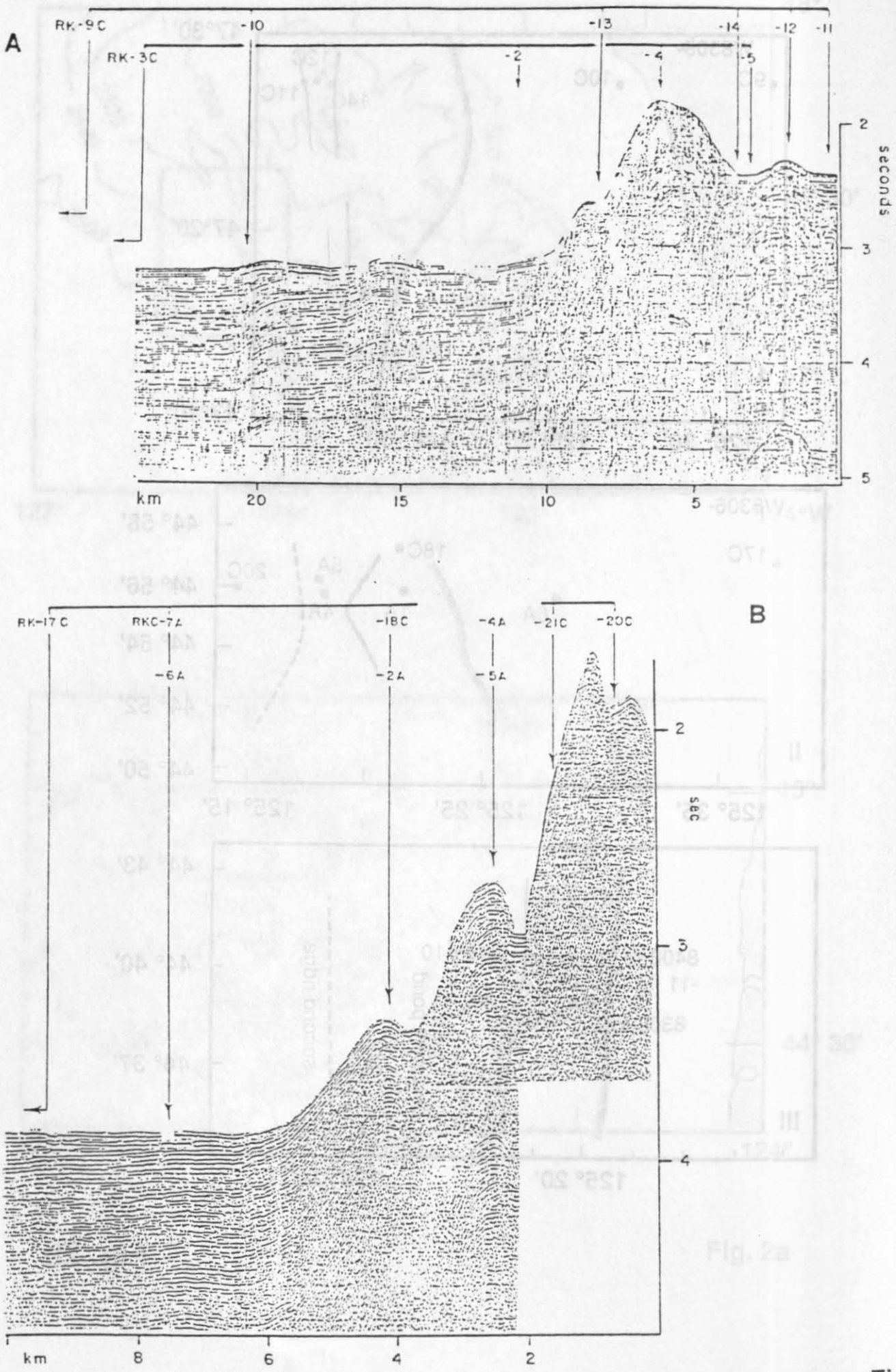
A
RK-9C
-10
-13
-14
-12
-11
RK-3C
-2
-4
-5
2
3
4
5
seconds
km
20
15
10
5
B
RK-17C
RKC-7A
-18C
-4A
-21C
-20C
-6A
-2A
-5A
2
3
4
sec
km
8
6
4
2

Fig. 3

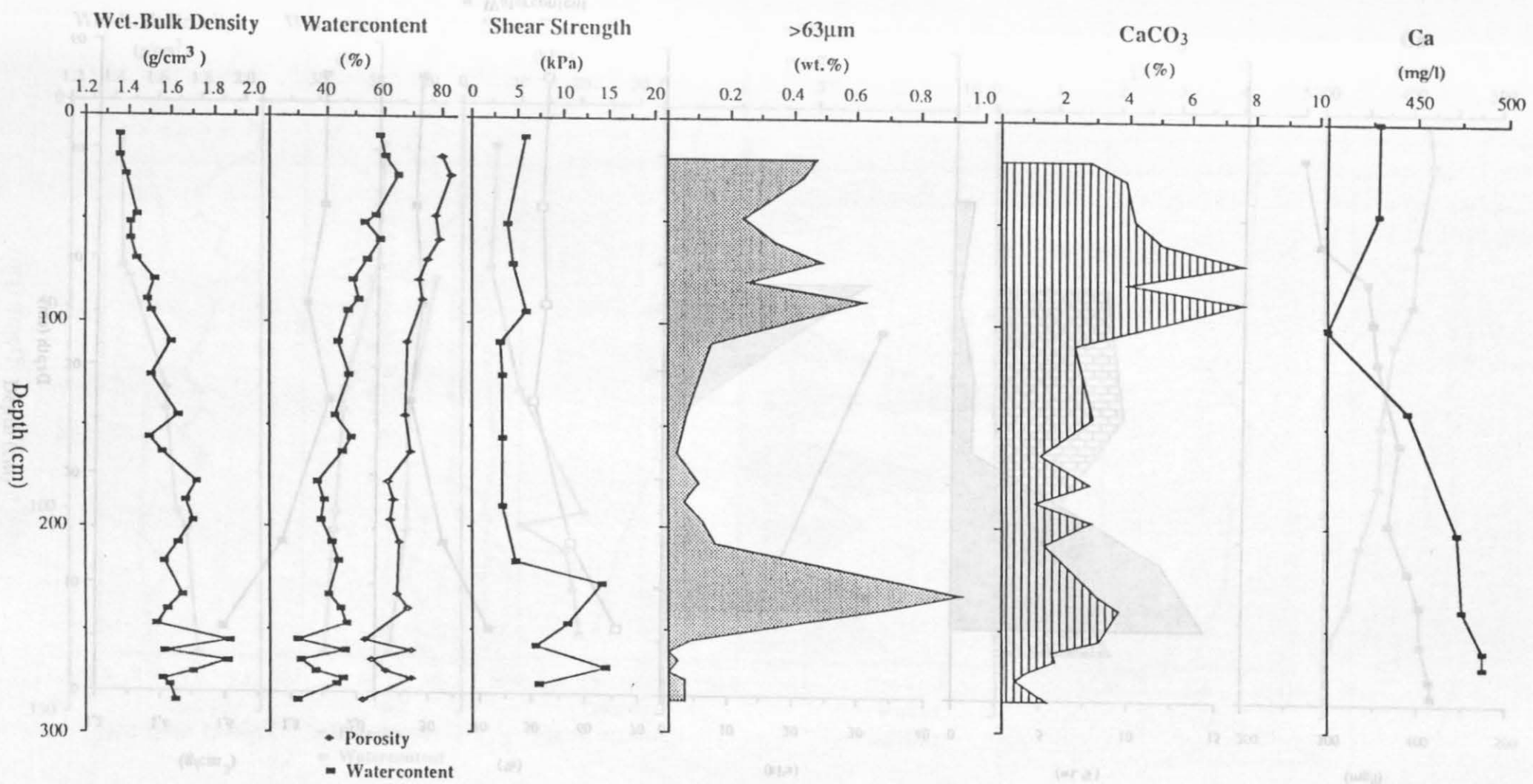
RK-09C
2370m (abyssal plain)
Wet-Bulk Density
(g/cm3)
1.2 1.4 1.6 1.8 2.0
Watercontent
(%)
40 60 80
Shear Strength
(kPa)
0 5 10 15 20
>63µm
(wt.%)
0.2 0.4 0.6 0.8 1.0
CaCO3
(%)
2 4 6 8 10
Ca
(mg/l)
450 500
0
100
200
300
Depth (cm)
Porosity
Watercontent

Fig. 4

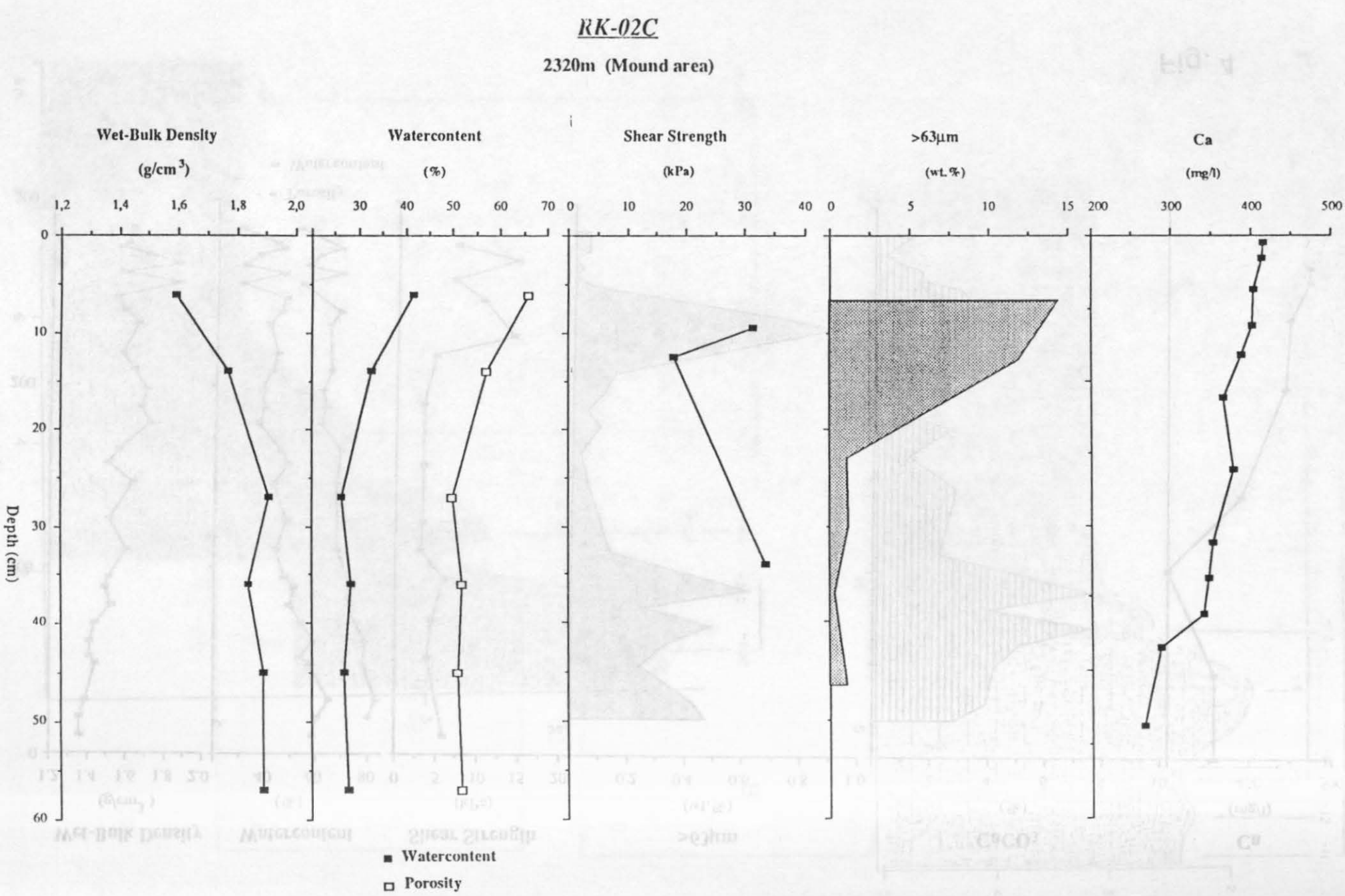
RK-02C
2320m (Mound area)
Wet-Bulk Density
(g/cm3)
Watercontent
(%)
Shear Strength
(kPa)
>63µm
(wt.%)
Ca
(mg/l)
Depth (cm)
Watercontent
Porosity

Fig. 5

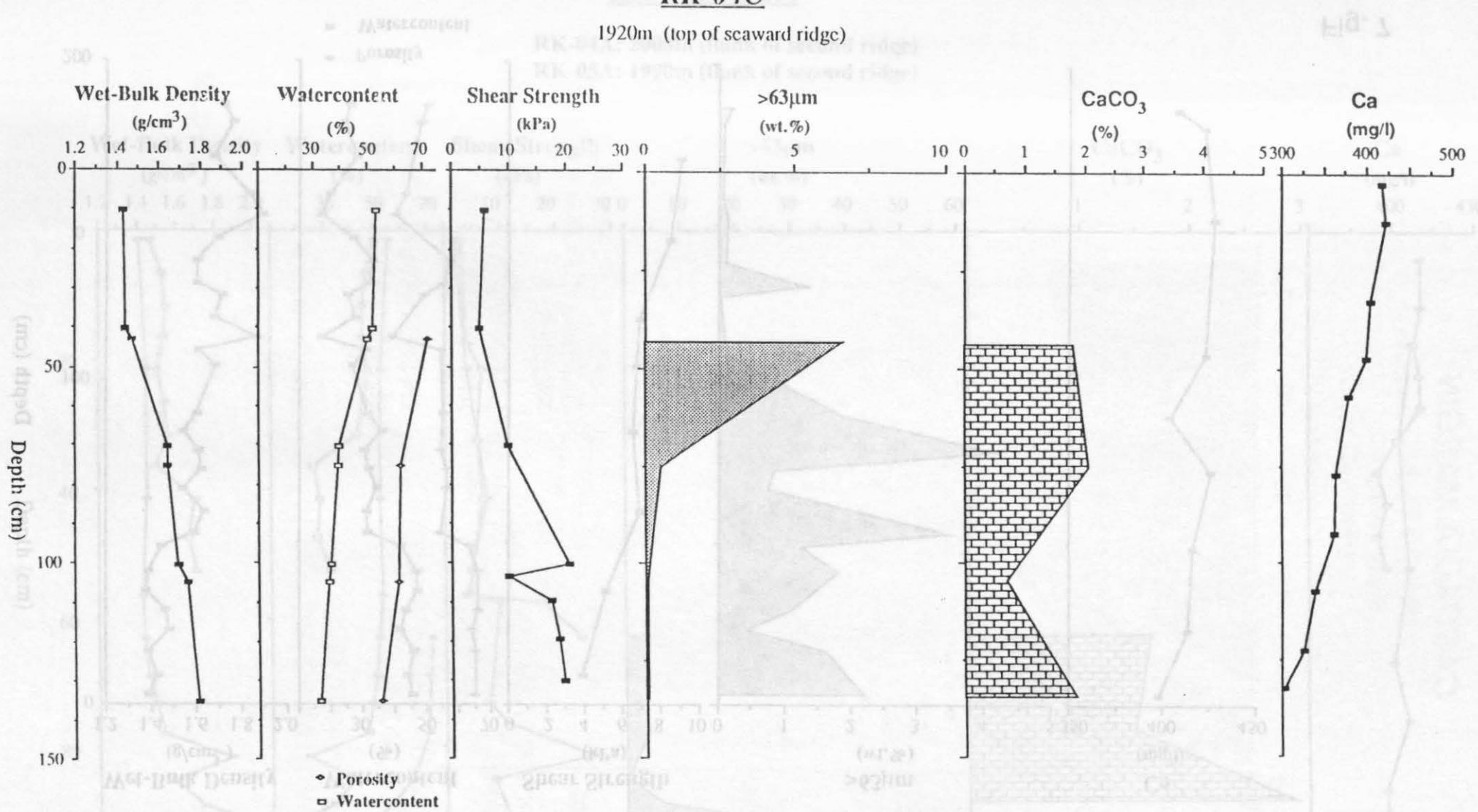
RK-04C
1920m (top of seaward ridge)
Wet-Bulk Density
(g/cm3)
1.2 1.4 1.6 1.8 2.0
Watercontent
(%)
30 50 70
Shear Strength
(kPa)
0 10 20 30
>63µm
(wt.%)
0 5 10
CaCO3
(%)
0 1 2 3 4 5
Ca
(mg/l)
300 400 500
Depth (cm)
0
50
100
150
Porosity
Watercontent

Fig. 6

RK-11C

1600m (sediment pond behind seaward ridge)

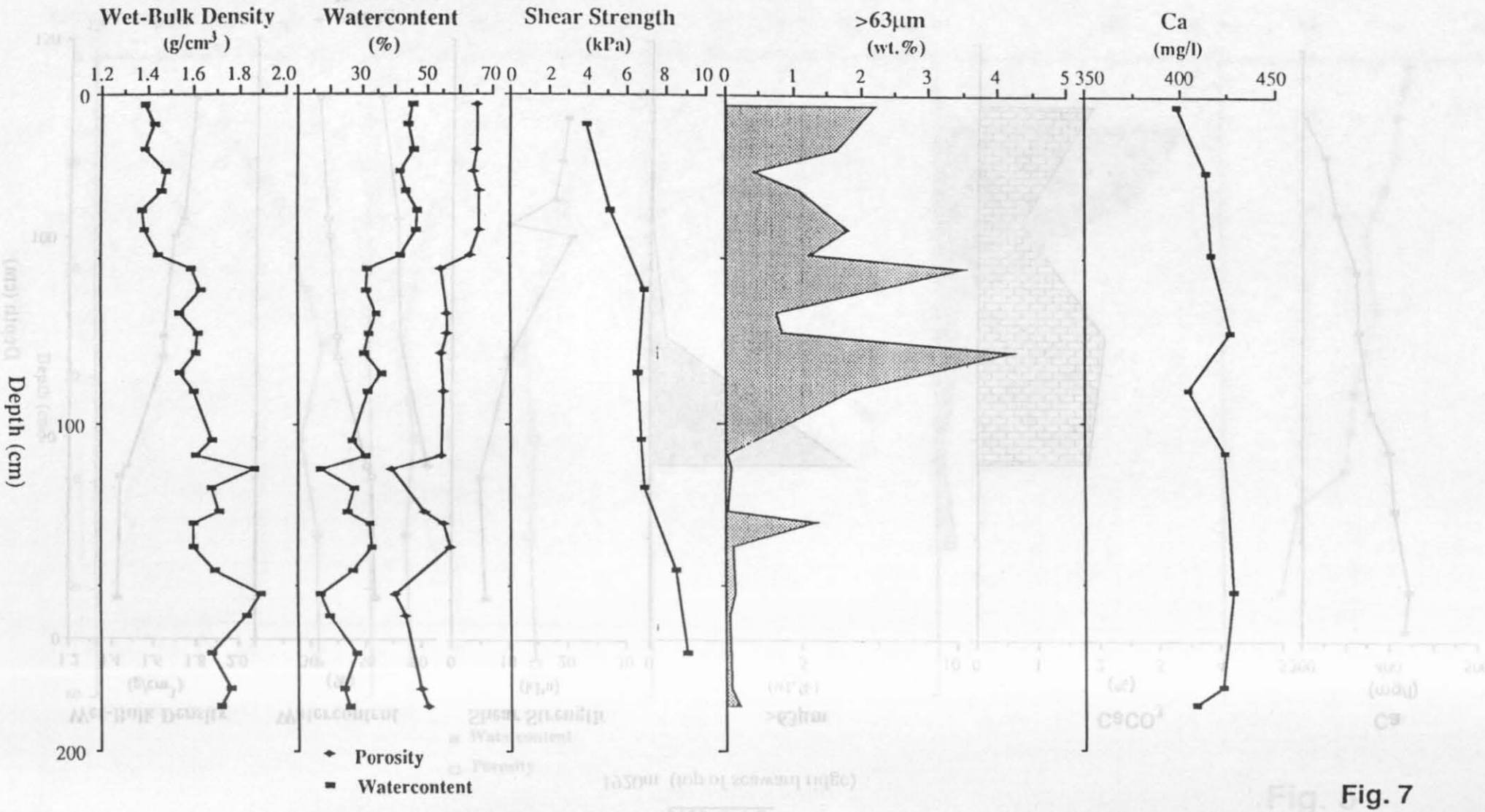

Fig. 7

RK-04A/-05A

RK-04A: 2008m (flank of second ridge)
RK-05A: 1990m (flank of second ridge)

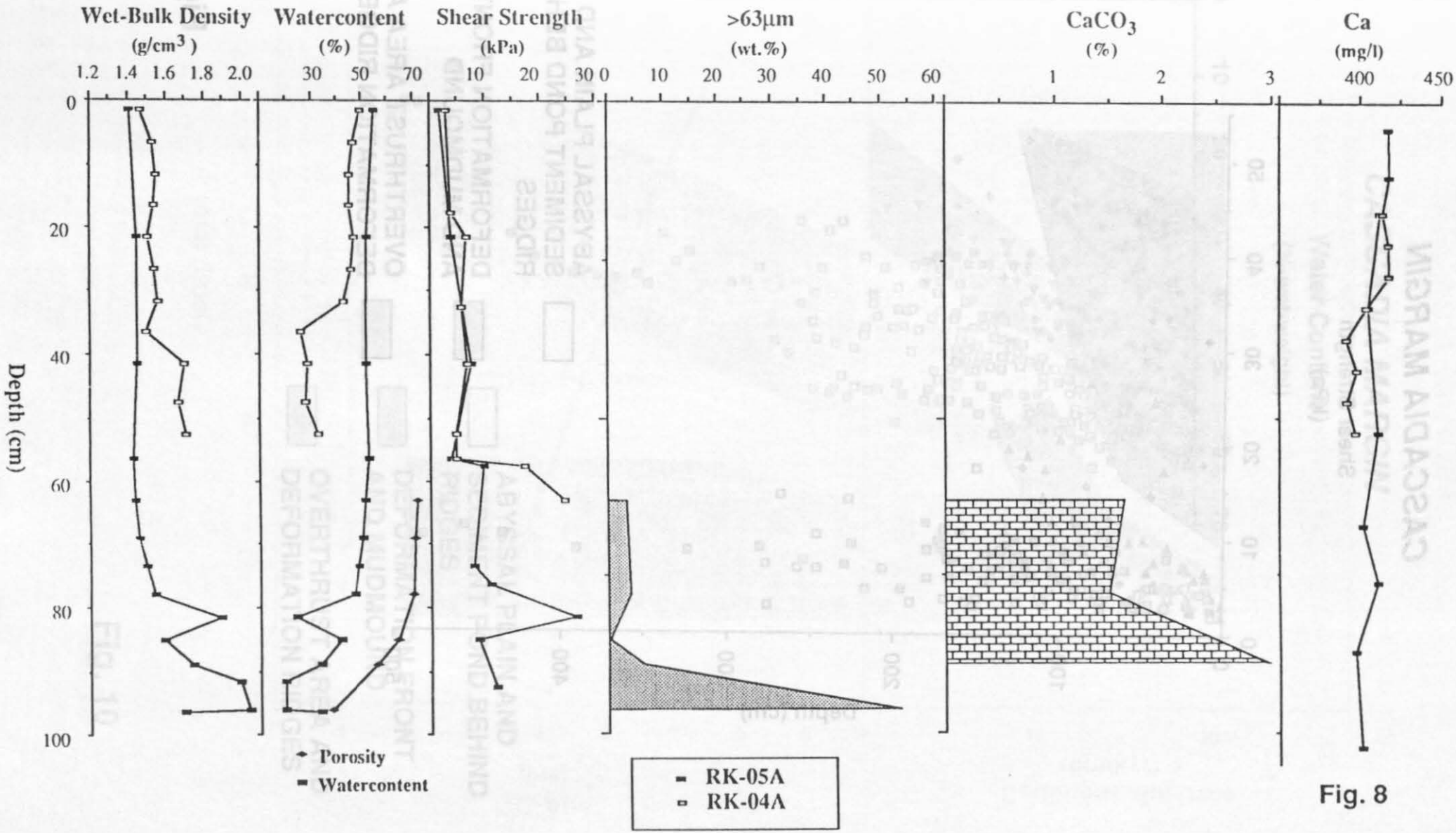

Fig. 8

CASCADIA MARGIN

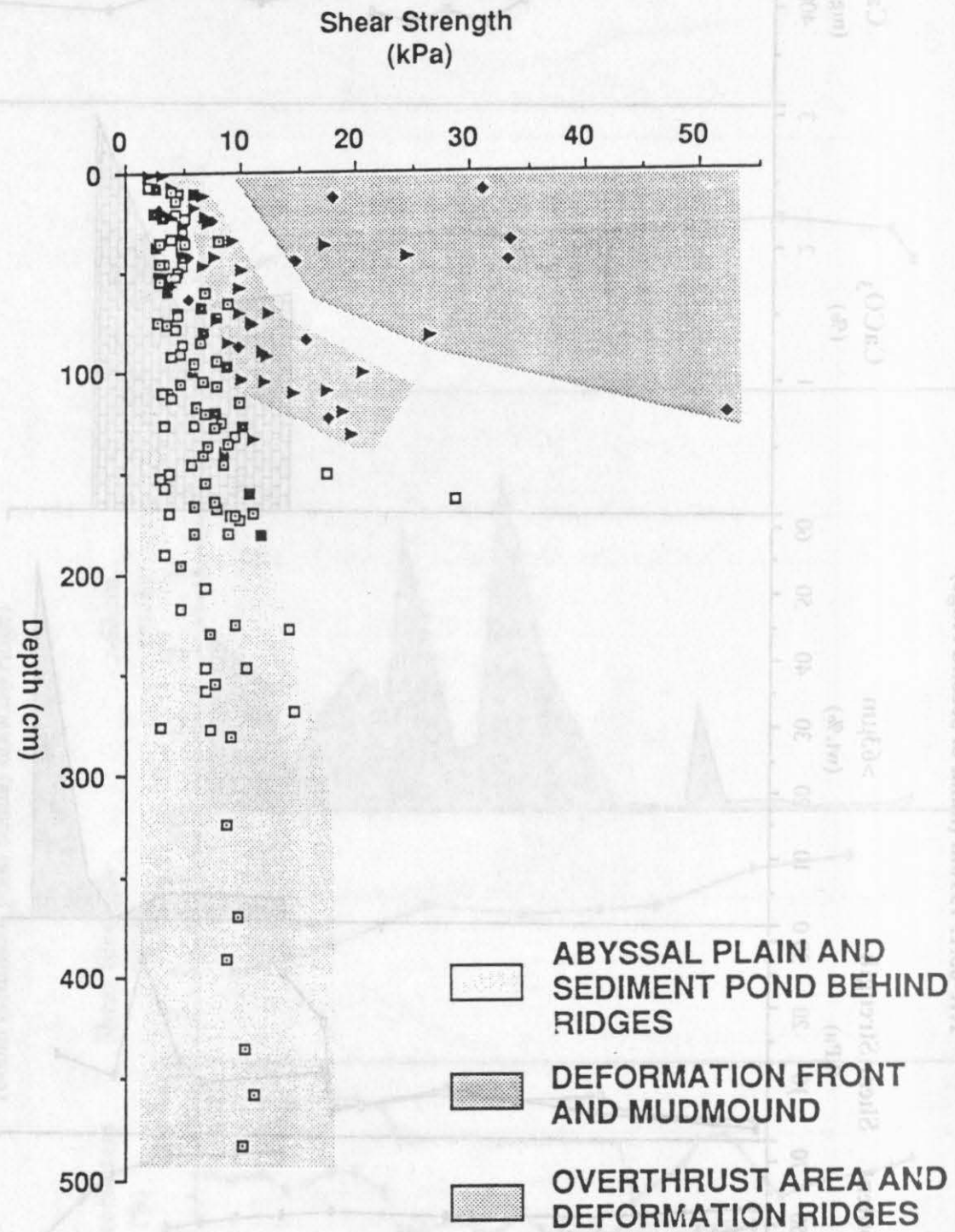

Fig. 9

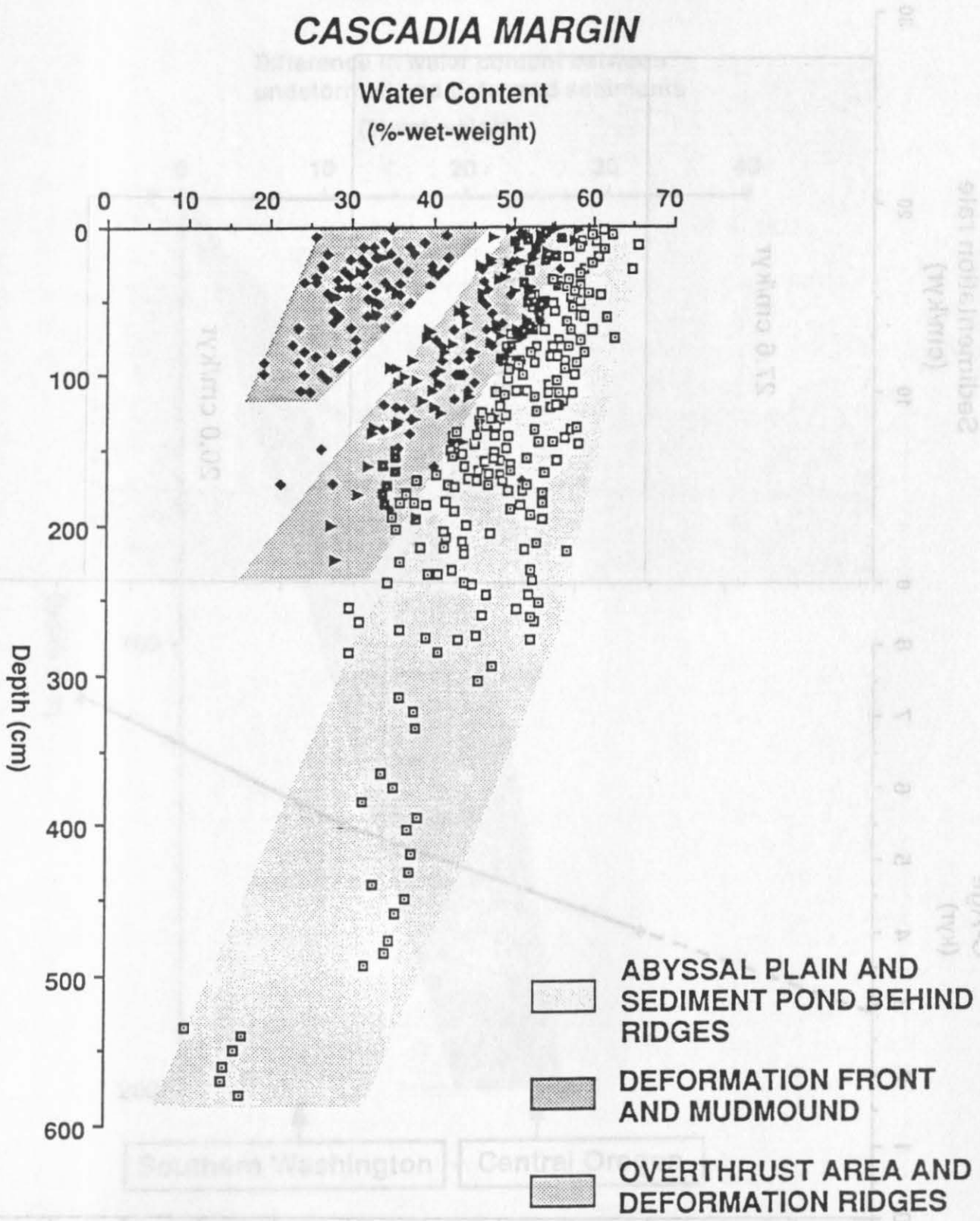
CASCADIA MARGIN
Water Content
(%-wet-weight)
0
10
20
30
40
50
60
70
0
100
200
300
400
500
600
Depth (cm)
ABYSSAL PLAIN AND SEDIMENT POND BEHIND RIDGES
DEFORMATION FRONT AND MUDMOUND
OVERTHRUST AREA AND DEFORMATION RIDGES

Fig. 10

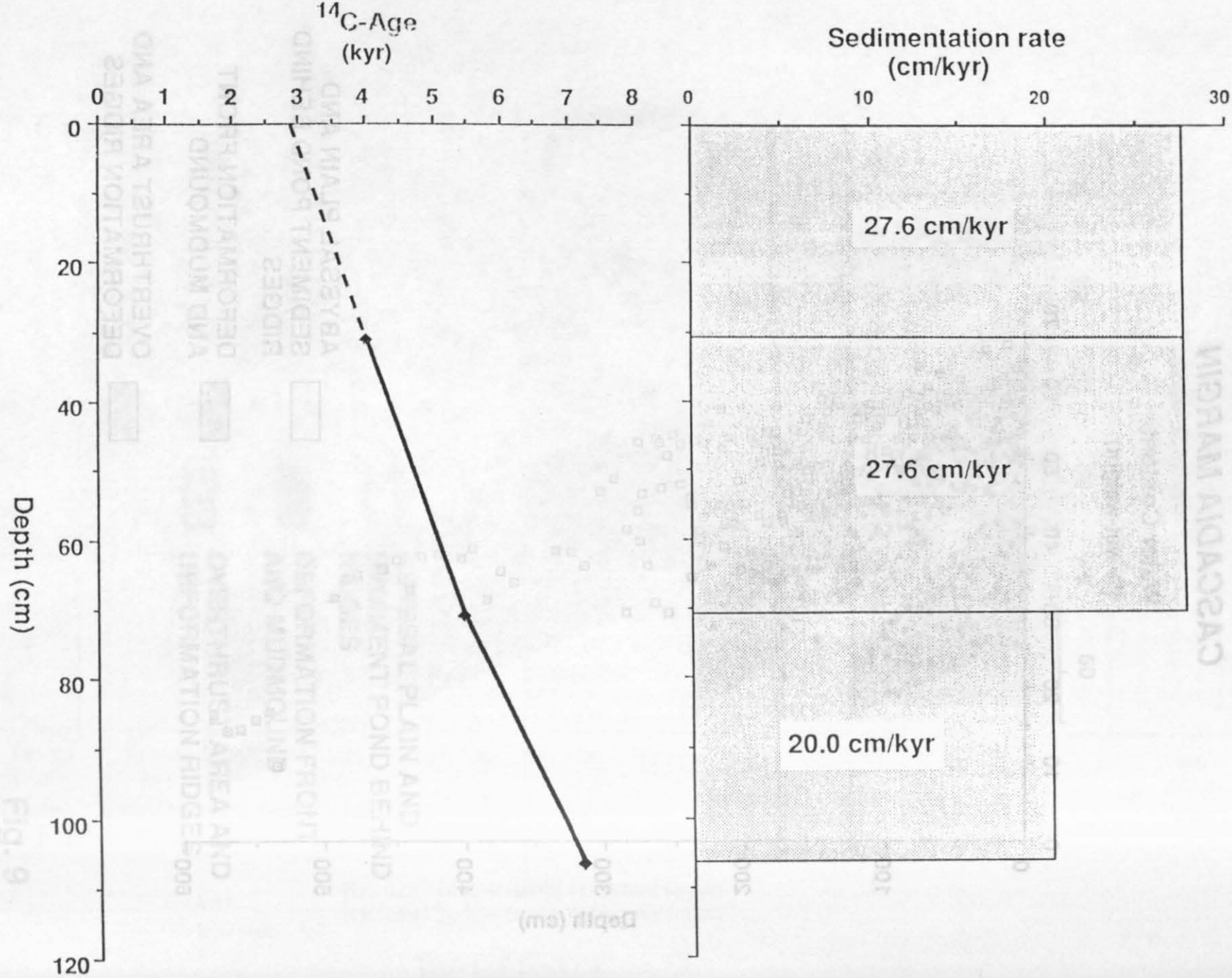
^{14}C-Age
(kyr)
0
1
2
3
4
5
6
7
8
Sedimentation rate
(cm/kyr)
0
10
20
30
Depth (cm)
0
20
40
60
80
100
120
27.6 cm/kyr
27.6 cm/kyr
20.0 cm/kyr

Fig. 11

CASCADIA MARGIN

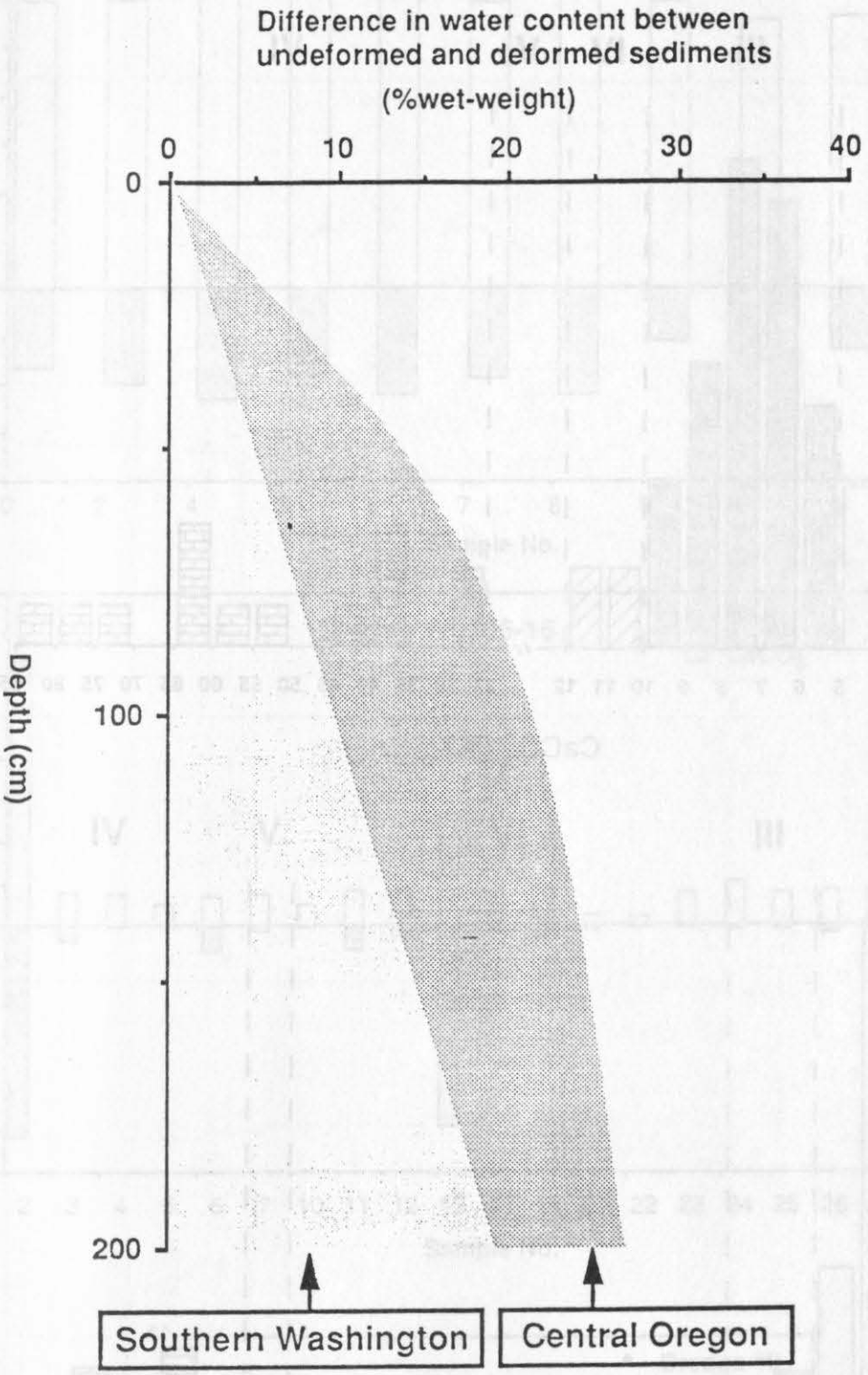

Fig. 12

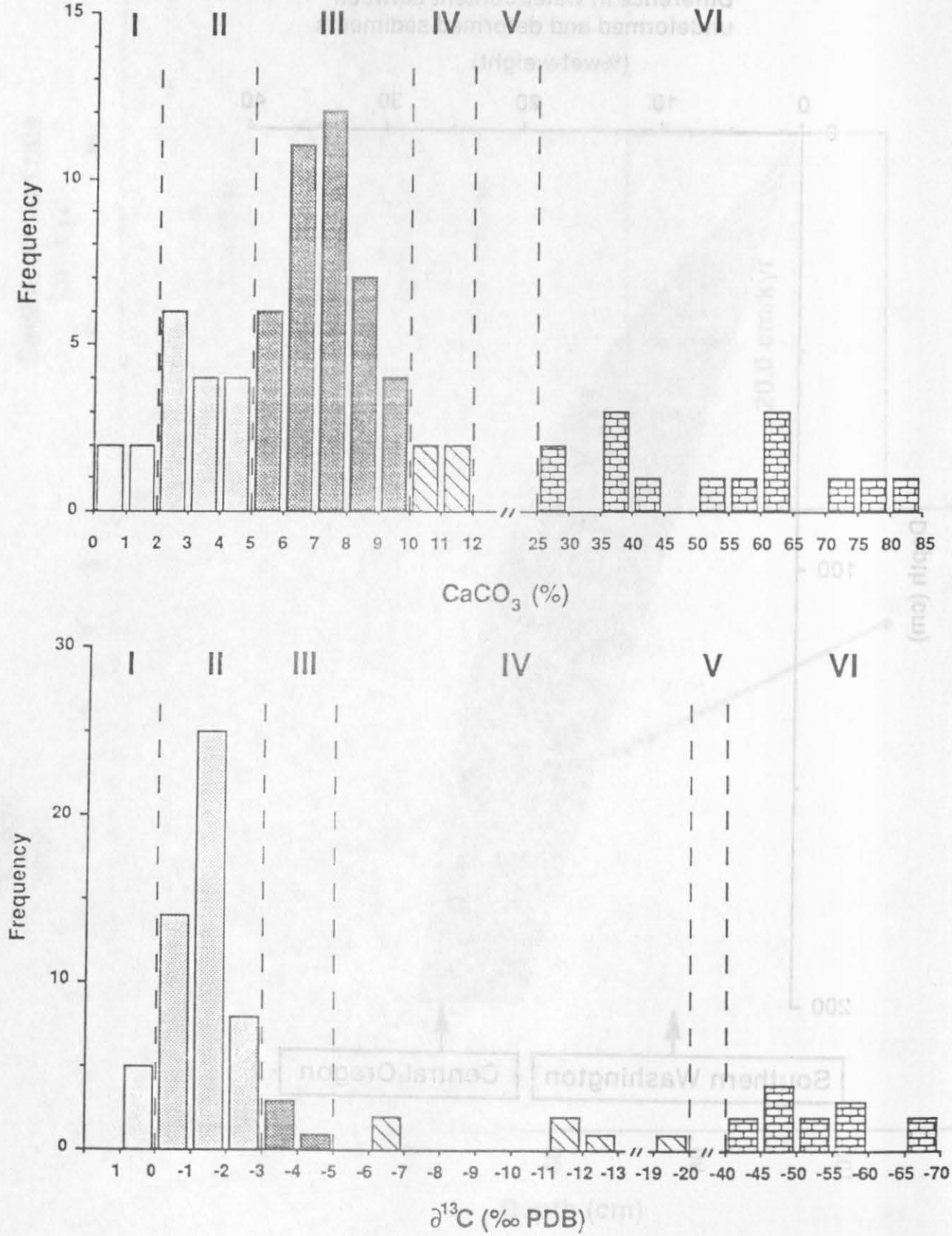
I
II
III
IV
V
VI
Frequency
15
10
5
0
0 1 2 3 4 5 6 7 8 9 10 11 12
25 30 35 40 45 50 55 60 65 70 75 80 85
CaCO3 (%)
I
II
III
IV
V
VI
Frequency
30
20
10
0
1 0 -1 -2 -3 -4 -5 -6 -7 -8 -9 -10 -11 -12 -13 -19 -20 -40 -45 -50 -55 -60 -65 -70
∂13C (‰ PDB)

Fig. 13

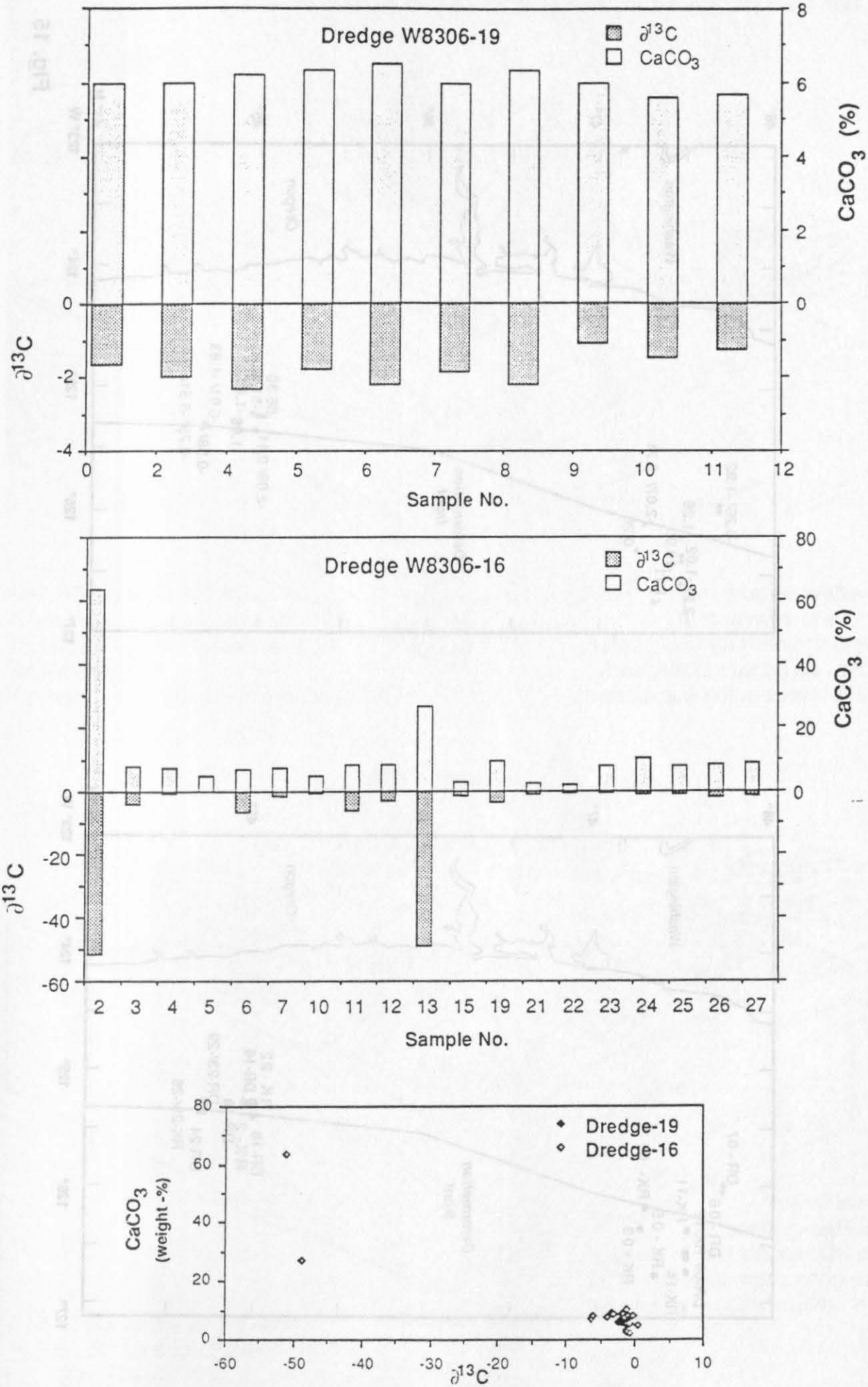
Dredge W8306-19
∂13C
CaCO3
∂13C
CaCO3 (%)
Sample No.
Dredge W8306-16
∂13C
CaCO3
∂13C
CaCO3 (%)
Sample No.
Dredge-19
Dredge-16
CaCO3 (weight -%)
∂13C

Fig. 14

Positions of surface samples at the Oregon and Washington continental margin

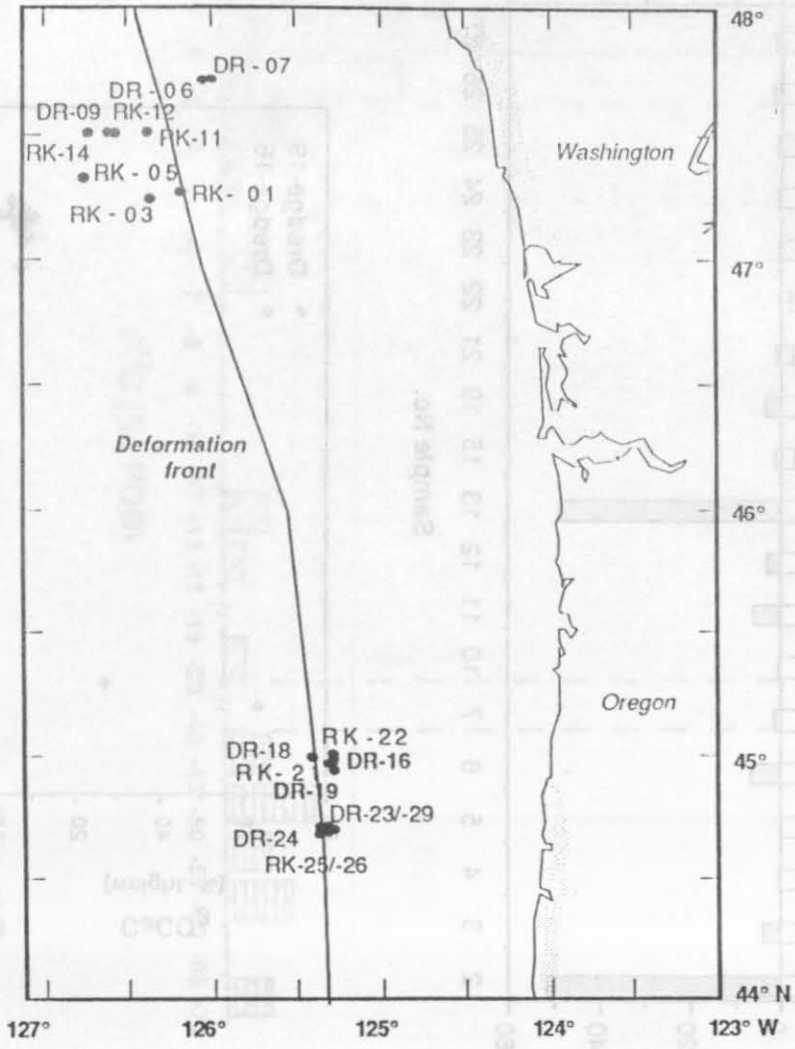

$\partial^{13}C$-isotopes from surface samples Location of deformation front after Davis & Hyndman (1989)

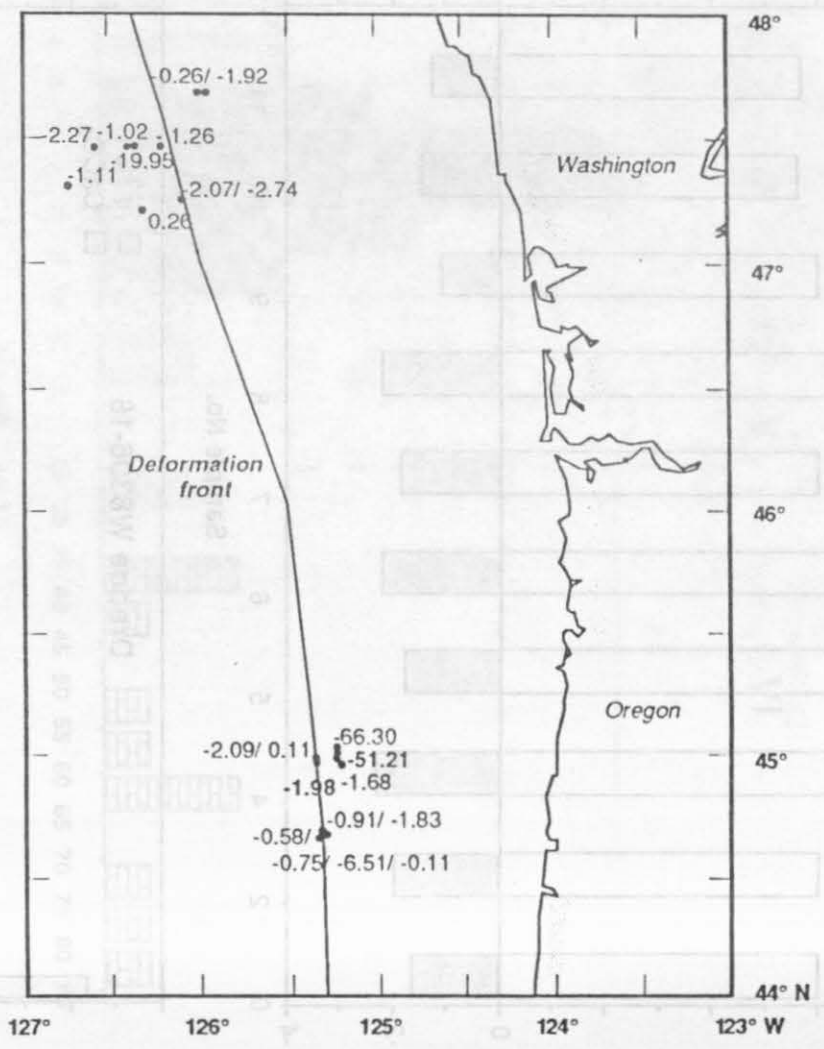

Fig. 15

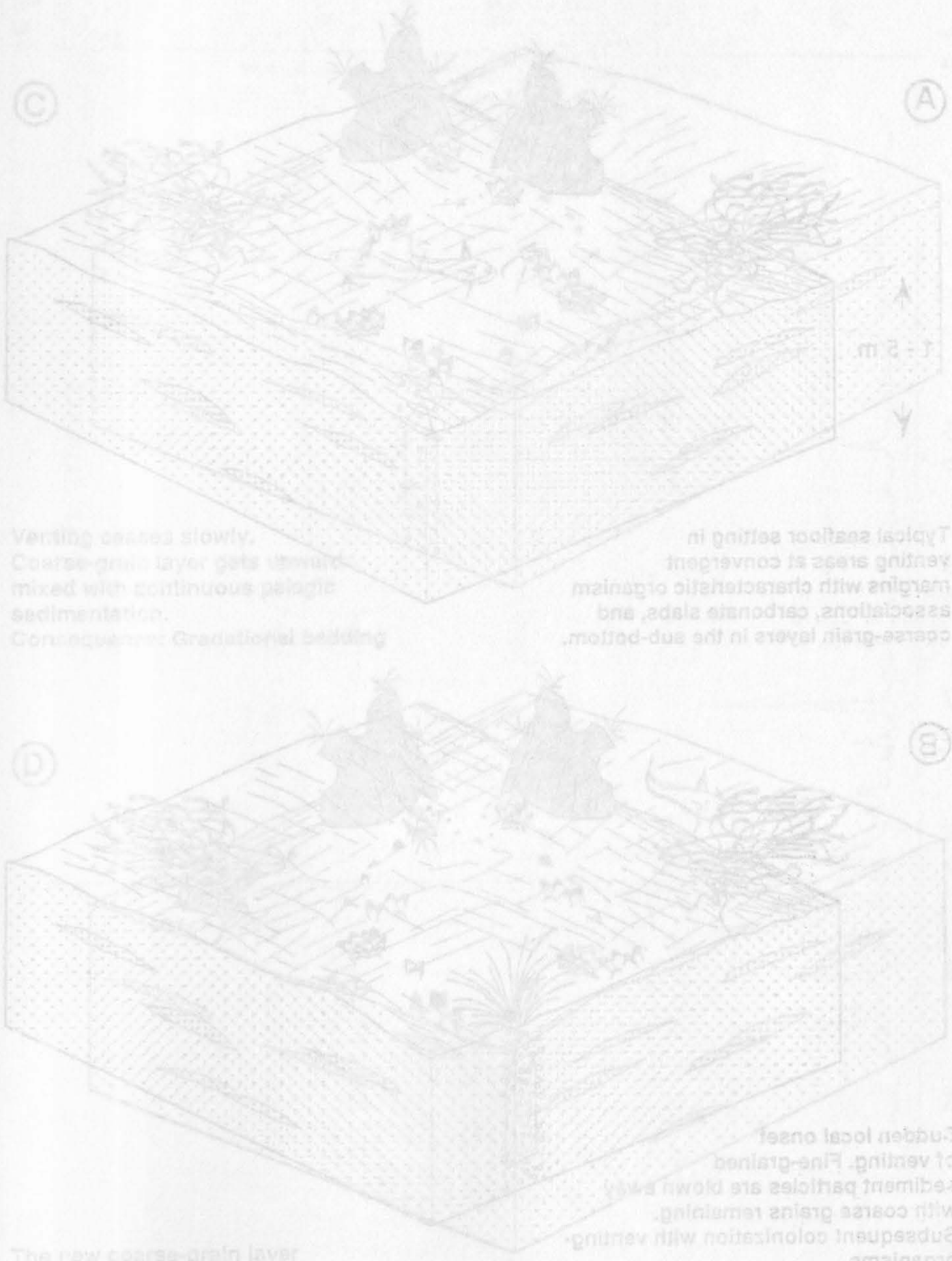
A
B
C
D

The origin of coarse-grain layers in venting areas

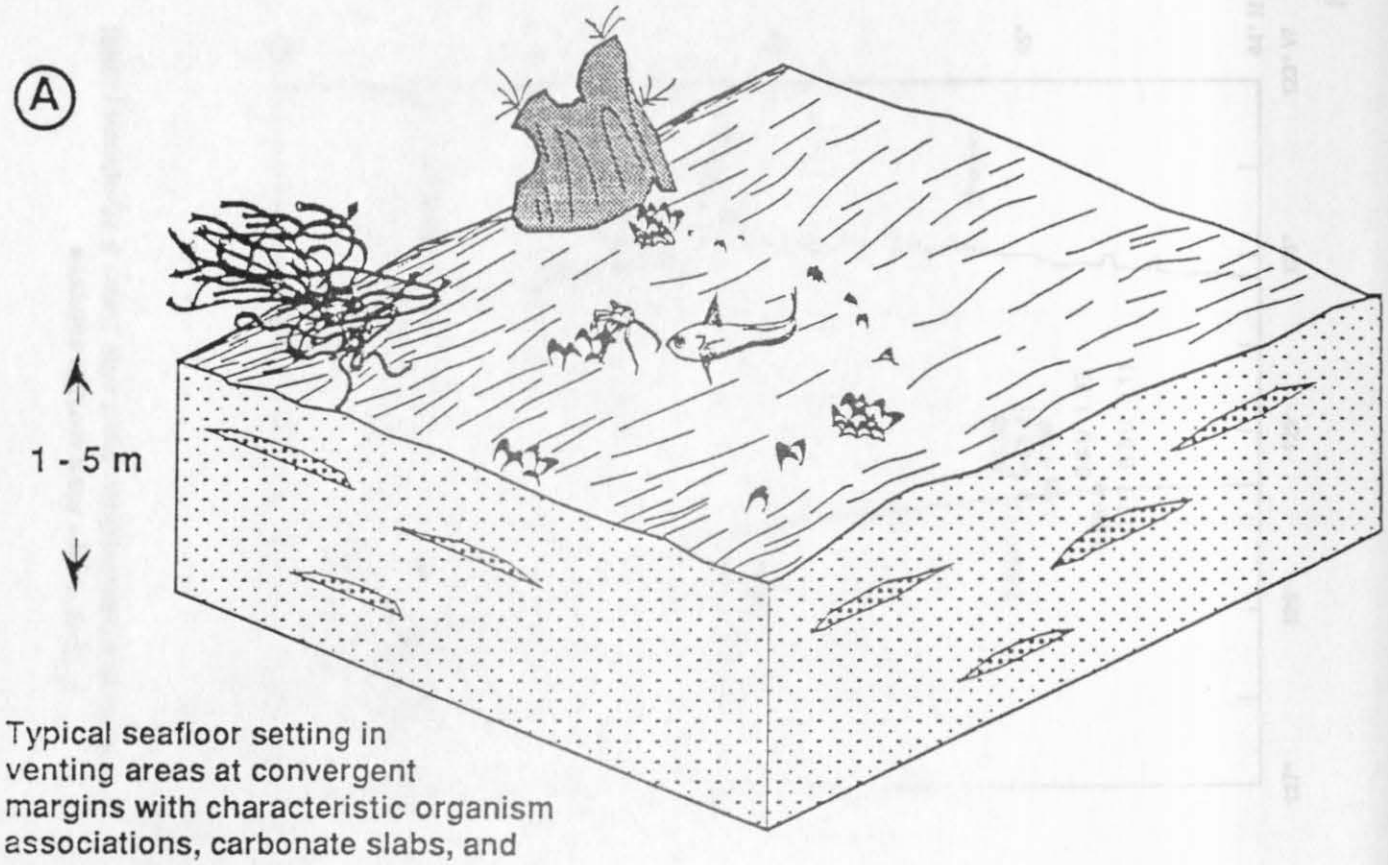

Typical seafloor setting in venting areas at convergent margins with characteristic organism associations, carbonate slabs, and coarse-grain layers in the sub-bottom.

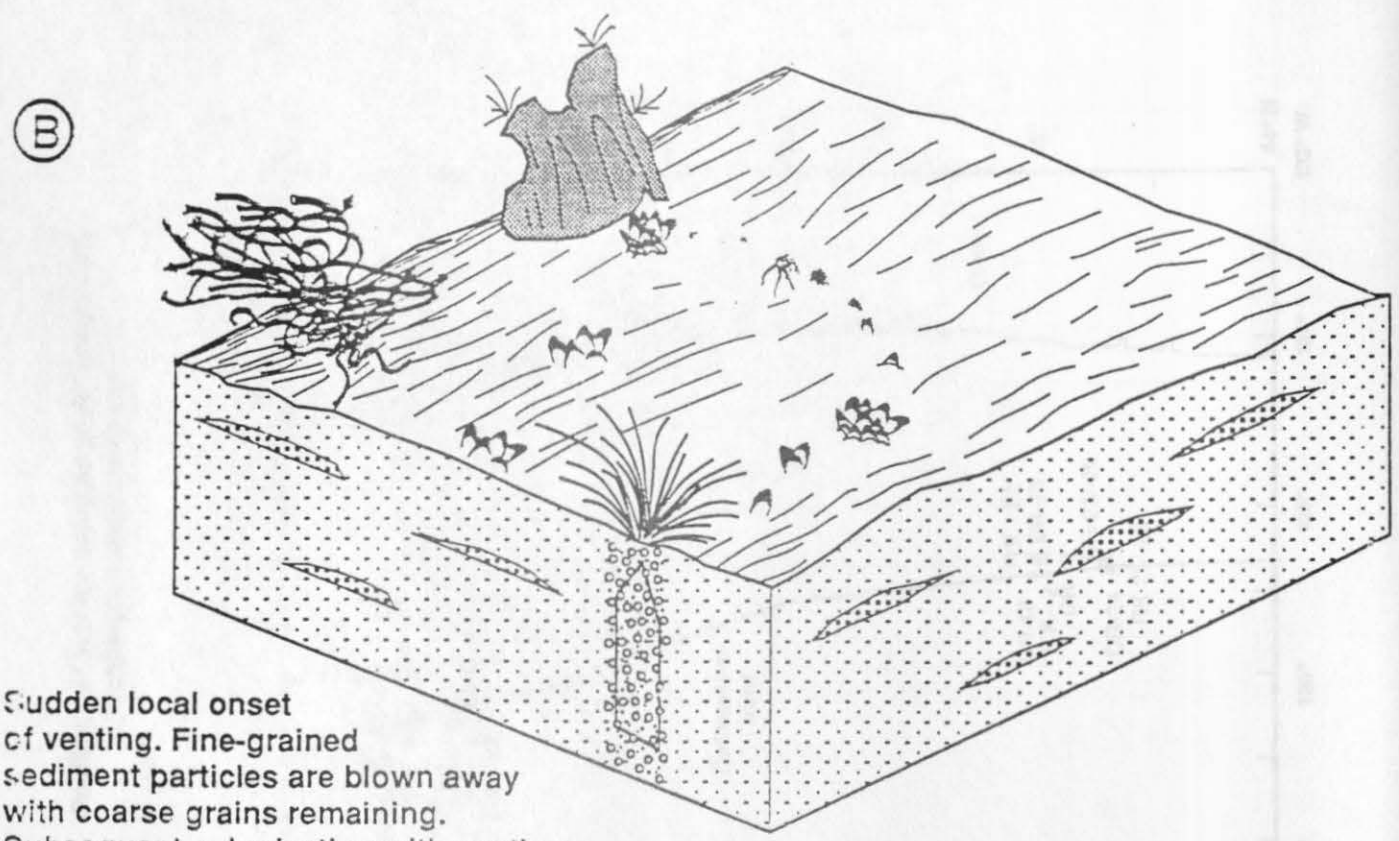

Sudden local onset of venting. Fine-grained sediment particles are blown away with coarse grains remaining. Subsequent colonization with venting-organisms.

Fig. 16

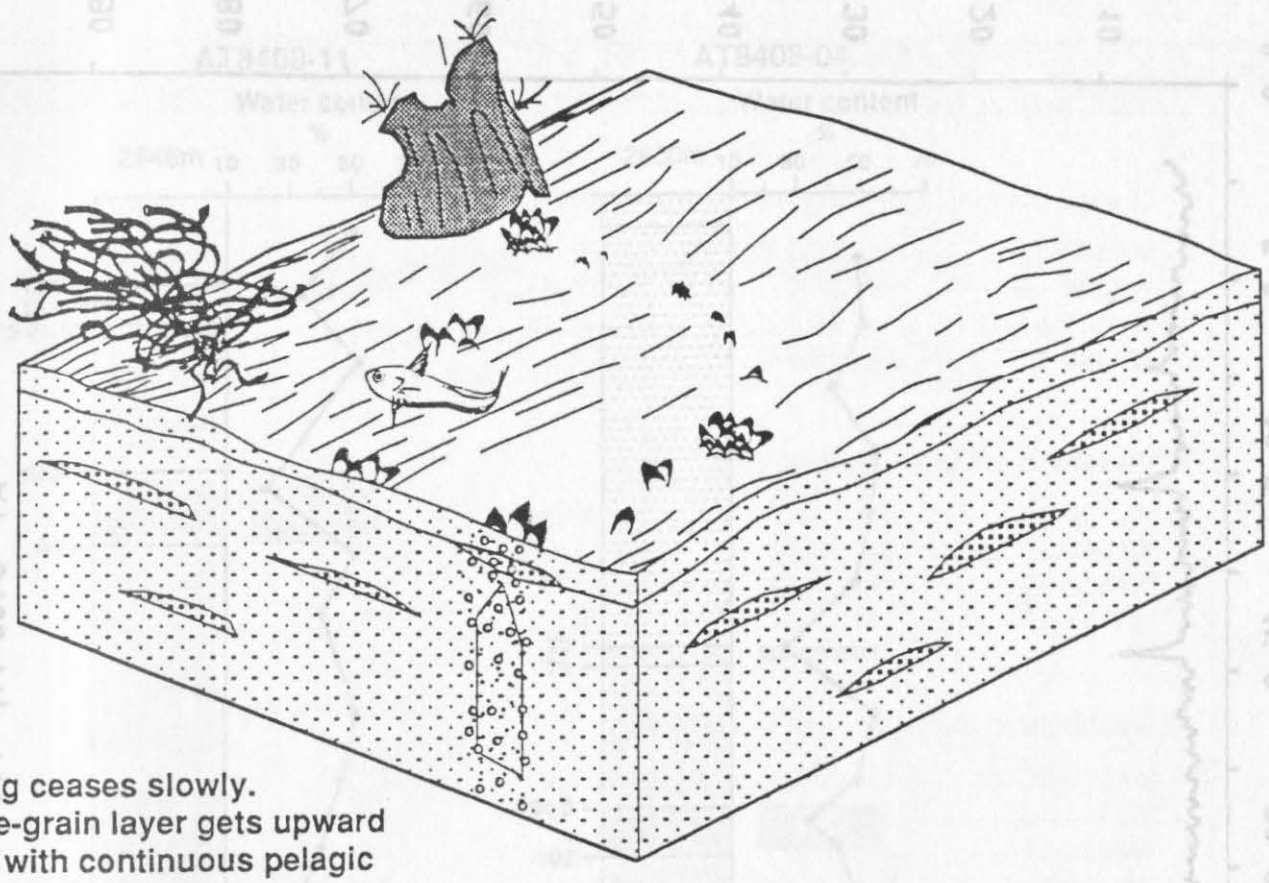

Venting ceases slowly.
Coarse-grain layer gets upward mixed with continuous pelagic sedimentation.
Consequence: Gradational bedding

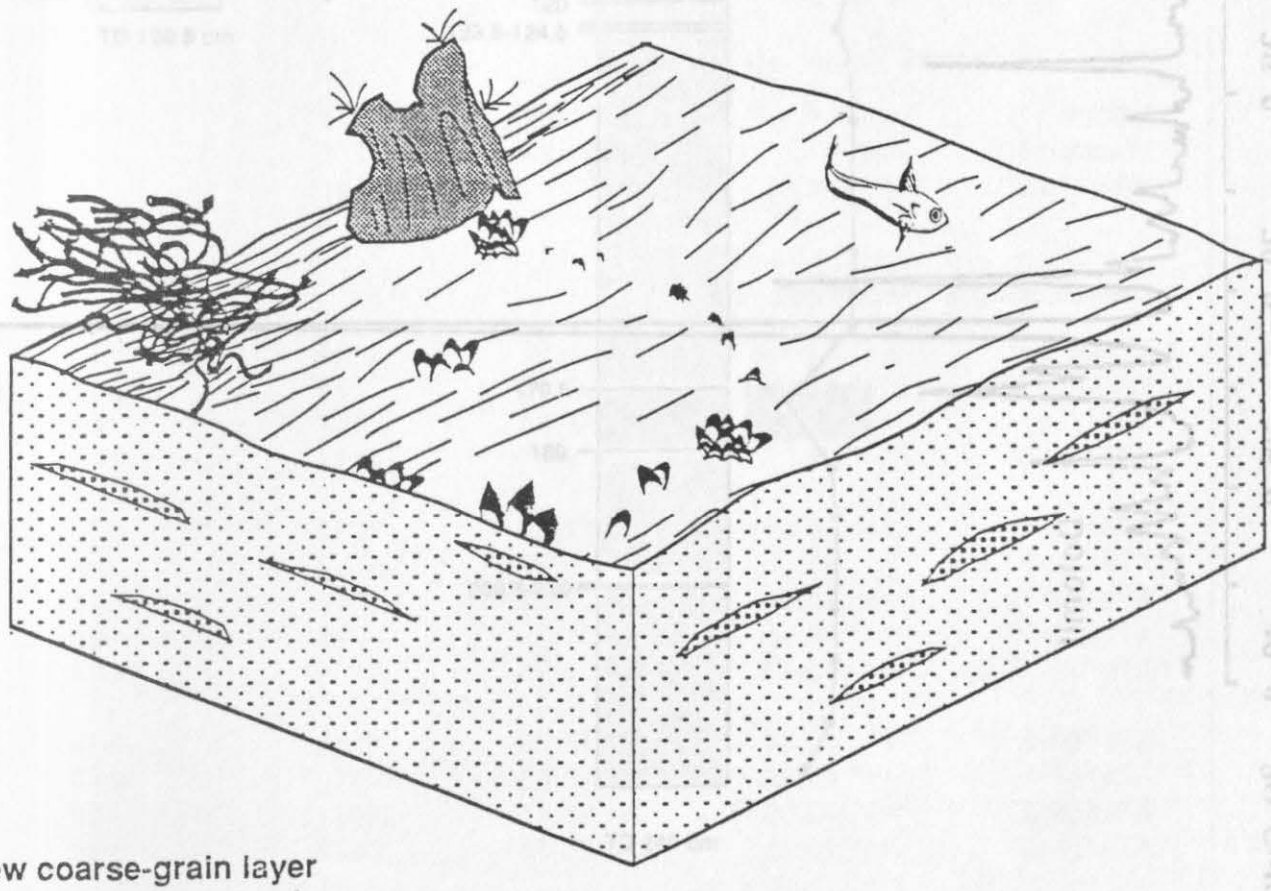

The new coarse-grain layer is part of the sediment column.

Fig. 16 cont.

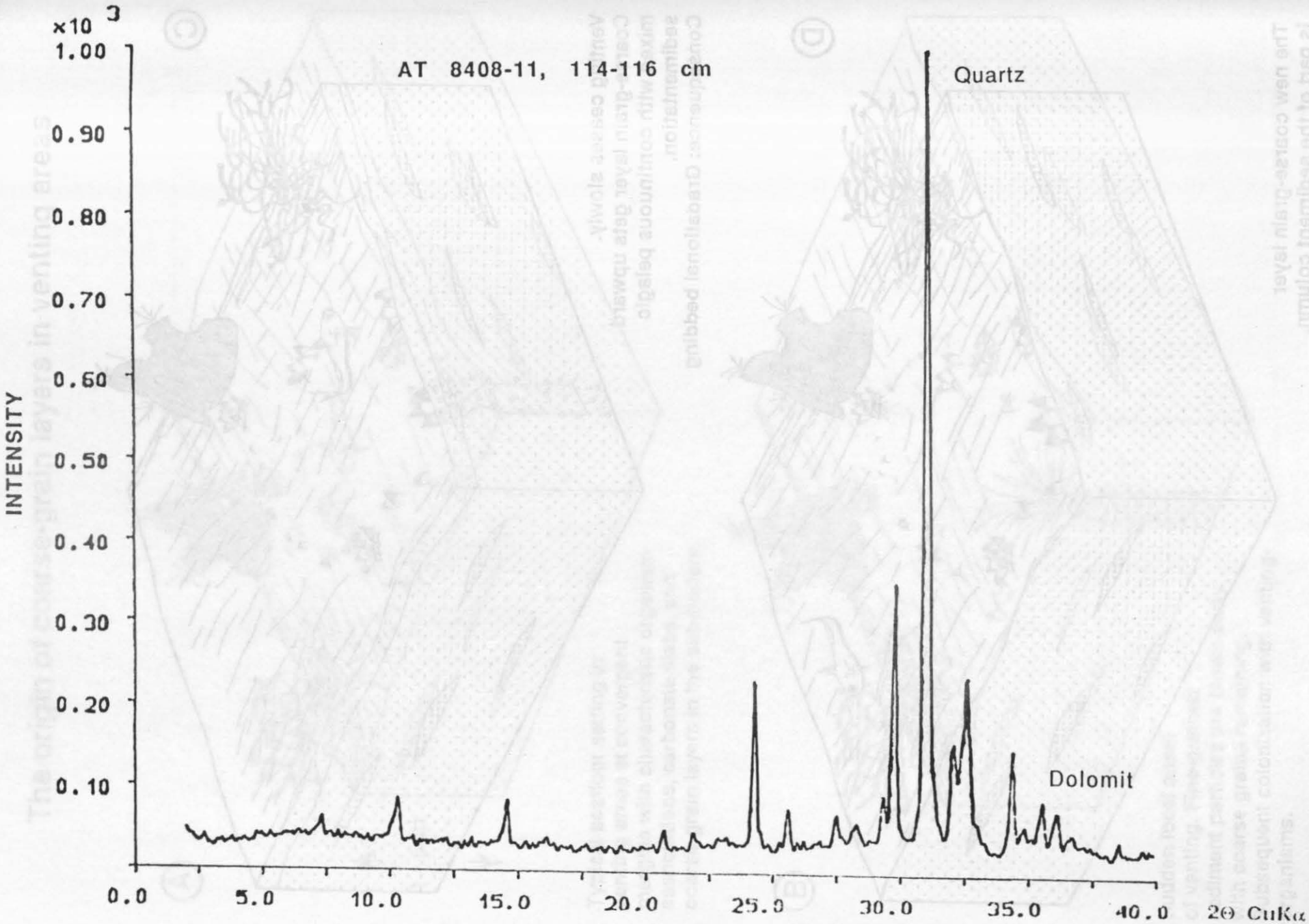
AT 8408-11, 114-116 cm
Quartz
Dolomit
INTENSITY
x10 3
1.00
0.90
0.80
0.70
0.60
0.50
0.40
0.30
0.20
0.10
0.0
5.0
10.0
15.0
20.0
25.0
30.0
35.0
40.0
2Θ CuKα

Fig. 17

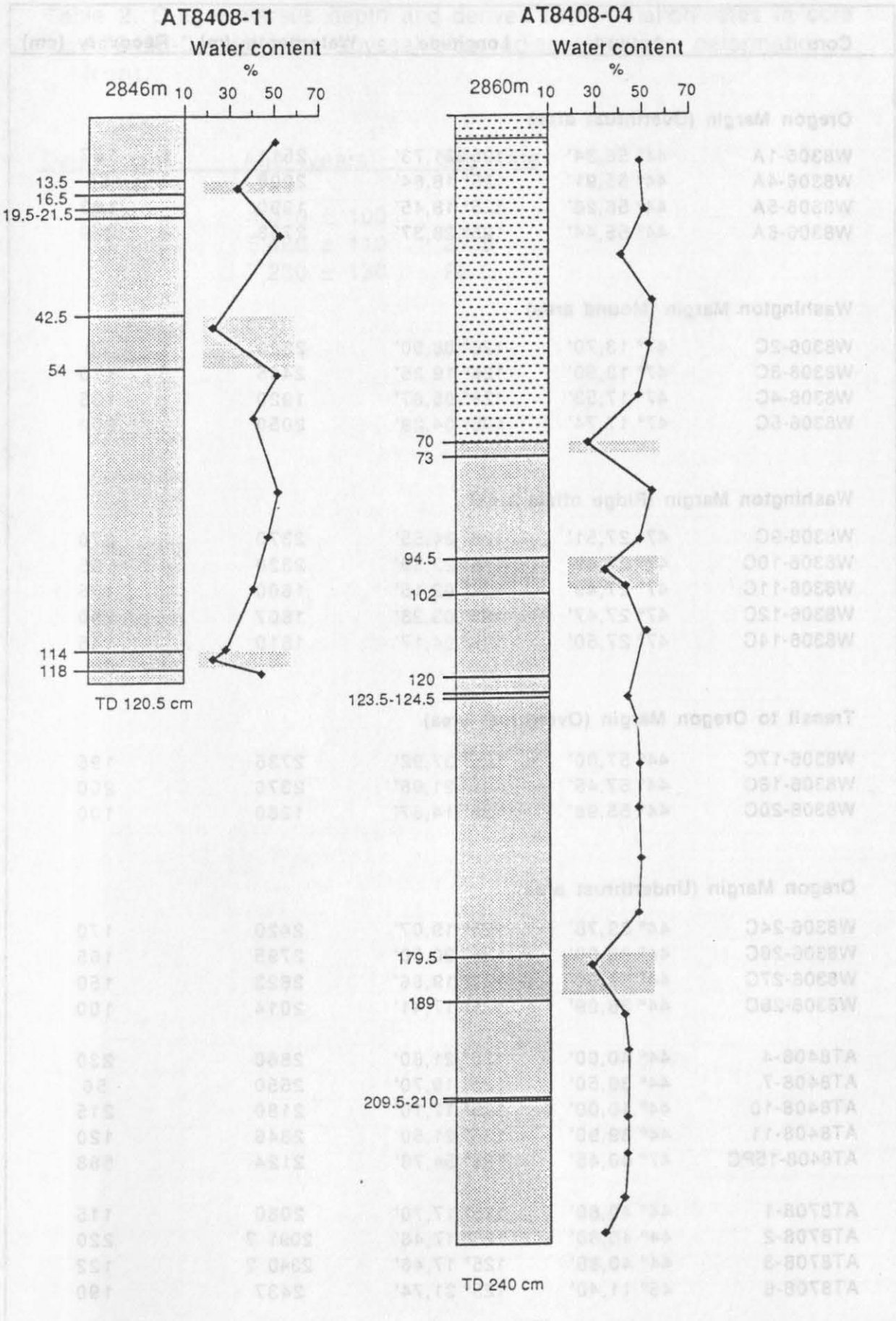
AT8408-11
Water content
%
2846m 10 30 50 70
13.5
16.5
19.5-21.5
42.5
54
114
118
TD 120.5 cm
AT8408-04
Water content
%
2860m 10 30 50 70
70
73
94.5
102
120
123.5-124.5
179.5
189
209.5-210
TD 240 cm
silty clay
sandy silt
very fine sand

Fig. 18

Table 1. Core localities, water depth, and recovery

Core	Latitude	Longitude	Waterdepth (m)	Recovery (cm)
Oregon Margin (Overthrust area)				
W8306-1A	44° 56,34'	125° 21,73'	2511	167
W8306-4A	44° 55,91'	125° 18,64'	2008	55
W8306-5A	44° 56,26'	125° 18,45'	1990	103
W8306-6A	44° 55,44'	125° 28,37'	2758	279
Washington Margin (Mound area)				
W8306-2C	47° 13,70'	126° 08,90'	2320	70
W8306-3C	47° 12,50'	126° 19,36'	2445	170
W8306-4C	47° 17,53'	126° 05,67'	1920	135
W8306-5C	47° 17,74'	126° 04,29'	2050	200
Washington Margin (Ridge offset area)				
W8306-9C	47° 27,51'	126° 34,55'	2370	270
W8306-10C	47° 27,42'	126° 23,89'	2320	195
W8306-11C	47° 27,49'	126° 02,15'	1600	195
W8306-12C	47° 27,47'	126° 03,28'	1807	250
W8306-14C	47° 27,50'	126° 04,17'	1810	145
Transit to Oregon Margin (Overthrust area)				
W8306-17C	44° 57,00'	125° 37,92'	2735	195
W8306-18C	44° 57,45'	125° 21,96'	2376	200
W8306-20C	44° 55,98'	125° 14,87'	1260	100
Oregon Margin (Underthrust area)				
W8306-24C	44° 39,78'	125° 19,07'	2420	170
W8306-26C	44° 39,00'	125° 20,50'	2795	165
W8306-27C	44° 39,00'	125° 19,66'	2623	150
W8306-28C	44° 38,99'	125° 17,41'	2014	100
AT8408-4	44° 40,00'	125° 21,60'	2860	230
AT8408-7	44° 39,50'	125° 19,70'	2550	56
AT8408-10	44° 40,00'	125° 17,10'	2180	215
AT8408-11	44° 39,90'	125° 21,50'	2846	120
AT8408-15PC	47° 00,45'	125° 54,78'	2124	588
AT8708-1	44° 40,80'	125° 17,70'	2080	115
AT8708-2	44° 40,80'	125° 17,46'	2091 ?	220
AT8708-3	44° 40,80'	125° 17,46'	2040 ?	122
AT8708-6	45° 11,40'	125° 31,74'	2437	190

W: RV WECOMA AT: RV ATLANTIS

Table 2. C-ages versus depth and derived sedimentation rates in core AT8408-04 from the abyssal plain adjacent to the deformation front.

Depth (cm)	Age (years)	Sed. rate
31	4,010 ± 100	
71	5,460 ± 110	27.5
106.5	7,230 ± 130	20.0

Table 3. Oxygen and carbon isotopic ratios and carbonate content of samples from Cascadia Margin

Sample device	Latitude	Longitude	Sample-ID	∂13O ‰	∂13C ‰	CaCO3 weight-%
W8306-01C	47° 13,68'	126° 08,76'	01/200	-8,20	-2,07	5,60
W8306-02C	47° 13,70'	126° 08,90'	02/300	-7,70	-2,74	2,80
W8306-03C	47° 12,50'	126° 19,36	03/100	-2,88	0,26	9,50
W8306-05C	47° 17,74'	126° 04,29'	05/100	-4,39	-1,11	8,10
			05/300	-4,06	-0,94	7,50
DR-06	47° 40,68'	126° 00,00'	06/300	-7,34	-0,26	1,20
DR-07	47° 40,68'	125° 57,96'	07/300	-1,58	-12,07	4,00
DR-07			07/900	-8,18	-1,92	2,80
W8306-09C	47° 27,51'	126° 34,55'	09/200	-11,12	-2,27	7,60
W8306-11C	47° 27,49'	126° 02,15'	11/100	-1,96	-19,95	7,40
W8306-12C	47° 27,47'	126° 03,28'	12/200	-4,75	-1,02	7,90
W8306-14C	47° 27,50'	126° 04,17'	14/100	-3,14	-1,26	9,70
			14/200	-5,77	-0,71	7,60
DR-16	44° 56,10'	125° 16,08'	16/200	4,31	-51,21	63,90
			16/300	2,14	-4,08	7,80
			16/400	-10,17	-0,44	7,40
			16/500	-11,78	0,38	4,90
			16/600	-8,26	-6,43	7,10
			16/700	-12,22	-1,51	7,60
			16/100	-12,86	-0,70	5,20
			16/110	-8,49	-6,04	8,30
			16/120	-8,50	-3,12	8,50
			16/130	3,69	-48,74	27,10
			16/150	5,59	-1,28	3,00
			16/190	-11,65	-3,38	9,30
			16/210	-7,67	-1,19	2,70
			16/220	-3,18	-0,74	2,10
			16/230	-10,82	-0,29	8,00
			16/240	-11,22	-1,23	10,40
			16/B	-12,05	-0,93	8,10
			16/C	-9,84	-1,89	8,70
			16/E	-10,91	-1,63	8,90
W8306-17C	44° 57,00'	125° 37,92'	17/35	-7,40	-2,09	0,90
W8306-18C	44° 57,45'	125° 21,96'	18/100	-4,39	0,11	7,30
			18/30	-5,55	-1,47	7,30
			18/70	-7,80	-2,07	1,10
			18/130	-7,90	-1,59	0,70
DR-19	44° 92,9'	125° 25,	19/20	-10,18	-1,68	6,00
			19/40	-8,58	-1,99	6,00
			19/60	-7,66	-1,80	6,30
			19/70	-7,88	-2,24	6,50
			19/80	-7,29	-1,88	6,00
			19/90	-9,52	-2,22	6,30
			19/100	-10,31	-1,11	6,00
			19/110	-10,25	-1,51	5,60
			19/120	-10,24	-1,28	5,70

cont. Table 3

Sample device	Latitude		Longitude		Sample-ID	∂13O ‰	∂13C ‰	CaCO3 weight-%
					19/105	-7,82	-2,35	6,20
W8306-21C	44°	56,10'	125°	16,14'	21/15	-7,41	-1,98	2,50
					21/30	-4,20	-3,07	2,60
DR-22	45°	00,00'	125°	27,00'	22/20	4,22	-66,30	39,30
					22/30	-3,76	-11,01	26,10
					22/60	4,72	-58,73	54,10
					22/80	-12,01	-1,31	11,60
					22/120	2,78	-66,70	35,40
					22/13	3,66	-56,10	36,10
DR-23	44°	40,20'	125°	19,86'	23/20	-11,02	-0,91	10,70
W8306-24C	44°	39,78'	125°	19,07'	24/20	-10,04	-0,58	6,70
W8306-25C	44°	39,84'	125°	18,30'	25/100	-1,91	-0,75	6,10
					25/35	-6,83	-1,90	3,70
W8306-26C	44°	39,00'	125°	20,50	26/100	-6,51	-0,95	6,40
					26/92	-10,80	-1,27	3,70
W8306-27C	44°	39,00'	125°	19,66	27/70	-4,20	0,11	3,80
DR-29	44°	39,00'	125°	19,56'	29/100	-10,36	-1,83	11,80
					29/40	-10,26	-1,28	5,90
					29/50	-7,96	-11,98	9,60
					29/60	-10,70	-0,29	4,70
					29/70	-11,65	-0,12	7,60
					29/80	-2,51	-0,71	5,50
					29/110	-9,09	0,28	4,30
DR-63	44°	39,00'	125°	30,48'	63/09	6,12	-51,81	62,00
DR-68	47°	31,20'	125°	58,38'	68/14	3,98	-41,31	70,00
DR-7914	47°	00,00'	125°	46,80'	79/14	4,75	-58,74	59,00
DR-7933	47°	51,60'	125°	09,36'	79/33	5,41	-49,60	43,00
DR-7934	48°	27,96'	125°	19,80'	79/34	5,80	-49,03	61,00
DR-9003	45°	45,48'	125°	10,98'	90/03	4,18	-44,14	76,00
DR-9028	47°	34,20'	125°	21,96'	90/28	6,13	-46,35	81,00

W8306-XX: Kasten corer

DR: Dredge

RK-01A

Depth (cm)	Watercont. wet. weight (%)	Wet-Bulk Den. (g/cm3)	Dry-Bulk Den. (g/cm3)	Shear Strength (kPa)
1,5	61	1,342	0,524	
6,5	56	1,404	0,621	2,75
21,5	54	1,419	0,652	3,33
36,5	51	1,455	0,707	2,75
51,5	54	1,417	0,658	2,94
66,5	52	1,454	0,696	6,67
96,5	49	1,479	0,749	8,83
126,5	49	1,502	0,768	10,20
156,5	46	1,515	0,814	13,73
165,5	46	1,535	0,827	19,61

RK-04A

Depth (cm)	Watercont. wt. %	Wet-Bulk Den. g/cm3	Dry-Bulk Den. g/cm3	Shear Strength kPa
1,5	49,6	1,471	0,741	3,14
6,5	46,6	1,525	0,815	3,92
11,5	45,2	1,549	0,848	6,67
16,5	45	1,543	0,849	5,88
21,5	47,1	1,507	0,798	6,86
26,5	45,9	1,538	0,832	4,90
31,5	43	1,555	0,886	4,90
36,5	25,9	1,502	1,113	17,16
41,5	28,5	1,703	1,218	24,52
47,5	27,8	1,666	1,203	
52,5	32,9	1,709	1,145	

RK-05A

Depth (cm)	Watercont. wet.weight (%)	Wet-Bulk Den. (g/cm3)	Dry-Bulk Den. (g/cm3)	Porosity (%)	Grain Den. (g/cm3)	Shear Strength (kPa)	>63 µm wet weight (%)	CaCO3 (%)	Corg (%)
1,5	55,20	1,41	0,63			1,96			
21,5	52,30	1,45	0,69			3,92			
41,5	52,00	1,45	0,70			7,65			
56,5	53,10	1,43	0,97			3,92			
57,5						9,80			
63,0	51,45	1,44	0,70	72	2,38		3,60	1,625	1,53
69,0	50,23	1,46	0,73	71	2,42		27,15		
73,5	48,30	1,50	0,78			7,85			
76,5						10,95			
78,0	46,97	1,54	0,81	70	2,61		4,26	1,5	1,5
81,5	24,10	1,89	1,44			26,48			
85,0	41,24	1,59	0,93	64	2,55	8,81	0,33		
89,0	33,64	1,74	1,15	56	2,58		6,55	2,95	0,53
91,5	19,80	1,99	1,60						
92,5						12,04			
96,0	19,70	2,04	1,64	38	2,58		53,90		
96,5	33,70	1,70	1,13						

RK-06A

Depth (cm)	Watercont. (%)	Wet-Bulk Den. (g/cm3)	Dry-Bulk Den. (g/cm3)	Porosity (%)	Grain Den. (g/cm3)	Shear Strength (kPa)	>63µm (%)	63-2µm (%)	<2µm (%)	CaCO3 (%)	Corg (%)
6,5	44,30	1,57	0,88			1,96					
37,0	55,80	1,39	0,61	75,00	2,37		1,02	69,40	29,66		
46,5	52,50	1,44	0,69			4,90					
47,0	51,96	1,45	0,70	72,00	2,43		6,26			1,33	1,37
57,0	55,03	1,40	0,63	75,00	2,44		1,61	68,95	29,43	0,99	1,53
67,0	51,65	1,48	0,71	73,00	2,58		4,36	62,61	33,01	0,99	1,34
77,0	55,64	1,41	0,63	75,00	2,45		1,05	59,49	39,44	1,08	1,45
86,5	55,70	1,41	0,63			4,90					
87,0	54,61	1,42	0,64	75,00	2,50		0,35			0,16	1,51
97,0	45,96	1,56	0,84	69,00	2,68		5,43	73,10	21,45	1,99	1,12
107,0	54,30	1,44	0,66	75,00	2,60		4,77			0,00	1,47
117,0	56,07	1,40	0,61	76,00	2,48		1,21	62,95	35,83	0,33	1,49
126,5	42,20	1,60	0,93			5,88					
137,0	57,02	1,38	0,59	76,00	2,42		0,76	62,29	36,93	0,16	1,54
157,0	55,18	1,42	0,63	76,00	2,60		0,25	62,11	37,63	1,16	1,61
166,5	48,40	1,51	0,78			7,85					
177,0	51,15	1,47	0,72	73,00	2,59		0,22				
187,0	50,81	1,49	0,73	73,00	2,66		1,21	56,59	42,18	0,08	1,42
197,0	53,68	1,44	0,66	74,00	2,52		0,13			0,00	1,48
206,5	47,00	1,52	0,81			6,86					
217,0	51,43	1,46	0,71	72,00	2,49		0,08			0,00	1,32
227,0	29,72	1,82	1,28	53,00	2,71		8,40			2,66	0,54
237,0	52,19	1,45	0,69	74,00	2,59		0,09			0,33	1,49
246,5	51,90	1,46	0,70			6,86					
257,0	50,41	1,49	0,74	73,00	2,65		0,14			0,66	1,34
261,0	52,62	1,45	0,69	74,00	2,59		0,11			0,25	1,53

RK-01C

Depth (cm)	Water cont. wet weight (%)	Wet-Bulk Den. (g/cm3)	Dry-Bulk Den. (g/cm3)	Shear Strength (kPa)
2,5	54,1	1,398	0,622	0,29
7,5	51,8	1,423	0,667	0,19
12,5	44,8	1,559	0,843	0,38
17,5	34,8	1,685	1,083	3,37
22,5	32,5	1,71	1,139	2,79
27,5	36,7	1,69	1,054	3,46
32,5	29,5	1,774	1,24	
37,5	29,1	1,783	1,25	
42,5	27,5	1,847	1,326	14,43

RK-02C

Depth (cm)	Water cont. wet weight (%)	Wet-Bulk Den. (g/cm3)	Dry-Bulk Den. (g/cm3)	Porosity (%)	Grain Den. (g/cm3)	Shear Strength (kPa)	>63µm (wt.%)	63-2µm (wt.%)	<2µm (wt.%)	CaCO3 (wt.%)	Corg. (wt.%)
6,0	41,58	1,59	0,93	66	2,75		22,7	58,04	29,16	0,91	0,865
9,5						31,18					
12,5						17,94					
14,0	32,6	1,77	1,19	57	2,81		0,93			1,9	0,549
27,0	26,42	1,91	1,4	50	2,82		0,87			0,75	0,412
34,0						33,38					
36,0	28,21	1,84	1,32	52	2,83		0,98			2,07	0,36
45,0	26,89	1,89	1,38	51	2,83		0,22			1,04	0,408
57,0	27,77	1,89	1,36	52	2,82		0,85			0,32	0,401

RK-3C

Depth (cm)	Watercont. wet weight (%)	Wet-Bulk Den. (g/cm3)	Dry-Bulk Den. (g/cm3)	Porosity (%)	Grain Den. (g/cm3)	Shear Strength (kPa)	>63µm (wt.%)	CaCO3 (wt.%)	Corg. (wt.%)
12,5	65,40	1,31	0,43						
22,5						5,09			
32,5	58,40	1,33	0,54			3,92			
52,5	54,90	1,40	0,61			4,30			
72,5	49,50	1,46	0,72			7,84			
78,5						4,34			
81,0	54,82	1,41	0,64	76,00	2,57		0,14	1,92	1,07
90,5						4,63			
91,5	52,60	1,45	0,67			3,92			
100,0	57,65	1,37	0,58	78,00	2,68		0,36	2,29	1,015
112,0	57,19	1,38	0,59	78,00	2,69		0,49	2,10	0,97
112,5	54,20	1,42	0,63			3,92			

RK-3C (cont.)

Depth (cm)	Watercont. wet weight (%)	Wet-Bulk Den. (g/cm3)	Dry-Bulk Den. (g/cm3)	Porosity (%)	Grain Den. (g/cm3)	Shear Strength (kPa)	>63µm (wt.%)	CaCO3 (wt.%)	Corg. (wt.%)
121,0	55,77	1,38	0,61	76,00	2,48		0,46	2,12	1,075
131,5						9,40			
132,5	41,10	1,64	1,05						
134,0	47,88	1,53	0,80	72,00	2,76		0,64	2,20	0,776
142,5	56,40	1,38	0,60	76,00	2,48		0,29	4,08	1,09
150,0						17,36			
151,0	47,54	1,86	0,98	71,00	2,78		0,15	2,86	0,237
152,5	43,50	1,61	0,89			2,94			
161,0	28,23	1,85	1,32	51,00	2,69		0,14	2,94	0,293
162,5						28,48			
166,0	28,81	1,96	1,39	55,00	3,07		0,36	2,70	0,179
172,5	25,20	1,91	1,42			9,80			

RK-04C

Depth (cm)	Water cont. wet weight (%)	Wet-Bulk Den. (g/cm3)	Dry-Bulk Den. (g/cm3)	Porosity (%)	Grain Den. (g/cm3)	Shear Strength (kPa)	>63µm (wt.%)	CaCO3 (wt.%)	Corg. (wt.%)
10,5	53,40	1,43	0,65			5,88			
40,5	52,00	1,44	0,67			4,90			
43,0	50,06	1,47	0,73	72,00	2,60		3,07	1,79	1,205
70,5	39,60	1,64	0,97			9,80			
75,0	39,12	1,64	1,00	62,00	2,62		0,28	2,05	0,477
100,5	36,40	1,69	1,06			20,59			
103,5						9,94	0,04	0,68	0,471
105,0	35,70	1,74	1,12	61,00	2,84				
109,5						17,38			
119,5						18,79			
130,5	35,60	1,70	1,08			19,61			
135,0	32,64	1,79	1,20	55,00	2,59		0,02	1,83	0,376

RK-05C

Depth (cm)	Water cont. wet weight (%)	Wet-Bulk Den. (g/cm3)	Dry-Bulk Den. (g/cm3)	Porosity (%)	Grain Den. (g/cm3)	Shear Strength (kPa)	>63µm (wt.%)	63-2µm (wt.%)	<2µm (wt.%)	CaCO3 (wt.%)	Corg. (wt.%)
6,0	62,35	1,34	0,50	80,00	2,45		0,12	61,89	37,97	0,67	1,65
14,0	58,40	1,35	0,54			4,30					
24,0	59,74	1,40	0,56	79,00	2,62		0,22			2,75	1,8
35,0	54,90	1,41	0,61			2,94					
44,0	57,65	1,40	0,59	78,00	2,57		2,06	76,71	21,19	0,99	1,92
55,0	57,40	1,39	0,57			2,94					

RK-05C (cont.)

Depth (cm)	Water cont. wet weight (%)	Wet-Bulk Den. (g/cm3)	Dry-Bulk Den. (g/cm3)	Porosity (%)	Grain Den. (g/cm3)	Shear Strength (kPa)	>63µm (wt.%)	63-2µm (wt.%)	<2µm (wt.%)	CaCO3 (wt.%)	Corg. (wt.%)
64,0	56,64	1,41	0,61	77,00	2,55		1,91	74,44	23,53	0,08	1,84
75,0	62,60	1,32	0,47			2,74					
84,0	58,88	1,38	0,57	78,00	2,62		0,27	61,95	37,77	2,42	1,47
95,0	56,20	1,35	0,57			5,88					
104,0	55,28	1,26	0,56	76,00	2,55		0,34	71,55	28,09	1,08	1,6
106,5						7,83					
115,0	52,60	1,44	0,66			9,80					
124,0	52,91	1,47	0,69	74,00	2,56		0,35			1,83	1,4
135,0	57,90	1,38	0,56			8,82					
140,5						6,74					
145,0	53,04	1,47	0,69	75,00	2,65		0,17	67,20	32,62	1,08	1,38
155,0	51,50	1,47	0,69			6,86					
164,0	49,54	1,51	0,76	72,00	2,59	7,66	0,13	79,22	20,63	0,75	1,33
171,0						9,44					
173,0	46,81	1,54	0,82	69,00	2,54		1,32	75,38	23,28	1,42	1,22
179,0	53,50	1,42	0,64			8,82					
189,0	49,57	1,49	0,75	72,00	2,58		0,43	69,95	29,25	1,25	1,2

RK-09C

Depth (cm)	Water cont. (wet weight. %)	Wet-Bulk Den. (g/cm3)	Dry-Bulk Den. (g/cm3)	Porosity (%)	Grain Den. (g/cm3)	Shear Strength (kPa)	>63 µm (wt. %)	CaCO3 (wt. %)	Corg. (wt. %)
10,0	58,50	1,36	0,54			5,88			
20,0	60,53	1,36	0,53	80,00	2,54		0,18	2,83	1,24
29,0	64,85	1,39	0,49	83,00	2,60		0,14	3,92	1,19
48,0	57,08	1,44	0,62	78,00	2,67		0,10	4,17	1,19
52,0	53,20	1,41	0,64			3,92			
60,0	58,36	1,41	0,59	79,00	2,69		0,14	5,04	1,00
70,0	53,91	1,44	0,66	75,00	2,64		0,22	7,57	0,76
71,5						4,52			
80,0	49,07	1,52	0,77	72,00	2,65		0,13	3,98	0,63
90,0	50,93	1,49	0,73	73,00	2,63		0,28	7,61	0,72
95,0	47,20	1,51	0,78			5,88			
110,0	44,01	1,60	0,90	68,00	2,74	3,11	0,08	2,30	0,46
126,0	47,80	1,51	0,77			3,33			
146,0	42,67	1,63	0,94	67,00	2,77		0,00	2,85	0,23
157,0	48,40	1,50	0,76			3,33			
164,0	45,55	1,56	0,85	69,00	2,66		0,02	1,18	0,50
178,0	36,71	1,72	1,09	61,00	2,73		0,06	2,75	0,19
187,0	39,20	1,67	1,02	63,00	2,69		0,03	1,05	0,45
189,5						3,29			
197,0	37,85	1,70	1,05	62,00	2,67		0,06	2,83	0,20
208,0	41,69	1,63	0,95	65,00	2,67		0,08	1,35	0,38
217,0	43,80	1,57	0,86			4,71			
227,5						14,11			
233,0	40,63	1,65	0,98	64,00	2,68		0,51	2,98	0,54
240,0	44,82	1,58	0,87	68,00	2,69		0,35	3,65	0,61
247,0	46,50	1,53	0,80			10,39			
255,0	29,69	1,87	1,31	53,00	2,73		0,04	3,06	0,19
257,5						6,90			
261,0	46,05	1,57	0,85	69,00	2,68		0,81	1,53	0,21
265,0	30,90	1,86	1,28	55,00	2,75		0,02	1,69	0,66
268,5						14,45			
270,0	35,95	1,70	1,09	60,00	2,69		0,00	0,74	0,47
274,0	45,33	1,56	0,85	69,00	2,71		0,03	0,43	0,66
277,0	43,10	1,59	0,88			7,26			
285,0	29,68	1,62	1,14	52,00	2,59		0,03	1,35	0,53

RK-10C

Depth (cm)	Water cont. (wet weight. %)	Wet-Bulk Den. (g/cm3)	Dry-Bulk Den. (g/cm3)	Porosity (%)	Grain Den. (g/cm3)	Shear Strength (kPa)	>63 µm (wt. %)	63-2µm (wt. %)	<2µm (wt. %)	CaCO3 (wt. %)	Corg. (wt. %)
10,0	60,40	1,34	0,51			4,51					
29,0	58,90	1,35	0,53			4,90					
50,0	58,30	1,37	0,55			4,41					
61,0	50,92	1,39	0,68	72,00	2,47		0,48	65,68	33,82	2,99	1,03
70,0	52,40	1,44	0,67								
81,0	55,79	1,42	0,63	76,00	2,52		0,23	66,24	33,52	3,91	0,97
90,0	56,20	1,39	0,59								
100,0	19,31	1,91	1,54	38,00	2,63		0,17	57,60	42,22	3,26	0,70
110,0	50,20	1,47	0,71			3,73					
121,0	48,40	1,52	0,78	69,00	2,44		29,71			2,02	0,17
132,0	45,90	1,54	0,81								
132,0	30,65	1,84	1,27	54,00	2,70		12,68	78,73	8,57	1,82	0,20
140,0	42,27	1,63	0,94	66,00	2,69		0,34	67,68	31,26	2,41	0,53
145,0	23,89	1,95	1,48	45,00	2,63		36,81	57,24	5,94	1,38	0,19
150,0	42,00	1,59	0,91			3,73					
161,0	43,91	1,56	0,88	66,00	2,49		1,59				
169,0	44,40	1,56	0,85			3,73	7,36	84,72	7,90	1,12	0,21
170,0	24,70	1,94	1,46	46,00	2,63						
177,0	49,41	1,47	0,74	70,00	2,39		0,26	61,49	38,23	2,99	0,85

RK-11C

Depth (cm)	Water cont. (wet weight. %)	Wet-Bulk Den. (g/cm3)	Dry-Bulk Den. (g/cm3)	Porosity (%)	Grain Den. (g/cm3)	Shear Strength (kPa)	>63 µm (wt. %)	63-2µm (wt. %)	<2µm (wt. %)	CaCO3 (wt. %)	Corg. (wt. %)
3,0	55,58	1,39	0,62	75,00	2,43		2,64	65,35	31,99	0,50	1,54
9,0	54,30	1,43	0,63			3,92					
17,0	55,72	1,39	0,62	75,00	2,43		1,85	66,71	31,42	0,66	1,64
23,0	51,62	1,48	0,71	74,00	2,72		0,43			3,32	0,97
29,0	53,61	1,46	0,68	76,00	2,71		1,26	56,53	42,19	5,75	1,16
35,0	56,80	1,38	0,58			5,10					
41,0	56,59	1,39	0,60	76,00	2,50		2,16	53,91	43,91	4,17	1,32
49,0	51,62	1,45	0,70	73,00	2,51		1,24			2,79	0,96
53,0	41,39	1,59	0,93	64,00	2,58		3,97	64,88	31,13	2,39	0,56
60,0	40,90	1,63	0,95			6,86					
67,0	44,00	1,54	0,86	66,00	2,51		0,75			2,93	0,27
73,0	41,83	1,62	0,94	66,00	2,76		0,93	60,83	38,23	3,43	0,38
79,0	40,35	1,61	0,96	64,00	2,60		4,20			2,27	0,27
85,0	45,70	1,54	0,82			6,47					
90,0	41,47	1,60	0,94	65,00	2,62		1,87			2,64	0,38
105,0	36,70	1,68	1,05			6,67					
110,0	40,78	1,61	0,95	64,00	2,61		0,04	63,82	36,13	2,10	0,32

RK-11C (cont.)

Depth (cm)	Water cont. (wet weight. %)	Wet-Bulk Den. (g/cm3)	Dry-Bulk Den. (g/cm3)	Porosity (%)	Grain Den. (g/cm3)	Shear Strength (kPa)	>63 µm (wt. %)	63-2µm (wt. %)	<2µm (wt. %)	CaCO3 (wt. %)	Corg. (wt. %)
114,0	27,06	1,86	1,36	49,00	2,64		0,08	86,31	13,59	2,47	0,31
120,0	37,10	1,68	1,04			6,86					
127,0	35,07	1,71	1,11	59,00	2,65		0,04	70,97	28,98	3,65	0,30
131,0	41,94	1,60	0,93	65,00	2,62		1,42	66,85	31,72	1,51	0,64
138,0	42,91	1,60	0,91	67,00	2,69		0,13	63,93	35,92	2,69	0,58
145,0	36,80	1,69	1,05			8,43					
152,0	26,87	1,89	1,38	50,00	2,72		0,15			3,17	0,27
159,0	29,60	1,83	1,29	53,00	2,69		0,05			4,25	0,25
170,0	37,90	1,68	1,03			9,02					
181,0	34,08	1,76	1,16	58,00	2,74		0,08	68,59	31,31	3,47	0,39
186,0	35,97	1,72	1,10	60,00	2,72		0,19			3,07	0,30

RK-12C

Depth (cm)	Water cont. (wet weight. %)	Wet-Bulk Den. (g/cm3)	Dry-Bulk Den. (g/cm3)	Porosity (%)	Grain Den. (g/cm3)	Shear Strength (kPa)	>63 µm (wt. %)	CaCO3 (wt. %)	Corg. (wt. %)
6,0	59,75	1,37	0,55	78,00	2,44		0,10	0,25	2,18
15,0	61,40	1,32	0,49						
31,0	58,18	1,37	0,57	76,00	2,24		0,03	0,21	1,93
45,0	59,20	1,34	0,53			2,94			
61,0	61,43	1,34	0,52	78,00	2,29		0,18	1,63	1,77
76,0	58,30	1,37	0,55			3,53			
85,0	52,17	1,46	0,70	72,00	2,42		0,28	3,12	0,82
93,0	50,58	1,46	0,72	71,00	2,41		0,31	3,09	0,79
99,0	51,12	1,46	0,71	72,00	2,47		0,40	3,58	0,85
106,0	45,80	1,54	0,82			4,71			
113,0	48,71	1,49	0,76	70,00	2,46		1,43	2,58	0,92
116,5						6,09			
125,0	23,13	2,00	1,54	44,00	2,67		27,45	1,94	0,24
127,5						7,58			
136,0	39,50	1,64	0,97			7,06			
139,0	33,14	1,76	1,18	56,00	2,63		0,28	2,82	0,30
149,0	29,49	1,82	1,29	52,00	2,61		0,04	3,59	0,22
154,0	42,23	1,60	0,92	66,00	2,65		0,27	2,23	0,41
166,0	40,30	1,65	0,97			5,88			
169,5						10,87			
173,0	41,73	1,64	0,96	64,00	2,56		0,03	2,95	0,30
180,0	36,59	1,69	1,07	60,00	2,57	5,89	0,12	2,83	0,29
185,0	37,51	1,68	1,05	60,00	2,56		0,07	2,68	0,31
195,0	34,80	1,82	1,17			4,71			
203,0	35,38	1,72	1,11	59,00	2,63		0,06	3,48	0,21

RK-12C (cont.)

Depth (cm)	Water cont. (wet weight. %)	Wet-Bulk Den. (g/cm3)	Dry-Bulk Den. (g/cm3)	Porosity (%)	Grain Den. (g/cm3)	Shear Strength (kPa)	>63 µm (wt. %)	CaCO3 (wt. %)	Corg. (wt. %)
208,0	30,78	1,80	1,24	54,00	2,65		0,18	2,81	0,28
215,0	41,37	1,69	0,99	64,00	2,54		0,05	3,67	0,23
225,0	35,90	1,70	1,07			9,41			
233,0	39,33	1,66	1,01	62,00	2,58		0,00	2,11	0,58

RK-14C

Depth (cm)	Water cont. (wet weight. %)	Wet-Bulk Den. (g/cm3)	Dry-Bulk Den. (g/cm3)	Porosity (%)	Grain Den. (g/cm3)	Shear Strength (kPa)	>63 µm (wt. %)	63-2µm (wt. %)	<2µm (wt. %)	CaCO3 (wt. %)	Corg. (wt. %)
3,0	57,93	1,38	0,58	77,00	2,40		1,26			0,50	1,69
10,0	57,60	1,37	0,56			6,08					
17,0	54,11	1,42	0,65	75,00	2,50		1,85	70,41	27,72		
23,0	50,91	1,46	0,72	72,00	2,49		1,90	65,09	32,99	1,33	1,27
29,0	49,55	1,59	0,80	71,00	2,57		2,71			2,67	1,00
34,0	48,80	1,48	0,74			9,22					
41,0	34,72	1,72	1,12	58,00	2,63		3,06	74,06	22,87	2,80	0,37
45,0	35,60	1,73	1,11	59,00	2,61		3,35			2,90	0,41
49,0	38,80	1,64	0,99			10,00					
59,0	33,00	1,76	1,18	56,00	2,62		4,09	72,03	23,86	2,31	0,43
70,0	39,40	1,65	0,99			12,36					
79,0	42,35	1,62	0,93	66,00	2,64		0,75	63,13	36,10	4,34	0,52
90,0	37,40	1,67	1,03			11,77					
97,0	40,73	1,61	0,95	64,00	2,65		0,18	62,81	37,00	1,72	0,42
103,0	37,93	1,64	1,02	62,00	2,65		0,11	63,78	36,09	0,94	0,43
110,0	39,80	1,63	0,97			14,51					
117,0	38,51	1,70	1,04	62,00	2,67		0,11	64,14	35,73		

RK-17C

Depth (cm)	Water cont. (wet weight. %)	Wet-Bulk Den. (g/cm3)	Dry-Bulk Den. (g/cm3)	Shear Strength (kPa)
20,0	56,80	1,38	0,58	4,31
46,0	60,70	1,36	0,51	3,33
70,0	59,90	1,36	0,14	4,51
96,0	56,30	1,40	0,59	
120,0	55,60	1,40	0,60	
146,0	58,00	1,37	0,56	5,69

RK-18C

Depth (cm)	Water cont. (wet weight. %)	Wet-Bulk Den. (g/cm3)	Dry-Bulk Den. (g/cm3)	Porosity (%)	Grain Den. (g/cm3)	Shear Strength (kPa)	CaCO3 (wt. %)	Corg. (wt. %)
7,0	51,88	1,44	0,69	72,00	2,46		1,16	1,83
13,0	52,70	1,44	0,68	73,00	2,47		1,24	1,79
19,0	55,20	1,40	0,61			2,55		
29,0	52,10	1,45	0,69	73,00	2,52		1,24	1,61
39,0	55,50	1,42	0,61			4,90		
50,0	51,80	1,45	0,70	72,00	2,41		0,99	1,69
59,0	53,40	1,41	0,64			3,73		
70,0	51,20	1,47	0,71	72,00	2,50		0,83	1,70
79,0	49,70	1,48	0,72			6,86		
90,0	48,87	1,51	0,77	71,00	2,52		1,16	1,64
99,0	49,10	1,48	0,73			5,88		
110,0	47,71	1,51	0,79	70,00	2,54		2,16	1,63
119,0	48,00	1,50	0,76			7,85		
130,0	45,76	1,53	0,83	68,00	2,55		1,41	1,51
139,0	47,50	1,50	0,77			8,63		
145,0	44,77	1,55	0,86	67,00	2,52		0,99	1,43
150,0	35,45	1,71	1,11	58,00	2,59		2,16	0,70
154,0	35,49	1,71	1,10	59,00	2,60		2,91	0,51
159,0	34,00	1,76	1,15			10,79		
164,0	35,32	1,73	1,12	59,00	2,63		3,49	0,55
169,0	38,10	1,66	1,03	62,00	2,65		4,41	0,67
173,0	34,27	1,74	1,14	58,00	2,65		2,66	0,50
179,0	33,90	1,75	1,15			11,77		
185,0	34,04	1,74	1,15	58,00	2,68		3,74	0,53

RK-20C

Depth (cm)	Water cont. (wet weight. %)	Wet-Bulk Den. (g/cm3)	Dry-Bulk Den. (g/cm3)	Porosity (%)	Grain Den. (g/cm3)	>63 µm (wt. %)	CaCO3 (wt. %)	Corg. (wt. %)
6,0	25,38	1,93	1,44	47,00	2,67	67,82	2,46	0,52
16,0	27,24	1,86	1,35	50,00	2,65	64,61	4,08	0,54
26,0	26,11	1,90	1,41	48,00	2,68	66,08	3,52	0,60
36,0	25,96	1,91	1,41	48,00	2,68	68,28	1,16	0,52
46,0	27,61	1,88	1,36	50,00	2,71	67,26	0,39	0,49
56,0	27,77	1,86	1,34	50,00	2,66	63,42	1,93	0,57
66,0	27,72	1,86	1,34	50,00	2,67	54,14	9,25	0,67
76,0	30,72	1,81	1,26	52,00	2,45	45,77	7,94	0,57
86,0	25,62	1,91	1,42	64,00	5,18	54,65		

RK-20C (cont.)

Depth (cm)	Water cont. (wet weight. %)	Wet-Bulk Den. (g/cm3)	Dry-Bulk Den. (g/cm3)	Porosity (%)	Grain Den. (g/cm3)	>63 µm (wt. %)	CaCO3 (wt. %)	Corg. (wt. %)
95,0	28,97	1,85	1,31	68,00	5,19	50,82	2,83	0,55
104,0	27,08	1,88	1,37	47,00	2,40	51,16	0,55	0,60

RK-24C

Depth (cm)	Water cont. (wet weight. %)	Wet-Bulk Den. (g/cm3)	Dry-Bulk Den. (g/cm3)	Porosity (%)	Grain Den. (g/cm3)	Shear Strength (kPa)	>63 µm (wt. %)	CaCO3 (wt. %)	Corg. (wt. %)
5,0	51,59	1,46	0,71	73,00	2,58		39,07	1,42	1,64
9,0	50,11	1,47	0,73	72,00	2,59		34,10	1,33	1,45
15,0	50,50	1,46	0,70			2,94			
21,0	33,00	1,77	1,18	57,00	2,69		0,16		
26,0	39,87	1,63	0,98	64,00	2,66		19,98	3,21	0,81
30,0	39,94	1,63	0,98	64,00	2,65		19,10	2,75	0,79
35,0	34,00	1,77	1,16			3,14			
40,0	31,94	1,79	1,22	56,00	2,72		17,40	4,18	0,59
46,0	35,84	1,69	1,09	59,00	2,63		19,77	4,43	0,59
50,0	46,12	1,53	0,83	69,00	2,61		19,70	2,58	1,36
55,0	41,40	1,62	0,93			4,31			
60,0	43,78	1,57	0,88	67,00	2,64		16,79	2,90	1,19
65,0	48,62	1,49	0,77	71,00	2,55		19,90	2,42	1,33
69,0	46,66	1,53	0,81	69,00	2,61		17,31	2,17	1,21
75,0	37,80	1,68	1,03			5,10			
81,0	41,16	1,61	0,94	64,00	2,61		17,30	2,92	1,07
86,0	27,49	1,88	1,36	51,00	2,74		18,96		
90,0	50,20	1,48	0,74	73,00	2,64		18,22	1,50	1,53
95,0	48,60	1,50	0,75			6,28			
100,0	42,75	1,58	0,90	66,00	2,59		19,02	2,90	1,15
105,0	40,80	1,61	0,95	64,00	2,64		14,85	1,08	1,13
110,0	33,00	1,76	1,18	56,00	2,66		18,05	4,02	0,82
115,0	38,10	1,68	1,03			7,85			
121,0	35,49	1,71	1,10	59,00	2,67		23,35	2,64	0,76
126,0	45,96	1,55	0,83	67,00	2,42		14,11	1,50	1,34
129,0	47,02	1,53	0,81	68,00	2,43		29,08	0,90	1,49
135,0	34,00	1,76	1,15			9,41			
140,0	45,37	1,55	0,84	67,00	2,42		20,40	1,17	1,65
145,0	42,42	1,58	0,91	64,00	2,39		17,62	1,92	1,56
149,0	35,57	1,69	1,09	57,00	2,41		16,66	1,42	1,34
155,0	40,50	1,64	0,96	10,79		10,79			
161,0	40,11	1,65	0,99	63,00	2,59		17,42	1,50	1,47
170,0	51,01	1,49	0,73	72,00	2,51		14,70	2,08	1,14

RK-26C

Depth (cm)	Water cont. (wet weight, %)	Wet-Bulk Den. (g/cm3)	Dry-Bulk Den. (g/cm3)	Porosity (%)	Grain Den. (g/cm3)	Shear Strength (kPa)	>63 µm (wt. %)	63-2µm (wt. %)	<2µm (wt. %)	CaCO3 (wt. %)	Corg. (wt. %)
4,0	50,73	1,46	0,72	71,00	2,42		28,94			3,66	1,36
11,0	53,12	1,43	0,67	73,00	2,34		23,00			3,41	1,34
18,0	52,50	1,45	0,67			2,94					
23,0	49,90	1,46	0,73	70,00	2,32		23,93			2,33	1,56
28,0	55,71	1,39	0,62	74,00	2,32		8,99			2,58	1,46
32,0	31,29	1,81	1,24	54,00	2,64		33,54			4,41	0,60
37,0	46,27	1,52	0,81	68,00	2,49		20,95				
42,0	46,80	1,52	0,79			5,49					
47,0	49,66	1,48	0,75	70,00	2,43		10,17				
53,0	46,70	1,52	0,81	68,00	2,47		11,25			4,58	1,22
58,0	47,35	1,51	0,79	69,00	2,47		5,06			4,08	1,28
64,0	53,40	1,43	0,65			5,49					
69,0	47,95	1,50	0,78	69,00	2,45		13,72			3,91	1,22
75,0	50,29	1,47	0,73	71,00	2,42		9,98			4,58	1,47
80,0	47,37	1,53	0,80	69,00	2,50					2,16	1,39
88,0	44,50	1,57	0,85			9,81					
90,0	43,19	1,59	0,90	65,00	2,50		12,82			1,49	1,36
100,0	40,17	1,62	0,97	63,00	2,53		7,65			2,33	0,99
110,0	23,55	1,97	1,51	45,00	2,64		92,44			1,41	0,24
116,0	23,25	1,99	1,53	44,00	2,64		68,38			2,58	0,36

RK-27C

Depth (cm)	Water cont. (wet weight, %)	Wet-Bulk Den. (g/cm3)	Dry-Bulk Den. (g/cm3)	Porosity (%)	Grain Den. (g/cm3)	Shear Strength (kPa)	>63 µm (wt. %)	CaCO3 (wt. %)	Corg. (wt. %)
2,0	34,85	1,72	1,12	57,00	2,54		10,70	3,49	0,68
7,0	53,70	1,41	0,63						
13,0	31,43	1,79	1,22	54,00	2,55		35,15	2,66	0,67
18,0	37,70	1,68	1,05	61,00	2,62		2,43	2,16	0,92
23,0	35,51	1,73	1,11	58,00	2,58		30,61	3,41	0,89
28,0	46,17	1,58	0,85	69,00	2,59		7,10	2,16	1,10
33,0	40,60	1,65	0,98	63,00	2,52		5,83	2,58	0,87
38,0	35,88	1,72	1,10	59,00	2,56		19,61	3,24	0,64
44,0	32,80	1,77	1,17			14,71			
50,0	39,08	1,67	1,02	62,00	2,59		13,07	2,83	0,76
55,0	40,16	1,66	0,99	62,00	2,50		12,56	2,66	0,80
60,0	32,91	1,77	1,19	57,00	2,69		24,90	3,58	0,57
65,0	37,44	1,69	1,05	61,00	2,61		23,12	2,66	0,75
70,0	42,58	1,61	0,92	65,00	2,58		7,16	2,41	0,95
77,0	40,42	1,64	0,97	64,00	2,59		11,78	2,49	1,01

RK-27C (cont.)

Depth (cm)	Water cont. (wet weight. %)	Wet-Bulk Den. (g/cm3)	Dry-Bulk Den. (g/cm3)	Porosity (%)	Grain Den. (g/cm3)	Shear Strength (kPa)	>63 µm (wt. %)	CaCO3 (wt. %)	Corg. (wt. %)
84,0	44,60	1,55	0,84			15,69			
90,0	40,98	1,64	0,97	64,00	2,60		7,54	3,41	0,92
95,0	33,76	1,76	1,17	57,00	2,65		8,51	3,24	0,73
99,0	43,82	1,59	0,89	66,00	2,56		13,55	1,66	1,06
105,0	45,20	1,58	0,87	68,00	2,59		6,98	2,49	1,12
111,0	44,22	1,57	0,87	67,00	2,55		3,87	1,33	1,06
116,0	42,72	1,61	0,92	65,00	2,56		1,61	2,75	0,88
123,0	36,40	1,69	1,06			17,65			
129,0	37,30	1,69	1,06	61,00	2,64		3,63	2,16	0,74
136,0	33,81	1,75	1,16	57,00	2,59		22,46	1,91	0,66
139,0	37,15	1,70	1,07	60,00	2,60		9,99	1,33	1,01

RK-28C

Depth (cm)	Water cont. (wet weight. %)	Wet-Bulk Den. (g/cm3)	Dry-Bulk Den. (g/cm3)	Porosity (%)	Grain Den. (g/cm3)	>63 µm (wt. %)	CaCO3 (wt. %)	Corg. (wt. %)
6,0	44,57	1,56	0,86	67,00	2,59	33,05	1,74	1,30
15,0	43,68	1,57	0,88	66,00	2,54	50,18	1,41	1,21
25,0	47,11	1,52	0,80	69,00	2,52	30,80	1,49	1,43
35,0	48,09	1,49	0,78	70,00	2,49	29,52	1,66	1,35
45,0	45,98	1,52	0,82	68,00	2,49	31,10	1,58	1,29
55,0	43,94	1,57	0,88	67,00	2,66	29,25	1,49	1,27
65,0	44,21	1,58	0,88	68,00	2,66	27,22	1,58	1,17
75,0	44,53	1,55	0,86	67,00	2,54	24,54	1,41	1,23
85,0	44,97	1,53	0,84	67,00	2,51	35,30	1,33	1,35

AT 8408-04

Depth (cm)	Water cont. (wet weight. %)	Wet-Bulk Den. (g/cm3)	Dry-Bulk Den. (g/cm3)	Porosity (%)	Grain Den. (g/cm3)	>63 µm (wt. %)	CaCO3 (wt. %)	Corg. (wt. %)
10,0	50,03	1,33	0,67	72,00	2,57		1,58	1,52
20,0	51,59	1,45	0,70	74,00	2,63		2,33	1,62
30,0	42,08	1,62	0,93	66,00	2,70		3,92	0,76
40,0	55,98	1,40	0,62	77,00	2,60		1,50	1,57
50,0	53,88	1,43	0,66	75,00	2,62		1,92	1,49
60,0	49,07	1,51	0,77	72,00	2,63			
70,0	27,45	1,87	1,35	50,00	2,66		4,17	0,27
80,0	54,95	1,42	0,64	76,00	2,55		1,92	1,66
90,0	49,66	1,50	0,75	72,00	2,63		1,92	1,44
97,0	34,59	1,72	1,13	58,00	2,63		3,17	0,74
100,0	43,24	1,58	0,90	66,00	2,63		2,25	1,06
110,0	51,50	1,46	0,71	73,00	2,62		0,90	1,44
124,0	44,36	1,58	0,88	68,00	2,64		1,92	1,27
130,0	48,22	1,51	0,78	71,00	2,67		2,49	1,28
140,0	49,33	1,49	0,75	71,00	2,57		1,25	1,48
149,0	49,05	1,49	0,76	71,00	2,61		0,92	1,41
160,0	49,63	1,48	0,75	72,00	2,61		1,17	1,40
170,0	48,46	1,55	0,80	70,00	2,50		1,90	1,14
181,0	28,91	1,84	1,31	52,00	2,68		4,10	0,50
191,0	42,56	1,59	0,91	66,00	2,60		1,08	1,28
200,0	44,04	1,58	0,88	67,00	2,62		2,17	1,16
211,0	43,68	1,57	0,88	66,00	2,56		1,17	1,24
220,0	43,91	1,53	0,85	68,00	2,69		1,25	1,56
230,0	42,32	1,63	0,94	66,00	2,70	18,99	1,42	1,23
238,0	34,42	1,77	1,16	58,00	2,71	40,64	3,08	0,59

AT 8408-07

Depth (cm)	Water cont. (wet weight. %)	Wet-Bulk Den. (g/cm3)	Dry-Bulk Den. (g/cm3)	Porosity (%)	Grain Den. (g/cm3)	Shear Strength (kPa)	>63 µm (wt. %)
13,0	37,02	1,53	0,96	61,00	2,64		40,80
20,0	41,90	1,59	0,92	65,00	2,65		40,90
23,5						7,41	
29,0	41,35	1,61	0,94	65,00	2,67		13,34
39,0	39,58	1,62	0,98	63,00	2,64		8,85
44,5						33,29	
52,0	37,08	1,72	1,08	62,00	2,85		5,70

AT 8408-10

Depth (cm)	Water cont. (wet weight. %)	Wet-Bulk Den. (g/cm3)	Dry-Bulk Den. (g/cm3)	Porosity (%)	Grain Den. (g/cm3)	>63 µm (wt. %)	CaCO3 (wt. %)	Corg. (wt. %)
5,0	53,25	1,42	0,66	75,00	2,68	38,13	1,25	1,69
15,0	50,59	1,46	0,72	74,00	2,73	16,70	1,92	1,45
25,0	49,31	1,48	0,75	73,00	2,73	20,85	2,08	1,48
35,0	40,60	1,62	0,96	65,00	2,70	12,43	4,23	0,79
45,0	51,81	1,45	0,70	74,00	2,65	28,60	2,17	1,58
57,0	43,04	1,57	0,89	67,00	2,68	37,38	2,25	1,10
65,0	47,86	1,52	0,79	72,00	2,81	16,63	2,50	1,42
70,0	29,91	1,81	1,27	54,00	2,74	65,06	2,29	0,64
75,0	51,04	1,45	0,71	73,00	2,61	26,77	1,50	1,60
85,0	49,26	1,50	0,76	73,00	2,76	25,18	1,08	1,61
95,0	35,42	1,67	1,08	58,00	2,58	28,03	2,28	0,86
99,0	33,75	1,73	1,14	57,00	2,68	58,32	1,94	0,69
105,0	40,53	1,53	0,91	64,00	2,61	27,91	1,83	1,25
115,0	44,34	1,56	0,87	68,00	2,63	24,67	1,60	1,40
125,0	40,85	1,58	0,93	63,00	2,53	31,94	1,75	1,26
135,0	47,10	1,53	0,81	71,00	2,72	26,32	1,92	1,31
145,0	43,60	1,57	0,89	68,00	2,72	21,85	1,50	1,57
155,0	47,49	1,51	0,79	70,00	2,66	22,44	1,25	1,90
165,0	46,85	1,53	0,81	70,00	2,66	17,40		1,84
175,0	42,99	1,58	0,90	66,00	2,65	13,01	1,58	1,71
185,0	41,71	1,60	0,93	66,00	2,70	18,27	0,42	1,52
195,0	37,97	1,68	1,04	62,00	2,74	23,88	1,75	1,29
205,0	41,42	1,62	0,95	65,00	2,70	25,07	0,58	1,53
215,0	38,62	1,67	1,03	63,00	2,69	15,97	1,99	1,39
223,0	27,87	1,86	1,34	51,00	2,71	55,74	2,70	0,88

AT 8408-11

Depth (cm)	Water cont. (wet weight. %)	Wet-Bulk Den. (g/cm3)	Dry-Bulk Den. (g/cm3)	Porosity (%)	Grain Den. (g/cm3)	CaCO3 (wt. %)	Corg. (wt. %)
5,0	51,26	1,48	0,72	74,00	2,70	1,60	1,82
15,0	34,13	1,75	1,15	59,00	2,76	2,75	0,88
25,0	53,20	1,46	0,68	76,00	2,79	1,25	1,98
45,0	23,46	1,96	1,50	45,00	2,75	3,89	0,20
55,0	52,40	1,45	0,69	75,00	2,67	0,58	1,60
64,0	41,53	1,61	0,94	66,00	2,74	1,83	1,05
80,0	52,90	1,45	0,68	75,00	2,69	0,08	1,82
89,0	48,21	1,51	0,78	72,00	2,74	0,58	1,43
100,0	41,44	1,61	0,94	66,00	2,76	2,17	1,06
113,0	29,45	1,85	1,31	53,00	2,76	3,12	0,57

AT 8408-11 (cont.)

Depth (cm)	Water cont. (wet weight. %)	Wet-Bulk Den. (g/cm3)	Dry-Bulk Den. (g/cm3)	Porosity (%)	Grain Den. (g/cm3)	CaCO3 (wt. %)	Corg. (wt. %)
115,0	23,04	1,98	1,52	45,00	2,76	3,03	0,35
118,0	44,95	1,56	0,86	69,00	2,69	1,92	1,23

AT 8408-15PC

Depth (cm)	Water cont. (wet weight. %)	Wet-Bulk Den. (g/cm3)	Dry-Bulk Den. (g/cm3)	Porosity (%)	Grain Den. (g/cm3)	Shear Strength (kPa)	>63 µm (wt. %)	CaCO3 (wt. %)	Corg. (wt. %)
30,0	53,34	1,44	0,67	74	2,5		36,84	1,35	0,33
34,5						8,00			
40,0	58,24	1,39	0,58	78	2,51		33,27	1,43	0,41
60,0	58,02	1,4	0,59	78	2,51		25,59	1,51	0,33
65,5						8,85			
70,0	57,08	1,39	0,6	76	2,42		44,25	1,49	1,08
80,0	56,8	1,4	0,61	76	2,43		39,45	1,38	1,24
91,0	57,75	1,4	0,59	78	2,57		41,02	1,6	1,24
94,5						7,92			
112,0	55,51	1,44	0,64	77	2,68		43,35	1,44	1,66
121,0	54,56	1,41	0,64	74	2,37		32,66	1,47	0,49
124,5						8,16			
137,0	52,49	1,46	0,69	73	2,47		14,32	1,43	0,91
145,0	54,78	1,42	0,64	75	2,43		28,29	1,41	0,83
160,5						10,87			
165,0	53,9	1,43	0,66	74	2,49		26,27	1,14	1,66
173,0	51,56	1,49	0,72	74	2,67		17,49	1,25	2,24
186,0	53,63	1,42	0,66	74	2,45		19,42	1,37	2,33
189,5						6,91			
194,0	51,98	1,47	0,7	73	2,49		16,34	1,12	3,33
213,0	52,89	1,45	0,68	74	2,5		16,72	1,36	3,08
218,0	56,47	1,4	0,61	76	2,49		34,46	1,69	1,66
230,0	52,18	1,45	0,69	73	2,5	7,19	15,67	1,09	2,08
239,0	43,86	1,55	0,87	67	2,61		45,45	0,94	3,49
252,0	53,07	1,47	0,69	74	2,58		40,53	1,28	1,66
254,5						7,56			
262,0	52,09	1,47	0,7	73	2,56		41,16	1,39	2,83
275,0	39,05	1,67	1,02	63	2,65		0,34	0,54	2,08
280,5						8,95			
285,0	40,62	1,67	0,99	65	2,74		0,39	0,48	2,99
295,0	47,4	1,55	0,81	71	2,69		8,98	0,85	2,74
304,0	45,69	1,57	0,85	68	2,54		14,73	1,1	2,99
315,0	35,88	1,73	1,11	59	2,65		1,9	0,32	3,91
323,5						8,55			

AT 8408-15PC (cont.)

Depth (cm)	Water cont. (wet weight. %)	Wet-Bulk Den. (g/cm3)	Dry-Bulk Den. (g/cm3)	Porosity (%)	Grain Den. (g/cm3)	Shear Strength (kPa)	>63 µm (wt. %)	CaCO3 (wt. %)	Corg. (wt. %)
325,0	37,74	1,7	1,06	62	2,7		4,63	0,45	2,58
335,0	37,95	1,7	1,05	62	2,71		0,83	0,34	3,49
365,0	33,67	1,79	1,19	58	2,78		20,8	0,34	3,16
369,5						9,54			
375,0	35,21	1,75	1,13	59	2,68		1,68	0,4	3,33
385,0	31,38	1,81	1,24	55	2,7		0,66	0,32	3,66
390,5						8,57			
395,0	38,14	1,69	1,04	62	2,71		2,47	0,46	2,41
404,0	36,77	1,72	1,08	61	2,67		3,86	0,54	1,91
420,0	37,34	1,71	1,07	62	2,78		1,56	0,29	3,74
432,0	37,15	1,71	1,08	61	2,72		0,74	0,38	2,66
435,5						10,22			
440,0	32,55	1,79	1,21	57	2,73		1,23	0,45	2,16
450,0	36,52	1,71	1,09	61	2,71		2,67	0,26	2,66
457,5						10,93			
460,0	35,41	1,74	1,12	60	2,77		0,34	0,29	2,66
477,0	34,59	1,77	1,16	59	2,76		0,85	0,33	3,16
482,5						9,94			
485,0	34,06	1,76	1,16	58	2,74		0,36	0,3	3,08
493,0	31,6	1,83	1,25	56	2,75		3,16	0,61	0,83
534,0	9,78	2,38	2,15	22	2,72		89,06	0,16	0,75
540,0	16,79	2,17	1,8	35	2,72		61,83	0,3	0,83
550,0	15,71	2,2	1,85	33	2,72				
560,0	14,52	2,22	1,9	31	2,7				
570,0	14,3	2,23	1,91	31	2,71		86,4	0,18	0,41
580,0	16,39	2,17	1,81	34	2,71		82,24	0,19	0,66

AT8708-01

Depth (cm)	Water cont. (wet weight. %)	Wet-Bulk Den. (g/cm3)	Dry-Bulk Den. (g/cm3)	Porosity (%)	Grain Den. (g/cm3)	Shear Strength (kPa)	>63 µm (wt. %)	CaCO3 (wt. %)	Corg. (wt. %)
8,0	34,31	1,78	1,17	57	2,61		64,65	0,99	0,77
20,0	33,57	1,76	1,17	57	2,69		58,27	1,41	0,73
21,5						6,95			
30,0	30,80	1,80	1,25	54	2,65		62,29	0,66	0,69
40,0	34,40	1,74	1,14	58	2,66		56,12	1,08	0,86
46,5						6,63			
50,0	32,90	1,76	1,18	56	2,66		47,36	1,41	0,83
60,0	32,36	1,79	1,21	56	2,70		54,91		
70,0	33,54	1,73	1,15	57	2,63		49,10		
74,5						10,79			

AT8708-01 (cont.)

Depth (cm)	Water cont. (wet weight. %)	Wet-Bulk Den. (g/cm3)	Dry-Bulk Den. (g/cm3)	Porosity (%)	Grain Den. (g/cm3)	Shear Strength (kPa)	>63 µm (wt. %)	CaCO3 (wt. %)	Corg. (wt. %)
80,0	30,75	1,79	1,24	54	2,65		49,64	0,91	0,82
90,0	30,38	1,81	1,26	53	2,66		53,25	1,66	0,62
100,0	26,65	1,81	1,33	48	2,61		52,49	1,99	0,63
104,5						11,88			
110,0	28,17	1,83	1,32	51	2,64		55,48	1,08	0,75

AT 8708-02

Depth (cm)	Water cont. (wet weight. %)	Wet-Bulk Den. (g/cm3)	Dry-Bulk Den. (g/cm3)	Porosity (%)	Grain Den. (g/cm3)	>63 µm (wt. %)
20,0	30,01	1,83	1,28	53	2,69	63,1
30,0	29,34	1,84	1,30	52	2,69	62,27
40,0	30,13	1,80	1,25	53	2,64	61,09
49,0	32,10	1,74	1,18	55	2,58	43,57
60,0	35,20	1,69	1,10	58	2,58	44,72
69,0	34,15	1,69	1,11	57	2,55	49,65
79,0	33,17	1,75	1,17	57	2,68	41,53
89,0	29,07	1,81	1,28	51	2,61	50,38
100,0	29,85	1,80	1,26	53	2,65	49,22
110,0	31,16	1,77	1,22	54	2,61	53,16
122,0	40,07	1,61	0,97	63	2,60	29,54
127,0	28,90	1,81	1,29	51	2,63	40,52
130,0	37,67	1,66	1,03	61	2,62	30,94
139,0	32,34	1,75	1,18	56	2,68	39,56
150,0	26,71	1,88	1,38	49	2,67	30,43
161,0	31,84	1,76	1,20	55	2,63	41,37
170,0	27,78	1,87	1,35	51	2,70	44,66
175,0	21,44	2,03	1,60	42	2,71	76,42
180,0	30,66	1,79	1,24	54	2,65	53,56
190,0	34,91	1,71	1,11	58	2,62	20,68
200,0	27,44	1,86	1,35	50	2,70	40,61

AT 8708-03

Depth (cm)	Water cont. (wet weight. %)	Wet-Bulk Den. (g/cm3)	Dry-Bulk Den. (g/cm3)	Porosity (%)	Grain Den. (g/cm3)	CaCO3 (wt. %)	Corg. (wt. %)
11,0	38,90	1,65	1,00	63,00	2,68	0,67	0,91
23,0	31,35	1,79	1,23	55,00	2,71	1,33	0,60
35,0	24,30	1,92	1,46	46,00	2,68	0,90	0,42

AT 8708-03 (cont.)

Depth (cm)	Water cont. (wet weight. %)	Wet-Bulk Den. (g/cm3)	Dry-Bulk Den. (g/cm3)	Porosity (%)	Grain Den. (g/cm3)	CaCO3 (wt. %)	Corg. (wt. %)
45,0	35,36	1,70	1,10	59,00	2,64	0,83	0,86
60,0	28,62	1,83	1,31	52,00	2,69	2,34	0,53
70,0	23,51	1,95	1,49	45,00	2,68	2,55	0,46
80,0	22,83	1,99	1,54	44,00	2,74	9,44	0,36
90,0	23,23	1,96	1,51	45,00	2,70	3,58	0,22
100,0	24,30	1,94	1,46	46,00	2,68	2,48	0,40
110,0	25,48	1,91	1,42	47,00	2,68	1,88	0,51

AT 8708-06

Depth (cm)	Water cont. (wet weight. %)	Wet-Bulk Den. (g/cm3)	Dry-Bulk Den. (g/cm3)	Porosity (%)	Grain Den. (g/cm3)	>63 µm (wt. %)	63 - 2 µm (wt. %)	<2 µm (wt. %)	CaCO3 (wt. %)	Corg. (wt. %)
50,0	55,38	1,42	0,63	77,00	2,69				2,25	1,44
60,0	55,35	1,42	0,63	77,00	2,64	11,82	68,65	19,32	2,17	1,45
70,0	54,03	1,43	0,66	76,00	2,64				2,50	1,05
80,0	52,45	1,46	0,69	75,00	2,70				2,51	0,99
90,0	49,45	1,49	0,75	72,00	2,64	0,29			7,58	0,3
100,0	37,97	1,69	1,05	63,00	2,78				3,42	0,65
110,0	43,82	1,57	0,88	68,00	2,71				3,42	0,56
120,0	43,17	1,61	0,91	67,00	2,64				1,92	0,54
130,0	42,98	1,56	0,89	67,00	2,70				3,75	0,38
140,0	54,41	1,49	0,68	74,00	2,37	20,85			2,83	0,92
150,0	52,42	1,46	0,69	75,00	2,68				3,67	1,18
160,0	51,58	1,48	0,71	74,00	2,73				4,42	1,09
170,0	43,30	1,59	0,90	67,00	2,68				4,50	0,54

Tectonic history of a non-accreting active margin during the past 400 ka. Results of a submersible survey of the Peru Trench at 5-6°S. Part I.

J. Bourgois[1], Y. Lagabrielle[2], P. de Wever[1], E. Suess[3] and the Nautiperc team*

1 Université Pierre et Marie Curie, Paris, France

2 Université de Bretagne Occidentale, Brest, France

3 GEOMAR, Kiel, Federal Republlic of Germany

* L. Aquilina, Université Pierre et Marie Curie (UPMC), Paris; P. Chotin, UPMC, Paris; A. Dia, INSU-CNRS, UPMC, Paris; A. Duperret (UPMC, UBO); A. Fiala-Medioni, UPMC, Banyuls, France; J. P. Foucher, IFREMER, Brest; E. Fourcade, INSU-CNRS, UPMC, Paris; F. Harmegnies, IFREMER, Brest; T. Juteau, UBO, Brest; J. Machare, IFEA, Lima, Peru; B. Mercier de Lepinay, INSU-CNRS, Sophia-Antipolis, France; F. Michaud, UPMC, Villefranche sur Mer, France; F. Monge, IGP, Lima; M. Sosson, INSU-CNRS, Sophia-Antipolis; M. v. Breymann, GEOMAR, Kiel, Federal Republic of Germany; R. v. Huene, GEOMAR, Kiel.

ABSTRACT

The Recent tectonic history of the northern Peru convergent margin can be retraced using data collected during deep sea dives of the submersible Nautile combined with a recent Hydrosweep survey conducted off Peru at 5-6°S by the R/V Sonne. During the past 400 ka, a wide rollover fold developed in the middle slope area, in relation to a major seaward dipping detachment fault. A catastrophic debris avalanche occured as the result of an oversteepening of the landward flank of the rollover fold. The gravity failure of the slope, previously recognized by SeaBEAM mapping, occured 13.8 ± 2.7 ka ago and displaced enough material to produce a destructive tsunami.
The sedimentary sequence has been intensively sampled along the main scarp of the middle slope area. It consists of Upper Miocene (8-9 Ma) to Pleistocene siltstone, sandstone and rare dolostone. Based on micropaleontological data, a main unconformity, at the base of the Quaternary sequence has been documented.

INTRODUCTION

Tsunamis generated at convergent plate boundaries may be caused by gravity slides of large amounts of sediments combined with relatively low amplitude earthquakes in basement rocks (Kanamori, 1972; Beck and Nishenko, 1990). Deep sea dives conducted with the NAUTILE along the northern margin of Peru during the NAUTIPERC cruise in March-April 1991 (Fig. 1) provide new insight into the tectonic processes that allow massive tsunamogenic gravity failure to occur at convergent margins (von Huene et al., 1989).
The primary objectives of the NAUTIPERC cruise included geological observations and chemical studies of venting fluids at a convergent margin devoid of accretionnary prism and where subduction erosion (Scholl et al., 1980; Hussong and Wipperman, 1981; Aubouin et al., 1984; von Huene and Culotta, 1989; Bourgois et al., 1990; von Huene and Lallemand, 1990; von Huene and Scholl, 1992), normal faulting and massive subsidence (Kulm et al., 1984; Kulm et al., 1988; Suess, von Huene et al., 1988a; Suess, von Huene et al., 1988b; von Huene, Suess et al., 1988; Moore and Taylor, 1988; Resig, 1989) are active.

We report hereafter the main results of the geological study based on submersible observations. Geochemical results of the cruise are presented in a separate paper (Dia et al., this issue).
The geological data collected *in situ* from the submersible are combined with the results of a recent hydrosweep survey by the R/V Sonne (Cruise 78, March-April, 1992) conducted off northern Peru. These data provide more detailed constraints on the geology of the continental margin and of the trench and allow to propose a high resolution tectonic history of the past 400 ka (Bourgois et al., 1992).

PREVIOUS STUDIES OF THE PERU MARGIN OFF PAITA

Three MCS lines, trending E-W, were shot during the Nazca Plate Project (Kulm et al., 1981) in an area of the landward slope of the Peru Trench between 5° and 12° S. According to the interpretation of one of these lines (line CDP3, offshore Paita), Sheperd and Moberly (1981) concluded that the upper slope is deformed by block faulting and that the lower slope exhibits the diffraction pattern of an accretionary prism. Reprocessing of the line and comparison with data from on-shore industry wells allowed Miller et al. (1986) to project the geological data from the shelf to the middle slope area.
In 1986, in preparation for ODP Leg 112, the knowledge of the structure of the middle slope area was greatly improved by SeaBEAM bathymetry (Fig. 1) acquired simultaneously with four multichannel seismic profiles (von Huene et al.,1989) shot perpendicular to the CDP3 line. The main morphological features which have been distinguished in the surveyed area include : 1) a 400 to 700 m high scarp (Upper Slope Scarp : USS, Fig. 2). It is concave seaward and separates the upper slope from the middle slope. The seismic data have shown that this scarp corresponds to a major detachment fault dipping 45° seaward and penetrates deeply into the continental margin down to 3-5 km below seafloor (Bourgois et al., 1988; von Huene et al.,1989); 2) a 1000 to 1200 m high curved scarp (Middle Slope Scarp : MSS, Fig. 2), also concave seaward. It is located 10 km seaward from the USS; 3) a 300 to 500 m high scarp (Subduction Scarp : SS, Fig. 2) located at the base of the lower slope; 4) a chaotic topography, with closed highs and lows, between the MSS and SS which represents the surface of a debris avalanche detached from the MSS, 5) Isolated mounds on the flat floor of the trench indicating that the debris avalanche travelled down to the trench axis.

In 1989, von Huen et al. have proposed that the USS und the MSS bound a landward tilted block detached along a listric fault, and that the MSS represents the boundary of an area voided by slumping. They emphasized that the detachment of the block (20 x 33 km) was catastrophic. It produced the debris avalanche that covered the lower slope and extended across the trench axis. The volume of the displaced materails is thought to be sufficient to produce a destrcutive tsunami.

THE MIDDLE SLOPE SCARP (MSS)

Eighty four samples of sediment were collected along the MSS. They constrain the geology as illustrated in Figure 2. The reconstructed lithostratigraphic succession of the middle slope area consists, from bottom to top: 1) of 400 m of Upper Miocene mudstone and sandstone which include: the early Late Miocene (8 to 9 Ma) documented at the base of the sequence from a diatom assemblage and the latest Miocene (5 to 6 Ma) indentified by a radioalarm assemblage: 2) of 300 to 400 m of massive siltstone and sandy mudstone. An earliest Pliocene age (5.3 ot 4.5 Ma) is documented at the base of the sequence by a diatom and sillicoflagellate assemblage. A diatom assemblage allows to inditfy the latest Pliocene (2.3 to 1.8 Ma); 3) of 0 to 500 m of datom and radiolarian bearing mudstones of Quaternary age (0.4 to 1.5 ma). They exhibit a maximum thickness along the EW trending section of the MSS. To the south, this formation wedges in between the Pliocene and the Late Pliocene sequences; 4) of 50 to 75 m of pelagic diatom ooze which unconformably overlies the older sequence. A Late Pleistocene age, more recent than 0.4 Ma, for this section is based on the occurence of *Lamprocyrtis nigriniae* (Johnson and Nigrini, 1985) and the last occurence of *Stylatractus universus* (Morley and Schackleton, 1978).

The sixteen dives performed along the MSS have shown a succession of small cliff exposing bare rock outcrops (Fig. 3A) separated by narrow step covered with recent pelagic sediments. In detail, the topography is complicated by a succession of small canyons separated by sharp ridges that underline a dense network of fractures. Fresh screes are observed at the foot of small scarps. Fractures and screes are associated frequently with clam colonies and serpula thickets related to fluid vents. In general, the freshness of the outcrops (Fig. 3A) suggests that the failure of MSS was catastrophic and occured recently.

Two dives along the westernmost EW trending section of the MSS have shown beds dipping seaward. This is at variance with the dip expected from the „landward tilted block" model (von Huene et al., 1989) that predicts landward

dipping bed in this area. The middle slope area is not a simple, rigid, tilted block but a wide anticline with a N-S trending axis within a separate block down-dropped toward the trench (Fig.2). The post 0.4 Ma pelagic sedimentary cover (Fig.2) accumulated during the time that the anticline structure developed.

THE UPPER SLOPE SCARP (USS).

Two deeply incised canyons cut through the USS at the upper-middle slope boundary. They were the site of three dives of the NAUTIPERC cruise. Two main results of the geological survey must be pointed out : 1) in contrast to the MSS, the post 0.4 Ma pelagic sedimentary cover is very thick, leading to a smooth topography, indicating that the detachment fault scarp is totally burried (Fig.3B);.2) active fluid vents (Fig.3B) occur along the USS.
According to von Huene et al., (1989), the detachment along the USS fault was catastrophic and would have occurred very shortly before (or after) the failure which affected the MSS. Therefore, the USS should exhibit morphological characteristics similar to that of the MSS.
The major detachment fault related to the USS (Bourgois et al., 1988; von Huene et al., 1989) cuts the upper plate down to 5 km (von Huene et al., 1989). We assume that the anticline which extends seaward across the middle slope area is linked to the detachment fault and thus would be a rollover fold. The time when the rollover began to form can be estimated. The detachment cuts the Quaternary sequence (0.4 to 1.5 Ma), as shown by MCS data (von Huene et al., 1989). The detachment scarp is covered progressively by the post 0.4 Ma pelagic sediment as the middle slope area subsided. Thus, we assume that the detachment and the related middle slope rollover fold began to form 0.4 Ma ago.

DISCUSSION

AGE OF THE DEBRIS SLIDE.

The exact timing when the debris avalanche occurred cannot be estimated directly, however, can be inferred quite reliably. Assuming that the debris flow travelled across the trench floor down to the seaward wall of the trench and that the debris were subsequently transported back toward the east by plate convergence, the timing can be determined as a function of the distance between the front of the debris flow today and its original position. During March-April 1992, a complementary Hydrosweep survey was conducted along the Peru Trench during the R/V Sonne Cruise 78 to the north and to the south of the area

mapped during the R/V Jean Charcot cruise in 1986 (Fig1 and 4). These data show that the eastern border of the chaotic zone, representing the frontal part of the debris avalanche in the trench, narrows to the north, approaching the subduction front and widens to the south. Between 5°45´ and 5°50´ S, the debris front is 1 km away from the 150 m high scarp of the normal fault bounding the trench seaward. If we assume that : 1) the debris flow stopped against such a fault scarp and, 2) the trench has maintained a constant width as it evolved through time, we may infer that the front of the slide debris travelled landward 1 km since it occured. According to different authors, plate convergence rates in this area range between 6 and 8.9 cm/yr (6.3+/- 0.3 cm/yr : SL7.1 model, Smith et al., 1990; 8.1 cm/yr : NUVEL1 model, DeMets et al., 1990; 8.9 cm/yr : AMO2 model, Minster and Jordan, 1978). Taking into account the assumptions presented above, we may thus conclude that the slide occurred between 16.5 and 11.1 ka ago.

GEOLOGY AND EVOLUTION OF THE MARGIN.

According to the interpretation of the CDP3 line by Miller et al., (1986) including the geology projected from the shelf (Sheperd and Moberly, 1981), sedimentary rock of Eocene and Cretaceous ages were supposed to crop out along the USS and the MSS. Such interpretation should be reconsidered in light of the samples recovered during the NAUTIPERC cruise. The oldest sedimentary rock sampled at the southern toe of the MSS is Upper Miocene in age (8-9 Ma). The main unconformity, imaged by the MCS data along the middle slope area (von Huene et al., 1989) is at the base of the Quaternary sequence.

The pre-detachment fault topography (Fig. 5A) of the slope landward of the MSS was reconstructed (von Huene et al., 1989) by matching the subsurface geology and aligning the sea floor topography along the CDP3 line (Fig. 2). A complementary constraint was obtained by aligning landward dipping reflectors cut by the detachment fault at about 5 km depth. Thus, from 400 ka ago, when the detachment fault began to form, to the present time, the landward flank of the middle slope rollover fold had rotated 5° landward. The slope in this area became undercritical (Fig. 5B and C). During the same time, the seaward flank of the middle slope rollover fold had rotated 5° seaward (Fig. 5B). The restored slope of the seaward flank dips about 12°, which is slighty greater than the 11° slope of the northern intact part of the seaward flank of the middle slope rollover fold. Thus, the slope in this area oversteepened (Fig. 5B) dramatically and became overcritical. The catastrophic debris avalanche which occurred between 16.5 and 11.1 ka ago, removed the seaward flank of the middle slope rollover

fold (Fig.5C). The volume of material involved in the avalanche debris (more than 400 km3) is sufficient to generate a large tsunami. The tectonic process which conducted to generate such a large tsunami includes : 1) a major seaward dipping detachment fault located at the upper-middle slope boundary, and 2) the contemporary development of a 18 km wide rollover in the middle slope area. The strain released along the detachment fault was stored partly along the middle slope rollover fold during the past 400 ka and then catastrophically released through the failure of the middle slope area. The processes that cause the initiation of the detachment faulting must be discussed. Subduction erosion working at depth, change in the angle of subduction, occurrence of reliefs on the subducting plate and compressional forces within the sedimentary sequence of the margin may act separately or together to increase the slope angle of the middle slope area.

The unloading induced by the catastrophic failure and the subsequent avalanche debris would diminish the pore fluid pressure and accelerate the upward migration of fluid. Indeed, a major zone of fluid vents was found at the break in slope of the MSS (black dot Fig. 2) that is at the intersection between the NS and EW main structural directions of the middle and upper slopes (Dia et al., 1992, this issue). Murachi and Ludwig (1980) have suggested that upward migration of fluid released during subduction is a mechanism able to soften the base of the upper plate. Such softening might help subduction erosion of the base of the upper plate. Therefore, the catastrophic failure of the middle slope area is a process that may increase locally subduction erosion.

REFERENCES CITED

Aubouin, J., Bourgois, J., and Azema, J., 1984, A new type of active margin : the convergent-extensional margin, as exemplified by the Middle America Trench off Guatemala: Earth and Planetary Science Letters, v.87, p. 111-126.

Beck, S.L., and Nishenko S.P., 1990, Variations in the mode of great earthquake rupture along the central Peru subduction zone: Geophysical Research Letters, v.17, p. 1969-1972.

Bourgois, J., Pautot, G., Bandy, W., Boinet, T., Chotin, P., Huchon, P., Mercier de Lepinay, B., Monge, F., Monlaü, J., Pelletier, B., Sosson, M., and von Huene, R., 1988, Seabeam and seismic reflection imaging of the tectonic regime of the

Andean Continental margin off Peru (4 S to 10 S): Earth and Planetary Science Letters, v.87, p. 111-126.

Bourgois, J., Huchon, P., and Pautot, G., 1990, Tectonics of the Peru Active margin: Proceeding of the 28th IGC, Washington, July 1989; Tectonics of the Circum-Pacific Continental margins, VSP edited by J. Aubouin and J. Bourgois, p. 77-137.

Bourgois, J., Michaud, F., von Breymann, M., Suess, E., von Huene, R., Lagabrielle, Y., Juteau, T., Foucher, J.P., Harmegnies, F., Chotin, P., De Wever, P., Fourcade, E., Mercier de Lepinay, B., Sosson, M., Aquilina L, Dia, A., Marchare, J., Monge, F., 1992, Northern Peru convergent margin : massive slides from the upper plate into the trench axis observed from a Submersible: E.O.S., vol.73, n°14, p.152.

DeMets, C., Gordon, R.G., Argus, D.F., and Stein, S., 1990, Current plate motions: Geophysic. J. Intl., v. 101., p. 425-478.

Dia, A.N., Aquilina L., Suess E., von Breymann M., Boulègue J., Bourgois J., and the Nautiperc Shipboard Scientists, Continent-derived fluids from the convergent margin off Peru. Deep sea dives of the Nautiperc cruise, Part 2: Geology (this issue).

Hussong, D.M., and Wipperman, L.K., 1981, Vertical movement and tectonic erosion of the continental wall of the Peru-Chile Trench near 11 30´`S latitude: *in* Nazca Plate: Crustal formation and Andean convergence edited by L.D. Kulm, J. Dymond, E.J. Dasch, and D.M. Hussong, Memoir Geological Society of America, 154, p. 509-524.

Johnson, D.A., and Nigrini C., 1985, Synchronous and time-transgressive Neogene radiolarian datum levels in the equatorial Indian and Pacific Oceans: Marine Micropaleontology, 9, p. 489-524.

Kanamori, H., 1972, Mechanism of tsunami earthquakes: Phys. Earth Planet. Inter., v.5, p. 346-359.

Kulm, L.D., Dymond J., Dasch E.J., Hussong D.M., and Roderick R., 1981, Nazca Plate : Crustal Formation and Andean Convergence: Geological Society of America, Memoir 154, 824 p.

Kulm, L.D., Suess, E., and Thornburg, T.M., 1984, Dolomites in organic-rich muds of the Peru forearc basins: Analogue to the Monterey Formation, *in* Garrison, R.E., Kastner, M., and Zenger. D.H., eds., Dolomites of the Monterey Formation and other organic-rich units: Society of Economic Paleontologists and Mineralogists, Pacific section, Special Publication 41, p. 29-47.

Kulm, L.D., Thornburg, T.M., Suess, E., Resig J., and Fryer, P., 1988, Clastic, diagenetic, and metamorphic lithologies of a subsiding continental block: Central Peru forearc, *in* Proceedings of the Ocean Drilling Program, initial reports (Volume 112): College Station, Texas Ocean Drilling Program, p. 91-107.

Miller, J., Hussong, D.M., and von Huene R,, 1986, Seismic images of modern Convergent Margins, tectonic structures, edited by R. von Huene: A.A.P.G. Stud. Geol., 26, p. 32-33.

Minster, J.B., and Jordan, T.H., 1978, Present-day plate motions: Journal of Geophysical Research, v. 92, p. 4798-4804.

Moore, G.F., and Taylor, B., 1988, Structure of the Peru Forearc from multichannel seismic-reflection data: *in* Proceedings of the Ocean Drilling Program, initial reports (Volume 112), College Station, Texas Ocean Drilling Program, p. 71-76.

Morley, J.J., and Shackelton N.L., 1978, Extension of the Radiolarian Stylatractus universus as a biostratigraphic datum to the Atlantic Ocean: Geology, v. 6, p. 309-311.

Murauchi, S., and Ludwig, W.G., 1980, Crustal structure of the Japan Trench : the effect of subduction of ocean crust, *in* Scientific Party, Initial Reports of the Deep Sea Drilling Project, 56, 57 (part 1): Washington D.C., US Government Printing Office, p. 463-470.

Resig, J.,1989, Benthic foraminiferal stratigraphy and paleoenvironment off Peru, Ocean Drilling Project Leg112: Proceedings of the Ocean Drilling Project, scientific results, College Station, Texas, Ocean Drilling Program, p. 203-235.

Scholl,W.D., von Huene, R., Vallier, T.L., and Howell D.G., 1980, Sedimentary masses and concepts about tectonic processes at underthrust ocean margins: Geology, v.8, p. 564-568.

Sheperd G.L., and Moberly R., 1981, Coastal structure of the continental margin, northward Peru and southwest Ecuador: Crustal formation and Andean convergence edited by L.D. Kulm, J. Dymond, E.J. Dasch, and D.M. Hussong: Memoir Geological Society of America, 154, p. 551-591.

Smith, D.E., Kolenkiewicz, R., Dunn, P.J., Robbins, J.W., Torrence, M.H., Klosko, S.M., Williamson, R.G., Pavlis, E.C., Douglas, N.B., and Fricke S.K., 1990, Tectonic motion and deformation from the Satellite Laser Ranging to LAGEOS: Journal of Geophysical Research, v.95, p. 22,013-22,041.

Suess, E., von Huene, R., et al., 1988a, Proceedings of the Ocean Drilling Program, initial reports (Volume 112): College Station, Texas Ocean Drilling Program.

Suess, E., von Huene, and Leg 112 shipboard Scientists, 1988b, Ocean Drilling Program Leg 112, Peru continental margin: Part 2, sedimentary history and diagenesis in a coastal upwelling environment: Geology, v.16, p. 939-943.

von Huene, R., Suess E., and Leg 112 shipboard Scientists, 1988, Ocean Drilling Program Leg 112, Peru continental margin: Part 1, Tectonic history: Geology, v.16, p. 934-938.

von Huene, R., Bourgois, J., Miller, J., and Pautot, G., 1989, A large tsunamogenic landslide and debris flow along the Peru Trench: Journal of Geophysical Research, v. 94, p. 1703-1714.

von Huene, R., and Culotta, R., 1989, Tectonic erosion at the front of the Japan Trench convergent margin: Tectonophysics, v. 160, p. 75-90.

von Huene, R., and Lallemand, S., 1990, Tectonic erosion along the Japan and Peru convergent margins: Geological Society of America Bulletin, v.102, p. 704-720.

von Huene, R., and Scholl, D.W., 1992, Observations at convergent margins concerning sediment subduction, subduction erosion, and the growth of continental crust: Reviews of Geophysics, 29, p. 279-316.

ACKNOWLEGMENTS

The NAUTIPERC cruise was supported by IFREMER, INSU-CNRS and GEOMAR. We thank the Captain and the crew of the R/V Nadir for their efficient work and the representants of the Peruvian Navy, Lieutenants Gaviola and Valdez. The help of the IFEA and the French Embassy in Lima and Quito was greatly appreciated. Diatom, silicoflagellate and radiolarian assemblages were identified by J. Barron and E Fourtanier, P. Dumitrica and J.P. Caulet respectively.

CAPTION OF FIGURES

Fig. 1- Location of dives during the NAUTIPERC cruise. Line with barbs indicates Peru Trench convergence zone. The main area discussed in this paper was surveyed during the Leg 1, off Paita. The arrow shows the direction of the subducting Nazca Plate relative to the South America Plate, the numbers above the arrow are the convergence rates (in cm/yr) determined by the SLR solution (Smith et al., 1990), the AMO2 model (Minster and Jordan, 1978) and the NUVEL1 model (DeMets et al., 1990), respectively.

Fig. 2- 3D diagram showing the main geologic and tectonic features identified in the Paita area. USS = Upper Slope Scarp, MSS = Middle Slope Scarp, SS = Subduction Scarp. The 3D diagram is from a mesh net perspective diagram of SeaBEAM bathymetry (Bourgois et al., 1988). The black dot and the open dot indicate locations of figures 3 and 4, respectively. The thick line along the CDP3 profile refers to section on figure 5C.

Fig. 3- A: The MSS exhibits bare rock outcrop without any pelagic deposit. It does not show a unique fault plane but a dense fracture network without privileged orientation. MSS is a very fresh scar. Active fluid venting associated with Clam colonies, bacteria veals, Serpula thickets and thick baryte deposits occurs along the MSS (Dia et al., 1992, this issue). B: The USS is covered by pelagic sediment, thus constracting from the typical aspect of the MSS.

Fig. 4- Hydrosweep (R/V Sonne cruise 78, March-April 1992) and SeaBEAM (SEAPERC cruise of the R/V Jean Charcot, July 1986) surveys of the Peru Trench off Paita (see fig. 1 for location). The slide debris traveled across the flat trench floor to the seaward slope and were subsequently carried back toward the deformation front by plate convergence. The mass wasting occured 13.8 ± 2.7 ka. 1-turbidite infill of the trench, 2-slide debris, 3-slide direction of the debris flow, 4-front of the slide debris in the trench, 5-deformation front, 6-normal fault.

Fig. 5-Tectonic evolution of the middle slope area during the past 400 ka. A-Slope condition 400 ka ago prior initiation of the detachment fault. The steep slope was under stable conditions along the middle slope area. B-The downslope slip movement along the detachment fault was accomodated seaward by a rollover fold which extends throughout the middle slope area. The landward flank of the rollover fold subsided 800 m. The seaward flank was greatly oversteepened, the slope became overcritical. C-Failure of the seaward flank of the rollover fold.

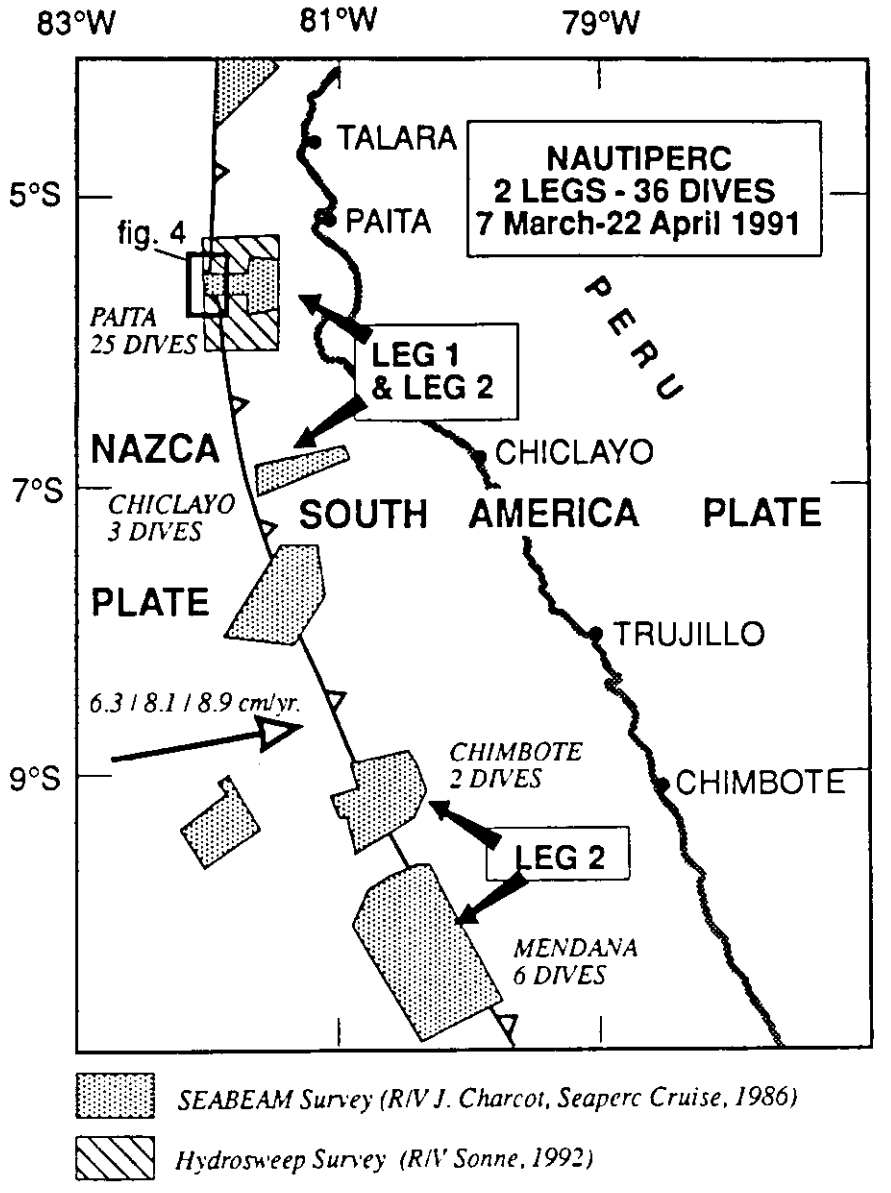
83°W
81°W
79°W
5°S
7°S
9°S
TALARA
PAITA
NAUTIPERC
2 LEGS - 36 DIVES
7 March-22 April 1991
fig. 4
PAITA
25 DIVES
LEG 1
& LEG 2
PERU
NAZCA
CHICLAYO
CHICLAYO
3 DIVES
SOUTH AMERICA PLATE
PLATE
TRUJILLO
6.3 / 8.1 / 8.9 cm/yr.
CHIMBOTE
2 DIVES
CHIMBOTE
LEG 2
MENDANA
6 DIVES
SEABEAM Survey (R/V J. Charcot, Seaperc Cruise, 1986)
Hydrosweep Survey (R/V Sonne, 1992)

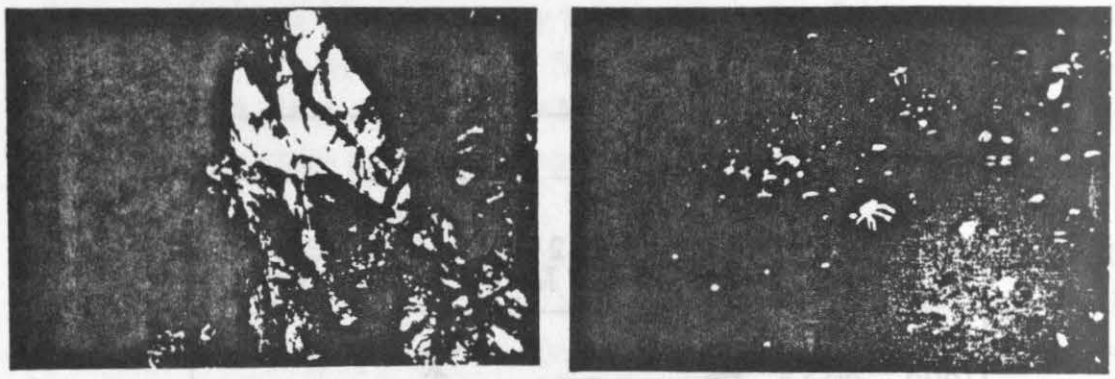

A B

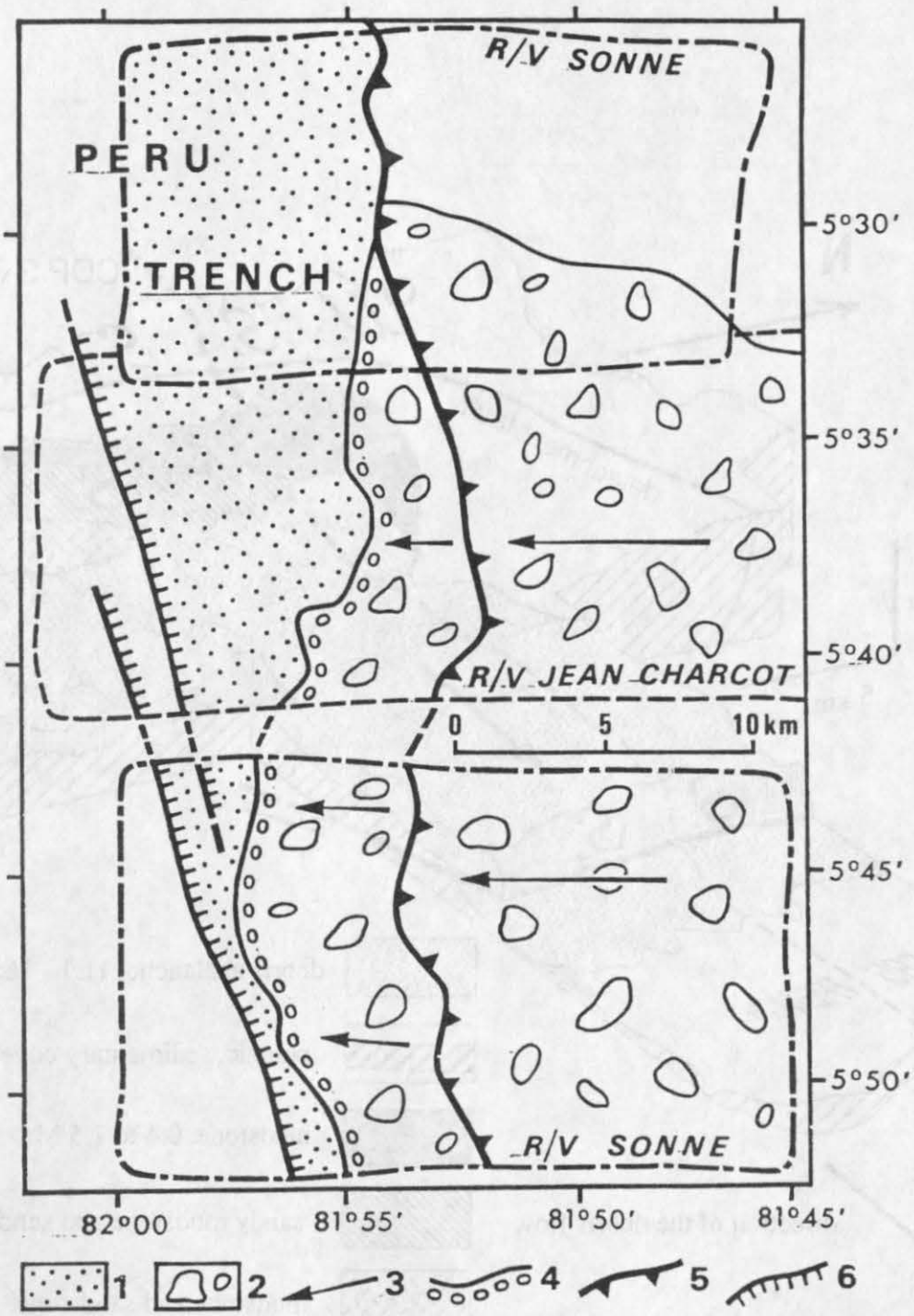
R/V SONNE
PERU
TRENCH
5°30'
5°35'
5°40'
R/V JEAN CHARCOT
0 5 10km
5°45'
5°50'
R/V SONNE
82°00
81°55'
81°50'
81°45'
1
2
3
4
5
6

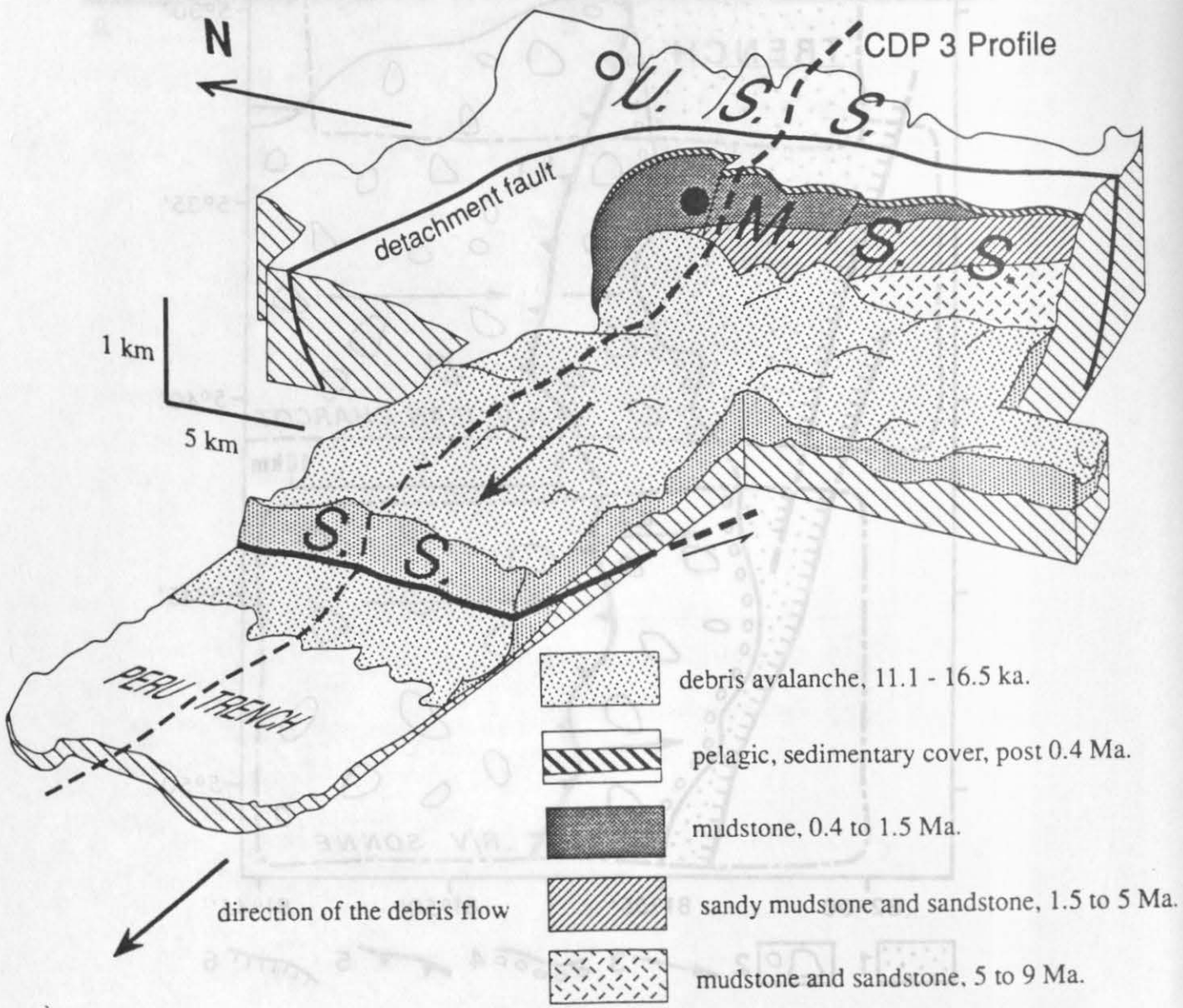
N
CDP 3 Profile
U. S.
detachment fault
M. S. S.
1 km
5 km
S. S.
PERU TRENCH
direction of the debris flow
debris avalanche, 11.1 - 16.5 ka.
pelagic, sedimentary cover, post 0.4 Ma.
mudstone, 0.4 to 1.5 Ma.
sandy mudstone and sandstone, 1.5 to 5 Ma.
mudstone and sandstone, 5 to 9 Ma.

Continent-derived fluids from the convergent margin off Peru. Deep sea dives of the Nautiperc cruise, Part II.

A. N. Dia[1], L. Aquilina[1], E. Suess[2], M. Torres[2], J. Boulègue[3], J. Bourgois[4], and Nautiperc Shipboard Scientists*

1 Laboratoire de Géochimie et Métallogénie, Tour 26-16, E5, Université Pierre et Marie Curie, Paris, France
2 GEOMAR, Wischhofstr. 1-3, 2300 Kiel 14
3 INSU-CNRS, UPMC, Laboratoire de Géochimie et Métallogénie, Paris, France
4 INSU-CNRS, UPMC, Laboratoire de Géodynamique, Tectonique et Environnement, Paris, France

* P. Chotin, UPMC, Paris, France
P. de Wever, INSU-CNRS, UPMC, Paris, France
A. Fiala-Médioni, UPMC, Banyuls, France
J. P. Foucher, IFREMER, Brest, France
E. Fourcade, INSU-CNRS, UPMC, Paris, France
F. Harmégnies, IFREMER, Brest, France
T. Juteau, UBO, Brest, France
Y. Lagabrielle, INSU-CNRS, UBO, Brest, France
J. Machare, IFEA, Lima, Peru
B. Mercier de Lépinay, INSU-CNRS, Sophia-Antipolis, France
F. Michaud, UPMC, Villefranche, France
F. Monge, IGP, Lima, Peru
M. Sosson, INSU-CNRS, Sophia-Antipolis, France
R. v. Huene, GEOMAR, Kiel, Germany

submitted to Geology

Abstract

The collection of 15 fluid samples from venting sites during the Nautiperc cruise, off the northern Peru convergent margin, provided the base of a geochemical (major and trace element contents) and Sr isotopic investigation, on the origin of fluids in Andean type subduction zones.

The venting sites are associated to large benthic biological communities as it has been often observed elsewhere in convergent margins. However, as a difference in this case, the venting is also closely related to large barite deposits.

Major (K, Ca and Mg) and trace element (Li, Rb, Sr, Pb, Cd, Mo, Mn, Cu and Co) do not reveal any significant variation as compared to bottom seawater. But, the Ba content shows some enrichment in these fluids as referred to seawater.

The $^{87}Sr/^{86}Sr$ isotopic ratios reveal a shift towards more radiogenic values compared to seawater. To explain such elevation, we propose either the influence of a fluid characterized by more radiogenic signature (continental fluid) or reaction between seawater and the underlying continental crust and/or with clastic sediments. The presence of this non local continental component is more strongly marked on the $^{87}Sr/^{86}Sr$ ratios measured in the associated barite deposits. Therefore, the fluids responsible for the barite deposition were mostly continent-derived and thus the fluids collected are, at least in a part, continent related.

CH_4 fluxes and therefore associated water flow rates were estimated through CH_4 contents measured with a benthic chamber.

Introduction

The nature and as a consequence the origin of fluids in convergent margins has been previously investigated widely through geochemical and isotopic studies of venting fluids, as well as pore fluids (Boulègue et al., 1987a; Elderfield et al., 1990; Kastner et al., 1990; Kastner et al., 1991). During the past ten years, extensive work was done along active margins exhibiting well developed accretionary prism, these include Nankai (Claypool et al., 1986; Boulègue et al., 1987a,b), Barbados (Brown and Westbrook, 1988; Foucher et al., 1990) and Oregon Cascadia (Carson et al., 1988) margins.

During the same time little was done regarding the fluid regime of Andean type convergent margin along which related-subduction erosion processes are working. Such type of convergent margin shows: widespread extensional tectonic regime, low developed accretionary wedge and massive subsidence, instead of compressional tectonic regime, well developed accretionary wedge and uplift as known along the Nankai, Barbados and Oregon-Cascadia margins. The first significant work regarding pore fluids of an Andean type convergent margin was done from samples recovered during the ODP Leg 112 (Suess et al., 1988; Kastner et al., 1990) off Peru.

One of the main purpose of the Nautiperc cruise (March-April, 1991), using the deep sea submersible Nautile, was to acquire new insights into the hydrogeological system along the non accreting convergent margin off Peru. Therefore, fluids and associated barite deposits from vents located along the Andean (convergent) margin between 5 and 7° south latitude have been sampled, at depth ranging from 2500 to 5400 m down to the trench (Bourgois et al., 1992a).

Subduction zone fluids can have two types of sources: internal and external. The possible internal sources could be: 1) pore fluids included in the sediment and/or the fluids contained in the oceanic crust expelled by porosity reduction processes (Bray and Karig, 1985; Bangs et al., 1990; Davis et al., 1990), 2) fluids formed through diagenetic or metamorphic dehydration, or produced from the breakdown of hydrous minerals (Kastner et al., 1991), and 3) fluids due to biogenic or thermogenic decomposition of organic matter (Kastner et al., 1990; Peacock, 1990; Vrolijk et al., 1990).

As external sources, seawater and/or mixing with meteoric or deep water transported through a complex system of faults can be considered (Kastner et al., 1990; Le Pichon et al., 1990a; Le Pichon et al., 1990b).

One would expect that the primary geochemical and isotopic features of the collected venting fluids, have to be affected by fluid-solid exchange reactions, and by

mixing with the infinite reservoir of ambient seawater. The use of different geochemical and isotopic tracers can help to distinguish, at least, the main sources of such fluids, in spite of the complexity of the system.

Therefore, from a geochemical point of view, our investigation on the major and trace-element composition of the fluids coupled with Sr isotope measurements (firstly done off Peru on venting fluids and not as previously done on pore fluids), was aimed at elucidating the nature of the fluids and thus at a characterization of their possible sources. Indeed, the determination of the origin of such venting fluids, reinferred by Sr isotope data, could provide clues to better constrain fluid migration in subduction zones. During the same cruise, fluids were sampled through a benthic chamber for CH_4 content measurements with the aim of estimating methanefluxes and fluid venting rates.

Geological setting

The deep water samples were collected during the Nautiperc cruise from four sites (Paita, Chiclayo canyon, Chimbote and Mendana areas) (Fig.1); this paper is focussed only on data from the Paita and Chiclayo areas, where thick barite deposits were discovered in close relation to the venting.

The Paita and Chiclayo canyon are located off northern Peru between 5 and 7°10' south latitude (Fig. 1). Knowledge of both areas was greatly improved by SEABEAM bathymetry, which has been thoroughly discussed by Bourgois et al., 1988. The main morphological features distinguished in the Paita area include : 1) a 400 to 700 m high scarp at the upper slope-middle slope boundary, this Upper Slope Scarp (USS) is a major detachment fault dipping 45° seaward, which penetrates into the continental margin down to 3-5 km below seafloor (Bourgois et al., 1988; Von Huene et al., 1989); 2) a 1000 to 1200 m high scarp (MSS=Middle Slope Scarp) located 10 km seaward from the USS; 3) a 300 to 500 m high scarp (SS=Subduction Scarp) located at the base of the lower slope. This complex scarp system (USS, MSS and SS) which trends N-S, parallel the trench and exposes sediments younger than upper Miocene (Bourgois et al., 1992a; Bourgois et al., this issue).

The Chiclayo canyon (Sosson et al., 1992) is 100 km south of the Paita area, extending in the east north east-west south west direction, perpendicular to the trench axis. It is 1500 to 2000 m deep and provides the only opportunity to complete a geological cross-section through the Andean Continental Margin. Paleozoic basement was recovered at three sites located at 15, 25 and 50 km landward from the trench axis, respectively. The data collected from the three dives along the canyon and comparison with results from the MCS and wells on the shelf, allow a projection of geological data

information from the shelf to the lower slope area. The Paleozoic basement of the Amotope-Bayovar Massif extends down to the lower slope: the E-W trending normal faults which deeply penetrate the basement rock onland also extend seaward.

Assuming that the Chiclayo canyon is a window opened on the deep structure of the margin, the complex drainage network of fluids across the continental margin off Peru may include: 1) an E-W trending normal fault network which extends across the continental margin and, 2) a N-S trending fault network which includes a major detachment fault in the Paita area; both penetrating deeply the continental basement of the margin.

Fluid venting occurrence

In the Paita and Chiclayo canyon areas, the venting is associated with the presence of dense biological communities. Indeed, the fluid expulsion indicated by fluid seeps or vents, is marked by intense biological activity as already seen elsewhere on convergent margins (Suess et al., 1985; Kulm et al., 1986; Boulègue et al., 1987b; Dron et al., 1987; Le Pichon et al., 1987; Tarney et al., 1991; Moore and Vrolijk, 1992).

In the Paita area (Fig.1), the fluid samples were collected in the SS and the MSS as well as along the USS. The largest vent site at present known on active margins, in term of the density of the distribution of benthic organisms, was discovered in the area where MSS trend changes from EW to NS . This is assumed to be an indirect evidence of the intensity of the venting rate itself. In the Chiclayo canyon, fluid vents were sampled during two dives (Fig.1) located at respectively 15 and 25 km landward from the trench axis.

The fluids were collected with titanium syringes above the sediment interface, or in the sediment itself in the biological communities. Local reference bottom seawater samples were collected at different depths outside any evidence of venting and biological activity.

Origin of the fluids : geochemical and isotopic constraints

The determination of pH and alkalinity on the samples were done on board. Samples for shore-based analysis of major, trace-element and Sr isotope were filtered (Nuclepore 0.1 μm) and acidified with ultrapure nitric acid. Major and trace-element concentrations were determined either by FAA, ZCFAA, ICP or IC. More details on the analytical procedure could be found elsewhere (Aquilina et al. in prep.).

Sr isotopic compositions were determined by TIMS. The measured $^{87}Sr/^{86}Sr$ ratios were normalized to $^{86}Sr/^{88}Sr = 0.1194$, but have not been normalized to a

particular value for a standard. A mean value of 0.710259±26 for 25 repeated analyses of the NBS 987 standard and of 0.709192±13 for modern seawater (IAPSO) have been obtained over the course of the study. Errors aregiven at 95% confidence limit.

The main chemical parameters measured on these fluids reveal that, in all the fluid samples the pH is comparable to common seawater. The chloride content is slightly higher than that of IAPSO standard seawater (546 mM), and that of the local reference bottom seawater (546 mM). We observe values ranging from 551 and 567 mM for the fluids collected on the Paita zone, and from 558 and 560 mM for Chiclayo canyon fluids. Clay membrane filtration and subsequent formation of saline fluids may explain such elevation of the chloride content as previously suggested for pore fluids recovered by deep sea drilling in the Peru margin (Suess et al., 1988; Kastner et al.1991). The sulfate content measured in thesesamples from Paita and Chiclayo (26.90 to 28.40 mM) does not reveal any significant variation from the reference water (28.23 mM).

Alkalinity values plotted against the total dissolved carbonate (Fig.2) clearly shows that all these fluids are located above the expected range for deep Pacific Ocean water (Broecker and Peng, 1982). Thus, suggesting an evolution compatible with carbonate dissolution and degradation of organic matter. Therefore, in order to decouple the original signatures of the fluid, we need tracers not affected by diagenesis. Furthermore, we have to find tracers whose contents are not modified by the passage through the biological communities; i.e. chemical parameters which are not affected by the metabolism of the dense benthic colonies of clams.

The alkali metals (Li, K and Rb), the alkaline earth metals (Mg, Ca and Sr) display variations within the range of common bottom seawater. Co, Pb, Cd, Cu and Mo concentrations do not show any variation relative to reference water of IAPSO.The concentration of these elements may have been shown to be affected by the metabolism of the clams, in the Japan accretionary margin (Boulègue et al., 1987b).

Barium is the only trace-element that shows significant variations in the two sampled sites, as shown on Figure 3. If the enrichment in water is real and does not reflect the effects of the metabolism of the biological communities, it could be related to advection of deep water enriched in Ba relative to the seawater content. It is therefore unfortunately that major and trace element appear to be inadequate to characterize the fluid sources in this context .

The Sr isotope analysis done on the fluids from paita and Chiclayo show values higher or at least equivalent to common bottom seawater (0.709192±13; this study and Dia et al., 1992b). These radiogenic values are as high as 0.709323±19 (Fig.4) (Dia et

al.; 1992a, Aquilina et al., in prep.). To explain such elevation of the Sr isotopic ratios relative to seawater, we need either the influence of a fluid characterized by more radiogenic signature (continental), which can result from reaction between seawater with the underlying continental crust or with radiogenic clastic sediments. Hence, the major result which stems from this set of data, is that even when the seawater isotopic composition is strongly recorded in these fluids, another component characterized by a "continental" signature must also be present. Indeed, it is obvious that because of the way of collecting the samples, the dilution by the ambient seawater is large, and thus the isotopic signature of this advected end-member is not strongly marked, even it is significant with respect to the analytical error bars. The question is then to identify this non local component.

The low (as compared to seawater) Sr isotopic ratios measured in sediments collected at venting sites clearly rules out the hypothesis of interaction between sediments and seawater to explain the origin of these fluids. But, the high Sr isotopic ratios measured in the massive barite deposits (0.710152±10 to 0.711118±12; Aquilina et al., 1992; Aquilina et al., in prep.), occurring in the vicinity of the venting, reveal a radiogenic component for the fluid responsible of the deposition of such barites. Therefore, these fluids were mostly continental and thus, the fluids collected during the Nautiperc cruise are at least in a part continent related. They could either come directly from continental aquifers through a complex plumbering, or be due to underplating of continental material removed continent-ward by subduction erosion.

Methane and fluid venting rates

A benthic chamber previously described by Carson et al. (1990) and Linke et al. (1992) and used at the Cascadia convergence zone off NW America was deployed during Dive 35 on the Upper Slope Scarp (USS). Briefly, the benthic chamber is an open-bottomed barrel with an exhaust port at the top. It is placed over an active vent, and sequentially activated bottles inside are tripped to obtain water samples for determining time-dependent chemical changes caused by fluid venting.

Conceptually, the effluent from a vent gradually displaces the ambient bottom water inside the chamber and with time a mixture develops with increasing amounts of vent fluid. This causes a gradual change in concentration of certain tracers, i.e. dissolved methane or helium, from which mass flux rates, or if the composition of the source water is known, fluid venting rates can be calculated. In addition, the temperature is monitored inside the chamber for the duration of the deployment (Fig.5).

The topography at the selected vent site along the USS was rough and steep, making the deployment so difficult that the device needed to be held in place by the submersible for about two hours. The data collected during the successful deployment are shown in Table 2.

Two highly significant chemical signals of venting were observed: a relatively high flux of methane from the seafloor and a peculiarly ^{13}C-depleted ΣCO_2 input. The methane flux calculated from the change in concentration amounts to 5 mmol m^{-2} day^{1}. This is in good agreement with rates previously observed along the Cascadia subduction zone (Carson et al., 1990; Linke et al., 1992), whose associated water flow rate was on the order of 200L m^{-2} day^{-1}. These are minimum rates since CH_4 oxidation inside the chamber during the deployment is not taken into consideration.

Most extraordinary is the enrichment in ^{12}C in the dissolved ΣCO_2 of the vent effluent (Table 2). Although the data do not document a time dependent change in carbon isotope composition, the values of -10‰ PDB can only be explained by a significant input of methane-derived carbon (Suess and Whiticar, 1989). At this time, it is unclear whether the CH_4 oxidation, from which the $^{12}CO_2$ originates, takes place at the sediment interface, i.e. by the dense chemosynthetic community at the vent site, or that the ^{12}C -enriched ΣCO_2 is actually expelled from greater depth; both mechanisms are possible. In any case, the data from the first successful deployment of the benthic barrel along the Peru convergent margin confirms the predominance of methane and methane-derived carbon as a criteria for mass flux from convergent margins. Furthermore, the temperature recorded during the deployment (Fig.5) clearly identifies the vents on the USS off Paita as "cold seeps".

Summary and conclusions

Major and trace-element analysis coupled with Sr isotope measurements on samples of venting fluids and associated barite deposits (recovered for the first time off Peru), allows to characterize the origin of fluids. The sample analysis reveal 1) most trace element contents do not show changes relative to seawater composition, 2) a Ba enrichment of fluids was nevertheless observed at all sites, and 3) a Sr isotope ratio of the fluids and barite deposits indicating that the fluids responsible for the barite deposition were mostly continental. We conclude that the Ba enrichment of fluid collected during the Nautiperc cruise can be related to advection of non local deep water enriched in Ba relative to the seawater composition. The fluids of the northern continental margin off Peru are at least in a part continent related.

Finally, the first successful deployment of a benthic barrel along the Peru convergent margin allowed the calculation of methane fluxes and fluid venting rates in this geodynamical setting.

Acknowledgments

The Nautiperc cruise supported by IFREMER, INSU-CNRS and GEOMAR would not be possible without the help of the crew of the R/V Nadir, the Peruvian Navy and the French embassies in Lima and Quito. Part of the analytical work was done by Dr A.-M.De Kersabiec, F.Vidot, D.Dubarry and Y.Meinnel. Pr C.J.Allègre is thanked for allowing A.N.Dia to access to mass spectrometry facilities.

References

Aquilina, L., Dia, A.N., Boulègue, J, Fouillac, A.-M., Suess, E., Von Breymann, M. and Bourgois J., 1992, Geochemistry of barite and carbonate deposits associated with fluid vents in the Peru convergent margin off Paita: EOS, vol 73, N°14, 153.

Aquilina, L., Dia, A.N., Cros, P., Boulègue, J. and Fouillac A.-M., in prep., Geochemistry of fluid and solid samples from the convergent margin off Peru: implications for fluid circulation within subduction zones.

Bangs, N., Westbrook, G.K., Ladd, J.W. and Buhl, P., 1990, Seismic velocities from thre Barbados Ridge Complex: indicators of high pore fluid pressure in an accretionary complex: J.Geophys.Res. 95, 8767-8782.

Boulègue, J., Iiyama, J.T., Charlou, J.-L. and Jedwab, J., 1987a: Nankai Trough, Japan Trench and Kuril Trench: Geochemistry of fluids sampled by submersible "Nautile": Earth Planet.Sci.Lett. 83, 363-375.

Boulègue, J., Bénédetti, E.L., Dron, D., Mariotti, A. and Létolle, R., 1987b, Geochemical and biogeochemical observations on the biological communities associated with fluid venting in the Nankai Trough and Japan Trench subduction zones: Earth Planet.Sci.Lett. 83, 343-355.

Bourgois, J., Pautot, G., Bandy, W., Boinet,T., Chotin, P., Huchon, P., Mercier de Lépinay, B., Monge, F., Monlau, J., Pelletier, B., Sosson, M and Von Huene, R., 1988, Seabeam and seismic reflection imaging of the tectonic regime of the Andean continental margin off Peru (4S to 7S): Earth Planet.Sci.Lett. 87, 116-126.

Bourgois, J. , Lagabrielle, Y., DeWever, P., Suess, E. and the Nautiperc cruise shipboard scientists, 1992a, Tectonic history of a non accreting active margin during the past 400 ka. Results of a submersible survey of the Peru Trench at 5-6°: submitted to Geology.

Bourgois, J., Michaud, F., Von Breymann, M., Suess and the Nautiperc cruise shipboard scientists, 1992b, Northern Peru convergent margin: massive slides from the upper plate into the trench axis observed from a submersible: EOS, vol 73, N° 14, 152.

Bray, C.J. and Karig, E.D., 1985, Porosity of sediments in accretionary prisms and some implications for dewatering processes: J.Geophys.Res. 90, 768-778.

Broecker, W.S. and Peng, T.H., 1982, Tracers in the sea: Eldigio Press, N.Y., 690 pp.

Brown, K. and Westbrook, G.K., 1988, Mud diapirism and subcretion in the Barbados ridge accretionary complex: the role of fluids in accretionary processes: Tectonics, 7, 613-640.

Carson, B., Suess, E. and Strasser, J.C., 1990, Fluid flow and mass flux determinations at vent sites on the Cascadia margin accretionary prism: J.Geophys.Res. 95, 8891-8897.

Claypool, G.E., Vuletich, A.K. and Kvenvolden, K.A., 1986, Isotopic composition of interstitial fluids in sediment of the Nankai Trough: Init.Rep.DSDP 87, 857-860, Washington D.C.

Davis, E., Hyndman, R.D. and Villinger, H, 1990, Rates of fluid expulsion across the Cascadia accretionary prism: constraints from new heat flow and multichannel seismic reflection data: J.Geophys.Res.95, 8869-8889.

DeMets, C., Gordon, R.G., Argus, D.F. and Stein, S., 1990, Current plate motions: Geophysic. J. Int., 101, 425-478.

Dia, A.N., Aquilina, L., Boulègue, J., Suess, E., Von Breymann, M. and Bourgois, J., 1992a, Fluids from the Peru subduction vents: Trace element and isotopic constraints, EOS: vol 73, N° 14, 153.

Dia, A.N., Cohen, A.S., O'Nions, R.K. and Shackleton, N.J., 1992b, Seawater Sr isotope variation over the past 300 kyr and influence of global climate cycles: Nature 356, 386-388.

Dron, D., Boulègue, J., Taira, A. and Rangin, C., 1987, Geochemisrty of the Teryu Canyon deep-sea fan biological community (Kaiko): Earth Planet.Sci.Lett. 83, 356-362.

Elderfield, H., Kastner, M. and Martin, J.B., Compositions of sources of fluids in sediments of the Peru subduction zone:J .Geophys.Res. 95, N°B6, 8819-8827.

Foucher, J.P., Le Pichon, X., Lallemant, S., Hobart, M.A., Henry, P., Bénédetti, M., Westbrook, G.K. and Langseth, M.G., 1990, Heat flow, tectonics and fluid circulation at the toe of the Barbados accretrionary prism: J.Geophys.Res. 95, 8851-8897.

Kastner, M., Elderfield, H., Martin, J.B., Suess, E., Kvenvolden, K.A. and Garrison, R.E., 1990, Diagenesis and interstitial water chemistry at the Peruvian continental margin-major constituents and strontium isotopes: Proc.DSDP, Sci. Res., vol. 1123, 413-440.

Kastner, M., Elderfield, H. and Martin, J.B., 1991, Fluids in convergent margins: what do we know about their composition, origin, role in diagenesis and importance for chemical fluxes?: Philos.Trans.R.Soc.London, Ser.A, 335, 275-288.

Kulm, L.D. et al., 1986, Oregon subduction zone:venting, fauna and carbonates:Science 231, 561-566.

Le Pichon, X. et al., 1987, Nankai Trough and Zenisu Ridge: deep-sea submersible survey, Earth Planet.Sci.Lett. 83, 285-299.

Le Pichon , X., Foucher, J.P., Henry, P., Lallemant, S., Bénédetti, M., Avedik, F. and Marriotti 1990a, Mud volcano field seaward of the Barbados accretionary complex: a submersible survey: J.Geophys.Res. 95, 8931-8943.

Le Pichon, X., Henry, P. and Lallemant , S., 1990b, Water flow in the Barbados accretionary complex: J.Geophys.Res. 95, 8945-8967.

Linke, P., Suess, E., Torres, M., Martens, V., Rugh, W.D., Ziebis, W., M., Carson, B. and Kulm, L.D., submitted (1992), Determination of flud flow from subduction zone vents: Deep Sea Res.

Peacock, S.M., 1990, Fluid processes in subduction zones: Science, 248,321-337.

Minster, J.B. and Jordan, T.H., 1978, Present-day plate motions: J.Geophys.Res., 92, 4798-4804.

Moore, J.C. and Vrolijk, P., 1992, Fluids in accretionary prisms: Reviews of Geophysics, 30, 2, 113-135.

Smith, D.E., Kolenkiewicz, R., Dunn, P.J., Robbins, J.W., Torrence, M.H., Klosko, S.M., Williamson, R.G., Pavlis, E.C., Douglas, N.B. and Fricke, S.K., 1990, Tectonic motion and deformation from the Satellite Laser Ranging to LAGEOS: J.Geophys.Res., 95, 2013-2041.

Sosson, M., Mercier de Lépinay, B., Bourgois, J., DeWever, P., Michaud, F., Barron, J., Fourtanier, E., 1992, Deep sea dives in the Chiclayo Canyon northern Peru: tectonic regime in the Andean convergent margin: EOS, vol 73, N°14, 152.

Suess, E., Carson, B., Ritger, S., Moore, J.C., Jones, M., Kulm, L.D. and Cochrane, G., 1985, Biological communities at vent sites along the subduction zones off Oregon: in The Hydrothermal Vents of eastern Pacific: An overview, edited by M.L. Jones.

Suess, E., Von Huene, R. and Leg 112 Shipboard Scientists, 1988, Ocean Drilling Program, leg 112, Peru continental margin: Part 2 sedimentary history and diagenesis in a coastal upwelling environment: Geology, 16, 939-943.

Suess, E. and Whiticar, M.J., 1989, Methane derived CO_2 in pore fluids expelled from the Oregon subduction complex: Paleogeogr., Paleoclimat., Paleoecolo., 71, 119-136.

Tarney, J., Pickering, K.T., Knipe, R.J. and Dewey, J.F., (eds), 1991, The behaviour and influence of fluid in subduction zones, Royal Society London, pp192.

Von Huene, R., Bourgois, J., Miller, J. and Pautot, G., 1989, A large tsunamogenic landslide and debris flow along the Peru Trench: J.Geophys.Res. 94, 1703-1714.

Vrolijk et al., 1990, Stable isotope ratios of interstitial fluids from the northern Barbados accretionary prism: Proc.ODP Sci.Res., vol 110B, 181-205, College Station, TX.

Figure captions

Fig.1 General map of the dives performed during the Nautiperc cruise. The arrow shows the convergence direction of the subducting Nazca Plate relative to the South America Plate (convergence rate above the arrow are from Minster and Jordan, 1978; DeMets et al., 1990 and Smith et al., 1990). ABM = Amotope-Bayovar Massif, USS = Upper Slope Scarp, MSS = Middle Slope Scarp and SS = Subduction Scarp.

Fig.2 Alkalinity (in mM) is plotted in this diagram against the total dissolved carbonate content (in mM). The open circles are representing Paita area samples and full circles the Chiclayo canyon area samples. Local reference values are shown by arrows. The pattern area is representing the domain delineated by samples from common Pacific bottom waters (Broecker and Peng, 1982).

Fig.3 $^{87}Sr/^{86}Sr$ isotopic ratios are plotted (with their respective error bars at 95% confidence limit) against the depth (in meters) in this diagram as for fluids from the Paita area (open circles), as well as for fluids from the Chiclayo Canyon (full circles). The local reference fluids are shown by arrows, and the IAPSO value is plotted on the y axis with its associated error bar (2σ).

Fig.4 Ba content expressed in nM is plotted versus depth (in meters). Open circles are representing fluids from Paita and full circles fluids from Chiclayo canyon. The local reference samples are shown by black arrows.

Fig. 5 Temperature record obtained during deployment of the benthic barrel during Dive 35 on the Upper Slope Scarp off Paita, which clearly shows ambient bottom water temperature.

Table captions

Table 1 Location, fluid samples and associated alkalinity and total dissolved carbonate content expressed both in mM, are plotted in Table 1, as well as the depth (in meters), the $^{87}Sr/^{86}Sr$ isotopic ratios and their error bars at 95% confidence limit, and the Ba content (expressed in nM). More details on the analytical work could be found elsewhere (Aquilina et al., in prep.).

Table 2 Sulfate (mM), chloride (mM), alkalinity (meq/L), $\delta^{13}C$ and methane concentrations (nL/L) are reported during the barrel deployment (Dive 35) through time.

Location	Sample	Alkalinity (mM)	ΣCO_2 (mM)	Depth (m)	$^{87}Sr/^{86}Sr$	2σ	Ba (10^{-9}M)
Paita upper slope F1	NP 1-5	2.82	2.70	2582	0.709194	0.000016	27.67
	NP 1-17	2.56	2.37	2632	0.709206	0.000015	24.75
Paita middle slope F2A	NP 1-2	2.59	2.29	3347	0.709203	0.000010	27.67
	NP 1-3	2.62	2.44	4000	0.709161	0.000011	26.94
	NP1-4	2.56	2.38	3554	0.709323	0.000019	25.48
	NP 2-32b	2.70	2.32	3534	0.709268	0.000009	136.16
	NP 2-32r	2.75	2.50	3549	0.709189	0.000009	86.64
Paita middle slope F2B	NP 1-13	2.75	2.40	3006	0.709284	0.000010	52.42
Paita lower slope	NP 1-8-1	2.65	2.40	5187	0.709280	0.000016	26.21
	NP 1-9	2.52	2.20	5040	0.709211	0.000012	22.57
	NP 1-11	2.62	2.22	5131	0.709274	0.000018	32.77
	NP 1-8-2	3.25	2.92	4950	0.709272	0.000018	——
	NP 1-12	2.80	2.61	4842	0.709255	0.000012	29.85
Chiclayo	NP 2-33	2.82	2.50	3711	0.709191	0.000010	122.32
	NP 2-34	2.62	2.32	4174	0.709268	0.000013	73.54
	Std IAPSO	——	——	——	0.709192	0.000013	——

Nautiperc

Table 1

NP2-35 barrel data

Time min.	SO4 mmol/L	Cl mmol/L	Alk. meq/L	∂13CΣCO2‰	CH4 nL/L	Sample I.D.
0	27.81	546.4	2.40	-9.8	142	NP.35-Nisk
22	27.12	542.0	2.55	-10.9	2084	NP.35-1336
57	27.33	541.0	2.55	-10.7		NP.35-1335
82	26.68	542.1	2.60		8046	NP.35-1340
107	25.69	541.6	2.74	-10.6		NP.35-1339

Table 2

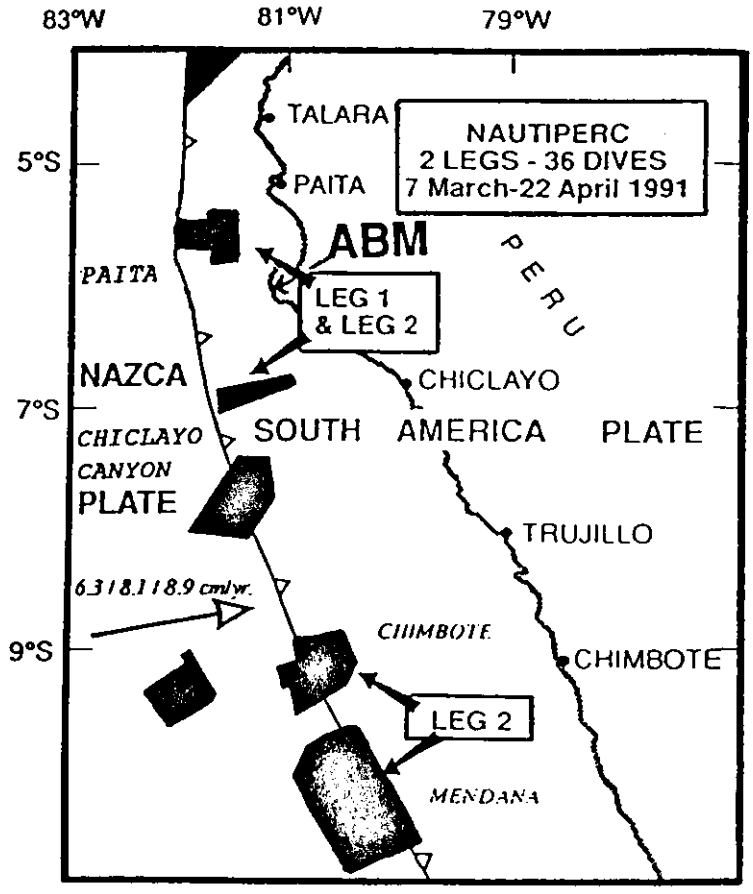
83°W
81°W
79°W
5°S
7°S
9°S
TALARA
PAITA
NAUTIPERC
2 LEGS - 36 DIVES
7 March-22 April 1991
ABM
PAITA
LEG 1
& LEG 2
PERU
NAZCA
CHICLAYO
CHICLAYO
CANYON
PLATE
SOUTH AMERICA PLATE
TRUJILLO
6.3 18.1 18.9 cm/yr.
CHIMBOTE
CHIMBOTE
LEG 2
MENDANA

Fig.1

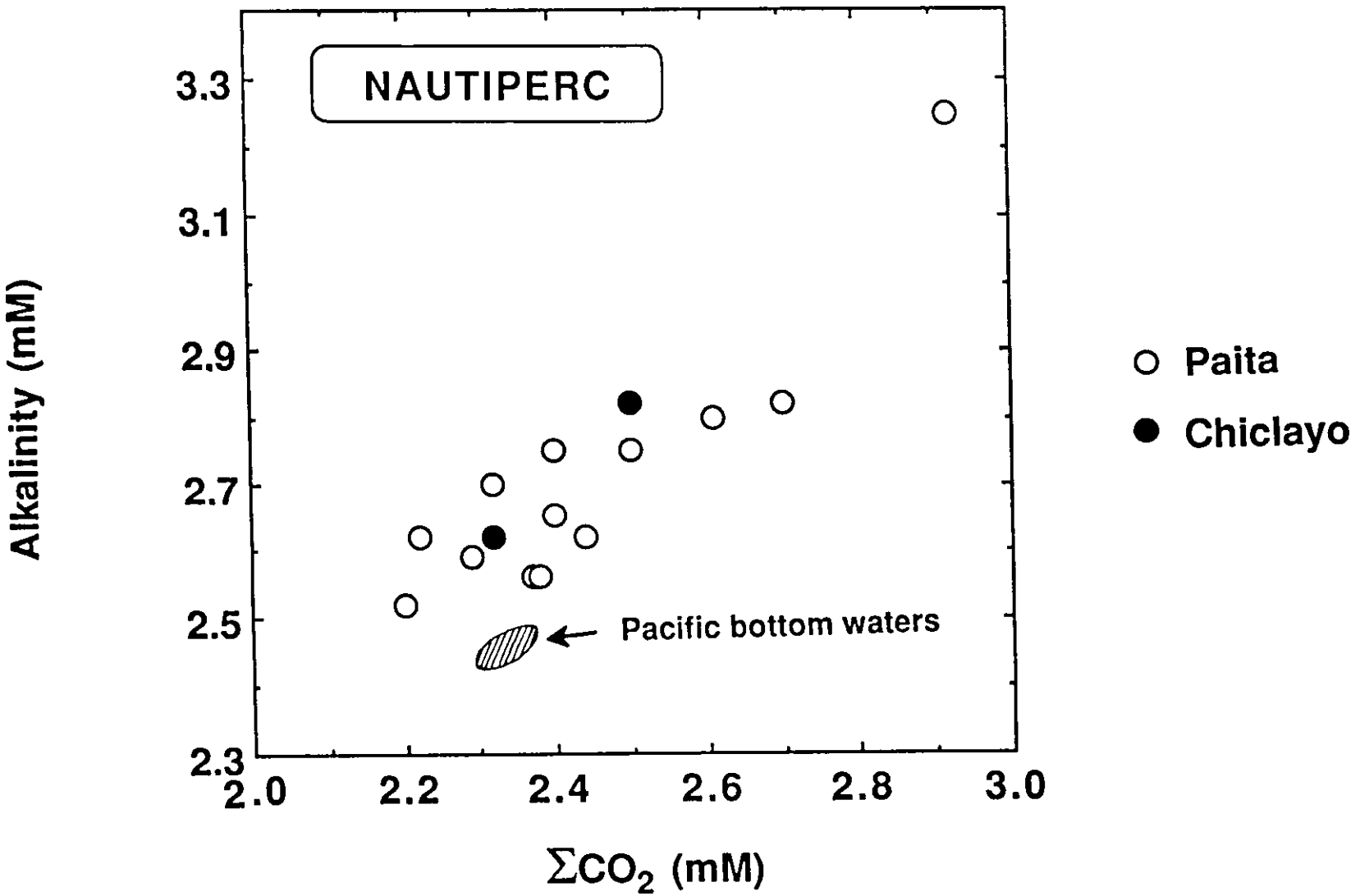
NAUTIPERC
Alkalinity (mM)
3.3
3.1
2.9
2.7
2.5
2.3
2.0
2.2
2.4
2.6
2.8
3.0
ΣCO2 (mM)
Pacific bottom waters
Paita
Chiclayo

Fig.2

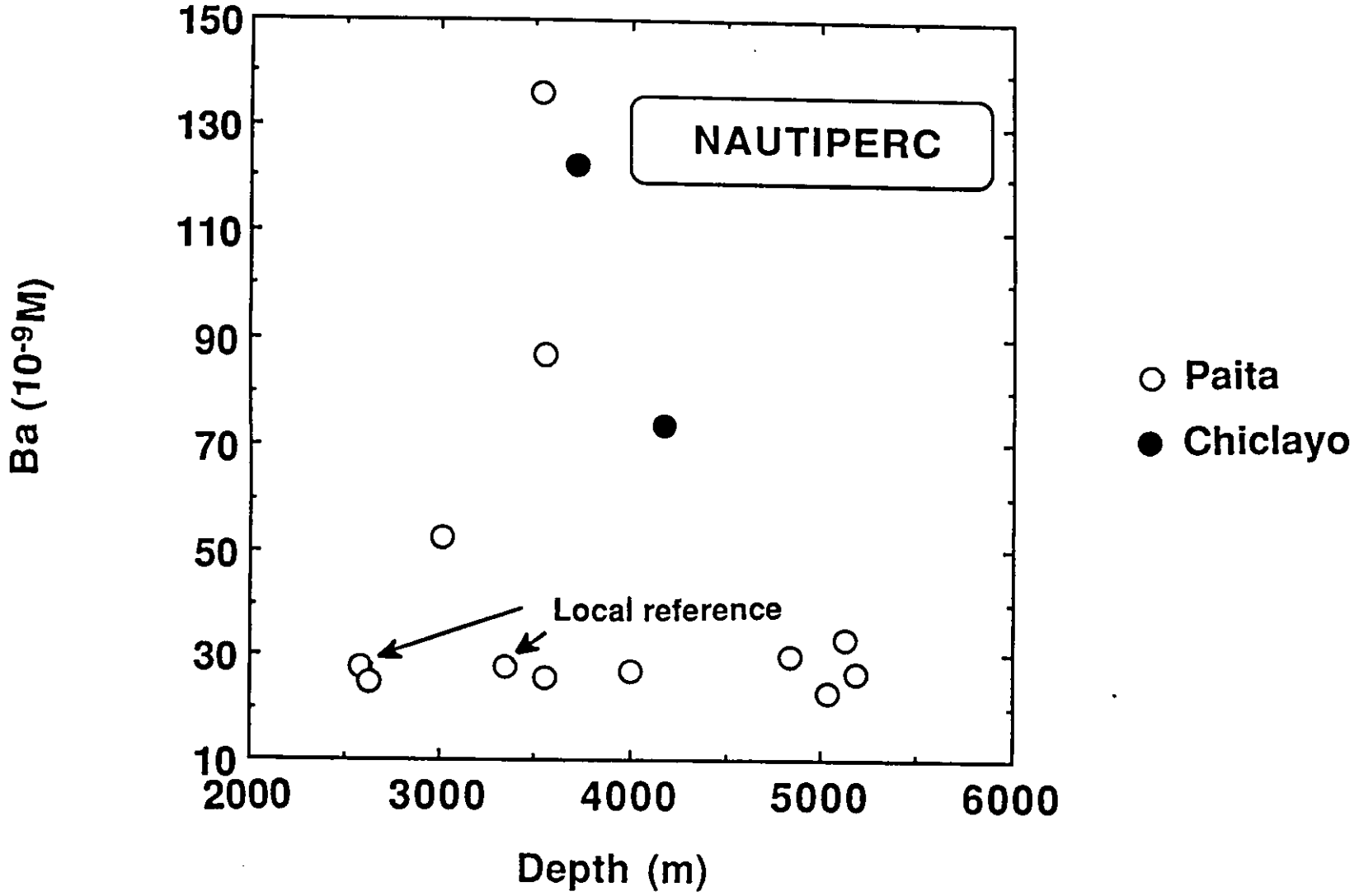
NAUTIPERC
Local reference
Ba (10^{-9}M)
Depth (m)
150
130
110
90
70
50
30
10
2000
3000
4000
5000
6000
Paita
Chiclayo

Fig.3

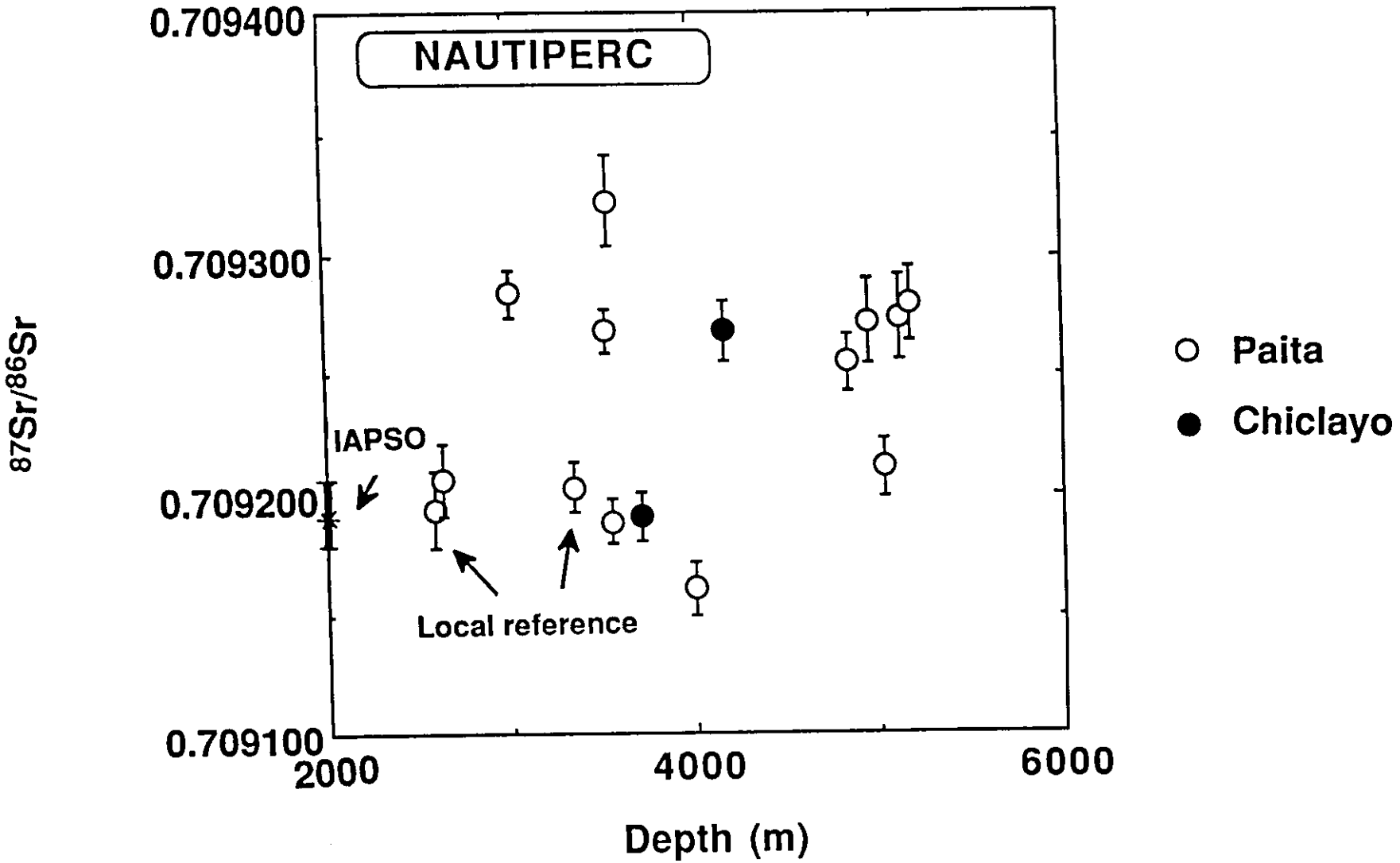
NAUTIPERC
0.709400
0.709300
0.709200
0.709100
$^{87}Sr/^{86}Sr$
IAPSO
Local reference
2000
4000
6000
Depth (m)
Paita
Chiclayo

Fig.4

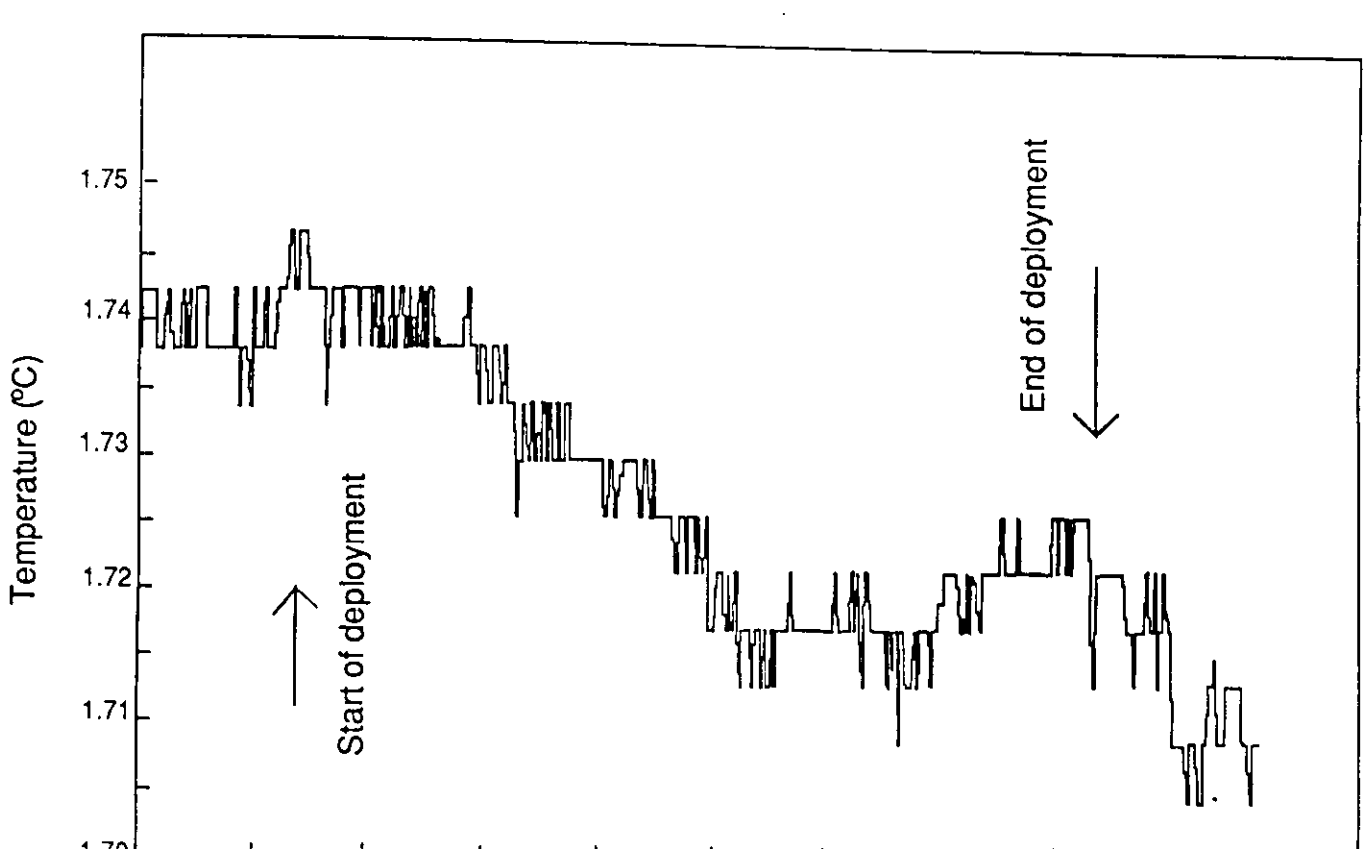
Temperature (°C)
1.75
1.74
1.73
1.72
1.71
1.70
Start of deployment
End of deployment
12:55:26
13:25:26
13:55:26
14:25:26
14:55:26
Local time

Fig.5

Expulsion of shallow gas in the Skagerrak - evidence from sub-bottom profiling, seismic, hydroacoustical and geochemical data

P. Hempel[1], V. Spieß[2], and R. Schreiber[3]

[1] GEOMAR, Wischhofstraße 1-3, 2300 Kiel 14

[2] Fachbereich Geowissenschaften, Universität Bremen, Bibliothekstr., 2800 Bremen 33

[3] Atlas Elektronik GmbH, P. O. Box 448545, 2800 Bremen

submitted to Estuarine, Coastal and Shelf Sciences

ABSTRACT

A combined high resolution seismic, subbottom profiling, and multibeam echo-sounding survey in the Skagerrak (Danish sector of the Nroth Sea) together with gas analyses at a station along the profile exhibit the expulsion of gas (mainly methane) from and the presence of gas-charged sediments at shallow depth. The echo-soundings yield detailed insight in the distribution and shape of typical sea floor features associated with gas seepage, such as pockmarks. The pockmarks reach dimensions of 800 in length, 300 m in width, and 15 m in depth, with the long axis running parallel to the slope of the Norwegian Trench. Processing of the multi-channel high resolution seismic data and the digitally recorded subbottom profiler signals indicate an internal compressional velocity of about 1050 m/s within the gas-charged sediments reaching from the sea-floor to a subbottom depth of about 23 m. Using the lateral distribution and thickness of the gas-charged sediments in conjunction with a mean concentration of gas of 3,000 ppb, the present amount of trapped gas is estimated to be 6.45 $x\ 10^{11}$ g CH_4. The flux of methane through the seabed into the water column appears to be 7.2 x 10^{10} g CH_4 per year. To explain the small difference in size between the methane pool in near surface sediments and the annual flux through the seabed a constantly high supply of methane from leaking hydrocarbon reservoirs at greater depths has to be active.

INTRODUCTION

The seepage of gas and fluids through the sea-floor is a worldwide phenomenon, known from mid-ocean ridges, convergent margins and at shelf seas of passive margins. In the last two cases one observes cold seeps resulting mainly from vertical or lateral sediment compaction. Fluid expulsion from the sea-floor occurs along fracture planes and at stratigraphic horizons or is associated with diapirism. Areas of recent intense investigations are the Gulf of Mexico (Brooks et al., 1986; Brooks et al., 1987; Anderson and Bryant, 1990; Kennicutt II, 1990; Neurauter and Bryant, 1990) the Florida Escarpment (Paull et al., 1984; Paull et al., 1985), the Laurentian Fan in the NW-Atlantic (Mayer et al., 1988), the Cascadia continental margin off Oregon (Carson et al., 1990), the Nankai Trough off Japan (LePichon et al., 1987; Okada and Cadet (eds.), 1989) and the North Sea area (LePichon, 1987; Hovland and Judd, 1988; Hovland and Thomsen, 1989; Hovland, 1990; Dando et al., 1991). Most of these investigations are based on direct observations from deep-diving submersibles or remotely operated vehicles. Further evidence of enhanced fluid and gas flow within sedimentary complexes were provided by Ocean Drilling at collision zones e.g. (Moore, Mascle et al., 1988; Suess, Huene, et al., 1987; Hill, Taira et al., 1991).

Unless the expulsion of gas through the seabed is indicated by rising bubbles in shallow waters, most convincingly shown for the methane escape off Paramushir Island in the Sea of Okhotsk (Zonenshayn et al., 1987), seep locations at the sea-floor are characterized by a specific community of benthic organisms and mostly by carbonate precipitations of shapes and forms, like chimneys and carbonate crusts. These manifestations range in diameter from a couple of decimeters to several meters. Bathymetric evidence for fluid expulsion at shallow water depth are local crater-like depressions at the sea-bed, so-called pockmarks. Pockmarks are local depressions which are formed in soft, fine-grained sea-floor sediments, (King and MacLean 1970) and are reported from the North Sea area of normally to be 10-300 m in diameter and perhaps up to 15 m deep (McQuillin and Fannin, 1979; Hovland, 1981; Hovland and Judd, 1988). The underlying gas-charged sediment-body is often characterized on shallow seismic profiles and sub-bottom profiler records as an acoustically turbid or

transparent zone. Several studies have focussed on the distribution of pockmarks (Hovland and Judd, 1988; and references therein) and the associated gas-fields, by using techniques such as the echo-sounder, side scan sonar and shallow seismics using various sound sources. Up to now, anomalous zones indicating gas have only been described on analogue seismic records. With the availability of modern wide angle multi-beam echo-sounders and sub-bottom profilers delivering digital data with high vertical and lateral resolution, new insights into gas seepage are possible. So far, digital sub-bottom profiler data have only been used for paleoceanographic studies, focussing on the correlation of high frequency sedimentological and physical properties of near surface sediments with seismic data (Mayer, 1979; Rostek et al., 1991; LeBlanc, 1992).

Gases (mainly methane?) stored in and expelled from near-surface sediments originate either from leaking hydrocarbon reservoirs at greater depth (Baker, 1990; Max et al., 1992) or is produces in rapidly accumulating organic-rich sediments at shallow depth below the sea-floor. Both sources have distinctly different stable carbon-isotopic signatures (Schoell, 1980; Whiticar et al., 1985). Since methane, per mole, has a global warming potential 3.7 times that of carbon dioxide (Lashof and Ahuja, 1990), it is one of the most important greenhouse gases in the atmosphere. Methane contained in and seeping from shallow marine sediments represents a vast, but largely uncharted source which is of environmental importance. Gas in the seabed at shallow depth is also of economic interest in the case of offshore constructions because it affects the stability of the subsurface. On the other hand it is an indicator of potential gas reservoirs as well if the gas has the "proper" carbon isotopic signature indicative of thermogenic sources.

The aim of this study is to survey and evaluate the order of magnitude of the natural discharge of methane in the Skagerrak by applying a combined geochemical, hydro-acoustical, and seismic effort. We present the seismic evidence for the presence of gas by processing high resolution multi-channel seismic data, with specific attention on the distribution of seismic velocities in the near-surface sediments. This technique allows a first order estimate on the thickness of the gas-charged sediments. However, the vertical resolution of the seismic data prevents the identification of the sub-surface depth of the surface

of the gas-charged sediments. This drawback will be overcome by simultaneous sub-bottom profiler records along the same trackline, which yield the necessary information to image the lower surface of the gas-charged zone. These registrations were stored digitally and allow us to focus specifically on the processing capabilities of digital sub-bottom profiler data, which give a detailed picture of the acoustic response of the gas-charged sediments. All of the indirect evidence for the presence of gas in near-surface sediments is supported by the analysis of methane in the sediments recovered at a station along the seismic line.

Regional setting and depositional environment

The study area is situated in the southern part of the Skagerrak, a semi-enclosed basin in the Danish sector of the northeastern North Sea, bordered to the north and east by the coastlines of Norway and Sweden and in the south by the shoals of northern Denmark (Fig. 1). Its bathymetry is characterized by the Norwegian Channel, a 700 deep trench that curves around southern Norway and eventually exits into the Northern Atlantic at the continental margin.

The Norwegian Channel separates the crystalline basement of the Scandinavian Shield to the north from the Norwegian-Danish Basin, as part of the Northwest European sediment basin (Sellevoll and Aalstad, 1971) to the south. In the southwestern Skagerrak Mesozoic strata with hydrocarbon potential reach a thickness of about 5 km above the basement (Weigel et al., 1970). At the southern slope of the Norwegian Channel the Mesozoic strata are covered by only a thin blancket of Quaternary deposits.

Erosional processes associated with the Pleistocene glaciations had the greatest impact on the modern topography of the Skagerrak. Melting of the ice caps and oscillations of the ice front during interglacial periods lead to the generation of moraines and the deposition of fine grained sediments, partly rich in organic carbon. Degradation of these carbon-rich sediments could be a source for biogenic methane formation.

Distribution of gassy sediments

Great attention has been spent in recent years on the presence of gassy sediments in the Skagerrak, indicated by acoustically turbid zones in sub-bottom profiler records (Van Weering et al., 1973; Van Weering, 1982; Hovland, 1991). Based on the numerous records the distribution of gas-charged sediments has been mapped with some accurracy, showing a widespread occurrence at the southwestern slope and along the eastern part of the Skagerrak (Fig. 1). This shallow gas-field could be connected with the gas occurrences of northern Denmark and the Kattegat, where active seepage and carbonate cementation are currently being studied (Jørgensen et al., 1990; Jørgensen, 1992; Jensen et al., 1991 (subm.)). There is also evidence for the occurrence of gas-charged sediments north of the Norwegian Channel on a submarine plateau off Arendal (Hempel, 1985).

Stable carbon isotopic analyses on gases in surface sediments in the vicinity of seep locations and on exposed carbonate cements in the Skagerrak and Kattegat area indicate that the methane is of primarily biogenic origin (Jørgensen, 1992; Schmaljohann et al., 1990). However, the sediments also contain methane and heavier hydrocarbons of a thermogenic origin (Schmaljohann et al., 1990). Distinctive carbon 13/12 ratios indicate that the authigenic carbonates originate from an extremely ^{13}C depleted reservoir, which is commonly associated with oxidation products of methane (Rosenfeld and Silvermann, 1959), like authigenic carbonate precipitations. Methane oxidation is believed to take place either in the anoxic environment by sulphate-reducing bacteria or in the oxic environment through the activities of aerobic methane-oxidizing bacteria (Jørgensen, 1992). These bacteria form the nutrient supply for invertebrates often found at seep locations (Schmaljohann and Flügel, 1987; Schmaljohann et al., 1990), establishing a locally restricted endosymbiontic ecosystem. The seeping gas of the Jutland-Kattegat field is composed of 85-90% methane, 10-15% CO_2 and 0.1-1% H_2S (Fenchel, 1989). Most recent gas analyses by Laier et al. (in press) reveal gas compositions of 98-99% methane in the same area. In the following calculations of gas content in the sediments and seepage through the seabed the gas has been considered to be purely methane.

Methods

Echosounding and subbottom profiling

A transit cruise of RV *Polarstern* in 1990 from Bremerhaven to Oslo was used for echo-sounding and sub-bottom profiling along a reflection seismic line shot by RV *Gauss* in 1981 in the Skagerrak. The profile extends from 57° 42.11'N - 08° 33.51'E in the southwest to 58° 00.12'N - 09° 43.41'E in the northeast, a distance of about 60 km (Fig.1). The profile runs parallel to the slope of the Norwegian Trench in a water depth of 220-250 m.

RV *Polarstern* is equipped with a modern multibeam echosounding system (HYDROSWEEP) and a built in sub-bottom profiler (PARASOUND) by Atlas Elektronik (Bremen, F.R.G.). HYDROSWEEP is designed for efficient hydrographic surveying in shallow and deep water, with the special feature of a large sea-floor coverage of 2 x 45°. The resulting swath width on the seabed is equal to twice the water depth underneath the ship. A generated frequency of 15.5 kHz provides good signal quality even at larger angles and allows precise depth determination of ± 1 % of the water depth (Schreiber and Schenke, 1990), resulting in a detailled image of the topography and the pockmarks in particular, with about 2 m vertical resolution. This is achieved because the signal is reflected from the true bottom rather than penetrating the surface sediments. The system is fully compensated for heave, roll and pitch motions of the vessel (Grant and Schreiber, 1990).

Sub-bottom profiling with the PARASOUND sub-bottom profiler was conducted parallel to the echo-sounding survey. The PARASOUND technique offers the possibility to achieve very high vertical and lateral resolution, facilitating the detection of fine-layers of sediment, while giving good penetration from a hull-mounted transducer (Grant and Schreiber, 1990). PARASOUND emittes two sonic frequencies, a constant primary frequency of 18 kHz and a secondary variable frequency of 20.5 to 23.5 kHz. The superposition of these two frequencies results in the so-called nonlinear parametric effect, leading to energy emission in the band of the difference in frequencies, i.e. to energy emission between 2.5 and 5.5 kHz (Rostek et al., 1991). The emitted sounding cone has an angle of only 4°, which reduces the area of reflecting bottom surface considerably, compared to

conventional sub-bottom profiling systems. In areas of rough topography, with slope inclinations of more than 4°, no signals can be registered by the shipboard receivers, caused by the generated narrow beam. This effect has been observed at the slopes of some pockmarks.

The main advantage of PARASOUND to this study here, is the possible access to seismogram data via an interface for digital data aquisition. These data are stored on industry standard magnetic tapes, and offer the possibilty for seismic processing steps, known for single channel seismic data.

The PARASOUND data recording system on board RV *Polarstern* consists of a modular data aquisition unit, equipped with a high speed digital voltmeter. A 80386/87 microcomputer is used as the central processing unit, with a 100 Megabyte disc and a color monitor, which also executes storage and graphic display tasks. The PARASOUND-signals were set to be 4 kHz by using 4 sinusoid oscillations and sampled at a frequency of 40 kHz, with a registration length of 133 ms, which represents a penetration of about 100 m into the sediment. A more detailed description of the system is given by Spieß (in prep.). Shore-based processing of the PARASOUND-data included band-pass filtering, spectral analysis of the reflected amplitudes, and a variety of graphical displays. These processing steps are standard processes of the GEOSYS-software package of GECO-PRAKLA (Hannover, F.R.G.). Prior to processing these data were converted to SEGY-format and resampled in time to a rate of 4 msec, instead of the original 0.025 msec, acceptable for GEOSYS. This resampling had no influence on the ratio of the sample rate to the number of samples and to the registered signal amplitudes.

Although the frequency of the generated signals were set at 4 kHz, we performed at selected traces spectral analysis of the amplitudes of the registered signals. This allowed the precise determination of the low- and high cut frequencies of the band-pass filter. All processes were performed on a Convex 3220 (10 MFLOP's, 256 MB, 10 GB disc space).

Plotting the digitally recorded PARASOUND-data at enlarged scales exhibits details on the succession of reflectors previously impossible to detect on analog records of conventional 3.5 kHz

subbottom profiling systems. It allows to trace certain reflections more easily over some distances and the carefull analysis of single seismograms. This carefull trace analysis enables to reveal the influence of gas on the seismic response.

Multi-channel seismic data

The high resolution reflection seismic profile was shot using an air gun with a chamber volumes of 1.6 ltr., at ambient pressure of 140 bar, and shot intervals of 8 seconds. A multi-channel streamer of GECO-Prakla, with a total length of 450 m, consisting of 8 active segments, each 50 m in length, allowed the registration of the returned signals with 10 seperately registrating channels. The streamer was towed at a ship's speed of 6 knots and predefined water depths of 3-5 m. The ratio of streamer length to mean water depth of 250 m along the surveyed profile fulfilled the requirements for common-depth-point-(CDP) stacking. The arrangement of the hydrophones within each channel led to a linear focussing of the reflected signals and an improvement of the signal to noise ratio. A NOVA 3 (Data General), 16 bit computer, was used on board as a central processing unit (CPU), in combination with a 12 bit analogue-digital-converter (Preston GMAD), amplifiers (Preston DX-AL), analogue filter for low and high cut (KEMO VBF/20), and a tape unit (Cipher 900) with densities of 800 bpi and 1600 bpi. Parallel to the digital recording a registration of the band pass filtered and amplified analogue signals of one channel were transferred to a line scan recorder. A more detailed description about the equipment and the registration procedure is given by (Schreiber, 1983). Frequencies of the band pass filter were set at 150 and 60 Hz for the low and high cut, respectively, since the dominant frequency of the reflected sea-floor signal was about 100 Hz.

Shore based processing of the seismic data included velocity analyses, since the distribution of compressional velocities are first order indications for the presence of gas in the sediments. The registrations fulfilled the requirements for standard CDP-velocity analyses, which were performed at selected parts of the seismic lines, where acoustically turbid zones are observed at the analogue record.

The precision of the calculated interval velocity within a discrete sediment layer depends on the accuracy of the stacking velocity and the determinations of the travel times at the layer boundaries. A precise determination of the stacking velocities was achieved using a coherency measurement (semblance) of the reflections in all traces belonging to one CMP gather. The technique searches along hyperbolic trajectories. The reflections that best fit these trajectories have a high semblance. Semblance analyses are, in general for the interpretation of air gun seismic registrations very useful, and in particular for the analysis of interval velocities of thin beds, because it considers only the amplitude of the first arrival of the signal. Hence, this method is not affected by the long signal consisting of several oscillations generated by bubble reveberations. Calculating the semblance coefficient is based on the algorithm of Taner and Koehler (1969). Errors of the interval velocity are proprotional to the ratio of the mean depth of the interval to its thickness.

Sediment degassing and methane analyses

Sediment samples were taken from a box-core and a giant kasten corer (KAL II; 57°46.4'N, 8°42.7'E, 245 m waterdepth) recovered from a position about 2 km off the seismic line (Fig.1). The samples were preserved in liquid nitrogen for later CH_4-determination. Prior to analysis, adsorbed and dissolved gases were separated from the sediment samples. This degassing was performed in a closed evacuated "blender" system, where the samples are heated under constant stirring and addition of phosphoric acid. The CO_2 released is removed by a saturated KOH-solution and the remaining gas is collected in a graduated part of the system from which aliquots can be taken through a septum. The system is decribed in detail

GC-analyzes

The gas aliquots were injected into a SHIMADZU 14A FID gas-chromatograph, equipped with a PORAPAK packed column and driven with N_2 stripping-gas. The precision of the CH_4-determination in sediment samples was ≥93%. The methane concentrations listed in table 2 are given in ppb of the total sediment wet-weight.

Results and Discussion

Characteristics of pockmarks

Pockmarks are visible both on the high resolution multi-channel seismic profile and on the combined HYDROSWEEP- and PARASOUND-profile. Both profiles are seperated by less than 5 km (Fig. 2). As indicated on figure 2, different pockmarks were recorded on both profiles, revealing a quite dense occurrence in this region along the southern slope of the Norwegian Trench. The number of pockmarks along the air gun profile increases laterally towards the east, whereas on the nearly parallel running PARASOUND-profile pockmark occurrences increase towards the west (Fig. 2).

The pockmarks along the surveyed profiles are up to 1 km in length and 300 m across, reaching depths of 20-25 m below the surrounding sea-floor (Fig. 3). These dimensions are in the same order as those reported by Hovland (1991) from the eastern Skagerrak. The precise depth informations given by HYDROSWEEP allows an imaging of the sea-floor with 2 m isobathes and thus enables a detailed architecture of the individual pockmarks. Mapping by means of multi-beam echo-sounding revealed their isolated occurrence and their elongated shape in southwest-northeasterly direction, parallel to the general strike direction of the Norwegian Trench. In the eastern Skagerrak, however, the elongation of the pockmarks appears to be in the northwest-to-southeast direction (Hovland, 1991), parallel to the slope of the Norwegian Trench in this part of the Skagerrak. HYDROSWEEP- and PARASOUND- records allow a three-dimensional image of the pockmarks, exhibiting a characteristic asymmetry in the steepness of their internal slopes. However, there is no generally favored side of the pockmarks where the steeper or the shallower slopes occur. The slope inclinations of some pockmarks are steeper than 4°, preventing the image of these slope surfaces on the PARASOUND-record, due to the narrow beam of the generated signals.

A characteristic feature of all pockmarks is a slightly elevated rim around them without any visible internal stratification, suggesting the deposition of the expelled sediments in the immediate vicinity

Two typical reflection patterns are associated with the pockmarks, generated by the expulsion of sediments and the subsequent collapse of the seabed, (1) subsurface-reflections either bend

downwards parallel to the sea-floor or (2) reflections wedge-out into the pockmark, at an angle almost perpendicular to the pockmark slope. These out-cropping horizons are of only minor extend, diminishing into the acoustically transparent zone. Down to 15 m beneath the base of the pockmarks there appear to be quite high amplitude reflections, extending laterally only a couple of tens of meters. They are real reflections from the subsurface and not a product of spherical focussing effects related to the synclinal topography of the sea-floor. Firstly, the footprint of the wavefront of the PARASOUND-signal on the sea-floor is only about 17 m in diameter (7% of 250 m waterdepth), which is neglegligable compared to the size of the pockmark slope. The focussed PARASOUND-beam effectively prevents most side echoes. Secondly, the reflectors are situated slightly off the center of the pockmark. The depth interval between the base of the pockmarks and these reflections is acoustically transparent.

Imaging of gas at shallow depth

Evidence from sub-bottom profiler records

In general the reflection patterns on the PARASOUND-record along the profile are fairly homogeneous. The penetration is restricted to about 8 to 10 m, which is remarkably low in unconsolidated, fine grained sediments. Internal reflectors within the reflecting uppermost 10 m of the sea-floor are incoherent, with a notable difference in the reflection pattern from west to east. At the western end of the profile the number of reflections are limited to about 2-3, occurring down to a depth of 2-3 m. Towards the east the number of reflectors increases to about 10, with unchanged penetration depth. The succession of reflectors indicate stratified sediments of some lateral extend. In most places the reflections run parallel to sub-parallel to the sea-floor. At minor depressions and ridge-like elevations, the internal cross-bedded stratification suggests enhanced lateral sediment transport (buried sand waves?) and erosional processes. In most of the downward section where the sediments reflect some energy, the reflection pattern is diffuse. This could be caused by the predominately fine-grained sediments, but could as well be the expression of randomly distributed upward migating gas-bubbles.

Below the reflecting sediment section follows an acoustically turbid zone, without any indications of internal reflectors. There is a gradual transition of diminishing reflections from the reflective section to the acoustically transparent section beneath. As mentioned earlier, deeper reflections are restricted to short segments beneath the base of the pockmarks. A close-up plot, shown in figure 7, illustrates the incoherent reflection pattern beneath the sea-floor down to a depth of 35 ms two-way traveltime (TWT). A gradual increase of the gas-content with depth successively reduces the acoustic impedance without generating a pronounced reflection with inverted phase.

On the analog record of the multi-channel seismic registrations, most of the near surface gas-charged sediments are masked by the relatively long signal of the air gun consisting of four reveberations and ghost reflections. Nevertheless, at various places incoherent reflections are visible above well stratified sediments. The area of incoherent and diffuse reflections extend from the east (left side of fig. 4) to about the center of the profile, where pockmark no. 4 occurs. Further westward, the number of pockmarks and the pronounced chaotic reflection patterns decrease considerably.

Although the analog record of the multichannel seismic profile gives only rather poor evidence about the presence of gas, it is suitable for the selection of those segments for which to perform detailed velocity analyses. For this purpose a segment has been choosen, situated between two pockmarks. The velocity analysis, following the procedure described by Schreiber (1983), involved the calculation of the semblance coefficients, which helped considerably to refine the stacking velocities and subsequently the determination of the interval velocity (V_{int}) between two reflectors as a reliable indicator for gassy sediments. Another advantage of semblance is that the subbottom depth of reflecting horizons can be determined with the greatest possible precision, because it actually takes the peak amplitude, which happens to be the first arrival. As a result from this precise analysis are the interval velocities in the uppermost 43 ms TWT (corresponding to a subbottom depth of 23 m) reduced to about 1050 m/s, a velocity reduction of 30 % compared to 1500 m/s in the overlying watercolumn, and about 40 % reduction compared to the directly underlying sediments

with interval velocities of 1600-1650 m/s, down to a depth of 113 ms TWT (≈ 80 m). At this depth the interval velocity increases drastically to about 2000 m/s, followed by an additional velocity increase to 2500 m/s at 217 ms (≈ 186 m) (Fig. 5; Tab. 1)

The calculated depths of these reflectors have to be handled with caution since the vertical resolution of the seismic data is under ideal conditions about 8 m at the sea floor. Physically the vertical resolution here is taken as l/2, controlled by the wavelength (l), which is proportional to the velocity (1500 m/s) and the frequency (100 Hz) (Sheriff and Geldart, 1985). Since the vertical resolution of the MCS-data prevented the determination of the surface of the gas-charged sediments with accuracy, the PARASOUND-registrations provide this information, with its vertical resolution of about 40 cm. Accordingly, the PARASOUND locates this boundary at a subbottom depth of 8-10 m. On the other hand the MCS-data provide evidence for the depth of the base of the gassy sediments located at a depth of 23 m, by the transition from low interval velocities (± 1000m/s) to velocities of ±1600 m/s. Based on the seismic and subbottom profiling, the thickness of the zone of gas-charged sediments appears to be 13-15 m ± 8 m, including the uncertainties of vertical resolution.

In support of the seismic evidence, the methane concentration in the sediments has been directly measured. The analyses were performed on samples from the kasten core (KAL II) recovered slightly off the profile lines (Fig.1) down to a depth of 5.4 m. A box core was taken parallel to the kasten core, for the recovery of undisturbed surface sediments, penetrating about 0.3 m into the sediment. Although kasten core KAL II did not reach the acoustically turbid zone, the methane concentrations in KAL II are very high compared to background values of "normal" marine sediments (Faber and Stahl,1984). The concentrations increase from about 160 ppb at the sea floor to maximum values of about 5,700 ppb CH_4 at 3 m below sea floor. There is a slight decrease to 4,340 ppb at the deepest sample taken from 5 m (Table 2). These high methane concentrations reveal that the gas zone is more extensive than indiated by PARASOUND acoustics. Taking into account the thickness overlying the acoustic turbidity, we come up with a total thickness of gas-charged sediments of 21-25 ±8m.

Different generations of pockmarks

The high methane concentrations in near surface sediments are first order indicators to relate the origin of pockmarks to gas-expulsion and the acoustic turbidity to gas-charged sediments. The restricted penetration of the PARASOUND signals to about 10 m is additional evidence for the presence of free gas in the sediment. Even in an area of suspected gas-charged sediments the penetration of PARASOUND reached some 40 m (Max et al., 1992). Free gas as bubbles in the pore space seems to absorb almost the entire energy of the generated pulses. The deeper reflections underneath the pockmarks indicate either that the available gas has been expelled from the pore spaces or that authigenic carbonate hard grounds with high reflectivity have developed through the steady upward flow of methane. The latter should not only be found underneath pockmarks but also in the otherwise methane-charged sediments. Along the profile not all pockmarks are characterized by deeply buried reflectors. This indicates various ages of pockmark formation. Pockmarks with deeper reflections are suspected to be the most recent ones where the eruption has expelled all available gas from this locality. As a result less seismic energy gets absorbed, allowing deeper reflections to be received. The other type of pockmark without any reflecting horizons is suspected to be older because a considerable amount of gas has accumulated since its generation, preventing reflected signals to be received from deeper levels.

Amount of methane at shallow depth

To estimate the amount of methane trapped in the shallow sediments, we calculated the area of gas appearance in the Skagerrak indicated in figure 1. The distribution of gassy sediments, particularly in the southern and eastern Skagerrak, is based on a map published by Van Weering (1975) and unpublished data from Theilen (Inst. für Geophysik, Kiel, FRG). Data from the area between the Skagerrak and Kattegat is too sparse to allow for reliable mapping of the shadow zones (Van Weering ,1975; Hempel,1985; Hovland,1991). Therefore, only the area north of the tip of Denmark has been considered in our estimation of the methane content.

From figure 1, the area of gas-charged sediments is calculated to be about 5,520 km^2. The thickness of the gas-charged sediments, as revealed by the combined records of subbottom profiling, high resolution seismic data and direct methane measurements is in the range of about 23 m (mean of 21 - 25 ± 8 m). Therefore, the resulting gas-charged sediment body has a volume of about 126 km^3. To determine the total amount of methane trapped in the sediments, the mass of the sediment body has to be calculated. Taking the mean wet-bulk density of the sediments as 1,700 kg/m^3 (Hass, pers. comm, 1992) results in a mass of 2.14×10^{14} kg for the entire sediment body. Assuming a mean methane concentration of about 3,000 ppb, the total amount of methane trapped in near surface sediments in the Skagerrak is about 6.45×10^{11} g.

Possible errors in this rough calculation involve (1) the distribution of gas charged sediments, (2) the thickness of this sediment body, and (3) the assumption of the methane concentration for the entire gas-charged sediments. The distribution of the gas-charged sediments as well as their thickness is based on a fairly good acoustical and seismic database of some 2,000 km. The methane concentration employed in this calculation is most likely too low to represent the entire gas-charged sediment body, since it represents the incoherent but nevertheless reflective part of the section, whereas no gas analyses exist from the acoustically transparent zone underneath, which probably exhibits much higher concentrations.

Methane flux rates through the sea-floor

In answering the question about the rate of methane escaping through the seabed into the water we are faced with the lack of flow measurements performed *in situ*. Hence we have to use rough estimates based on very sparse observations. Hovland et al. (in press) described a statistically based estimate of the methane flux through the seabed for different parts of the shelf seas. Their figures range from about 1 to 400 g $CH_4/m^2/yr$. An average estimate of 13 g $CH_4/m^2/yr$ is thought to represent any hydrocarbon-rich area with obvious seepage and intermittent ebullition. This mean value should be appropriate for an estimation of the methane flux in the Skagerrak, resulting in a annual flux of 7.17×10^{10} g CH_4 (5.516×10^9 m^2 x 13 g $CH_4/yr/m^2$). The most

recent estimate of the global atmospheric CH_4 production, as a sum of emission and consumption, by Reeburgh et al. (in press) results in an annual natural methane production of 5.8×10^{13} g CH_4. This figure is only about 800 times bigger than the estimated annual flux in the Skagerrak and suggests that most of the emitted methane is oxidized in the water column before it reaches the atmosphere. The area of gas seepage in the Skagerrak (5.5×10^3 km^2) is compared to the world ocean surface (3.61×10^8 km^2; Kossina,1921) a portion of 6.5×10^4. If we project this portion on the annual methane ebullition of the world ocean (5.8×10^{13} g CH_4) to the area of the Skagerrak we come up with a proposed methane emmittence of 8.8×10^8 g $CH_4/m^2/yr$. This in turn is about two orders of magnitude smaller than our estimated value of 7.2×10^{10} CH_4 $/m^2/yr$. We consider the difference as a reliable value for the loss of methane within the water column through oxidation processes. Presently has the methane consumption in the water column not been measured but there exsist certainly a substantial uptake of methane by biological processes.

All the above mentioned figures have to be handled with caution since they are all quite crude assumptions. They all lack sufficient measurements and are affected by uncertainties of unknown extend, e.g. the extend of methane oxidatioin in the water column and the constant or episodic seepage through the seabed. Nevertheless exists an surprising agreement in the results of the different estimates. between the estimates performed from different and is has to be kept in mind since Reeburgh et al. (in press) estimated the flux into the atmosphere, whereas our estimate represents the emission from the sea floor into the water.

Conclusions

An extensive area of gas-charged sediments exists in the southern and eastern Skagerrak. This has been mapped on the basis of acoustically transparent sediments and the distribution of pockmarks. Along a profile in the southern Skagerrak the multi-beam echo-sounding provides a detailed image of the isolated and elongated shape of the pockmarks. Gas-charged sediments are identified on the basis of high

resolution seismic recordings and subbottom profiler registrations. Processing of the seismic data revealed an interval velocity in the gas zone to be about 1050 m/s. A combined interpretation of the seismic and subbottom profiler records indicate a fairly constant thickness of the gas-charged sediments in the Skagerrak to be about the uppermost 23 m of the sediment column. The areal extend and the thickness of the gas-charged sediments have a volume of 126 km^3. Using a mean wet-bulk density of 1,700 kg/m^3, the total mass of the considered sediment body is estimated to be 2.15×10^{14} kg. A mean value of 3,000 ppb methane concentration measured on recovered sediments yields a total methane content (6.45×10^{11} g) in the near surface sediments. This is certainly a conservative estimate, since the sediment cores did not reach the main gas zone characterized by acoustic transparency.

Hovland et al. (in press) provided mean flux rates of methane through the seabed for different parts of the shelf seas under the consideration of hydrocarbon reservoirs at greater depth. A mean value is applied for the estimate on the annual seepage of methane in the Skagerrak. It results in 7.17×10^{10} g $CH_4/m^2/yr$. This value has been set in relation to the annual global methane production from the ocean into the atmosphere (5.8×10^{13} g CH_4) of Reeburgh et al. (in press). By comparing these flux rates with regard to the lateral extend of the seepage area in the Skagerrak compared to the ocean surface is the production of methane at the sea floor two oders of magnitude larger than what is expected from the Reeburgh et al. value to escape from the Skagerrak's sea surface to the atmosphere. This supports the assumption that there occurs a substantial consumption of methane by oxidation within the water column by biological processes.

Acknowledgements

The senior author wishes to express his sincere thanks to T. Dickmann, D. Kläschen and W. Weinrebe for their most valuable assistence with the processing of the PARASOUND data. We highly appreciated the most helpfull cooperation of the crews of RV *Gauss* RV *Polarstern* and *RV Planet.* C. Wold supported us with the algorithm to

calculate the area of gas-charged sediments. S. Lammers kindly performed the methane analyses and made the unpublished data available for us. S. Steinmetz is thanked for the processing of the HYDROSWEEP data. We highly appreciatedthe critical remarks and reviews of R. Keir, J. Leinbach, E.Suess and F. Theilen. P.H. received financial support through BMFT-grant 03R607.

References

Anderson, A.L. & Bryant, W.R. 1990. Gassy sediments occurrence and properties: Northern Gulf of Mexico. *Geo-Marine Letters* **10**, 209-220.

Baker, E.T. & Lupton, J.E. 1990. Changes in submarine hydrothermal 3He/heat ratios as an indicator of magmatic/tectonic activity. *Nature* **346**, 556-558.

Brooks, J.M., Cox, H.B., Bryant, W.R., Kennicutt II, M.C., Mann, R.G. & McDonald., T.J. 1986. Association of gas hydrates and oil seepage in the Gulf of Mexico. *Org. Geochemistry* **10**, 221-234.

Brooks, J.M., Kennicutt II, M.C., Fisher, C.R., Macko, S.A., Cole, K., Childress, J.J., Bidigare, R.R. & Vetter, R.D. 1987. Deep-sea hydrocarbon seep communities: Evidence for energy and nutritional carbon sources. *Science* **238**, 1138-1142.

Carson, B., Suess, E. & Strasser, J.C. 1990. Fluid flow and mass flux determinations at vent sites on the Cascadia Margin accretionary prism. *Journ. Geophys. Res* **95**, 8891-8897.

Dando, P.R., Austen, M.C., Burke, R.A. Jr., Kendall, M.A., Kennicutt II, M.C., Judd, A.G., Moore, D.C., O'Hara, S.C.M., Schmaljohann, R. & Southward., A.J. 1991. Ecology of a North Sea pockmark with an active methane seep. *Mar. Ecol. Prog. Ser.* **70**, 49-63.

Faber, E. & Stahl, W. 1984. Geochemical surface exploration for hydrocarbons in North Sea. *AAPG Bull.* **68**, 363-386.

Fenchel, T., 1989. Skorstene i Kattegat. *Hovedomradet Copenhagen Univ.* **19** (10), 10-11.

Grant, J.A. & Schreiber., R. 1990. Modern swathe sounding and sub-bottom profiling technology for research applications: The Atlas Hydrosweep and Parasound system. *Marine Geophysical Researches* **12** 9-19.

Hempel, P. 1985. Zur quartären Geschichte des Skagerrak - eine akustostratigraphische Interpretation reflexionsseismischer Messungen. **M.Sc. thesis**, Kiel University: 74pp.

Hill, I., Taira, H. & et al., 1991. *Proc. Init. Res., ODP.*, **131**, College Station, TX: Ocean Drilling Program.

Hovland, M., 1981. Characteristics of pockmarks in the Norwegian Channel. *Mar. Geol.* **39**, 103-117.

Hovland, M. & Judd, A.G. 1988. Seabed pockmarks and seepages. Graham and Trotman, London, 293pp..

Hovland, M. & Thomsen, E. 1989. Hydrocarbon-based communities in the North Sea? *Sarsia* **74**, 29-42.

Hovland, M. 1990. Suspected gas-associated clay diapirism on the seabed off Mid-Norway. *Mar. Petrol. Geol.* **7**, 267-276.

Hovland, M. 1991. Large pockmarks, gas-charged sediments and possible clay diapirs in the Skagerrak. *Mar. Petrol. Geol.* **8**, 311-316.

Hovland, M., Judd, A.G. & Burke Jr., R.A. (in press). The global flux of methane from shallow submarine sediments. *Chemosphere.*

Jensen, P., Aagard, I., Burke, R.A., Dando, P.R., Jørgensen, N.O., Kuijpers, A., Laier, T. & Schmaljohann, R. 1991 (subm.). Bubbling reefs in the Kattegat: methane-seeps with carbonate-cemented rocks attract a diverse ecosystem. *Mar. Ecol. Prog. Ser.*

Jørgensen, N.D., Laier, T., Buchardt, B. & Cederberg, T. 1990. Shallow hydrocarbon gas in the northern Jutland-Kattegat region, Denmark. *Bull. Geol. Soc. Denmark* **38**, 69-76.

Jørgensen, N. O., 1992. Methane-derived carboante cementation of marine sediments from the Kattegat, Denmark: Geochemical and geological evidence. *Mar. Geol.* **103**, 1-13.

Kennicutt II, M.C. & Brooks, J.M. 1990. Recognition of areas effected by petroleum seepage: Northern Gulf of Mexico continental slope. *Geo-Marine Letters* **10**, 221-224.

King, L.H. & MacLean, B. 1970. Pockmarks on the Scotian Shelf. *Geol. Soc. Amer. Bull.* **81**, 3141-3148.

Kossina, E. 1921. Die Tiefen des Weltmeeres. Berlin Univ., *Geogr. - naturwissen. Reihe*, **9**, 70pp.

Laier, T., Jørgensen, N.O., Buchardt, B., Cederberg, T. & Kuijpers, A. (in press). Accumulation and seepage of biogenic gas in northern Denmark. *Estuarine, coastal and shelf sciences.*

Lashof, D.A., & Ahuja, D.R 1990. Relative contribution of greenhouse gas emissions to global warming. *Nature* **344**, 529-631.

LeBlanc, L.R., Mayer, L., Rufino, M., Schock, S.G. & King, J. 1992. Marine sediment classification using the chirp sonar. *J. Acoust. Soc. Am.* **91** (1), 107-115.

LePichon, X., Iiyama, T., Boulegue, J., Charvet, J., Faure, M., Kano, K., Lallemant, S., Okada, H., Rangin, C., Taira, A. & et al. 1987. Nankai Trough and Zenisu Ridge: A deep-sea submersible survey. *Earth Planet. Sci. Letts.* **83**, 285-299

Max, M.D., Schreiber, R. & Cherkis, N.Z. 1992. Geological control of shallow gas and pockmarks in the Norwegian Channel; high resolution shallow suubottom profiling of small scale features. *Mar. Geophys. Res.*, **14**, 77-85.

Mayer, L.A. 1979. The origin of fine scale acoustic stratigraphy in deep-sea carbonates. *Journ. Geophys. Res.* **84**, 6177-6184.

Mayer, L.A., Shor, A.N., Clarke, J.H. & Piper, D.J.W. 1988. Dense biological communities at 3850 m on the Laurentian Fan and their relationship to the deposits of the 1929 Grand Banks earthquake. *Deep-Sea Research*, **35**, 1235-1246.

McQuillin, R. & Fannin, N.G.T. 1979. Explaining the North Sea's lunar surface. *New Scientist*, **1163**, 90-92.

Moore, J.C., Mascle, A. & et al. 1988. *Proc. Init. Res., ODP,* **110**, Ocean Drilling Program. College Station, TX.

Neurauter, T.W. & Bryant, W.R. 1990. Seismic expression of sedimentary volcanism on the continental slope, northern Gulf of Mexico. *Geo-Marine Letters* **10**, 225-231.

Okada, H. & Cadet, J.-P. (eds.) 1989. KAIKO Symposium: Geology, Geochemistry and Biology of the trench subduction zone. *Paleoclimat. Paleogeogr. Paleoecol.*

Paull, C.K., Hecker, B., Commeau, R., Freeman-Lynde, R.P., Neuman, C., Corso, W.P., Golubic, S., Hook, J.E., Sikes, E. & Curray, J. 1984. Biological communities at the Florida Escarpment resemble hydrothermal vent taxa. *Science* **226**, 965-967.

Paull, C.K., Tull, A.J.T., Tollin, L.J. & Linitz, T.1985. Stable isotope evidence for chemosynthesis in an abyssal seep community. *Nature* **317**, 709-711.

Reeburgh, W.S., Whalen, S.C., & Alperin, M.J. 1992 (subm.). The role of mirobially-mediated oxidation in the global CH_4 budget, *Nature*.

Rosenfeld, W.D. & Silverman, S.R. 1959. Carbon isotope fractionation in bacterial production of methane. *Science* **130**, 1658-1659.

Rostek, F., Spiess, V. & Bleil. U. 1991. Parasound echosounding: Comparison of analogue and digital echosounder records and physical properties of sediments from the equatorial South Atlantic. *Mar. Geology* **99**, 1-18.

Schmaljohann, R. & Flügel, H.J. 1987. Methane-oxidizing bacteria in pogonophora. *Sarsia* **72**, 91-98.

Schmaljohann, R., Faber, E., Whiticar, M.J., & Dando, P.R. 1990. Co-existence of methane- and sulphur-based endosymbioses between bacteria and invertebrates at a site in the Skagerrak. *Mar. Ecol. Prog. Ser.* **61**, 119-124.

Schoell, M., 1980. The hydrogen and carbon isotopic composition of methane from natural gases of various origins. *Geochim. et Cosmochim. Acta* **44**, 675-702.

Schreiber, R., 1983. Erstellung eines Programmpaketes für Geschwindigkeitsanalysen und CMP-Stapelungen von mehrkanaligen marinen reflexionsseismischen Daten. **M.Sc. thesis**, Kiel University:133pp.

Schreiber, R. & Schenke, H.W. 1990. Efficient hydrographic surveying of EEZ with new multibeam echosounder technology for shallow and deep water. In: *Ocean Resources*, Ardus, D.A. & Champ, M.A. (eds.) **1**, Kluwer Academic Publ., Netherlands, 73-87

Sellevoll, M.A. & Aalstad, I. 1971. Magnetic measurements and seismic profiling in the Skagerrak. *Marine Geophysical Researches* **1**, 284-302.

Sheriff, R.E. & Geldart, L.P. 1985. Exploration seismology. History, theory, and data acquisition. **Vol. 1.**, Cambridge Univ. Press, Cambridge:

Suess, E., Von Huene, R. & et al. 1987. *Proc. Init. Res., ODP* **112**, College Station, TX, Ocean Drilling Program.

Taner, M.T., & Koehler, F. 1969. Velocity spectra - digital computer derivation and applications of velocity functions. *Geophysics* **34** (6), 859-881.

Van Weering, T.C.E., Jansen, J.H.F., & Eisma, D. 1973. Acoustic reflection profiles of the Norwegian Channel between Oslo and Bergen. *Neth. Journ. Sea Res.* **6** (1-2), 241-263.

Van Weering, T.C.E. 1975. Late Quaternary history of the Skagerrak; An interpretation of acoustical profiles. *Geologie en Mijnbouw* **54** (3-4), 130-145.

Van Weering, T.C.E. 1982. Shallow seismic and acoustic reflection profiles from the Skagerrak; implications for recent sedimentation. *Proc. K. Ned. Akad. Wet. Ser. B* **85**(2), 129-154.

Weigel, W., Hjelme, J. & Sellevoll, M.A. 1970. A refraction profile through the Skagerrak from northern Jutland to southern Norway. *Geodaet. Inst. Medd.* **45**, 1-28

Whiticar, M.J., Suess, E., & Wehner, H. 1985. Thermogenic hydrocarbons in surface sediments of the Bransfield Strait, Antarctic Peninsula. *Nature* **314**, 87-90.

Zonenshayn, L.P., Murdmaa, I.O., Baranov, B.V., Kuznetsov, A.P., Kuzin, V.S., Kuz´min, M.I., Avdeyko, G.P., Stunzhas, P.A., Lukashin, V.N., Barash, M.S., Valyashko, G.M., & Demina, L.L. 1987. An underwater gas source in the Sea of Okhotsk west of Paramushir Island. *Oceanology* **27**, 598-602.

Figure captions

Figure 1. Location map and bathymetry of the Skagerrak in the NE-North Sea. Indicated are the positions of geological sampling and the general direction of profiling along the southern slope of the Norwegian Trench. The distribution of gassy sediment at shallow burial depth is taken from Hovland (1991).

Figure 2. Detailed trackchart of the reflection seismic profile and the combined HYDROSWEEP- and PARASOUND-profile. The heavy line marks the section of seismic velocity analyses shown in fig. 5. Along both profiles are the occurrences of pockmarks indicated.

Figure 3. Multibeam echosounding swath obtained with HYDROSWEEP along the profile shown in fig. 2, showing a typical in SW-NE-direction elongated pockmark with a lateral extend of up to 1 km by 300 m and a maximum depth of 20 m.

Figure 4. Analog record of the high resolution multichannel seismic profile. The numbers refer to pockmarks along this line. G: gas zone as revealed by the velocity analysis, M: multiple reflection, Q: base Quaternary, ME: mesozoic strata. The vertical scale is in milliseconds two-way traveltime. The location of the profile is shown by the heavy line in figure 2.

Figure 5. Section of the reflection seismic profile indicated in fig. 2 with the calculated interval velocities versus depth. The gas charged sediments at shallow depths are characterized by velocities of about 1000 m/s followed by velocities typical for unconsolidated marine sediments.

Figure 6. Sub-bottom profiler record produced by PARASOUND. The section shown has been bandpass-flitered between 3 and 5 kHz. The limited penetration into the sediments to about 10 m is caused by the presence of gas-charged sediments below this depth, attenuating the entire available energy. The top of the gassy sediments is marked by a relatively strong reflection.

Figure 7. Amplitude spectra of a selected PARASOUND-seismogram.

Figure 8. Detailed plot of 10 traces in an area of a succession of high amplitude reflections within the acoustically transparent zone.

Table captions

Table 1. Depths of reflectors in multi-channel seismic line, shown in fig. 5, below sea floor in two-way-traveltime (TWT), in metres, and the corresponding interval velocities, as revealed by seismic processing.

Table 2. Methane concentrations versus depth in kasten corer KAL II and the associated box corer GKG II.

Reflectors	TWT (ms)	Depth (m)	V_{int} (m/s)
Seafloor	0	0	
			1050
(1)	43	23	
			1650
(2)	70	45	
			1600
(3)	113	80	
			2050
(4)	217	186	
			2500

Table 1. Depths of reflectors in multi-channel seismic line, shown in fig. 5, below sea floor in two-way-traveltime (TWT), in metres, and the corresponding interval velocities, as revealed by seismic processing.

KAL II:

Depth (cm)	CH4 (ppb)
0	259
6	121
20	1019
100	653
300	5681
400	5163
500	4339

GKG II:

Depth (cm)	CH4 (ppb)
18	162
24	177

Table 2. Methane concentrations versus depth in kasten corer KAL II and spade box corer GKG II.

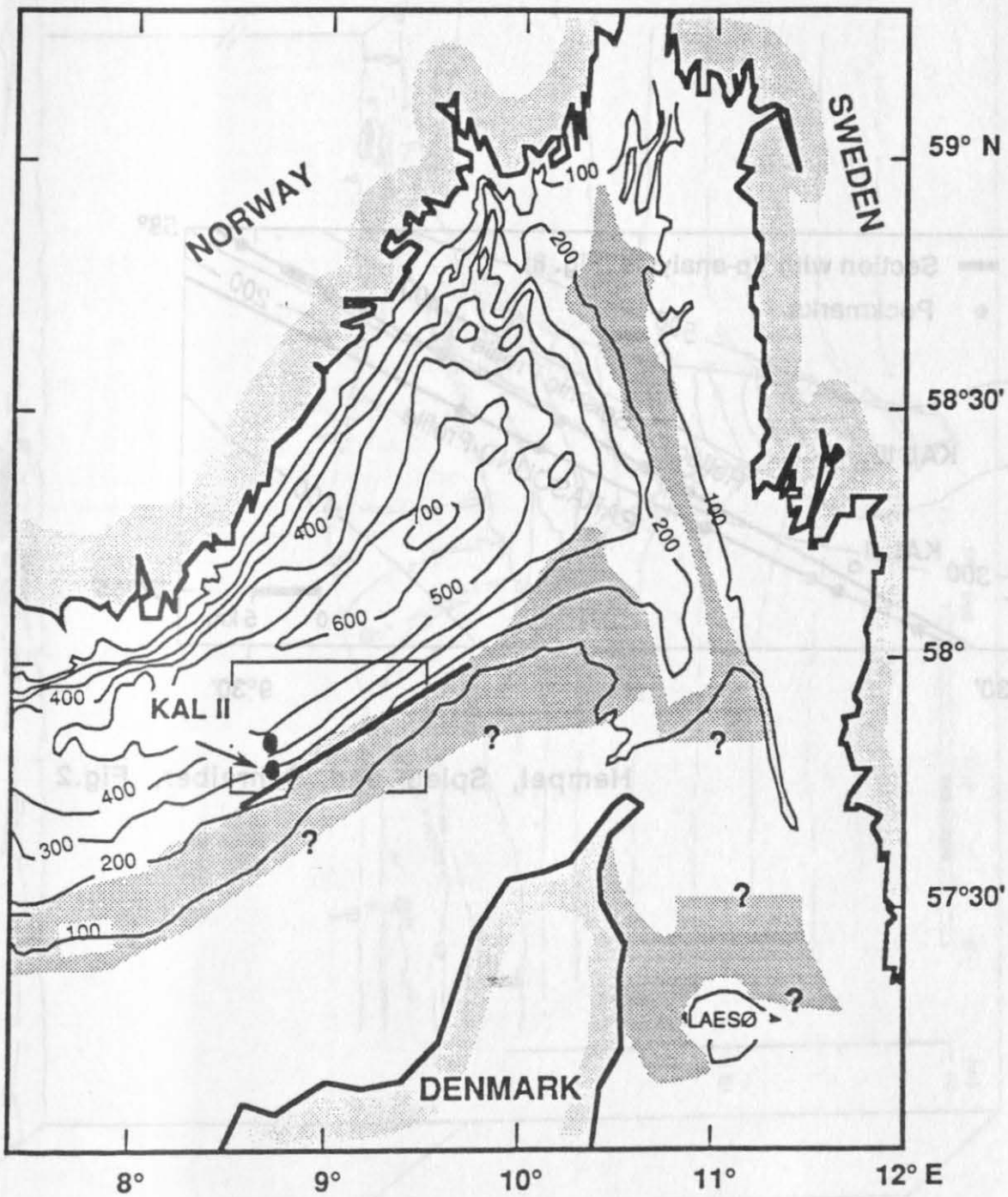

Hempel, Spieß and Schreiber, Fig.1

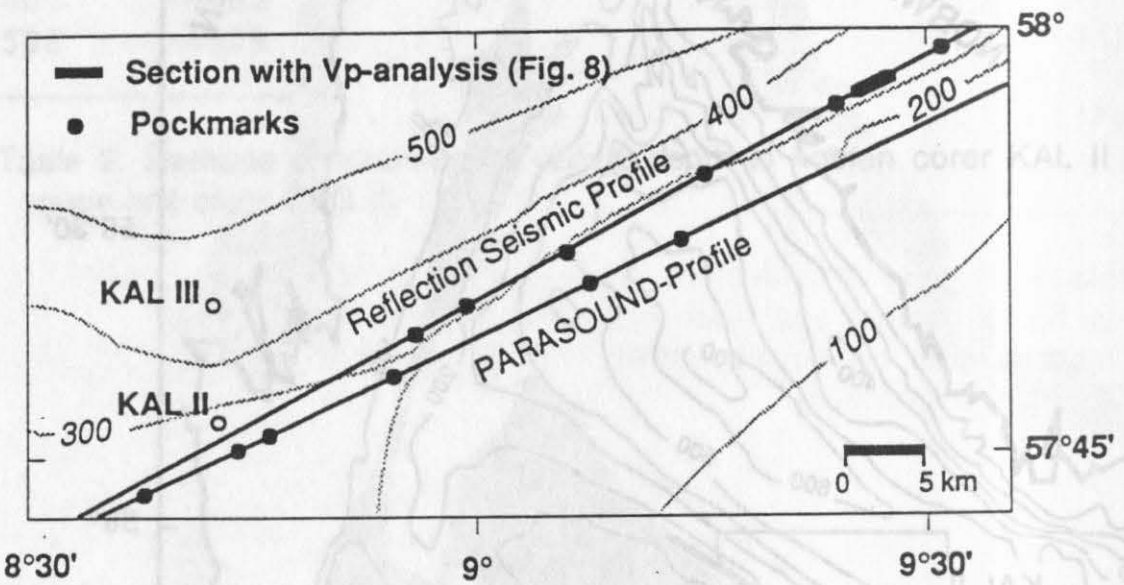

Hempel, Spieß and Schreiber, Fig.2

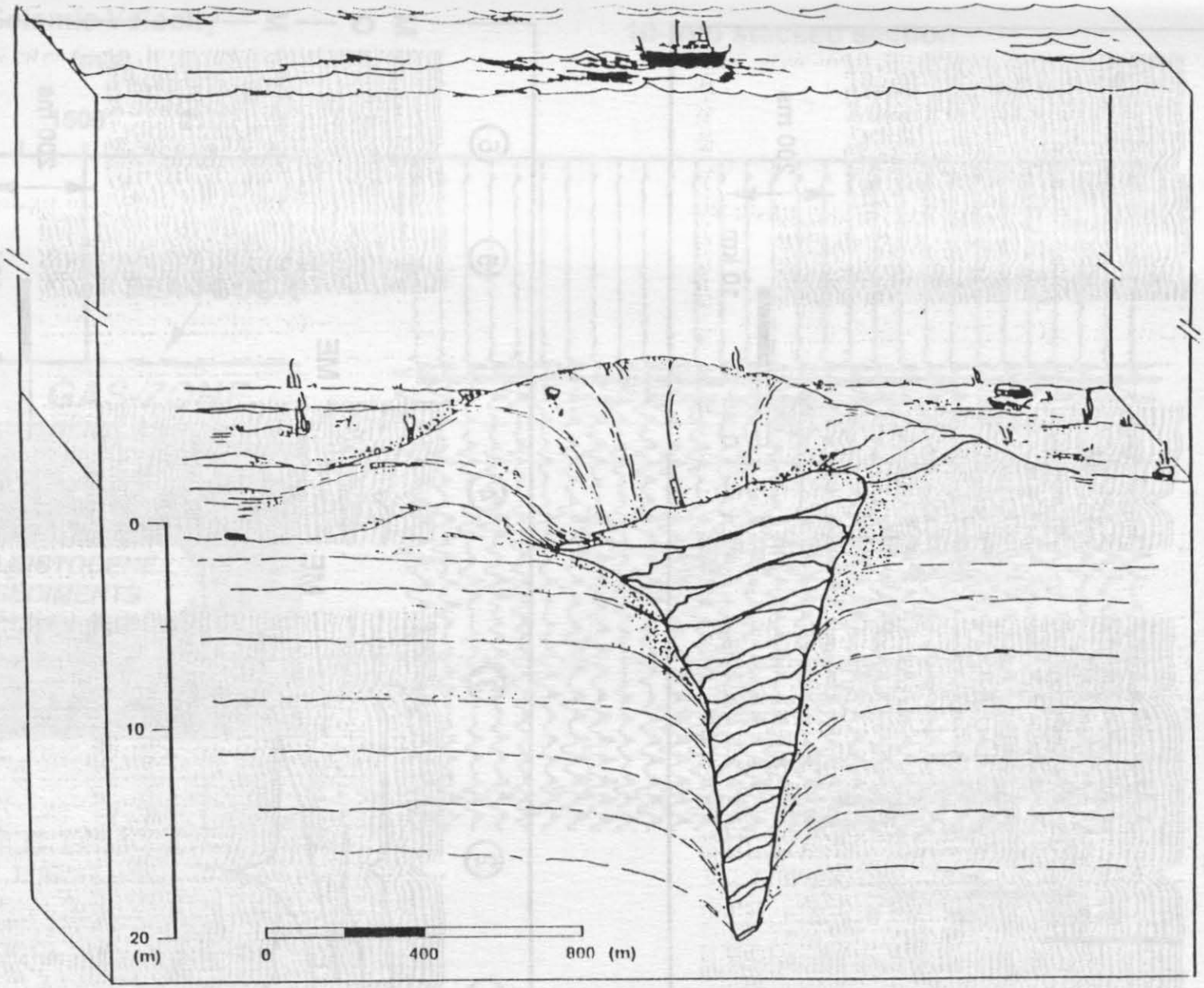

Hempel, Spieß and Schreiber, Fig.3

NE SW

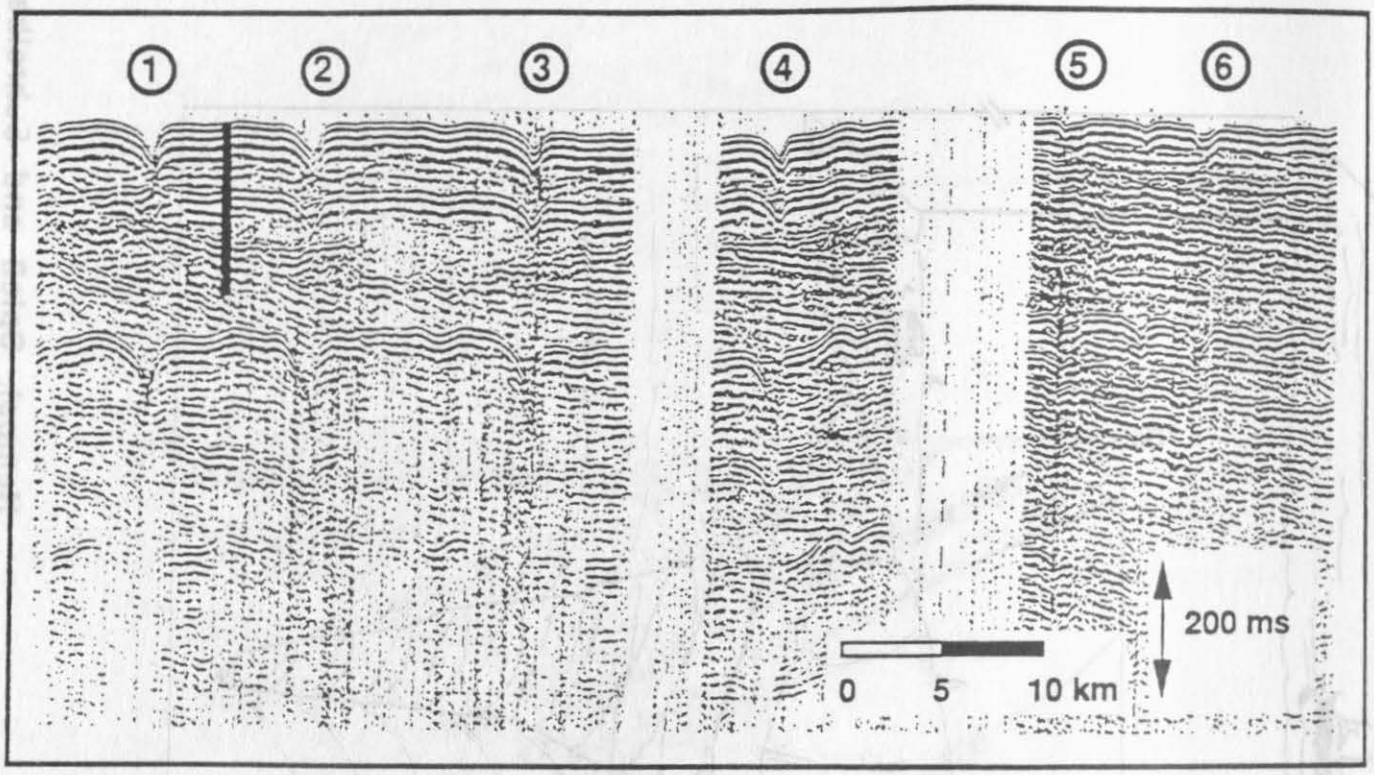

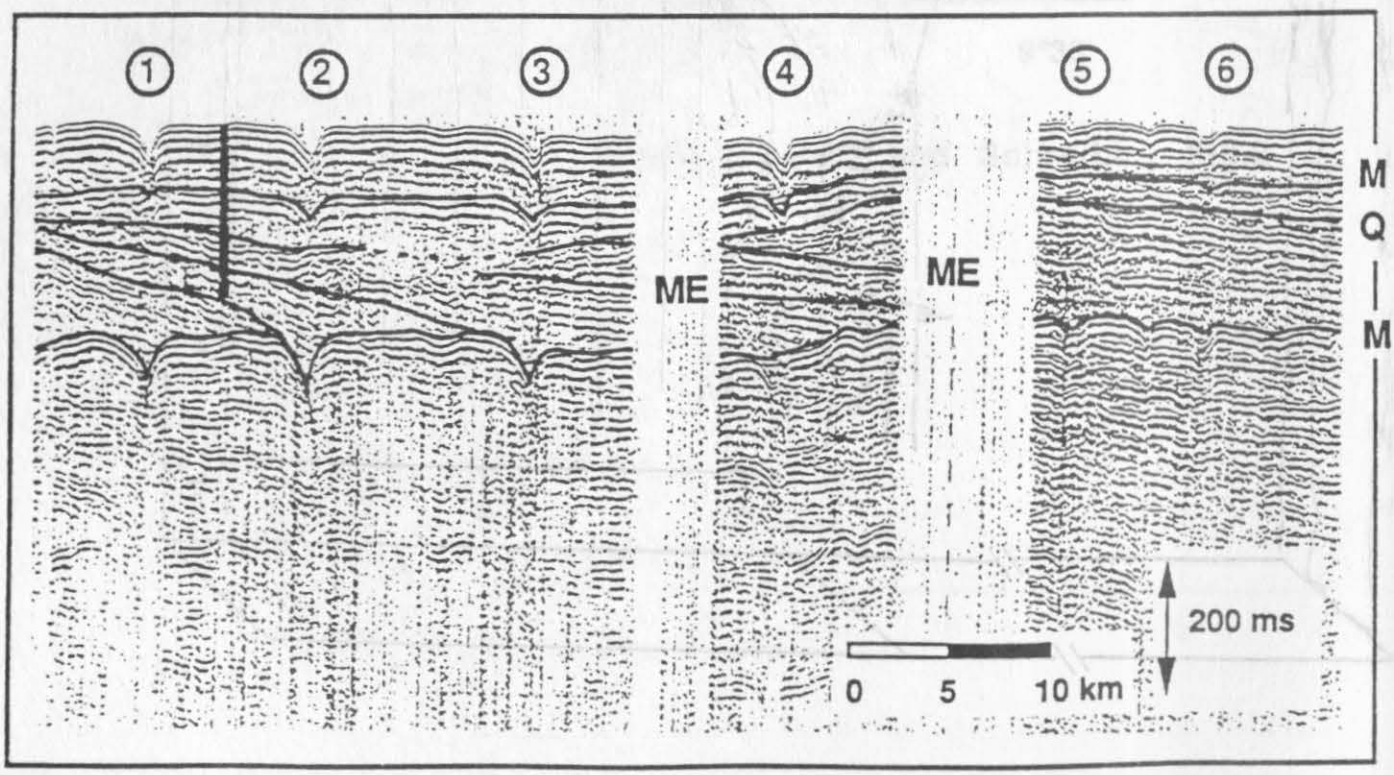

Hempel, Spieß and Schreiber, Fig.4

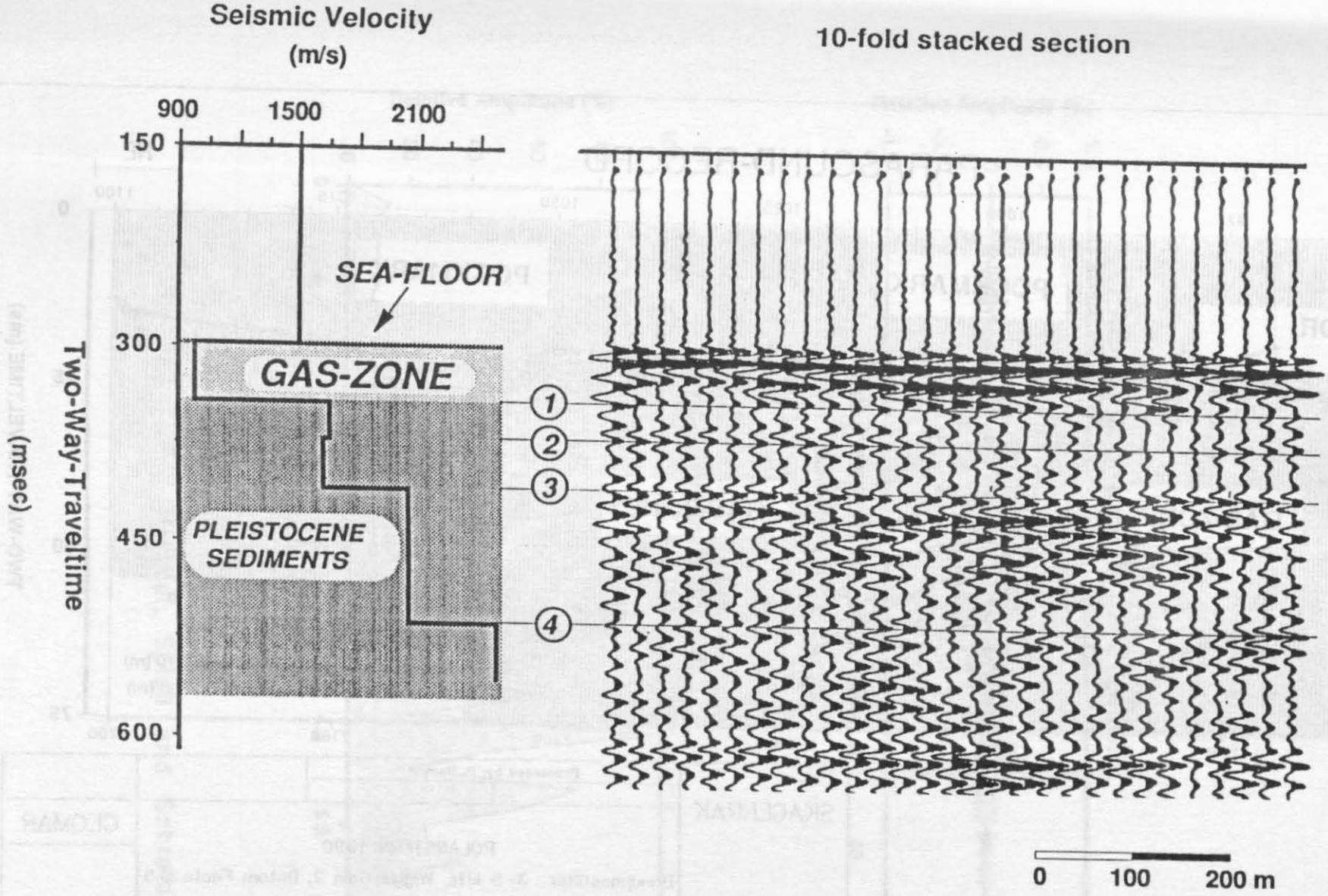

Hempel, Spieß and Schreiber, Fig.5

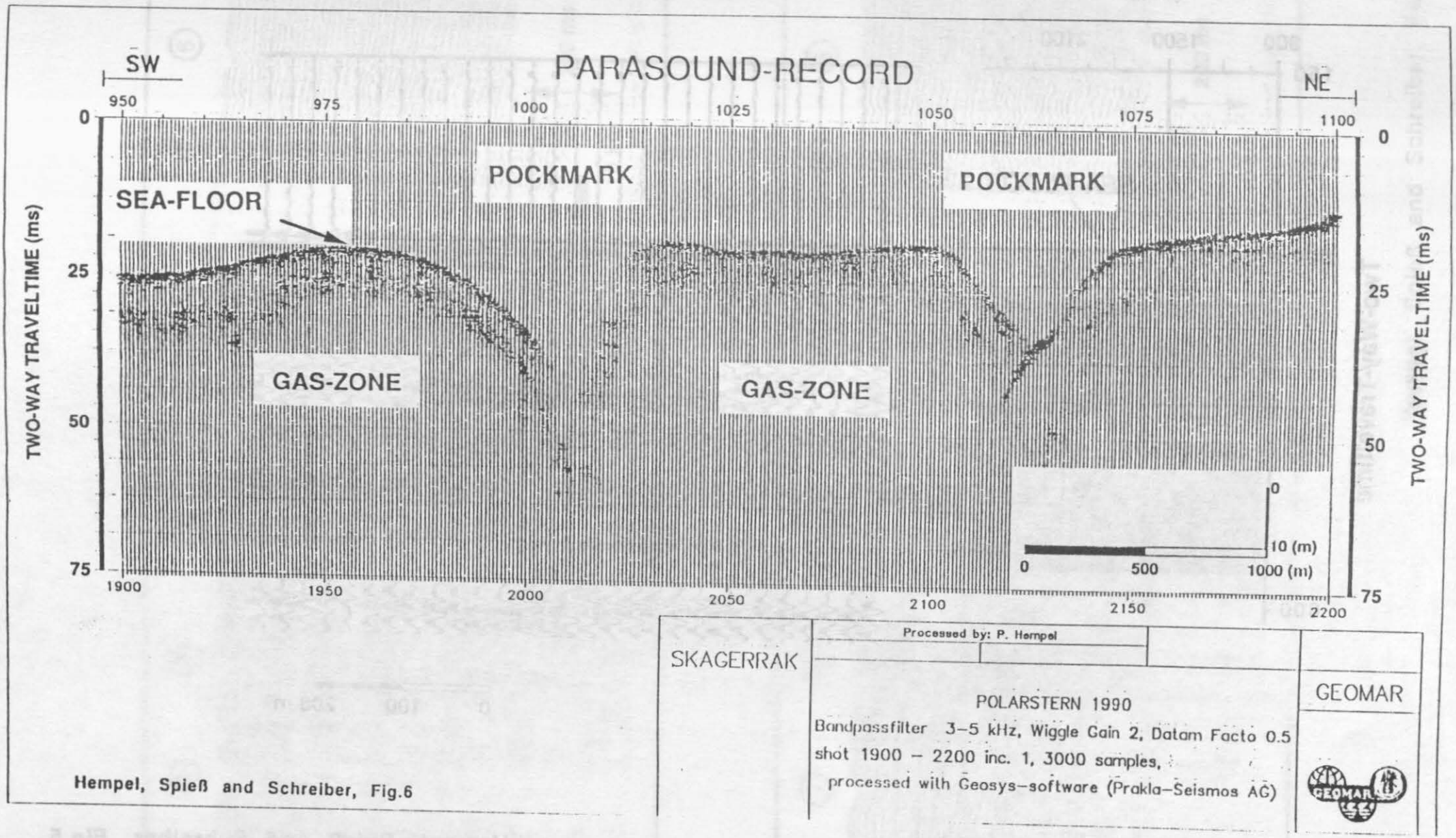

Hempel, Spieß and Schreiber, Fig.6

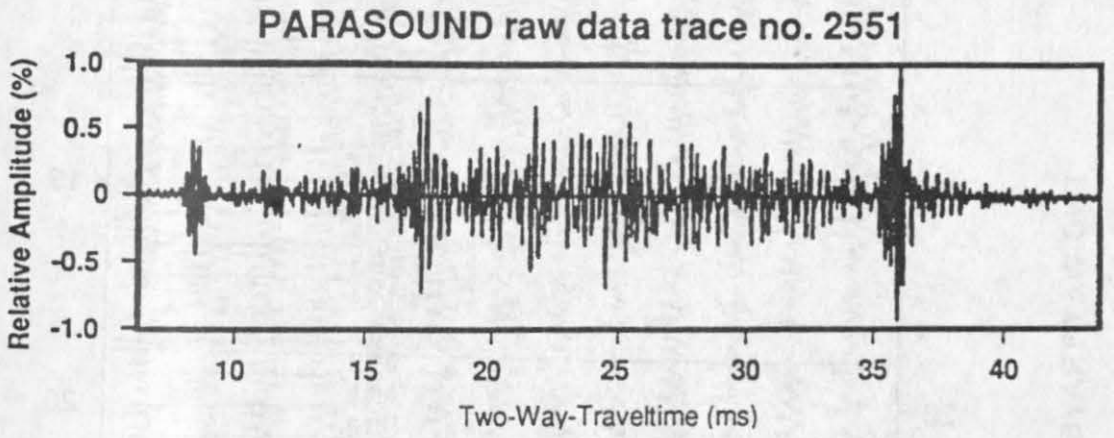

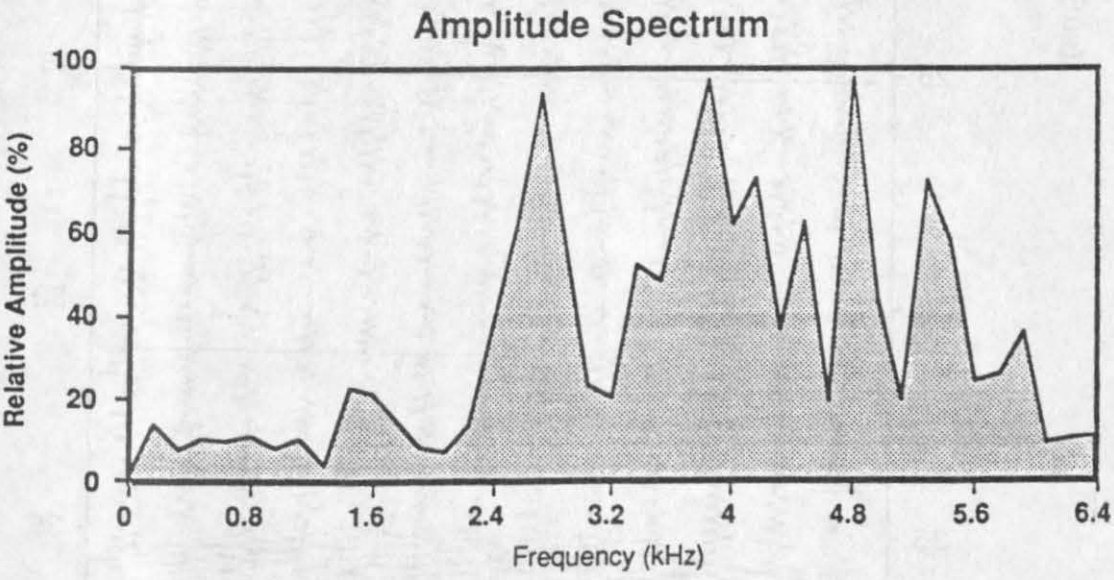

Hempel, Spieß and Schreiber, Fig.7

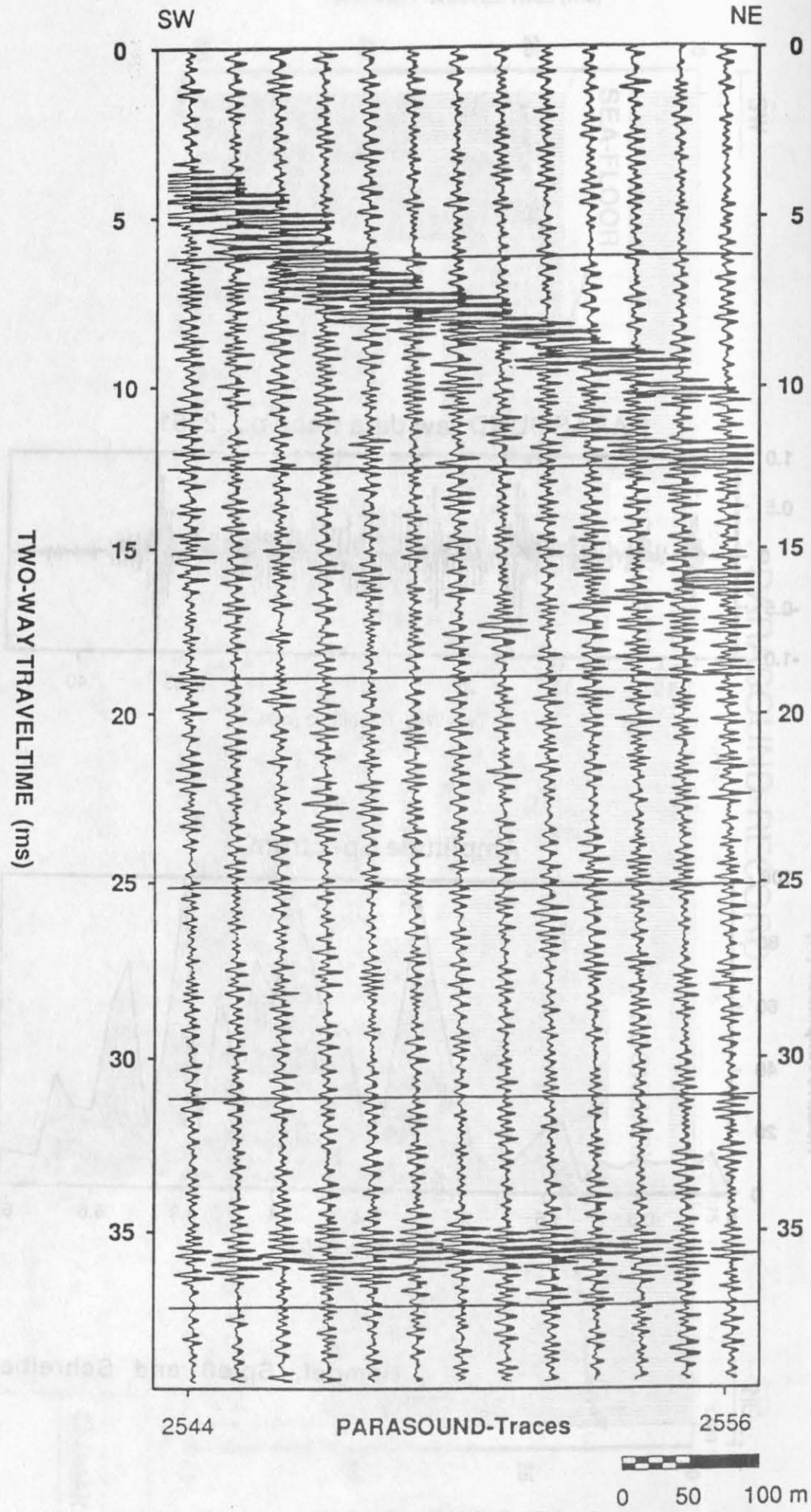

Hempel, Spieß and Schreiber, Fig.8

GAS-EXPULSION AT THE SEA-FLOOR IN THE SKAGERRAK; NE-NORTH SEA

P. HEMPEL

GEOMAR - Forschungszentrum für marine Geowissenschaften
Wischhofstr. 1-3
2300 Kiel 14
Germany

SUMMARY

Gas-expulsion at the sea-floor is a widespread phenomenon in the North Sea, particularly in the Skagerrak. Evidences are crater-like depressions, called pockmarks, acoustically transparent zones in the subsurface and enhanced methane concentrations in the sediments. A combined effort of multibeam echosounding, subbottom profiling, high resolution seismic data, and geochemical analyzes of sampled sediments, with respect to methane concentrations was performed to map the distribution of gas-charged sediments, and to calculate the volume of methane in these sediments.

INTRODUCTION

It is known from numerous studies that the Skagerrak area, bordered by the coastlines of Norway, Sweden and Denmark, is covered to a great extend by gas-charged sediments at shallow depth. Evidences for the presence of gas is the characteristic acoustically transparent reflection pattern on subbottom profiler registrations and the occurrence of pockmarks, which is suspected to be directly linked with gas in near surface sediments. Additionally support for the enhanced gas content in the sediments is delivered from geochemical analyzes and the findings of biological communities at the sea-floor, which are dependent on the expelled gases as a nutrient source.

About the distribution of gases in shallow marine sediments, their concentration and the rate of seeping into the watercolumn and the subsequent escape into the atmosphere is only very little known. Of particular interest is methane, as one of the most important greenhouse gases in the atmosphere, since methane, per mole, has a warming potential 3.7 times that of carbon dioxide (1). For a global estimate of the contribution of naturally derived gas emission it is crucial to aquire a basic understanding of the potential gas-flux in restricted areas of typical gas-charged sediments.

The aim of this paper is to demonstrate the most valuable combination of digitally recorded subbottom profiler registrations with high resolution multichannel seismic recordings and geological sampling for deciphering the extend of gas-charged sediments and to relate the seismic responses to actual methane concentrations.

RESULTS

As part of a high resolution multichannel seismic survey in the Skagerrak a profile was gathered at the southern slope of the Norwegian Trench indicating the presence of gas-charged sediments close to the seabed. The dense grid of seismic lines allowed a detailed mapping of these sediments, revealing a widespread occurrence in the southern and eastern Skagerrak. This is in good agreement with interpretations of (2). The seismic data were processed at selected sites with respect to the vertical distribution of compressional velocities. They reveal a zone of low interval velocities (<1000 m/s) below the sea-floor extending to a depth of about 25 m underlain by layers of velocities (1600-1650 m/s), typical for unconsolidated marine sediments. Velocities drastically reduced to values much lower than water velocity are known to be related to free gas in the pore spaces. Analyzes of sediments recovered by a giant kasten corer along the profile document a downcore increasing methane concentration from about 100 ppb at the sea-floor to about 4300 ppb at the total depth of coring in about 5 m, with maximum values reaching about 5700 ppb. Degassing of the sediments include all available gas, without indications of the state of the gas, whether free of disolved.

Subbottom profiling was performed with the modern narrow beam PARASOUND-profiler along the same line as the seismic investigation and supports the evidence for the presence of gas within the sedimentbody. All transmitted energy is absorbed within a depth range of about 10 m. Partly stratified reflections originated from surface sediments of 2-5 m in thickness are followed downward by an unstratified chaotic type of reflection. The data were stored digitally allowing to apply processing steps, like band pass filtering, calculation of amplitude spectra, and static stacking techniques. Advantages of this procedures are a significant improvement in the presentation and interpretation of the registrations.

Multibeam echosounding with HYDROSWEEP revealed a detailed image of the morphology and inter structures of the pockmarks, generated by the sudden expulsion of gas from the seabed into the watercolumn. The encountered pockmarks are isolated depressions in the sea-floor reaching a depth of about 20 m and an extend of 800 by 300 m. They are elongated in southwesterly-

northeasterly direction, paralleling the slope towards the Norwegian Trench.

The interpretation of the combined dataset of the seismic and subbottom profiler registrations allowed a confident calculation of the extend of the gas-charged sediments in the Skagerrak. These sediments cover an area of about 5.516 km^2. Assuming a mean thickness of 23 m of the gassy sediments the resulting sedimentbody has a volume of 126 km^3. A mean wet-bulk density of 1.600 kg/m^3 results in a mass of 1.89×10^{14} kg for the entire enrolled sedimentbody. Under the assumption of a mean methane concentration of about 3000 ppb a total amount of methane trapped in near surface sediments in the Skagerrak is about 6.3×10^5 t CH_4. This value is a conservative estimate, since the mean methane concentration for the entire gas-charged sediments is presumably higher than in the uppermost 6 m, as recovered by the sampler.

ACKNOWLEGEMENT

I am indebted to V. Spieß, T. Dickmann, D. Kläschen, and R. Schreiber for most valuable assistance with the registration and processing of the seismic and PARASOUND-data. The sediment cores were recovered by the crew of RV Planet under the supervision of C. Hass. S. Lammers performed the methane analyzes and generously made the unpublished results available. This work was funded by the BMFT under contract 03R6076 and MAST-CT89-0001-L.

REFERENCES

(1) LASHOF, D.A. and AHUJA, D.R. (1990). Relative contribution of greenhouse gas emissions to global warming. Nature, 344, 529-531.

(2) Van Weering, T.C.E. (1975). Late Quaternary history of the Skagerrak; An interpretation of acoustical profiles. Geologie en Mijnbouw, 54 (3-4), 130-145.

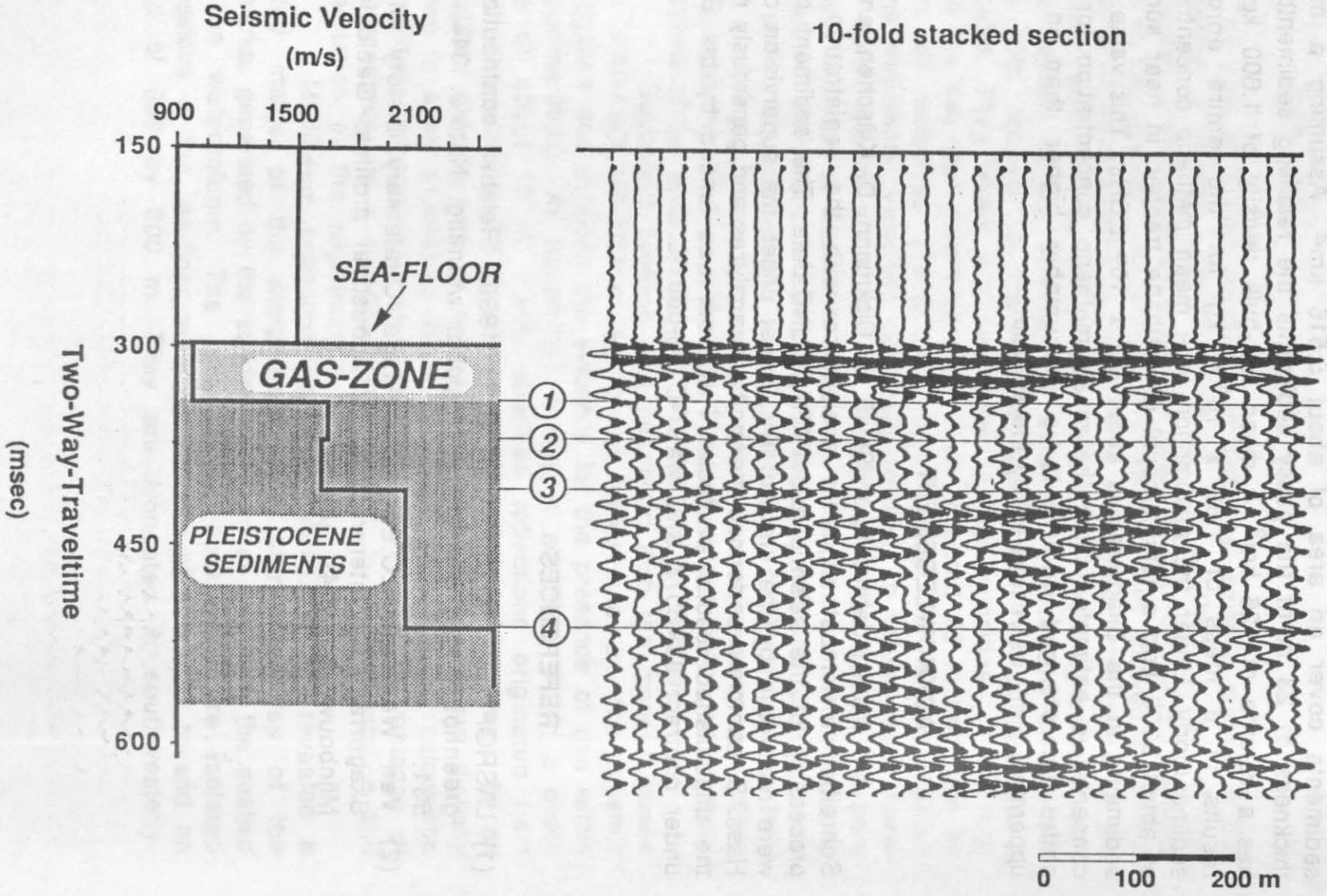
Seismic Velocity
(m/s)
900
1500
2100
150
300
450
600
Two-Way-Traveltime
(msec)
SEA-FLOOR
GAS-ZONE
PLEISTOCENE
SEDIMENTS
1
2
3
4
10-fold stacked section
0
100
200 m

Barite deposits from the Peru subduction zone

M. Torres[1], A.N. Dia[2], J. Boulègue[3], L. Aquilina[2], and E. Suess[1]

1 GEOMAR, Wischhofstraße 1-3, 2300 Kiel 14

2 Laboratoire de Géochimie et Métallogénie, Tour 26-16, E5, Université Pierre et Marie Curie, Paris, France

3 INSU-CNRS, UPMC, Laboratoire de Géochimie et Métallogénie, Paris, France

1993

In preparation

Introduction

In recent years a large effort has been devoted to study the processes of fluid venting from the ocean floor, because fluid circulation within the lithosphere and associated fluid-rock interactions profoundly affects global geochemical cycling and lithospheric geology. A program of dives with the deep submersible Nautile during the spring of 1991 (NAUTIPERC), has provided structural and stratigraphic data on the subducting plate boundary of the Peru margin (Bourgois et al., 1992). Communities of clams and serpulae as well as venting fluids were discovered and sampled during this project. Analyses of these materials have produced important information on the chemistry of fluids and vent organisms from this active margin (Dia et al., 1992; Boulegue et al, 1992). Of particular interest was the discovery of deposits of barite, in the form of crusts, concretions and chimneys which were recovered during the Nautile expedition and subsequently sampled during the R/V Sonne cruise 78 as well as confirming their ubiquitous occurrence and widespread distribution

High concentrations of microcrystaline barite (up to several weight percent) have been found in deep sea sediments underlying the equatorial divergence in the Pacific and Indian oceans (Goldberg and Arrhenius, 1958; Gurvich et al., 1978). Particle fluxes of barium and organic carbon in sediment trap samples have established a link between primary productivity and the barium flux to the ocean floor (Dymond et al., 1992). Remobilization of the biogenic barium by diagenesis has been proposed as the source of barite fronts in marginal basins (von Breymann et al., 1990; Torres et al., 1992). Barite formation from submarine hydrothermal vents has also been documented (Church, 1979; Koski et al., 1985; Koski et al., 1988). This paper presents geochemical data for large barite deposits from the Peru accretionary margin, in relation with their tectonic environment and chemistry of the venting fluids. We propose a new mechanism for the formation of these deposits uniquely related to fluid venting regimes of accretionary margins, and suggests an approach by which the magnitude of these deposits can be used to infer venting rates.

Geological setting

The Peru margin is one of the major areas of biogenic carbon production and burial in the world's ocean. The interplay of wind regime, oceanic circulation and biological productivity, results in deposition of a distinct sedimentary upwelling facies rich in organic matter and

biogenic silica (Suess et al., 1987, Reimers and Suess, 1981). The margin is also characterized by an active tectonic regime driven by the subduction of the Nazca Plate underneath the South American continent (Figure 1).

During the past 400 Kyr, a wide rollover fault developed in the middle slope section of the margin off northern Peru (Paita); subsequent oversteepening of the landward flank of the fold resulted in a debris flow avalanche at approximately 14 Kyr ago (Bourgois et al., 1992). This gravity failure has been documented by multibeam bathymetry, multichannel seismic studies and submersible observations (von Huene et al.,1989 and Bourgois et al,1992). The middle slope at this location is separated from the lower slope by a scarp 1000 to 1200 meters high and it has a mean slope angle of 45°. Observations at this lower scarp from the submersible Nautile revealed outcrops of massive claystone and mudstone and a very thin cover of pelagic sediments. Another scarp separates the middle slope from the upper slope. It ranges from 400 to 700 meters in height; the mean slope is of 45°, but is steeper between 3000 and 3400 m water depth. The outcropping rocks are mainly massive mudstone with very little sediment cover. The bench between the upper and lower scarps extends from 3500 to 3600 m, over a distance of about 450 m. In this area clam and serpulae colonies and associated venting of fluids were observed during the Nautile and Sonne (SO78) expeditions.

Venting activity in the Peru margin is not restricted to the Paita escarpment, but has also been observed in the Chiclayo canyon and offshore Chimbote. A survey of barite distribution was conducted using the French submersible Nautile, as well as with OFOS (Ocean-floor-observatory system) by the R/V Sonne. The areas investigated include both the upper and lower slope off Paita, the Chiclayo canyon and the slope in front of Chimbote (Figure 1). These surveys indicate that the barites are present only on the upper slope off Paita, with a few occurrences in the Chiclayo area (Figure 2). No barites were observed during the dives or OFOS surveys off Chimbote and the Paita lower-slope, nor were any samples recovered by coring or dredging in these areas. This is significant since venting of fluids in these areas is inferred by the presence of small colonies of clams.

Methods and Results

Barite samples were recovered from the slope of the Peru margin along a failure scarp as well as from the Chiclayo canyon using a submersible during the Nautiperc project, and by coring during the SO78 cruise. These barites occur in the form of light yellow to brown concretions or chimneys, up to 15 cm height, as well as white crusts only a couple of

millimiters thick. They are composed of very pure barium sulfate crystals either in dendritic arrangements or in concentric layers. No other phases were identified by XRD in either the chimneys nor in the crusts. Their porous nature results in a low bulk density, ranging from 2.8 to 3.4 g/cc, which is considerably lower than the material density of 4.5 g/cc for barium sulfate. Scanning electron micrographs (SEM) of the barites shown in Figure 3 display clean rosette-type structures for the barites recovered from chimneys; the crusts show several episodes of barite deposition, as indicated by concentric generations of the barite crystals.

Sulfate and oxygen isotope analysis of the barites was performed in the Department de Geochimie (BRGM) in Orleans and in the Geochemisches Institut of the University of Göttingen. Samples for Sr-isotope analysis were prepared and analyzed by A. N. Dia in the Laboratoire de Geochimie et Cosmochimie in Paris. The measured ratios were normalized to $^{86}Sr/^{88}Sr = 0.1194$. A mean value of 0.710259 $\pm$ 26 was obtained for 25 analysis of the NBS SRM 987 standard. Analysis of seawater standard (IAPSO) over the course of the study yielded a mean value of 0.709192 +13. The results for the isotopic composition of the barites are given in Table 1, with errors given at the 95% confidence limit.

Fluids from vents were collected by means of a titanium sampler during the Nautiperc expedition; the geochemistry of these fluids has been previously discussed by Dia et al., 1992. During the SO78 cruise, fluid samples were collected in a time sequence over a vent site using a benthic chamber deployed with a lander; a device which was developed at GEOMAR and has been named VESP (VEnt-SPider). This instrument has been described by Linke et al. (1993); it consists of a TV-controlled device for the deployment of five Niskin water samplers and a CTD-probe mounted inside a barrel and actuated by a time motor.

Water samples recovered with the benthic chamber were analyzed for barium by ICP-AES. Location of the deployments and the dissolved barium concentration are given in Table 2. The sequential water sampling using VESP showed significant changes in the chemical composition of the enclosed bottom water with time; changes in the barium concentration of the fluid are shown in Figure 4. During one of the deployments of the VESP at a vent site (Station SO78-180-4), a sediment sample was retrieved for analysing its pore fluid composition. Pore fluids were squeezed immediately after retrieval in a titanium hydraulic press; the dissolved barium content in the pore water was found to be 1260 nM.

Discussion

Source of the barium

It is important to determine the source of the barium in these deposits, as this knowledge might help elucidate the origin of the venting fluids, paths of fluid flow and venting rates. Two scenarios are possible: 1) the barites might have been deposited in association with hot barium-rich fluids which were discharged following the sediment slide by tapping into a hydrothermal reservoir; or 2) the barium associated with biogenic deposition in this high productivity region which is remobilized in the zone of sulfate depletion, could be subsequently transported with the fluids to the venting site where it precipitates upon mixing with ambient bottom water.

Deposition of barite from submarine hydrothermal sources along the East Pacific Rise (Church, 1979), the Gorda Ridge (Koski et al., 1988) and the Guaymas Basin (Koski et al., 1985; Peter and Scott, 1988) has been well documented. The sulfur isotopic composition of these barites is very close to the value of contemporaneous seawater sulfate (Koski et al., 1985; Kusakabe et al., 1982; Zierenberg et al., 1984); these results indicate that barite forms rapidly by mixing of barium-rich hydrothermal fluid with sulfate-rich seawater. In these cases, barite is found in association with other deposits characteristic of hydrothermal activity; namely, manganese and iron oxides, and polymetallic sulfides.

Barite deposits in the marine environment have also been observed in association with oceanic fracture zones such as in the California Borderland (Lonsdale, 1979) and in the Sea of Okhotsk. Lonsdale (1979) describes large masses of baritic sinter along the San Clemente fault in the California Borderland. As this author points out, there are no reports of active hydrothermal springs in this area, furthermore the barite deposits do not have coatings of manganese oxides nor are they associated with massive sulfide deposits. Inference of hydrothermal discharge as the origin of these barites was based solely on their association with vestimeniferan tube worms and other fauna typical of hydrothermal plumes at mid-ocean spreading centers.

Barite remobilization during diagenesis in sulfate-depleted environments has been postulated as the cause for the formation of barite fronts in several continental-margin settings. ODP drilling had previously recovered several modes of authigenic barites in the sediments of the Peru margin, an area where intensive high productivity results in a large flux of biogenic barium to the ocean

floor (von Breymann et al, 1992). In sediments undergoing strong anoxic diagenesis this labile biogenic-barium is partially dissolved in depth-intervals depleted of interstitial sulfate. In the absence of advective flow, upward barium diffusion to the sulfate reducing zone leads to the *in situ* formation of crystalline barite in these sediments. Barite precipitation is thought to occur in that section of the sediments where there is sufficient sulfate, generally supplied by downward diffusion, to cause supersaturation with respect to this mineral.

A possible source of barium for the barites recovered at the vent sites, is from the emanating fluids in which dissolved barium has accumulated as a result of sulfated depletion due to organic matter diagenesis, as in the case of the diagenetic barite front described above. Barium concentrations as high as 400 μM below the zone of sulfate depletionhave been measured in the pore fluids obtained by deep drilling in the Peru margin (von Breymann et al., 1990; Figure 5).

Temperature measurements (Foucher, personal communication) and geochemistry of the venting fluids (Dia et al., 1992) do not show any evidence for contemporaneous hydrothermal activity in the Peru slope; on the other hand, recent precipitation is suggested by the fragility of the deposits and by the absence of any significant sediment coating on the chimneys or infillings of the void space of the crystallites in an environment characterized by extremely high sediment accumulation rates. These observations lead us to postulate that the barium source is associated with remobilization of biogenic barium, and subsequent transport of the barium-rich reducing fluids to the cold-vent sites.

Isotopic evidence: Oxygen and sulfur

Sulfate fractionation during bacterial decomposition of organic matter results in a dissolved sulfate reservoir enriched in the heavy ^{34}S isotope (Goldhaber and Kaplan, 1980), so the diagenetic barites formed within the sediment column, and constituting the barite front, should be isotopically heavy relative to seawater. Such heavy barites (up to 84 $^{0}/_{00}$ CDT) have been recovered by deep sea drilling in the Japan Sea and the Peru margin (Torres et al., in preparation). These values contrast markedly with the results obtained from the barites recovered at the Chiclayo site, which indicate that the Chiclayo deposits formed at the seafloor, from the interaction of barium-rich fluids venting at the margin, with seawater sulfate. The slightly higher isotopic values in the samples from Paita ($\partial^{34}S$ = 25 to 30 $^{0}/_{00}$ CTD) may reflect a small component enriched in ^{34}S by bacterial reduction of sulfate during oxidation of organic matter which has either been being generated at the sediment water interface or has been transported up to the seafloor from deeper in the sediment section by the venting fluids.

The oxygen isotopes of the sulfate in the Chiclayo canyon barites are consistent with contemporary values for the dissolved seawater sulfate. The Paita samples, however show an enrichment of $S^{18}O_4$ relative to seawater ($\partial^{18}O$ = 17 to 18 $^{o}/_{oo}$). The hydrothermal barites recovered in the Guaymas hydrothermal field are, on the other hand, depleted in $S^{18}O_4$ ($\partial^{18}O$ = 6.9 to 7.8 $^{o}/_{oo}$), reflecting an elevated temperature of formation for these deposits of approximately 200 °C (Koski et al., 1985). The Peru barites are therefore not the result of precipitation from hot brines, as our above-mentioned first alternative would require. Therefore, we favor the second alternative and thus propose that the enrichment in the heavy oxygen isotope results from bacterial activity near the vent site.

During sulfate reduction, bacteria preferentially metabolize sulfate containing ^{16}O and ^{32}S (Mizutani and Rafter, 1973; McCready and Krouse, 1980), and thus the residual sulfate and hence the barites become progressively enriched in ^{18}O and ^{34}S. Using bacteria *Desulfovrio desulfuricans* as well as natural cultures from an estuarine sediment, Lloyd (1967; 1968) showed that even when the kinetic fractionation factor might depend on experimental conditions, it will always be negative, and the residual sulfate in solution will become progressively enriched in ^{18}O as the reaction proceeds.

The sulfate and oxygen isotopic composition of several barites from marine and continental deposits is shown in Figure 6. The composition of contemporaneous seawater is shown by the arrows on each axis. Samples from the Wairakei geothermal field in New Zealand (Rafter and Mizutani, 1967; Mizutani and Rafter, 1968) are shown to illustrate the enrichment in the light oxygen isotope relative to seawater. Similarly, samples recovered from the Guaymas hydrothermal deposits are also depleted in ^{18}O (Koski et al., 1985). The barite recovered from the Chiclayo canyon has an isotopic composition which is not significantly different from that of seawater, clearly indicating precipitation with seawater sulfate. The trend of increasing values of $\partial^{18}O$ and $\partial^{34}S$ for bacterially dominated systems includes the samples from Paita (this study), the Appalachian province (Nuelle and Shelton, 1986); Kaitara Harbor, New Zealand (Rafter and Mizutani, 1967); and samples dredged from the California Borderlands (Church, 1970). This trend indicates a progressive component of metabolized sulfate in a closed system with a continuous removal of the light isotopes. The slight enrichment in ^{34}S and ^{18}O in the Paita deposits thus indicates a component of biologically metabolized sulfate. This fractionation, which is only present in Paita and not in Chiclayo, is consistent with the higher sediment cover, stronger organic input, and the presence of bacterial mats observed in the Paita venting sites.

Venting rates

Barium concentrations in the barrel fluids clearly document a contemporaneous release of Ba to the bottom water from the vent sites (Fig 4). This demonstrates that barium can be remobilized from the sediments at low temperatures. Suess et al., (in preparation) have estimated water flow rates from these vents using the flux rates of dissolved components of the fluids. By assuming that: (1) the barium behaves conservatively during the period of deployment of approximately 30 minutes; and (2) that the barium content in the pore fluids feeding the vent is that measured just below the sediment surface, an estimate of fluid flow of approximately 970 $L/m^2/day$ was obtained using the barium flux rates from Station 180-4. The good correspondence of venting rates calculated with barium with those using other dissolved tracers (Suess et al., in preparation) indicates that the barium source is somehow coupled to the fluids which are enriched in metabolites from decomposition of organic matter.

The rates of flow discussed above represent the actual flow measured at the time of deployment; there is, however evidence that fluid flow from accretionary margins is not constant, but varies with time (e.g., Foucher et al., 1992). The fact that we know the age of the scarp at Paita (Bourgois et al., 1992), permits us to attempt to estimate of the integrated fluid venting rates over the last 14 Kyr using the barite deposits as a cumulative record of dissolved mass flux, and thereby fluid flow. For this estimate we assume that the barites cover 40% of the vent area and that the chimneys are on average 5 cm high. These assumptions are based on visual observations using the Nautile as well as the OFOS video records. Then, by knowing the density of the barite chimneys (3.1 g/cc), the concentration of barium in the venting fluids (1.3 μM) and the age of the debris flow avalanche which marks the start of the vent regime off Paita (14 Kyr; Bourgois et al, 1992), we arrive at an integrated fluid flow of approximately 68 $L/m^2/day$.

There is a difference of approximately one order of magnitude between the estimates using barite deposits and those calculated from the dissolved barium fluxes. This is reasonable since the assumptions of barite coverage represent average estimates, and furthermore, venting occurs at discrete episodes, as evidenced by SEM pictures of the barites showing the occurrence of various stages of barium deposition. Similar "events" of fluid flow have been documented by the presence of dead Calyptogena clam colonies in the Peru margin, and at depth in the sediments from the sea of Okhotsk.

Source of the fluid

The "instantaneous" flow rates estimated from the dissolved barium, are comparable with rates measured *in situ* along the Oregon margin. Several studies (Le Pichon et al., 1992; Carson et al.,1990: Linke et al., 1993) have argued that such high values cannot be explained solely by steady-state compactive dewatering processes, instead they imply that there must be a recharge zone for the fluids venting at accretionary margins.

Accumulation of dissolved barium is driven by the dissolution of barite in the sulfate depleted sediments. This observation establishes an upper limit on the depth of the penetration of the recharge fluids because they must be deeper than the thickness of the sulfate-containing zone. Furthermore, the strontium isotopic composition of the barites indicates that the fluid responsible for the transport of biogenic barium to the vent site may have a continental component (Table 1). This is in agreement with the results of Dia et al. (1992) which show a radiogenic strontium component of the fluids collected at the venting sites. Elderfield et al. (1990) have previously reported radiogenic values for isotopic composition of the dissolved strontium on sites drilled at approximately 9° north on the Peru margin, specifically at the site where accreted sediments were recovered (ODP Site 685). They attribute these high values ($^{87}Sr/^{86}Sr$ up to 0.70996) to a source involving reactions with the underlying continental crust, since isotopic analysis of bulk sediment samples from the drill sites do not reveal ratios as high as those recorded in the pore waters.

The fact that the barites recovered at the seafloor on the Paita scarp also have radiogenic $^{87}Sr/^{86}Sr$ ratios, indicates that fluid from the recharge zones must have reacted with continental crust. These observations clearly demonstrate that the fluids have either migrated from the continent or have reacted with a continental crust underlying the sediments. In either case, the fluids are not solely generated from within the sediment column due to loss of porosity during compaction, but instead must have migrated a considerable distance from their contact with continental crust. This implies that the circulation cell for the fluid venting at this margin is rather large; i.e., the recharge fluids cannot come from a small scale satellite convection around the vent.

Conclusions

The fact that there is barium being expelled at the vent site, is evidence that the barium source is currently active, and since there is

no high temperature anomaly associated with the vents, the fluids are filtering through the sediments. The radiogenic nature of the Sr isotopes suggests that the actual source of the fluids might be associated with a recharge area in the continent, or that the fluid penetration was deep enough to allow reaction with continental crust. The possibility of an original pulse of deep hot fluids as the parent-fluid for the barites does not seem likely, particularly given the oxygen and sulfur isotopic composition of the sulfate in these deposits.

Our hypothesis suggests an alternative origin for the barites recovered in association with faults in the California Borderland and Sea of Okhotsk. Both areas are characterized by high biogenic barium accumulation in the sediments, and it is possible that the fracture does provide an escape route to overpressured fluids, which bring with them a high concentration of barium that has been remobilized from sulfate-free, organic-rich sediments. This is particularly feasible in the San Clemente barites, since there is no other temperature or chemical data to suggest a hydrothermal source.

References

Boulegue, J., Mariotti, A., Fiala, A. and Bourgois, J. 1992. Geochemistry of clams from subduction zones. EOS 73, 153

Bourgois, J., Lagabrielle, Y., DeWever, P., Suess, E. and the Nautiperc cruise shipboard scientists, 1992. Tectonic history of a non-accreting active margin during the past 400 ka, Results of a submersible survey of the Peru trench at 5-6°. Part 1. Submitted to Geology.

Carson, B., Suess, E., and Strasser, J.C., 1990. Fluid flow and mass flux determinations at vent sites on the Cascadia margin accretionary prism. J. Geophys. Res. 95, 8891-8897.

Church, T.M. 1979, Marine Barite. In: Burns, R.G. ed., Marine minerals (Reviews in mineralogy, v.6.) Mineral Soc. America, 170-210.

Dia, A. N., Aquilina, L., Suess, E., Torres, M., Boulegue, J., Bourgois, J. and the Nautiperc shipboard scientists. 1992. Continent-derived fluids from the convergent margin off Peru. Deep sea dives of the Nautiperc cruise, Part 2. Submitted to Geology.

Dymond, J., Suess, E. and Lyle, M. 1991. Barium in deep sea sediment: a geochemical indicator of paleoproductivity. Paleoceanography

Elderfield, H., Kastner, M and Martin, J.B. 1990. Compositions and sources of fluids in sediments of the Peru subduction zone. J. Geophys. Res. 95, 8819-8827.

Foucher, J-P., Henry, P., Le Pichon, X. and Kobayashi, K. 1992. Time variations of fluid expulsion velocities at the toe of the eastern Nankai accretionary complex. Earth and Planet. Sci. Letters 109: 373-382.

Goldberg, E., D., and Arrhenius, G.O.S., 1958. Chemistry of Pacific pelagic sediments. Geochim. Cosmochim. Acta, 13:153-212.

Goldhaber, M.B. and Kaplan, I.R. 1980. Mechanisms of sulfur incorporation and isotope fractionation during early diagenesis in sediments of the Gulf of California. Mar. Chem., 9:95-143.

Gurvich, Y.G., Bogdanov, Y.A. and Lisitzin, A.P., 1978. Behavior of barium in Recent sedimentation in the Pacific. Geokhim., 3:359-374. (In Russian).

Koski, R.A., Lonsdale, P.F., Shanks, W.C., Berndt, M.E. and Howe, S.S., 1985. Mineralogy and geochemistry of a sediment hosted hydrothermal sulfide deposit from the southern trough of the Guaymas basin, Gulf of California. Jour. Geophys. Res., 90:6695-6707.

Koski, R.A., Shanks, W.C., Bohrson, W.A. and Oscarson, R.L., 1988. The composition of massive sulfide deposits from the sediment covered floor of Escanaba trough, Gorda Ridge: implications for depositional processes. Can. Mineral., 26:655-673.

Kusakabe, M., Chinba,H. and Ohmoto, H. 1982. Stable isotopes and fluid inclusion study of anhydrite from the East Pacific Rise at 21°N. Geochem. J., 16: 89-95.

Le Pichon, X., Kobayashi, K. and the Kaiko-Nankai scientific crew. 1992. Fluid venting activity within the eastern Nankai trough accretionary wedge: A summary of the 1989 Kaiko-Nankai results. Earth and Planet. Sci. Letter, 109: 303-318.

Linke, P., Suess, E., Martens, V., Rugh, W.D., Ziebis, W., Torres, M. and Kulm, L.D. 1993. Determination of fluid flow from active margin seeps. Submitted to Deep Sea Research.

Lonsdale, P. 1979. A deep-sea hydrothermal site on a strike-slip fault. Nature, 281: 531-535.

Lloyd, R.M. 1967. Oxygen-18 composition of oceanic sulfate. Science 156: 1228-1231.

Lloyd, R.M. 1968. Oxygen isotope behavior in the sulfate-water system.J. Geophys. Res. 73: 6099-6110.

McCready, R.D.L. and Krouse, H.R. 1980. Sulfur isotope fractionation by *Desulfovibrio vulgaris* during metabolism of $BaSO_4$. Geomicrobiology Jour., 2: 55-61.

Mitzutani, Y. and Rafter, A. 1973. Isotopic behavior of sulfate oxygen in the bacterial reduction of sulfate. Geochem. Jour., 6:183-191.

Nuelle, L. M. Lawrence and Shelton, K. L. 1986. Geologic and geochemical evidence of possible bedded barite deposits in Devonian rocks of the Valley and Ridge province, Appalachian mountains. Econ. Geol., 81: 1408-1430.

Peter, J.M. and Scott, S.D., 1988. Mineralogy, composition and fluid inclusion microthermometry of seafloor hydrothermal deposits in the Southern trough of Guaymas basin, Gulf of California. Can. Mineral., 26:567-587.

Rafter, T.A. and Mizutani., 1967. Oxygen isotopic composition of sulfates. Part 2. N. Z. J. Sci. 10:816-840.

Reimers, C.E. and Suess, E. 1981. Spatial and temporal patterns of organic carbon accumulation on the Peru continental margin. In Thiede, J., and Suess, E. (eds.) Coastal Upwelling: Its Sedimentary Record. Plenum, New York, 311-346.

Suess, E. , Kulm, L.D. and Killingley, J.S. 1987. Coastal upwelling and the history of organic-rich mudstone deposition off Peru. In Brooks, J. and Fleet, A.J. (eds.) Marine petroleum source rocks. Geological Society, London, Special Publication, 26, 181-197.

von Breymann, M. T., Emeis, K. C., and Camerlenghi, A., 1990. Geochemistry of sediments from the Peru upwelling area: results from Sites 680, 685 and 688. In Suess, E., von Huene, R., et al., Proc. ODP, Sci. Results, 112: College Station, TX (Ocean Drilling Program), 491-504.

von Breymann, M. T., Emeis, K. C. and Suess, E., 1992. Water-depth and diagenetic constraints in the use of barium as a paleoproductivity indicator. In Summerhayes, C. P., Prell, W. and Emeis, K. C. (Eds.), Evolution of Upwelling Systems since the Early Miocene. Geol. Soc of London. In press.

von Breymann, M. T., Brumsack, H. and Emeis, K. 1992. Depositional and diagenetic behaviour of barium in the Japan Sea. In Pisciotto, K., Ingle, J.C. von Breymann, M.T. Barron, J. (Eds.), Proc. ODP, Sci. Results, 128: College Station, TX (Ocean Drilling Program). In press.

von Huene, R., Bourgois, J., Miller, J. and Pautot, G., 1989. A large tsunamogenic landslide and debris flow along the Peru Trench. J. Geophys. Res. 94, 1703-1714.

Zierenberg, R.A., Shanks, W.C. and Bischoff, J.L. 1984. Massive sulfide deposits at 21°N, East Pacific Rise.: Chemical composition, stable isotopes, and phase equilibria, Geol. Soc. Am. Bull., 95, 922-929.

Figure captions

Figure 1. A) Location map showing the areas were barites were recovered (dashed blocks), as well as the location of seismic lines CDP-2 and CDP-3. B) Diagramatic representation or record CDP-3, showing the location of the scarpments off Paita, modified from von Huene et al., 1989.

Figure 2. Bathymetric contours indicating the areas surveyed by the Nautile (Nautiperc expedition) and the Sonne (cruise SO78). A) Paita area showing the location of the upper and lower venting sites. B) Chiclayo canyon. In both cases the barite deposits are indicated by open squares.

Figure 3. SEM pictures of barites showing the dendritic arrangement (A and B) and the concentric layer (C) structures of the barites.

Figure 4. Increase in dissolved barium concentration with time for two deployments of the VESP at the Paita venting site. Circles correspond to Station SO78-177-2 and squares represent data from Station SO78-180-4.

Figure 5. Downcore distribution of dissolved barium and sulfate at ODP Site 685, located at 5081 m of water on CDP-2. No barite deposits were recovered from this area, however, the high barium in the pore fluids (up to 400 μM) illustrates the remobilization of barium in the zone of sulfate depletion. The lithostratigraphic column shows the enrichment in diatomaceous components usually associated with high levels of biogenic barium accumulation.

Figure 6. Sulfate and oxygen isotopic composition of the sulfate in the barites recovered from the Peru margin (bold letters), compared with samples of hydrothermal origin, as well as with samples enriched in ^{34}S and ^{18}O which result from the preferential utilization of the lighter isotopes during bacterial consumption of sulfate. The composition of seawater is shown by the arrows at each axis.

Table 1. Isotopic composition of barites from the Peru margin.

Location	$\partial^{34}S_{(SO4)}$	$\partial^{18}O_{(SO4)}$	$^{87}Sr/^{86}Sr$
Paita	29.7	17	0.710152
	25.8	16.1	0.711118
Chiclayo	22.2	10.1	
Seawater	21-22	9-10	0.709192

Table 2. Concentration of barium in the sequentially activated bottles inside the benthic chamber deployed on the Paita scarp. Both deployment sites were in active vent fields.

Station	Water depth (m)	Time (min)	Ba (nM)
177-2	3352	5	109
		10	117
		15	131
		20	131
		25	136
180-4	3309	6	116
		12	117
		18	120
		24	131
		30	138

Fig. 1

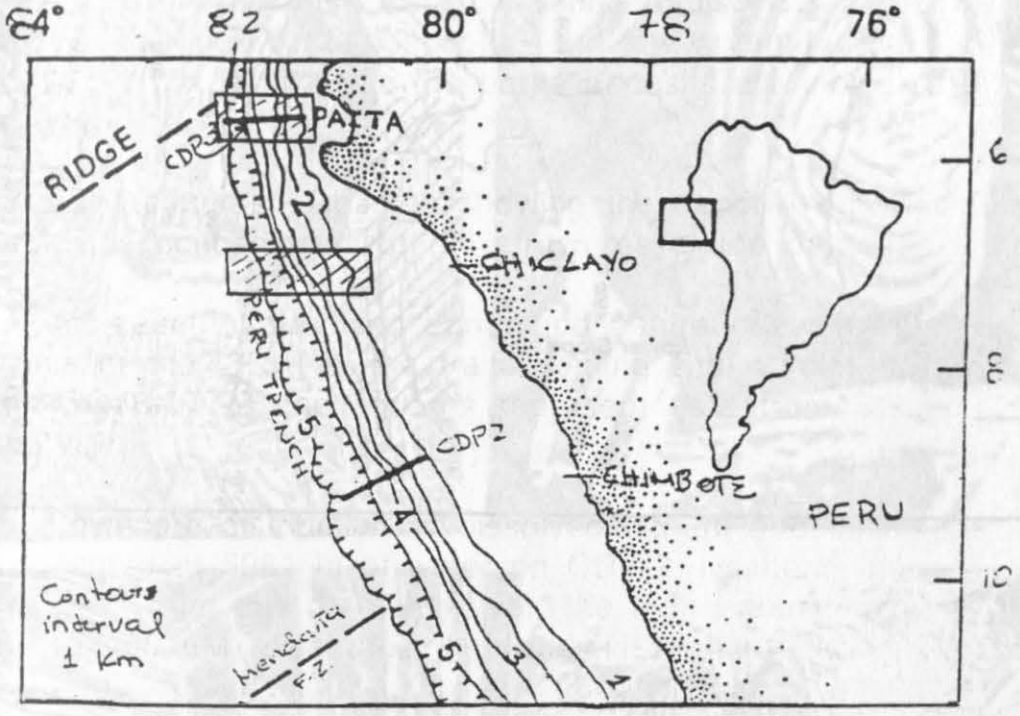
84°
82
80°
78
76°
RIDGE
CDP3
PAITA
CHICLAYO
PERU TRENCH
CDP2
CHIMBOTE
PERU
6
12
10
Contours interval 1 Km
Mendaña F.Z.
1
2
3
4
5

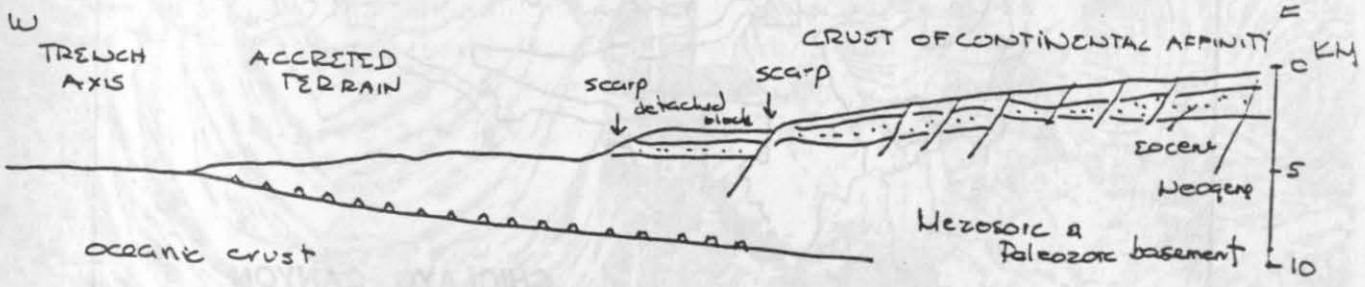
W
E
TRENCH AXIS
ACCRETED TERRAIN
CRUST OF CONTINENTAL AFFINITY
KM
0
scarp
detached block
scarp
Eocene
Neogene
5
Mezosoic & Paleozoic basement
10
oceanic crust

Fig. 2

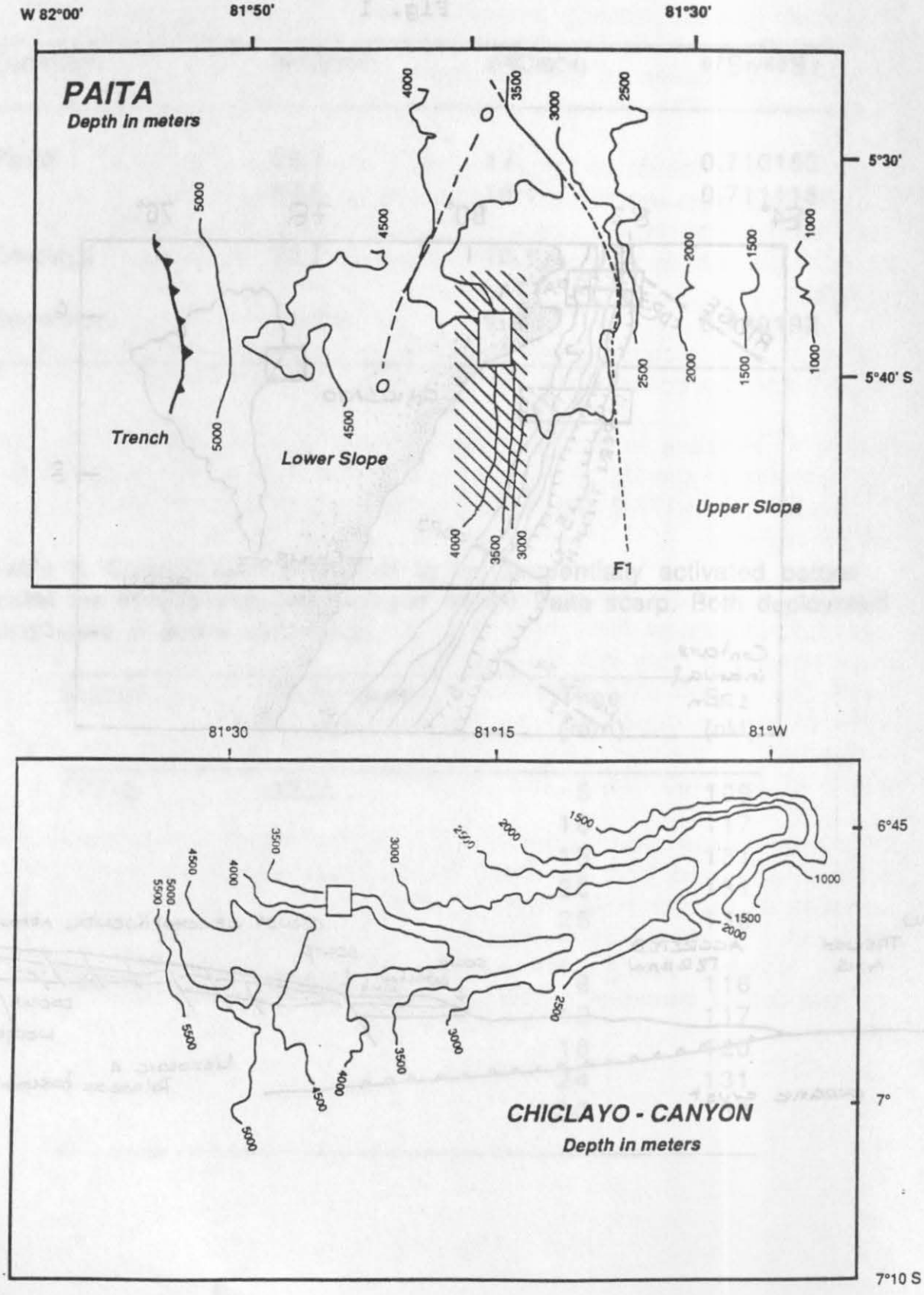
W 82°00'
81°50'
81°30'
PAITA
Depth in meters
5°30'
5°40' S
Trench
Lower Slope
Upper Slope
F1
81°30
81°15
81°W
6°45
7°
7°10 S
CHICLAYO - CANYON
Depth in meters

Fig. 3

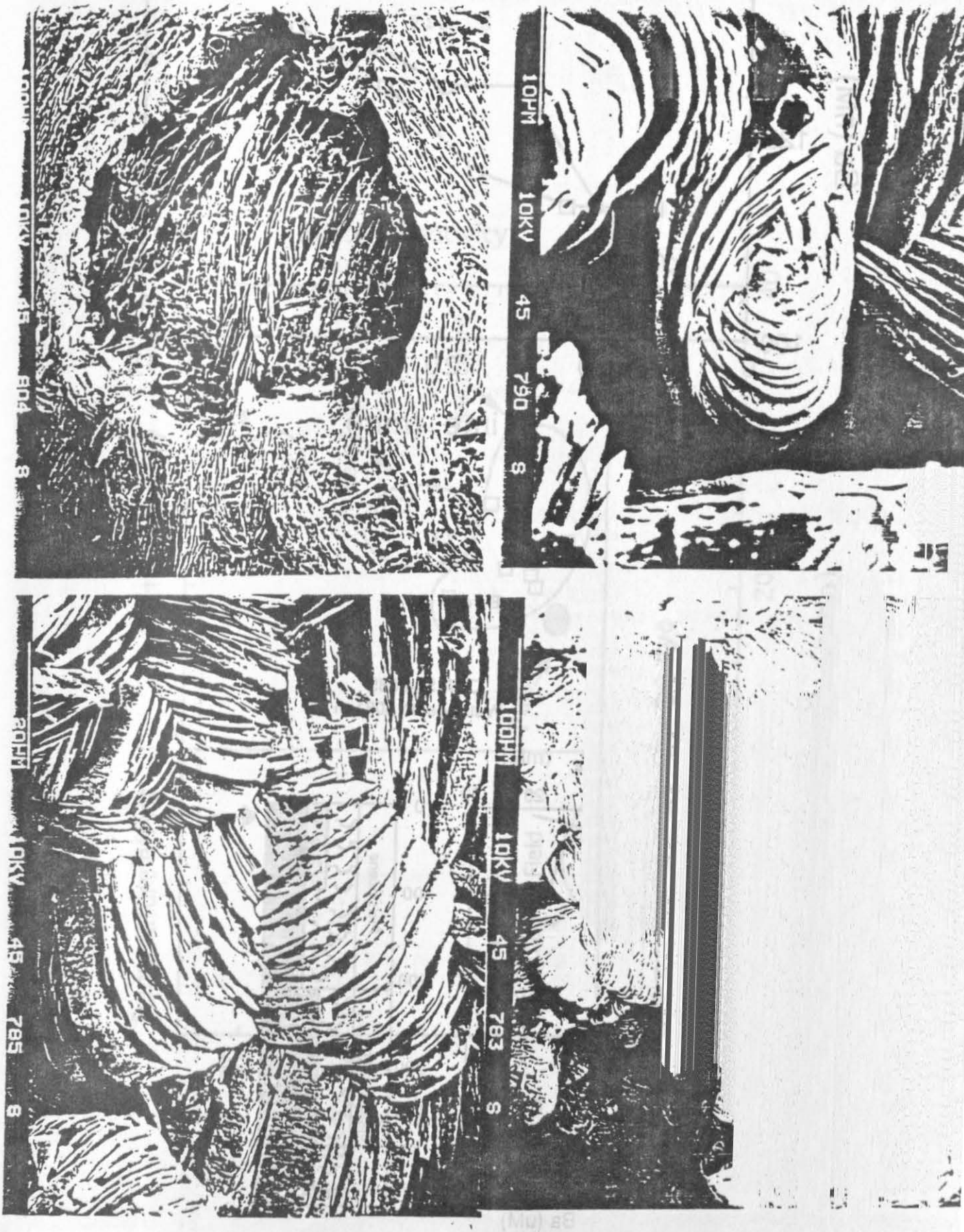
10HM
10KV
45
760
8
100HM
10KV
45
804
8
20HM
10KV
45
785
8
100HM
10KV
45
783
8

Fig. 4

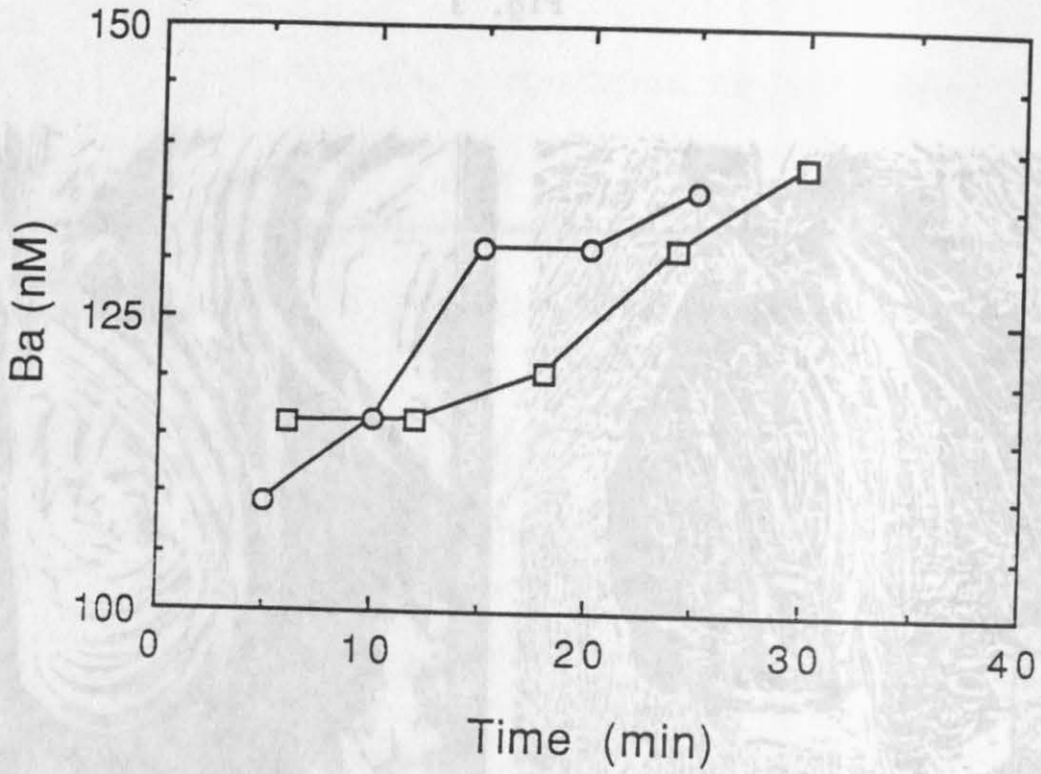
150
125
100
Ba (nM)
0
10
20
30
40
Time (min)

Fig. 5

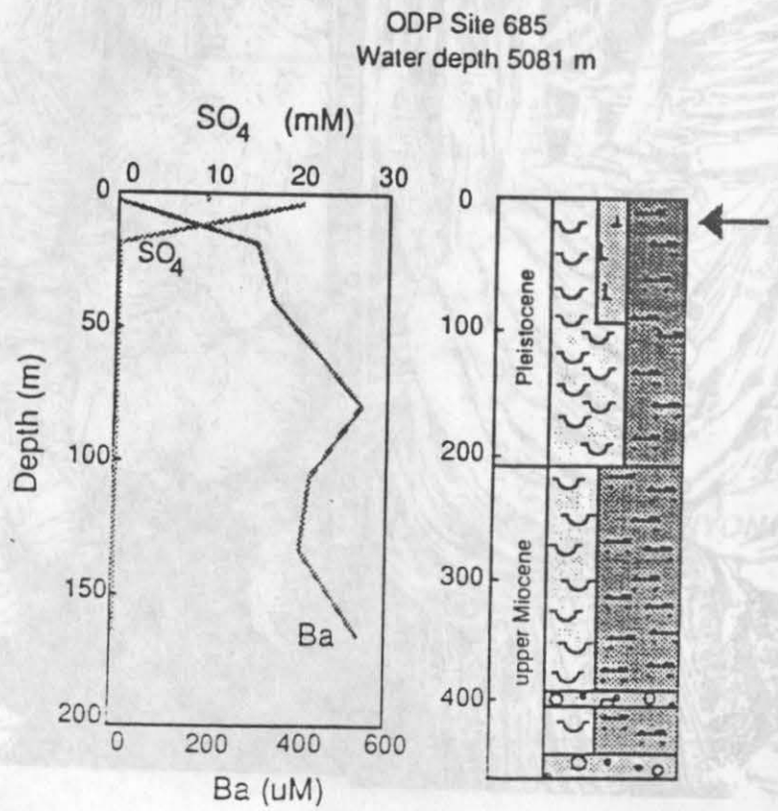
ODP Site 685
Water depth 5081 m
SO4 (mM)
0
10
20
30
SO4
Ba
Depth (m)
50
100
150
200
0
200
400
600
Ba (uM)
Pleistocene
upper Miocene
300
400

Fig. 6

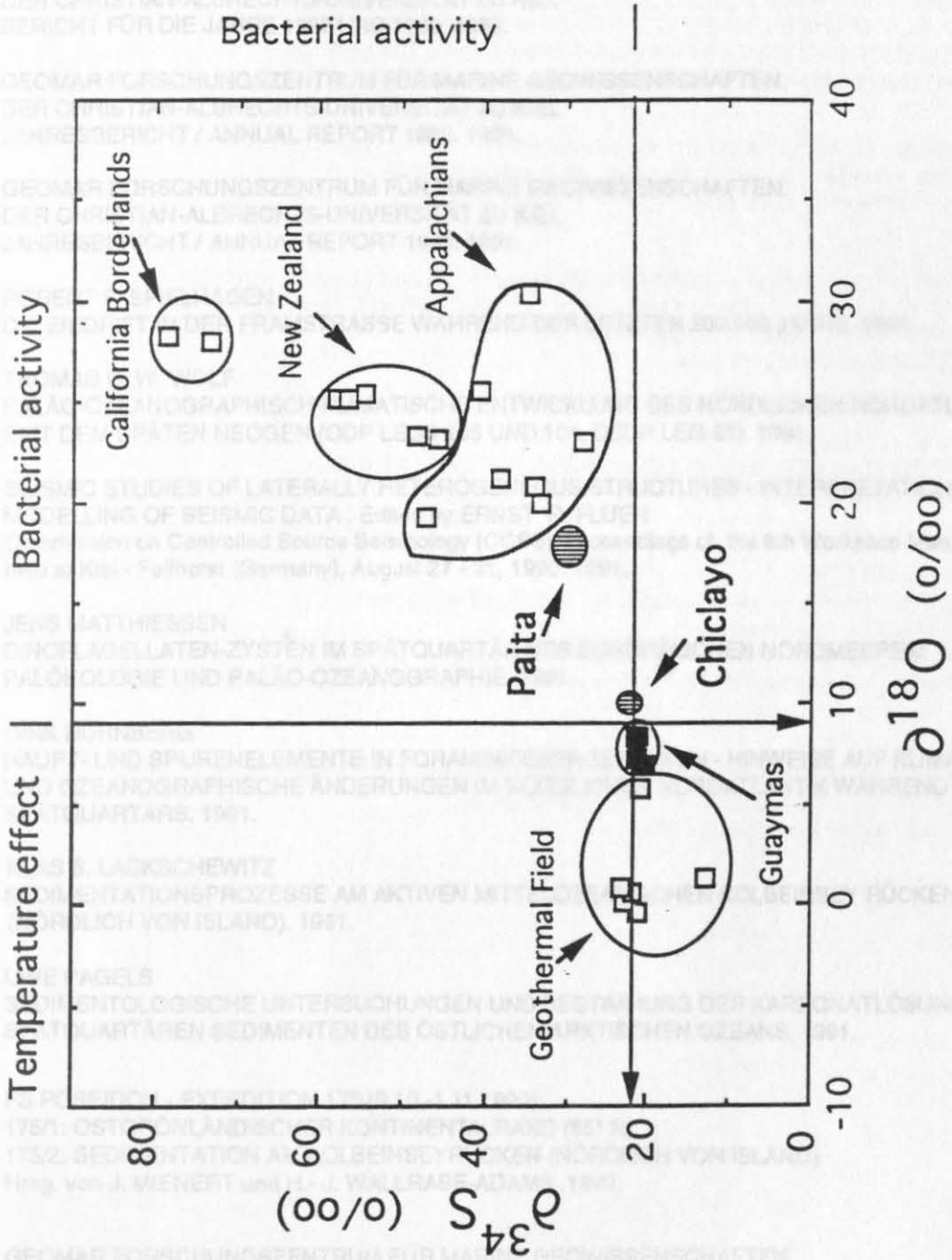
Bacterial activity
Temperature effect
Bacterial activity
California Borderlands
New Zealand
Appalachians
Paita
Chiclayo
Guaymas
Geothermal Field
$\partial^{34}S$ (o/oo)
$\partial^{18}O$ (o/oo)
80
60
40
20
0
-10
0
10
20
30
40